Development of Metabolomics and Lipidomics Workflows for Phosphorylated Metabolites Using Ultra-High-Performance Liquid Chromatography with Tandem Mass Spectrometry

Dissertation

der Mathematisch-Naturwissenschaftlichen Fakultät

der Eberhard Karls Universität Tübingen

zur Erlangung des Grades eines

Doktors der Naturwissenschaften

(Dr. rer. nat.)

vorgelegt von

Peng Li

Aus Jiangsu

China

Tübingen

2022

Gedruckt mit Genehmigung der Mathematisch-Naturwissenschaftlichen Fakultät der Eberhard Karls Universität Tübingen.

Tag der mündlichen Qualifikation: 21.07.2022

Dekan: Prof. Thilo Stehle

1. Berichterstatter: Prof. Dr. Michael Lämmerhofer

2. Berichterstatter: Prof. Dr. Stefan Laufer

Table of contents

I. Summary

Over the last decades, system biology and multi-omics have become an emerging field in life science. With the development of analytical instruments, especially the mass spectrometry (MS), MS based metabolomics are widely utilized to understanding the metabolic status. Due to significantly different properties of lipids, lipidomics became more and more an independent research discipline. Liquid chromatography coupled to tandem mass spectrometry (LC-MS/MS) is the most popular analytical platform in metabolomics and lipidomics. Recent progress in bioinformatical approaches has also facilitated the bottlenecking data processing steps.

Although some widely used methods were established for general metabolomics and lipidomics analysis, there are still some challenging analytes like phosphorylated metabolites/lipids, which showed compromised performance. Through highly regulated phosphorylation and dephosphorylation by enzymes, phosphorylated metabolites/lipids regulate many important cellular processes. Despite their importance, the performance of their current analytical methods is not satisfying. Generally, analysis of phosphorylated analytes by LC-MS/MS face the following challenges, including low abundance, low extraction recovery, instability, regioisomers, availability of standards, etc. In order to address these issues, we developed new methods based on phosphate methylation. Accordingly, complete workflows from sample preparation to data processing were developed and validated in biological matrix.

In the 1st project, a targeted LC-MS/MS method of fatty acyl-CoAs (acyl-CoAs) with different chain lengths was established. Acyl-CoAs are central metabolic intermediates in numerous biological processes. Due to diverse fatty acyl compositions, acyl-CoAs vary greatly in polarity, which poses great challenges to their chromatographic separation. Currently, short chain acyl-CoAs are separated by HILIC or acidic RP-LC, while medium-, long- and very long-chain acyl-CoAs are analysed in basic RP-LC. Additionally, carryover in LC-MS/MS instrumentation requires extra flushing/cleaning procedures. To address these problems, we developed phosphate methylation strategy for acyl-CoAs. In the sample preparation, mixed-mode SPE was optimized to be compatible with

methylation. SRM transitions in MS detection was constructed with fragmentation rule for all methylated acyl-CoAs. Uniformly 13C labelled yeast extract was used as internal standards for accurate quantification. Odd chain and stable isotope labelled analogs were used as surrogate calibrators. The LOQs were between 16.9 nM and 4.2 nM. The method was applied in cultured HeLa cells and human platelets of coronary artery disease patients. The results showed that the established method can be used to profile acyl-CoAs in biological samples.

In the 2nd project, an isomer selective LC-MS/MS method of PIPx was developed. PIPx is a family of low abundant phospholipids commonly found in eukaryotic cells. Starting from phosphoinositol (PI), PIPx family consists of three lipid classes (PIP, PIP2, and PIP3) according to phosphorylation degree. There are three distinct regioisomers in each class of PIP and PIP2. As phospholipids, PIPx has two fatty acyl groups at the sn1 and sn2 position of a glycerol backbone. Currently, methods capable of regioisomer separation and fatty acyl coverage are still missing. To develop a comprehensive method, we utilized polysaccharide chiral column with data independent acquisition technique. Stable isotope labelled PIPx were characterized and used as internal standards. The established method was applied to several biological samples, including NIST SRM1950 plasma, *Pichia Pastoris*, and cultured HeLa cells. The results indicate this method could effectively monitor PIPx profiles in real samples and facilitate our understanding of physiological and pathological conditions.

In the 3rd and 4th project, improved LC-MS/MS methods of IPx and SPx were developed. Compared to PIPx and acyl-CoAs, IPx and SPx are more polar and hydrophilic. To apply the phosphate methylation strategy, a new derivatization solvent mixture was developed and optimized. To improve extraction recovery, an extraction kit compromised of TiO2 and centrifuge filter was established. Differential isotope labelling methylation was utilized to generate stable isotope labelled analogs in both projects (internal standards in IPx project, surrogate calibrators in SPx project). Cholesterol-ether bonded RP column was used to separate IPx regioisomers, especially I(1,4,5)P3. Porous graphite carbon column was used to separate SPx in glycolysis pathway. After validation in biological matrix, the methods were applied in different biological samples, including NIST SRM1950 plasma, cultured HeLa cells, and human platelets.

II. Zusammenfassung

In den letzten Jahrzehnten haben sich die Systembiologie und die Metabolomik zu einem aufstrebenden Bereich der Biowissenschaften entwickelt. Mit der Entwicklung von Analyseinstrumenten, insbesondere der Massenspektrometrie (MS), wird die MS-basierte Metabolomik in großem Umfang zum Verständnis des Stoffwechselstatus eingesetzt. Aufgrund der Unterschiede in Struktur und Eigenschaften wurde die Lipidomik mehr und mehr zu einer eigenständigen Forschungsdisziplin. Flüssigchromatographie gekoppelt mit Tandem-Massenspektrometrie (LC-MS/MS) ist die beliebteste analytische Plattform in der Metabolomik und Lipidomik. Darüber hinaus haben die jüngsten Fortschritte in der Bioinformatik dazu beigetragen, die Datenverarbeitung zu vereinfachen.

Obwohl einige weit verbreitete Methoden für die allgemeine Metabolomics- und Lipidomics-Analyse etabliert wurden, gibt es immer noch einige schwierige Analyten wie phosphorylierte Metaboliten/Lipide, die eine kompensierte Leistung aufweisen. Durch stark regulierte Phosphorylierung und Dephosphorylierung durch Enzyme regulieren phosphorylierte Metaboliten/Lipide viele zelluläre Prozesse. Trotz ihrer Bedeutung ist die Leistung der derzeitigen Analysemethoden nicht zufriedenstellend. Im Allgemeinen ist die Analyse phosphorylierter Analyten mittels LC-MS/MS mit folgenden Problemen verbunden: geringe Häufigkeit, geringe Extraktionsausbeute, Instabilität, Regioisomere, Verfügbarkeit von Standards usw. Um diese Probleme zu lösen, haben wir neue Methoden entwickelt, die auf Phosphatmethylierung basieren. Dementsprechend wurden ganze Arbeitsabläufe, von der Probenvorbereitung bis zur Datenverarbeitung, entwickelt und in biologischer Matrix validiert.

Im ersten Projekt wurde eine gezielte LC-MS/MS-Methode für Fett-Acyl-CoAs (Acyl-CoAs) mit unterschiedlichen Kettenlängen entwickelt. Acyl-CoAs sind zentrale metabolische Zwischenprodukte in zahlreichen biologischen Prozessen. Aufgrund der unterschiedlichen Zusammensetzung der Fettacylgruppen sind Acyl-CoAs in ihrer Polarität sehr unterschiedlich, was ihre chromatographische Trennung vor große Herausforderungen stellt. Derzeit werden kurzkettige Acyl-CoAs durch HILIC oder saure RP-LC getrennt, während mittel-, lang- und sehr

langkettige Acyl-CoAs in basischer RP-LC analysiert werden. Außerdem erfordert die Verschleppung in LC-MS/MS-Instrumenten zusätzliche Spül-/Reinigungsverfahren. Um diese Probleme zu lösen, haben wir eine Phosphatmethylierungsstrategie für Acyl-CoAs entwickelt. Bei der Probenvorbereitung wurde die Mixed-Mode-SPE so optimiert, dass sie mit der Methylierung kompatibel ist. SRM-Übergänge in der MS-Detektion wurden mit Fragmentierungsregeln für alle methylierten Acyl-CoAs konstruiert. Einheitlich 13C-markierter Hefeextrakt wurde als interner Standard für die genaue Quantifizierung verwendet. Ungerade Ketten und mit stabilen Isotopen markierte Analoga wurden als Ersatzkalibratoren verwendet. Die LOQs lagen zwischen 16,9 nM und 4,2 nM. Die Methode wurde in kultivierten HeLa-Zellen und menschlichen Blutplättchen von Patienten mit koronarer Herzkrankheit angewandt. Die Ergebnisse zeigten, dass die etablierte Methode für die Profilierung von Acyl-CoAs in biologischen Proben verwendet werden kann.

Im Rahmen des zweiten Projekts wurde eine isomerenselektive LC-MS/MS-Methode für PIPx entwickelt. PIPx ist eine Familie von Phospholipiden mit geringem Vorkommen, die in eukaryontischen Zellen häufig vorkommen. Ausgehend von Phosphoinositol (PI) besteht die PIPx-Familie aus drei Lipidklassen (PIP, PIP2 und PIP3) je nach Phosphorylierungsgrad. In jeder Klasse von PIP und PIP2 gibt es drei verschiedene Regioisomere. Als Phospholipide haben PIPx zwei Fettacylgruppen an der sn1- und sn2-Position eines Glycerin-Grundgerüsts. Derzeit gibt es noch keine Methoden, die eine Regioisomerentrennung und Fettacylabdeckung ermöglichen. Um eine umfassende Methode zu entwickeln, haben wir eine chirale Polysaccharidsäule mit einer datenunabhängigen Erfassungstechnik verwendet. Mit stabilen Isotopen markierte PIPx wurden charakterisiert und als interne Standards verwendet. Die etablierte Methode wurde auf mehrere biologische Proben angewandt, darunter NIST SRM1950 Plasma, Pichia Pastoris und kultivierte HeLa-Zellen. Die Ergebnisse deuten darauf hin, dass diese Methode PIPx-Profile in realen Proben wirksam überwachen und unser Verständnis physiologischer und pathologischer Bedingungen erleichtern kann.

Im 3. und 4. Projekt wurden verbesserte LC-MS/MS-Methoden für IPx und SPx entwickelt. Im Vergleich zu PIPx und Acyl-CoAs sind IPx und SPx polarer und hydrophiler. Zur Anwendung der Phosphatmethylierungsstrategie wurde ein neues Derivatisierungslösungsmittelgemisch entwickelt und optimiert. Um die Extraktionsausbeute zu verbessern, wurde ein Extraktionskit mit TiO2 und Zentrifugenfilter entwickelt. Die Methylierung mit differentieller Isotopenmarkierung wurde in beiden Projekten zur Erzeugung stabiler isotopenmarkierter Analoga eingesetzt (interne Standards im IPx-Projekt, Ersatzkalibratoren im SPx-Projekt). Zur Trennung der IPx-Regioisomere, insbesondere I(1,4,5)P3, wurde eine RP-Säule mit Cholesterinbindung verwendet. Die Säule aus porösem Graphitkohlenstoff wurde für die Trennung von SPx im Glykolyse-Weg verwendet. Nach der Validierung in biologischer Matrix wurden die Methoden in verschiedenen biologischen Proben angewandt, darunter NIST SRM1950 Plasma, kultivierte HeLa-Zellen und menschliche Blutplättchen.

III. List of publications

Publication I

Li P, Gawaz M, Chatterjee M, Lämmerhofer M*. Targeted Profiling of Short-, Medium-, and Long-Chain Fatty Acyl-Coenzyme As in Biological Samples by Phosphate Methylation Coupled to Liquid Chromatography-Tandem Mass Spectrometry. *Anal. Chem.* 2021, 93 (9), 4342–4350. doi: 10.1021/acs.analchem.1c00664.

Publication II

Li P, Lämmerhofer M*. Isomer Selective Comprehensive Lipidomics Analysis of Phosphoinositides in Biological Samples by Liquid Chromatography with Data Independent Acquisition Tandem Mass Spectrometry. *Anal. Chem.* 2021, 93 (27), 9583–9592. doi: 10.1021/acs.analchem.1c01751.

Publication III

Li P, Gawaz M, Chatterjee M, Lämmerhofer M*. Isomer-Selective Analysis of Inositol Phosphates with Differential Isotope Labelling by Phosphate Methylation Using Liquid Chromatography with Tandem Mass Spectrometry. *Anal. Chim. Acta*. 2022, 1191, 339286. doi: 10.1016/j.aca.2021.339286.

Publication IV

Li P, Su M, Chatterjee M, Lämmerhofer M*. Targeted analysis of sugar phosphates from glycolysis pathway by phosphate methylation with liquid chromatography coupled to tandem mass spectrometry. *Anal. Chim. Acta*. 2022 (in revision)

IV. Author contributions

Publication I

Targeted Profiling of Short-, Medium-, and Long-Chain Fatty Acyl-Coenzyme As in Biological Samples by Phosphate Methylation Coupled to Liquid Chromatography–Tandem Mass Spectrometry.

Peng Li:
General idea generation
Method development
Sample preparation and analysis
Data processing and interpretation
Main writing of the manuscript

Prof. Dr. Meinrad Gawaz:
Organization of platelet samples
Proofreading of the manuscript

Dr. Madhumita Chatterjee:
Organization of platelet samples
Platelet isolation
Proofreading of the manuscript

Prof. Dr. Michael Lämmerhofer:
Generation, initiation, coordination and financing of the project
Discussion of results and interpretation
Proofreading and final approval of the manuscript
Corresponding Author

Publication II

Isomer Selective Comprehensive Lipidomics Analysis of Phosphoinositides in Biological Samples by Liquid Chromatography with Data Independent Acquisition Tandem Mass Spectrometry.

Peng Li:
General idea generation
Method development
Sample preparation and analysis
Data processing and interpretation
Main writing of the manuscript

Prof. Dr. Michael Lämmerhofer:
Generation, initiation, coordination and financing of the project
Discussion of results and interpretation
Proofreading and final approval of the manuscript
Corresponding Author

Publication III

Isomer-selective analysis of inositol phosphates with differential isotope labelling by phosphate methylation using liquid chromatography with tandem mass spectrometry.

Peng Li:
General idea generation
Method development
Sample preparation and analysis
Data processing and interpretation
Main writing of the manuscript

Prof. Dr. Meinrad Gawaz:
Organization of platelet samples
Proofreading of the manuscript

Dr. Madhumita Chatterjee:
Organization of platelet samples
Isolation of platelets
Proofreading of the manuscript

Prof. Dr. Michael Lämmerhofer:
Generation, initiation, coordination and financing of the project
Discussion of results and interpretation
Proofreading and final approval of the manuscript
Corresponding Author

Publication IV

Targeted analysis of sugar phosphates from glycolysis pathway by phosphate methylation with liquid chromatography coupled to tandem mass.

Peng Li:
General idea generation
Method development
Sample preparation and analysis
Data processing and interpretation
Main writing of the manuscript

Min Su:
Method development
Sample preparation and analysis
Data processing and interpretation
Proofreading of the manuscript

Prof. Dr. Meinrad Gawaz:
Organization of platelet samples
Proofreading of the manuscript

Dr. Madhumita Chatterjee:
Organization of platelet samples
Platelet isolation
Proofreading of the manuscript

Prof. Dr. Michael Lämmerhofer:
Generation, initiation, coordination and financing of the project
Discussion of results and interpretation
Proofreading and final approval of the manuscript
Corresponding Author

V. List of oral presentations

Oral presentation 1

The 17th International Symposium on Hyphenated Techniques in Chromatography and Separation Technology (HTC-17), Ghent, Belgium, May 18th - May 20th 2022.

Title: Targeted lipidomics analysis of phosphoinositide signaling network in biological samples by liquid chromatography with tandem mass spectrometry.

Peng Li, Michael Lämmerhofer

Oral presentation 2

Class I PI3K: disease modelling and drug targeting, online seminar, May 13th 2022.

Title: Isomer Selective Comprehensive Lipidomics Analysis of Phosphoinositides in Biological Samples by Liquid Chromatography with Data Independent Acquisition Tandem Mass.

Peng Li, Michael Lämmerhofer

Oral presentation 3

50th International Symposium and Exposition on High Performance Liquid Phase Separations and Related (HPLC 2022), San Diego, California, USA, June 18th - June 23rd 2022.

Title: Improved Metabolomics Analysis of Phosphorylated Metabolites from Single Sample Aliquot based on Sequential Extraction and Methylation Strategy using Liquid Chromatography coupled to Tandem Mass Spectrometry.

Peng Li, Michael Lämmerhofer

VI. List of poster presentations

Poster presentation 1

37th International Symposium on Microscale Separations and Bioanalysis (e-MSB 2021, Virtual Edition), Boston, USA, July 12th - July 15th 2021.

Tiltle: Targeted Profiling of Short-, Medium-, and Long-Chain Fatty Acyl-Coenzyme As in Biological Samples by Phosphate Methylation Coupled to Liquid Chromatography–Tandem Mass Spectrometry.

Peng Li, Michael Lämmerhofer

Awarded with the Best Poster Award

Poster presentation 2

Recent Developments in Pharmaceutical Analysis (RDPA 2019), Pescara, Italy September 8th – September 11th 2019.

Tiltle: Comprehensive profiling of short-, medium- and long-chain fatty-acyl-Coenzyme As in biological samples by phosphate methylation coupled to liquid chromatography–tandem mass spectrometry.

Peng Li, Michael Lämmerhofer

VII. Abbreviations

NMR	Nuclear magnetic resonance spectroscopy
GC-MS	Gas chromatography coupled to mass spectrometry
LC-MS	Liquid chromatography coupled to mass spectrometry
EI	Electron ionization
ESI	Electrospray ionization
FA	Fatty acyls
GL	Glycerolipids
GP	Glycerophospholipids
SP	Sphingolipids
ST	Sterol lipids
PR	Prenol lipids
SL	Saccharolipids
PK	Polyketides
Acyl-CoA	Fatty acyl-CoAs
PI	Phosphoinositol
PIPx	Phosphoinositide
PLC	Phospholipase C
DAG	Diacylglycerol
I(1,4,5)P3	Inositol 1,4,5-trisphosphate
IPx	Inositol phosphate
PP-IPx	Inositol pyrophosphates
PPP	The pentose phosphate pathway
TCA	The tricarboxylic acid cycle
ATP	Adenosine triphosphates
SPx	Sugar phosphates
SOPs	Standard operation procedures
LSI	Lipidomics-Standards-Initiative
LLE	Liquid-liquid extraction
SPE	Solid phase extraction
MTBE	Methyl tert-butyl ether
MOAC	Metal oxide affinity chromatography

TiO_2	Titanium dioxide
EDC	N-(3-Dimethylaminopropyl)-N-ethylcarbodiimide
SP	Stationary phase
RP-LC	Reversed-phase liquid chromatography
MP	Mobile phase
NP-LC	Normal-phase liquid chromatography
PEEK	Polyetheretherketone
ANP-LC	Aqueous normal phase liquid chromatography
HILIC	Hydrophilic interaction liquid chromatography
IEC or IEX	Ion chromatography or ion-exchange chromatography
CSP	Chiral stationary phase
UHPLC	Ultraperformance LC
FPP	Fully porous particle
SPP	Superficial porous particle
m/z	Mass-to-charge ratio
APCI	Atmospheric pressure chemical ionization
QqQ	Triple quadrupole
QTOF	Quadrupole time of flight
RF	Radiofrequency
DC	Direct current
CE	Collision energy
CID	Collision-induced dissociation
AC	Alternating current
KE	Kinetic energy
ADC	Analog-to-digital converter
TDC	Time-to-digital converter
LR	Low resolution
SIM	Selected ion monitoring
EPI	Enhanced product ion
HR	High resolution
DDA	Data-dependent acquisition
IDA	Information-dependent acquisition

VIII. Introduction

1. Metabolomics and lipidomics

1.1. Metabolites and metabolomics

Metabolites are endogenous small molecules (molecular weight usually less than 1500 Da), including amino acids, lipids, sugars, organic acids, etc. In cell metabolism, metabolites play critical roles as substrates, intermediates or end products. Metabolomics is the study of the whole family of metabolites in a system [1–3]. Rather than investigating individual metabolites, metabolomics analyzes all the metabolite features at a system-wide level. With the development of analytical chemistry and instrumental technology, metabolomics has become a powerful approach to studying the metabolic activity of organisms. Its ability to reveal unexpected changes in metabolites under different conditions makes it valuable for hypothesis generation. As shown in Figure VIII-1, compared to other omics studies, metabolomics is uniquely challenging due to its complexity and wide dynamic concentration range [4].

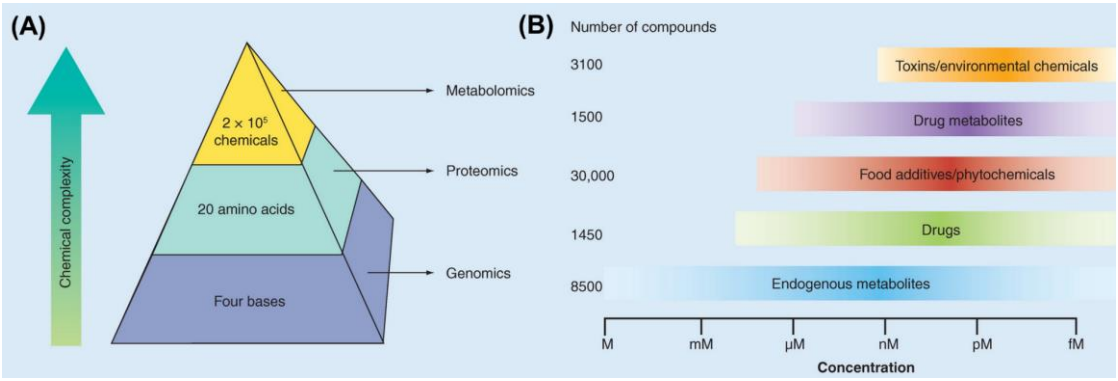

Figure VIII-1. Overview of metabolomics and other omics [4]. (A) Comparison of the complexity of analytes in different omics studies. (B) The concentration range of the human metabolome.

The workflow of metabolomics (Figure VIII-2) consists of experiment design, sample collection including quenching, extraction, data acquisition, data processing including identification and statistical analysis, and biochemical interpretation [5]. Data acquisition stage in metabolomics involves many analytical

techniques, including nuclear magnetic resonance spectroscopy (NMR) [6,7], gas chromatography coupled to mass spectrometry (GC-MS) [8,9], and liquid chromatography coupled to mass spectrometry (LC-MS) [10,11]. As summarized in Table VIII-1, they have distinct advantages and disadvantages according to their analysis principles [2].

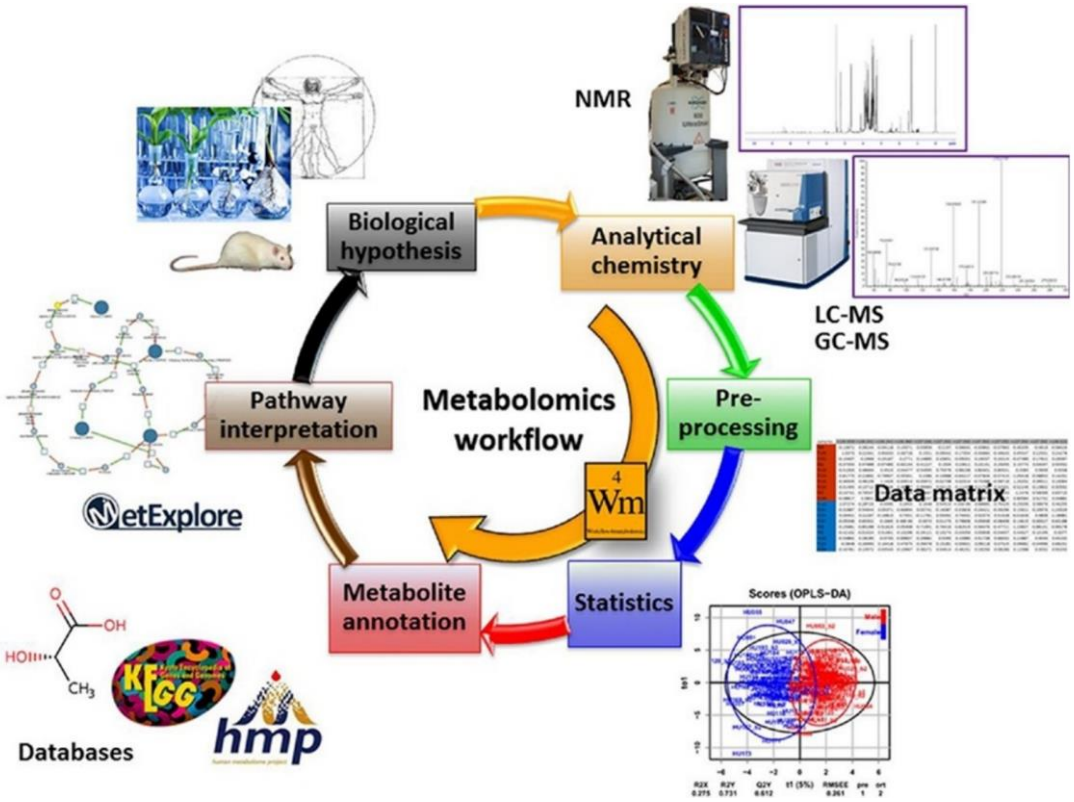

Figure VIII-2. Metabolomics workflow.

Across these different techniques, the identification of numerous metabolites remains challenging. To address this issue, the development of the computational approach has attracted more and more attention recently. Since the authentic standards remain limited. MS spectral library matching was the breakthrough to move forward for identification. Online databases are now available for electron ionization (EI) and electrospray ionization (ESI) techniques, including the human metabolome database (HMDB) [12], MassBank [13], Manchester Metabolomics Database (MMD) [14], and Tandem MS Database (METLIN) [15,16], Golm Metabolome Database (GMD) [17], FiehnLib [18], and NIST Database [19,20]. After being identified in different conditions, differential metabolites will be reviewed and validated in metabolic pathways. In this stage,

pathway databases like Kyoto Encyclopedia of Genes and Genomes (KEGG) [21], MetaCyc [22], etc. could be utilized for comprehensive analysis. Optionally, for metabolites involved in multiple pathways, metabolic flux analysis is performed to determine the metabolite interconversion. Stable isotopic tracers are often used in this approach [23].

Table VIII-1. Comparison of different analytical techniques in metabolomics [2].

Analytical platform	Advantages	Disadvantages	Special applications
LC-MS	Broad metabolite coverage Simple sample preparation High sensitivity Superior flexibility in compound separation and detection (i.e., options of LC column, mobile phase, or MS method settings) Various open-source software assisting data analysis	Cross-platform variation or batch effects that hinders standardization Not quantitative Destructive Inability to measure organic compounds that do not form molecular ion adducts (i.e., hydrocarbons)	Comprehensive (broad- coverage) metabolomics analysis
GC-MS	Broad metabolite coverage Analysis of gases or naturally volatile compounds High sensitivity Various open-source software assisting data analysis	Variations due to instrument type or conditions Not quantitative Destructive Not suitable for nonvolatile or thermally fragile molecules Complications from multiple derivatization products from a single metabolite	Petrochemical analysis
NMR	Real-time reaction monitoring at controlled temperatures Real-time in vivo measurements Deeper structural information Non-invasive	Low sensitivity Less metabolite coverage per run Less automated spectral processing High cost of equipment and maintenance	De novo compound structure elucidation Kinetics analysis of chemical reactions Real-time in vivo metabolic studies using stable isotope tracing Real-time imaging of live cells or animals

1.2. Lipids and lipidomics

Lipids are a diverse family of fatty acids and their naturally occurring derivatives, which are generally hydrophobic and soluble in nonpolar solvents. For clarification and homogenization, lipids are sorted into eight categories according to Lipid MAPS, an international consortium organized by lipid experts [24,25]. As shown in Figure VIII-3, eight lipid categories are fatty acyls (FA), glycerolipids (GL), glycerophospholipids (GP), sphingolipids (SP), sterol lipids (ST), prenol lipids (PR), saccharolipids (SL), and polyketides (PK).

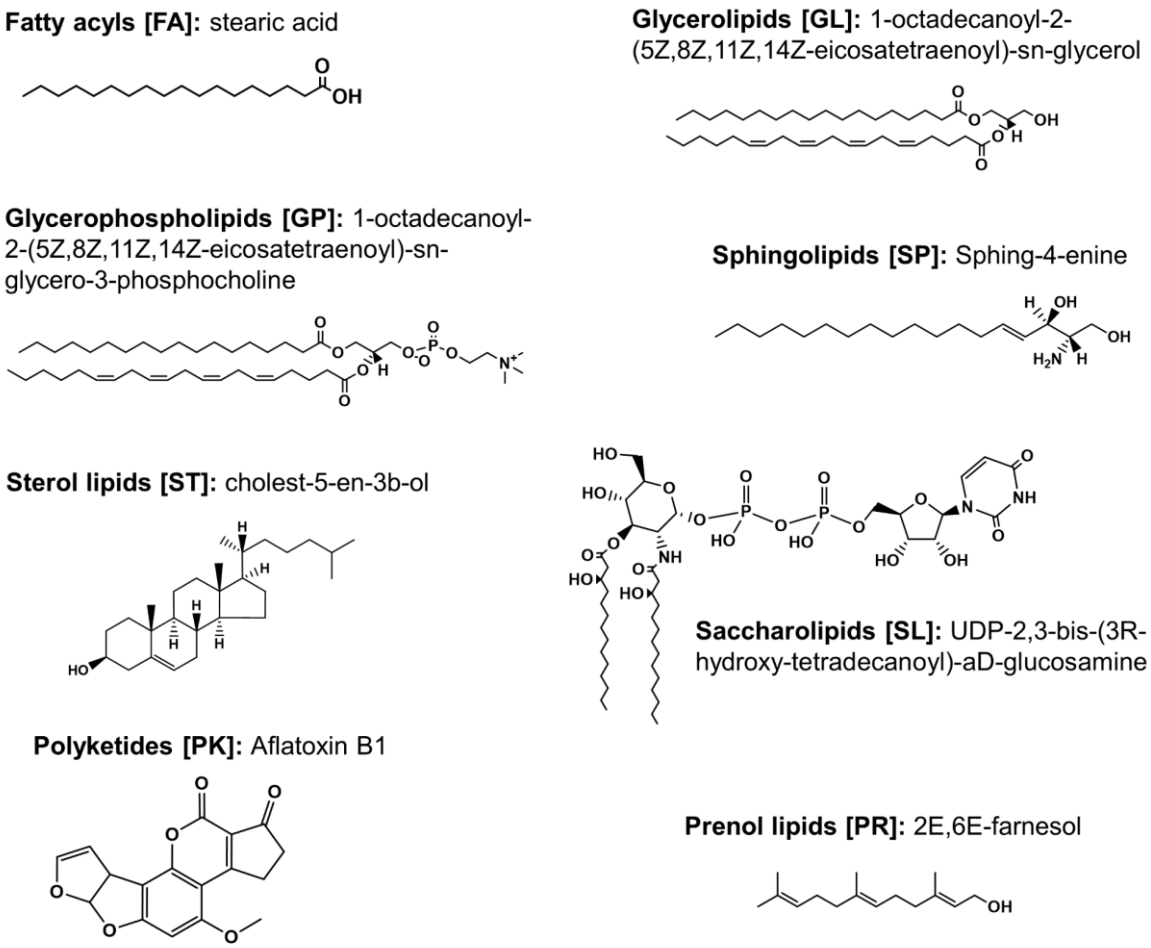

Figure VIII-3 Lipid classification system with representative structures in eight categories.

Furthermore, these categories are divided into classes and subclasses, which are summarized in Table VIII-2.

Table VIII-2 Lipid main classes and sub classes involved in this work with short annotations.

Lipid category	Main class	Sub class	Short annotation
Fatty acyls [FA]	Fatty acids	-	-
	Fatty esters	Fatty acyl cozyme A	Acyl-CoAs
Glycerolipids [GL]	Monoradylglycerolipids	Monoacylglycerols	MAG
	Diradylglycerolipids	Diacylglycerols	DAG
	Triradylglycerolipids	Triacylglycerols	TAG
Glycerophos-pholipids [GP]	Glycerophosphocholines	Diacylglycerophosphocholines	PC
		Monoacylglycerophosphocholines	LPC
		1-alkyl,2-acylglycerophosphocholines	O-PC
	Glycerophosphoethanol-amines	Diacylglycerophosphoethanolamines	PE
		Monoacylglycerophosphoethanolamines	LPE
		1-alkyl,2-acylglycerophosphoethanolamines	O-PE
	Glycerophosphoinositols	Diacylglycerophosphoinositols	PI
		Monoacylglycerophosphoinositols	LPI
		1-alkyl,2-acylglycerophosphoinositols	O-PI
	Glycerophosphoinositol monophosphates	Diacylglycerophosphoinositol monophosphates	PIP
	Glycerophosphoinositol bisphosphates	Diacylglycerophosphoinositol bisphosphates	PIP2
	Glycerophosphoinositol trisphosphates	Diacylglycerophosphoinositol trisphosphates	PIP3
Sphingolipids [SP]	Ceramides	Ceramide 1-phosphates	C1P
	Phosphosphingolipids	Ceramide phosphocholines	SM
	Sphingoid bases	Lysosphingomyelins and lysoglycosphingolipids	LSM
Sterol lipids [ST]	Sterols	Steryl esters	CE

To standardize the detailed description of lipid chemical structures, a nomenclature system was also introduced, which was used in this study as well. Lipidomics was first introduced by Han and Gross in 2003 [26]. As a subdiscipline of metabolomics, lipidomics stand out as a separate research field these years

as a significant difference in chemical structure thereby properties between lipids and other metabolites. A typical lipidomics workflow with mass spectrometry (MS) is shown in Figure VIII-4 [27]. After sample preparation, direct infusion or LC-based was performed prior to MS analysis. A broader coverage could be expected in direct infusion lipidomics (shotgun lipidomics) compared to the LC-based approach. However, due to co-extracted and co-ionized compounds, a significant matrix effect is usually observed in shotgun lipidomics. In order to separate isomers and reduce matrix effect, LC-MS-based lipidomics was used in this work to realize more accurate quantification.

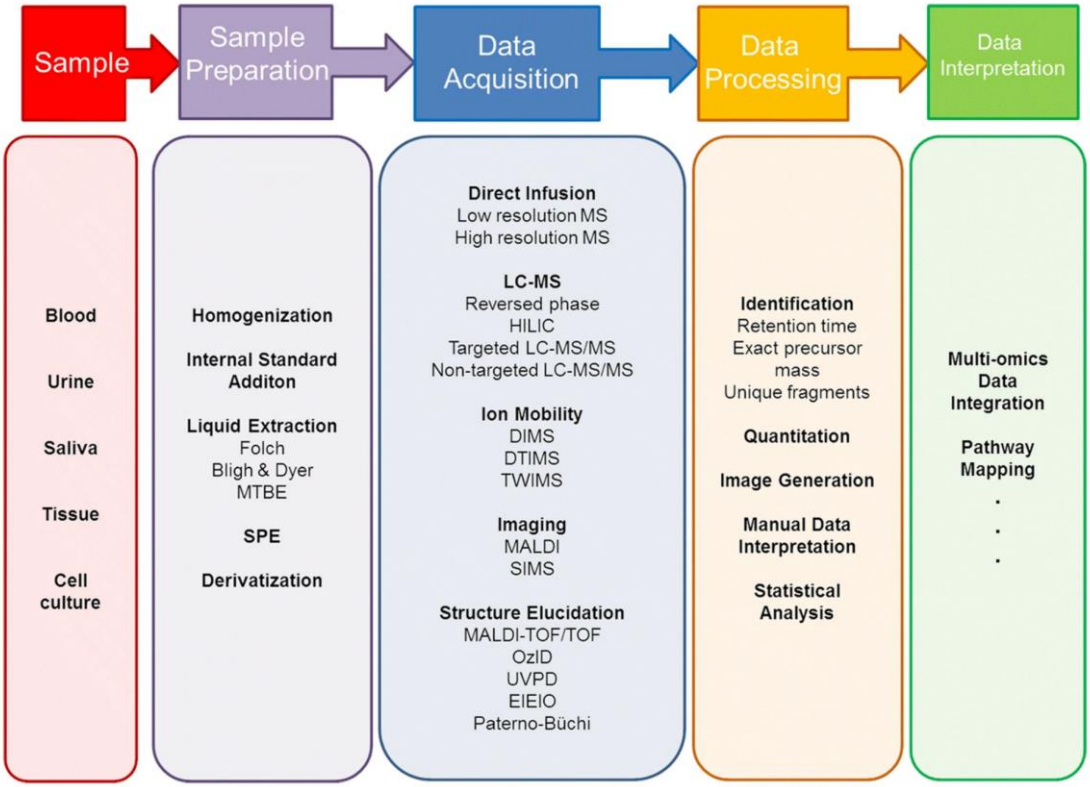

Figure VIII-4 Typical workflow in lipidomics study [27].

1.3. Targeted phosphorylated metabolites and lipids in this work

Phosphorylation and dephosphorylation are ubiquitous in biology. These reversible processes play critical roles in metabolic pathways, including signalling [28,29], energy metabolism, etc [30]. As reviewed before, the reason nature chose phosphate is the interplay between two counteracting facts: 1) phosphates are negatively charged so phosphate esters are inert for hydrolysis due to

charge-charge repulsion. 2) the charge-charge repulsion makes it possible to precisely regulate the phosphate ester hydrolysis by tuning the electrostatic environment. These facts make phosphate ester an ideal candidate for fine-regulated metabolism [31,32]. Below, some metabolic pathways involving targeted phosphorylated metabolites and lipids in this work are introduced.

1.3.1. Fatty acyl-CoA metabolism

Fatty acyl-CoAs (acyl-CoA) are important metabolic intermediates consisting of a 3'-phosphoadenosine diphosphate (ADP), pantothenate (Vitamin B5) and β-mercaptoethylamine [33]. They can also be regarded as an acyl group linked to coenzyme A by a thioester bond. As shown in Figure VIII-5, acyl-CoAs participate in many pathways as acyl donor/transfer [34]. In these pathways, acyl-CoAs are oxidized to provide cellular energy and are incorporated into proteins and lipids. Therefore, understanding the roles of acyl-CoAs in metabolic diseases is of ultimate importance. In this work, we developed an LC-MS/MS method to profile acyl-CoAs in biological samples.

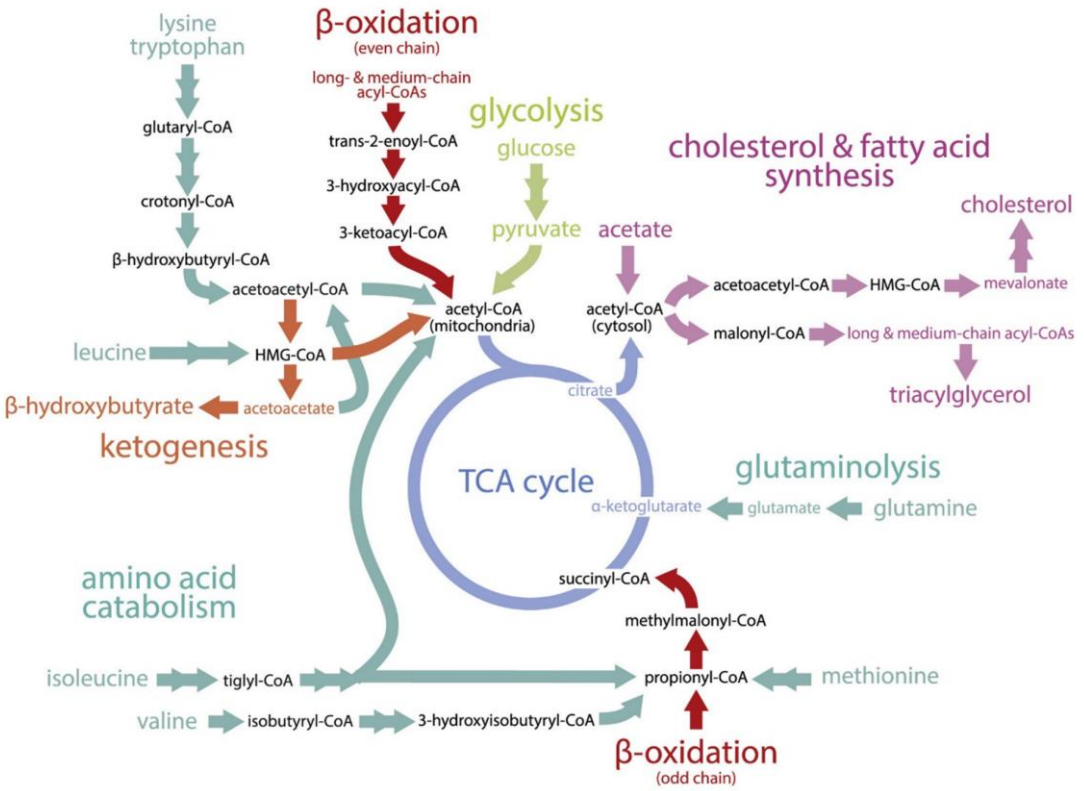

Figure VIII-5 Overview of acyl-CoA containing metabolic pathway [34].

1.3.2. Phosphoinositide network

As introduced previously, phosphoinositol (PI) belongs to glycerophospholipid. The chemical structure of PI is shown in Figure VIII-6, it has a glycerol backbone with two fatty acyl side chains at sn1/sn2 positions and inositol linked to phosphate at the sn3 position. Arising from phosphorylation and dephosphorylation at the 3', 4', and 5' positions at the inositol ring, a highly regulated phosphoinositide (PIPx) metabolic network is constructed (Figure VIII-6). The PIPx family consists of seven classes: phosphatidylinositol-3-phosphate (PI(3)P), phosphatidylinositol-4-phosphate (PI(4)P), phosphatidylinositol-5-phosphate (PI(5)P), phosphatidylinositol-3,4-bisphosphate (PI(3,4)P2), phosphatidylinositol-3,5-bisphosphate (PI(3,5)P2), phosphatidylinositol-4,5-bisphosphate (PI(4,5)P2), and phosphatidylinositol-3,4,5-trisphosphate (PI(3,4,5)P3) [35,36].

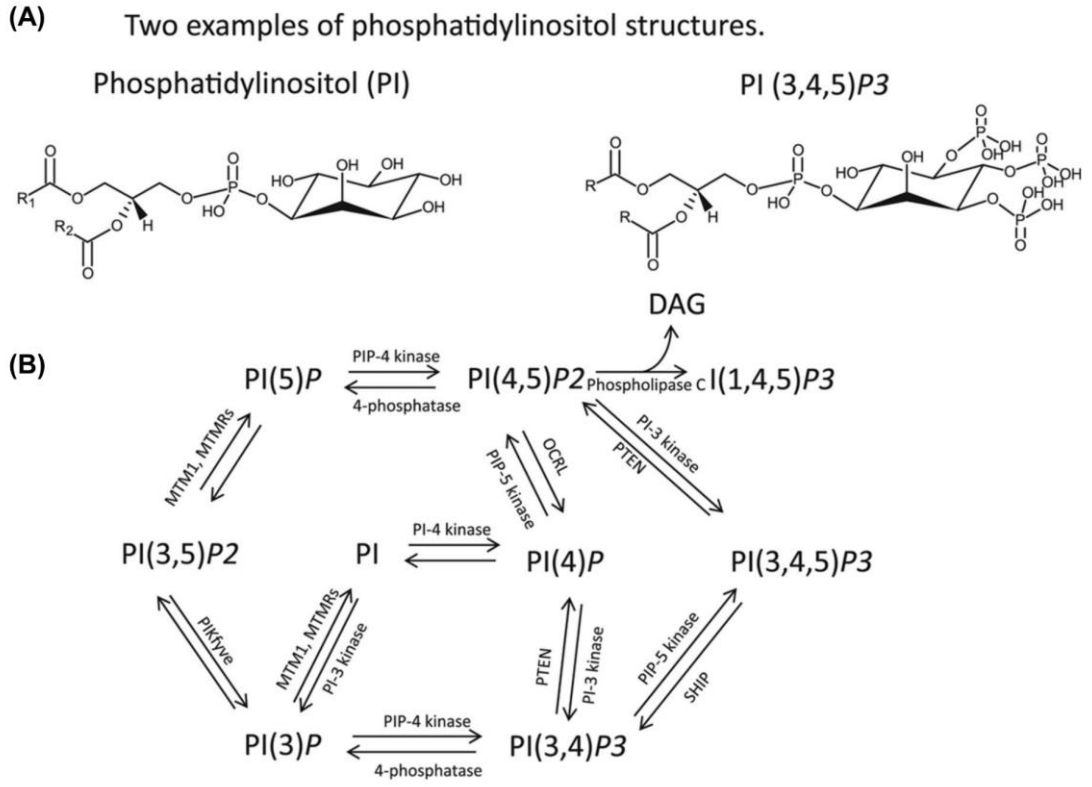

Figure VIII-6. Phosphoinositol structure and phosphoinositide network [35].

The PIPx network is ubiquitously found in eukaryotic cells. It plays central roles in a host of cell activities, including membrane trafficking, secretion, adhesion, migration, cell survival, replication, etc [37–39]. There are two widely investigated

pathways in this network. Phosphorylation of PI(4,5)P2 to generate PI(3,4,5)P3 was reported to be central in tumor biology, which makes the corresponding kinase (phosphoinositide 3-kinase, PI3K) a promising drug target for cancer treatment [40–42]. Besides, phospholipase C (PLC) was recognized to hydrolyze PI(4,5)P2 to generate second messengers diacylglycerol (DAG) and inositol 1,4,5-trisphosphate (I(1,4,5)P3) [43,44]. Apart from regioisomers indicated in Figure VIII-6, fatty acyl chains were reported to have specific metabolism [45,46]. For example, the fatty acyl profile of PI was remodeled and enriched to 38:4 (18:0 at sn1 while 20:4 at sn2) in platelets [47]. Analysis of PIPx remains challenging due to its instability, low abundance, presence of regioisomers, and rich negative charge. Currently, a comprehensive method for PIPx profiling that is able to provide information on fatty acyl chains and regioisomers is still in great demand. In this work, a comprehensive workflow integrating sequential extraction, phosphate methylation, chiral chromatography, and untargeted MS acquisition was developed and validated. The established workflow was applied to different biological samples to reveal its functionality.

1.3.3. Inositol phosphate network

Inositol phosphate (IPx) is a family of diverse phosphorylated derivatives of inositol. As shown in Figure VIII-7, the IPx family is diverse in structure due to combinations of different numbers and positions of phosphorylation [48]. As mentioned above, I(1,4,5)P3 was generated via hydrolysis of PI(4,5)P2 into the cytoplasm to trigger calcium release. Conversely, the ubiquitously expressed inositol phosphatases hydrolyze IPx to repress the calcium signaling. With further phosphorylation, IP6 can be a precursor for inositol pyrophosphates (PP-IPx). There are four common PP-IPx reported in nature: 5-diphosphoinositol (1,3,4,6)-tetrakisphosphate (5PP-IP4), 1-diphosphoinositol (2,3,4,5,6)-pentakisphosphate (1PP-IP5 or 1-IP7), 5-diphosphoinositol (1,2,3,4,6) pentakisphosphate (5PP-IP5 or 5-IP7) and 1,5-bisdiphosphoinositol (2,3,4,6) tetrakisphosphate (1,5PP2-IP4 or 1,5-IP8). Glycolysis and mitochondrial function were reported to be upregulated by PP-IPx, followed by increased cellular energetic activities [49,50]. Due to the structure similarity, instability, high polarity, and low abundance, the analysis of IPx remains challenging [51]. In this work, we developed a method

based upon SPE extraction, phosphate methylation, cholesterolether-bonded RP column, and targeted MS detection. The IP1 to IP6 was covered in this method and the biologically interesting messenger I(1,4,5)P3 was for the first time separated in RP condition with improved peak shape.

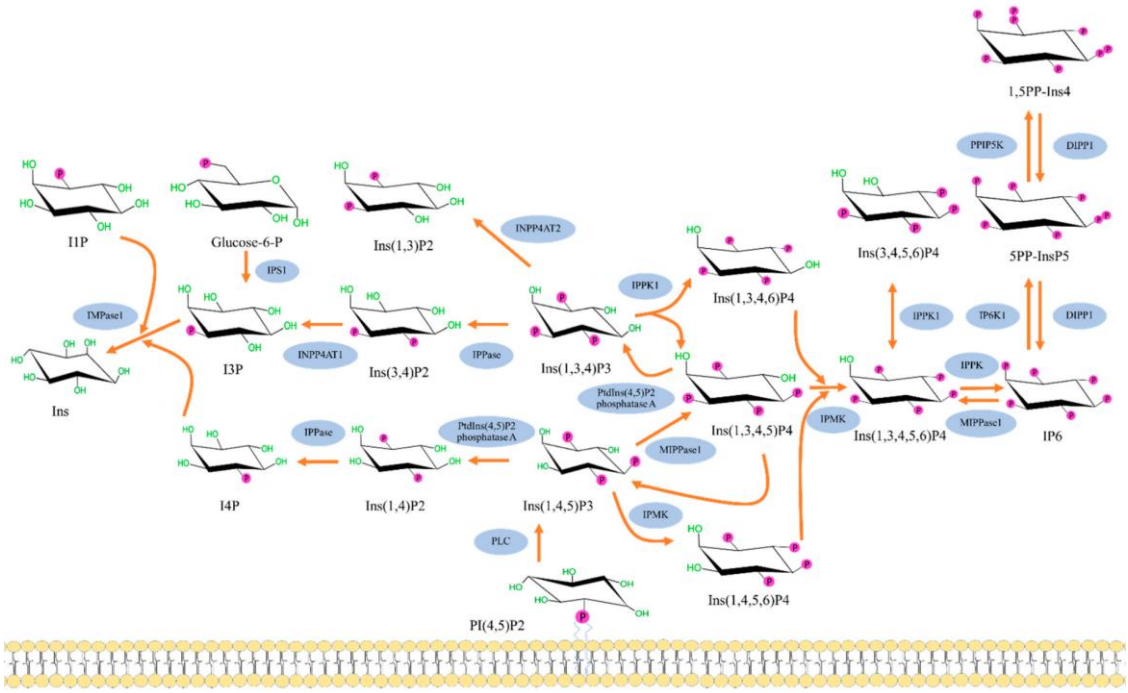

Figure VIII-7. inositol phosphate metabolic network [48].

1.3.4. Central carbon metabolism

The sugars are converted into metabolic precursors in the central carbon metabolism (shown in Figure VIII-8), which includes the glycolysis pathway, the pentose phosphate pathway (PPP), and the tricarboxylic acid (TCA) cycle [52]. As the starting point for most biosynthesis processes in vivo, central carbon metabolism plays a vital role in metabolism. In the glycolysis pathway, one molecule of glucose is broken down into two molecules of pyruvate, with the generation of a net of two adenosine triphosphates (ATPs). The pathway in a reverse direction leading to glucose generation is the gluconeogenesis pathway [53]. The PPP provides reduced nicotinamide adenine dinucleotide phosphate and ribose-5-phosphate, which is essential for the synthesis of nucleic acids. The TCA cycle is also known as the Krebs cycle and citric acid cycle. It is well investigated to support cellular activities by generating energy and biosynthesis

intermediates for many years. It is reported by Otto Warburg that cancer cells usually prefer anaerobic glycolysis over aerobic mitochondrial energy supply for ATP generation, which is named the Warburg effect [54,55]. As our understanding develops, some cancer cells still retain oxidative phosphorylation (OXPHOS) capacity and use it as the main energy source [56]. There is still a great need for improved analytical methods to monitor the central carbon metabolic network. In this work, we extend our derivatization strategy to polar sugar phosphate metabolites metabolites (SPx). As the proof of concept, the glycolytic SPx was taken for method development. The established method was utilized to profile SPx in different biological samples, including experimental human platelet samples.

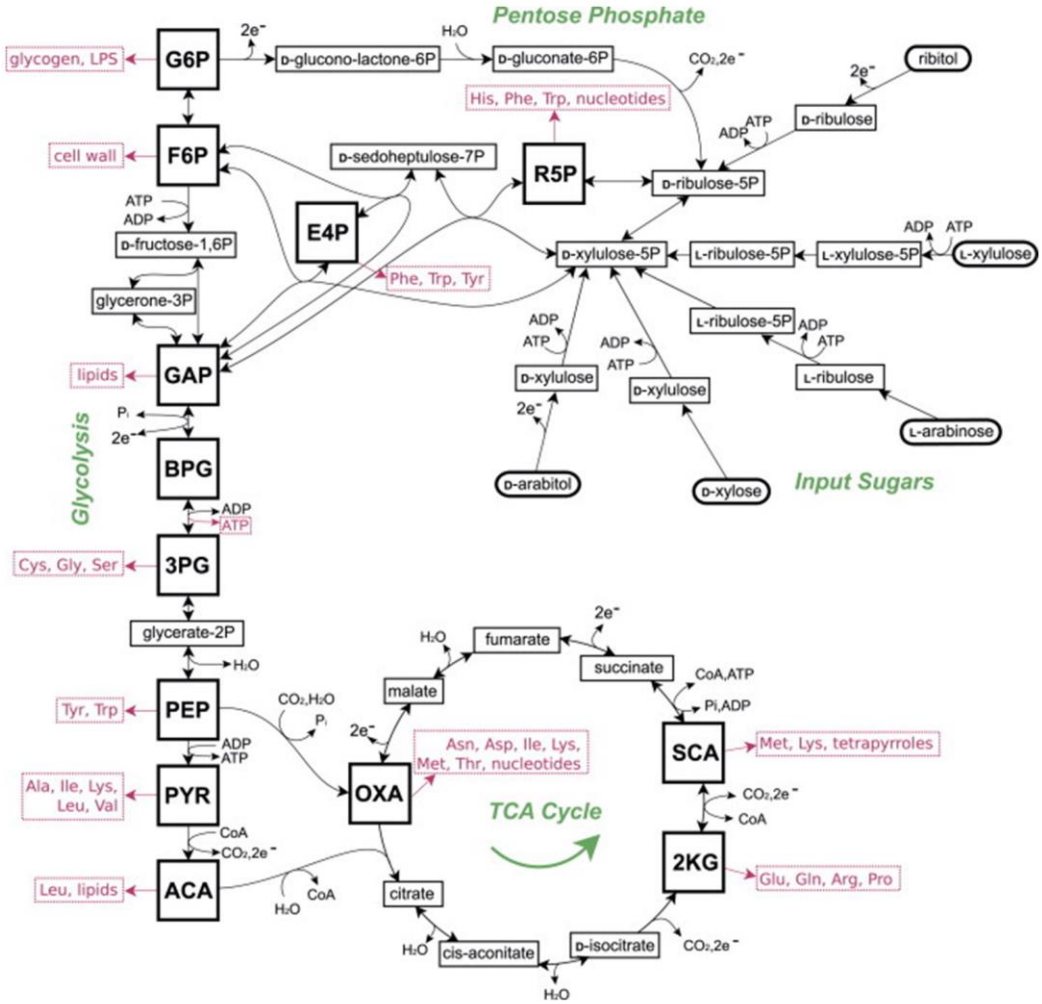

Figure VIII-8. The central carbon metabolism.

2. Sample preparation for metabolomics and lipidomics

2.1. Pre-analytical steps

The pre-analytical steps, including sample selection, sample collection, sample storage, etc., are crucial in metabolomics and lipidomics studies. Sample selection is the first step once the biological question is raised. There are several biological materials available for sampling, including biofluids (e.g., plasma, serum, urine, saliva, cerebral spinal fluid, bile, etc.), tissues (e.g., tumor tissues, muscles, brain, etc.), and cultured cells. The sample selection should be based on the research focus and the analytical methods. It should be noted that different sample types potentially provide complementary information. Sample collection with optional treatment should be carried out according to the specific standard operation procedures (SOPs), which is critical for reliable results. Collection time and variation sources should be carefully considered. As metabolite and lipid profile are the reflections of the metabolism status, which is sensitive to in vivo and in vitro environments. Therefore, nutritional status and circadian rhythm should be considered for sample collection time. More importantly, a good practice is always suggested to reduce variance, incusing low operation temperature, immediate metabolism quenching, optional addition of antioxidants and inhibitors, aliquoting whenever possible, avoiding repeated freeze-thaw cycles, etc. After collection, samples should be stored at -80 °C or lower for long-term purposes before analysis. As the best practice now, it is recommended by Lipidomics-Standards-Initiative (LSI) that: 1) Collect, prepare and store samples on ice; 2) Immediately flash-freeze in liquid nitrogen; 3) Long-time storage at -150°C - -80°C [57].

2.2. Extraction of metabolites and lipids

2.2.1. Cell disruption

To realize high efficiency from biological samples (e.g., tissues, cells, especially algal cells), cell disruption is usually required to release analytes from the sample matrix. In general, there are two main approaches to cell disruption: physical-mechanical methods and (bio-)chemical methods. Physical-mechanical methods

mainly utilize different technologies, involving temperature, pressure, electric field, ultrasonication, bead beading, which are summarized in Table VIII-3 [58].

Table VIII-3 Commonly used physical cell disruption methods with their advantages and disadvantages [58].

Method	Advantages	Disadvantages
Freeze-thaw	Gentle extraction of fragile compounds (protein, enzymes)	High energy and time-consuming, high maintenance cost, difficult to scale up, degradation of lipids
High-pressure homogenization	High efficiency; does not require biomass drying; easy scale-up	High energy consumption; temperature rise may lead to degradation of thermolabile compounds; rigid cell wall may hinder product release; very fine cell debris
Ultrasonication	Simple, short extraction time, high reproducibility, efficient	Moderate energetic costs, temperature rise, rigid cell wall hinders product release; production of reactive hydroxyl radicals; not applicable to large-scale, sonication; energy effective in small volume
Pulsed electric field treatment	Simple, highly energetically efficient, relatively fast, easy to scale up; can be combined with other methods	High maintenance costs, temperature rise, dependence on medium composition, decomposition of fragile compounds
Bead milling	Simple equipment, rapid process, high disruption efficiency, easy scale-up; suitable for large-scale, low labor intensity; low operating cost; can be applied on algal slurry	High energy consumption; requires extensive cooling for thermolabile compounds, formation of very fine cell debris
Microwave	Simple, rapid process; effective for robust species; easy to scale up; low operating costs; does not require dewatering of algal biomass	High energy consumption and maintenance costs, high temperature; recovery of thermolabile compounds may require cooling; lipid degradation and protein aggregation, denaturation, formation of free radicals

Cell disruption by chemicals usually uses acid/alkaline, ionic liquid, supercritical fluids, detergents, oxidizing agents, and so on. Compared to physical-mechanical methods, chemical approaches are generally low-energy consuming and more selective. However, the cost, quality, as well as compatibility with the LC-MS platform should also be taken into consideration. For example, detergent-based lysis buffers are widely used in the proteomics community, but they are less interested in the metabolomics/lipidomics community as extra steps are

required to remove MS-incompatible compounds. In large-scale metabolomics/lipidomics studies, bead beading, high-speed homogenization, and high-pressure homogenization are preferred due to their high efficiency, high throughput, and compatibility with LC-MS. The most critical problem of those homogenization techniques is the temperature rise which may lead to analyte degradation. Therefore, in this work, we took an efficient homogenizer with a temperature control function. Low temperature (typically 4 °C) could be maintained to minimize the enzymatic activity and compound degradation throughout the process.

2.2.2. Extraction

After being released from the sample matrix, metabolites/lipids are usually extracted and transferred into the interferent-free phase. Liquid-liquid extraction (LLE) and solid phase extraction (SPE) are commonly used. Different solvents or different solvent mixtures should be selected according to the polarity and octanol/water partition coefficient (log P) of targeted analytes. When further clean-up is desired, biphasic LLE is performed by using a water-immiscible organic solvent such as chloroform (CHCl3), hexane, and methyl tert-butyl ether (MTBE). The organic layer is obtained for lipophilic analytes like lipids while the aqueous phase is taken for polar metabolites like amino acids and nucleotides. For example, Folch [59], Bligh−Dyer [60], and the Matyash [61] methods are widely used for lipidomics analysis. SPE is usually used to concentrate or clean up analytes, in which sorbents of different mechanisms like reversed phase and ion exchange are used. Currently, LLE followed by SPE is adopted for challenging analytes. The extraction of phosphorylated analytes is challenging as they are prone to bind to proteins. Therefore, several acids including acetic acid, perchloric acid, trichloroacetic acid, and hydrochloric acid were reported to protonate analytes to achieve satisfying recovery. Additionally, similar to the extraction of phosphopeptides and phosphoproteins, metal oxide affinity chromatography (MOAC) is interesting for phosphorylated metabolites/lipids [62,63]. In this study, weak anion-exchange SPE and titanium dioxide (TiO2) based MOAC method was used for sample preparation.

2.3. Derivatization in metabolomics and lipidomics

2.3.1. Derivatization strategies

Chemical derivatization is an effective approach in LC-MS analysis to address problems regarding sensitivity, selectivity, analyte stability, chromatographic performance. As shown in Figure VIII-9, there are several derivatization strategies targeting functional groups of metabolites/lipids reported [64]. Ideally, the derivatization strategy should satisfy the following criteria: 1) reasonable reaction speed; 2) mild reaction (especially with unstable analytes); 3) robust and reproducible reaction yield; 4) ease to remove excessive reagent and by-products. When it comes to the application of real samples, it is important to ensure compatibility of derivatization and extraction, including the solvent composition, pH value, and buffer strength. Take phosphorylated analytes as an example, derivatization strategy is desired due to their poor performance in chromatography and MS. Phosphorylation makes the compound more polar and richer in negative charge, which leads to poor retention on commonly used reversed-phase LC columns.

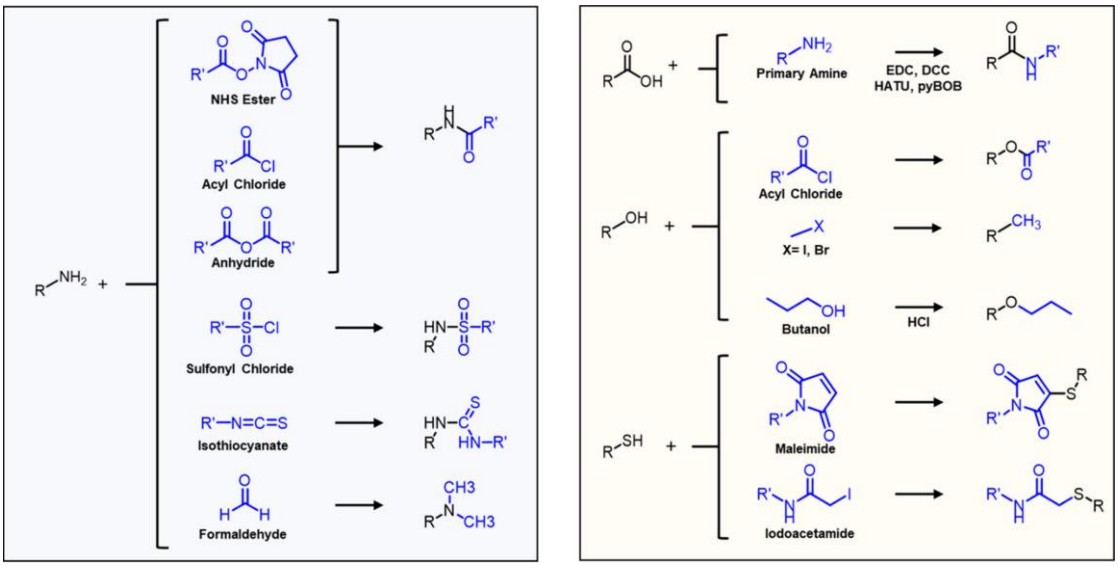

Figure VIII-9. Common derivatization reactions for functional groups in metabolomics/lipidomics methods [64].

Phosphorylated compounds are prone to stick to glassware and stainless steel, which are used in sample preparation and LC-MS instrumentations. After

derivatization, phosphate groups are neutralized. Alkyl is introduced to improve retention and ionization efficiency in MS. There are two main class strategies targeting phosphate groups: amine-based and diazo reagent-based [65]. In amine-based methods, phosphate groups are coupled with an amine in the presence of N-(3-Dimethylaminopropyl)-N′-ethylcarbodiimide (EDC). This reaction usually requires a relatively high temperature and long reaction time. In diazo reagent-based methods, phosphate groups are alkylated with nitrogen release in an almost instant manner, which produces quantitative derivatization efficiency. Diazomethane was reported to methylate phospholipids and nucleotides. Due to its explosive property, its safe alternative (trimethylsilyl)diazomethane was applied for the same purpose. Although diazo reagents are reactive, derivatization degrees should also be considered due to space resistance. Derivatization of phosphate groups may be incomplete for large alkyl groups. In this study, (trimethylsilyl)diazomethane was used due to the small methyl group. The sample preparation protocol was optimized to be compatible with derivatization accordingly.

2.3.2. Parallel derivatization strategy

Based on derivatization reaction, multiple advanced parallel derivatization strategies were proposed, among which isotopic and isobaric labeling is the most utilized ones. Most strategies were proposed for peptide analysis but they are inspiring in metabolomics/lipidomics according to the reaction principle. In the isotopic labeling strategy, stable isotopic analogs are used in replace (or in parallel with) original reagents. Mass shift then is introduced and distinguished by MS detection. This is quite useful to realize relative quantification in a complex matrix or absolute quantification when labeled compounds are not available. Usually, a decent mass shift (more than 3 Da) is introduced in these methods and could be distinguished by low-resolution MS. In this study, a differential stable isotope labeling strategy was developed to generate labeled analogs for quantification. In isobaric labeling methods, isotopes are distributed over the derivatization reagent. Once fragmented, reporter fragments with a difference in exact mass are generated. Multiple samples could be analyzed at once. Recently, a new approach combining isotopic and isobaric labeling was reported based on

dimethylation with light $(CH_3)_2$ and heavy $(^{13}C_2H_3)_2$ formaldehyde [26]. It was applied to the analysis of peptides and could be interesting for metabolites/lipids with amine groups as well.

3. Liquid chromatography for metabolomics and lipidomics

After sample preparation, there are two main analytical approaches in data acquisition: direct infusion and LC-MS. Direct infusion-based methods have advantages in coverage and throughput. However, direct infusion holds inherent disadvantages of matrix effect, difficulty in identification/alignment, and detector saturation. Therefore, chromatographic separation is widely adopted prior to MS detection in bioanalysis. The interactions in LC between analytes and the stationary phase (SP) are shown in Figure VIII-10 [66]. Different LC modes are selected according to the chemical and physical properties of analytes of interest. Respective mechanisms and applications are discussed in the following sections.

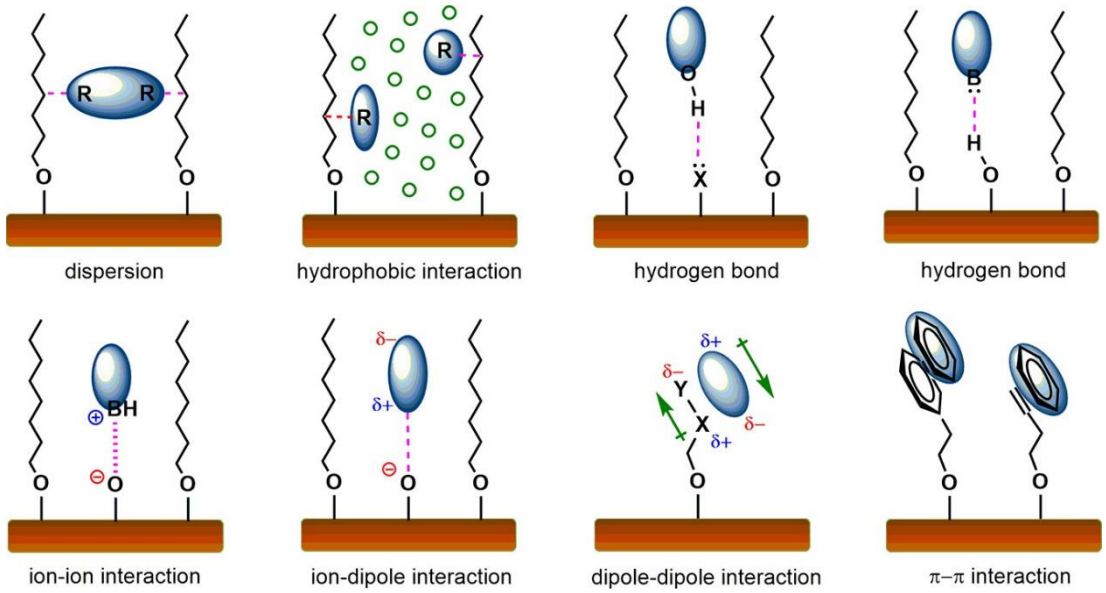

Figure VIII-10. Sample-column interactions in liquid chromatography [66].

3.1. Reversed phase liquid chromatography

There are many LC columns for different modes available on the market. Reversed-phase liquid chromatography (RP-LC) columns remain the most popular. In RP-LC, the polar mobile phase (MP) is made by water and water-miscible organic solvent (e.g., acetonitrile, methanol, isopropanol). As shown in

Figure VIII-11A [67], the unpolar SP consists of the silica or other supporting materials chemically bonded with hydrophobic groups. The most common ligand is the alkyl chains ranging from C1-C30, among which C18 (octadecyl chain) and C8 (octyl chain) are widely used. The retention of analytes is determined by polarity and hydrophobicity. The longer the carbon chain, the higher the SP hydrophobicity. Phenyl ring is bonded to provide π−π interaction, which could exhibit specific retention for analytes capable of forming it. Halogen like fluorine and compound like cholesterol are also bonded in order to provide different selectivity. To eliminate peak tailing arising from residual silanols of SP, end-capping with small molecules is commonly included in SP preparation. The columns which are end-capped with polar groups are suitable for polar and basic compounds. They could be operated in very low or even zero percentage of organic solvent in MP, which could be quite useful when the focusing step is needed at the beginning of the gradient [68].

As most metabolites are of low molecular weight and hydrophilic, they showed inadequate retention in RP-LC. However, the application of RP-LC in lipidomics studies is common practice due to its efficiency and robustness. Lipids usually carry diverse fatty acyl chains which could be separated in RP-LC. A specific elution pattern of lipids in RP-LC was reported, which was also used for lipid identification. Within the lipid class, retention time increases with carbon number and decreases with unsaturation [69,70]. Furthermore, a new strategy named Equivalent Carbon Number was reported to predict retention time for different lipid classes [71]. In this study, the targeted analytes are highly polar and rich in negative charge. After derivatization was proposed, the RP-LC approach was adopted for separation, which is robust and reproducible. To achieve specific selectivity, several RP-type LC columns were tested, including the C30 column and cholesterolether-bonded column, etc.

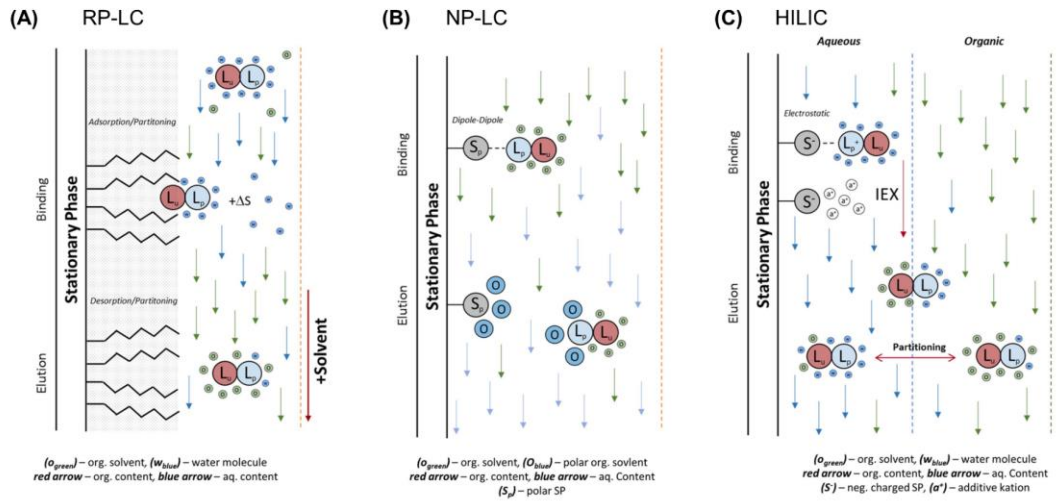

Figure VIII-11 Separation principles in (A) reversed phase liquid chromatography (RP-LC), (B) normal phase liquid chromatography (NP-LC), and (C) hydrophilic interaction liquid chromatography (HILIC) [67].

3.2. Normal phase chromatography

In normal-phase liquid chromatography (NP-LC), SP is polar (silica or bonded silica). Unpolar organic solvent (e.g., hexane, heptane) with miscible polar organic solvent (e.g., isopropanol, chloroform) are used as in MP. Special care should be taken when polyetheretherketone (PEEK) tubing is used with THF and chloroform. As shown in Figure VIII-11B [67], polar MPs elute the analytes binding to SP by increasing the polarity, after which a long equilibrium time is required. Silanols are of high affinity to water. Therefore, even a trace amount of water could lead to low reproducibility and NP-LC should be operated under strict exclusion of water. When hyphenated to MS, NP-LC carries some inherent disadvantages. In the ionization process, low conductivity and high resistance of MP might lead to unstable spray and low ionization efficiency. Furthermore, the high flammability of unpolar solvents should also be considered for safety reasons. To address the above issues and improve the application range, aqueous normal phase (ANP) LC was introduced. As shown in Figure VIII-12, compared to conventional SP in NP-LC, silica is replaced with hydride silica [72]. ANP-LC has dual hydrophobic-hydrophilic property. ANP LC-MS was reported in metabolomics to show great potential in terms of flexibility [73].

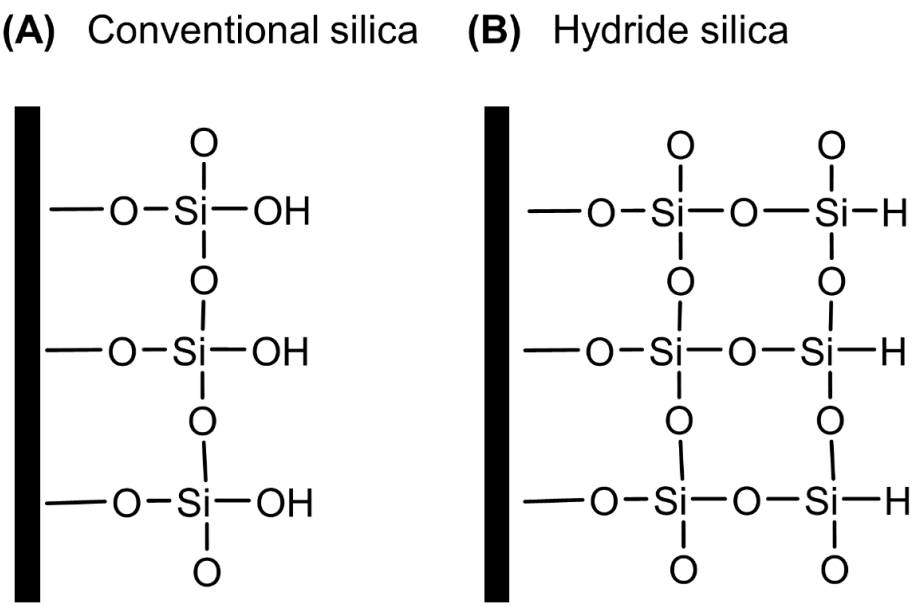

Figure VIII-12 Structures of (A) conventional silica in NP-LC and (B) hydride silica in ANP-LC.

3.3. Hydrophilic interaction liquid chromatography

As discussed above, RP-LC could separate hydrophobic compounds, NP-LC could separate hydrophilic compounds, and ANP-LC could separate both. Hydrophilic interaction liquid chromatography (HILIC) is the popular choice for polar-ionic analytes. In HILIC (shown in Figure VIII-11C) [67], the SP is polar (silica or functionalized silica). MP consists of water-miscible organic solvent and water. Water in MP usually counts for more than 2.5% to form the water layer on SP. Analytes are separated according to their partition between the water layer (the actual SP) and MP. At the same time, the analytes in the water layer can interact with charged SP, which introduces the ion exchange mechanism. When coupled to MS, HILIC has the advantage in sensitivity due to the high content of organic solvent [73].

3.4. Ion exchange chromatography

Ion chromatography or ion-exchange chromatography (IEC or IEX) separate analytes by their charge. Different ligands containing acids/bases were introduced in IEX. The analytes interact with charged SP and are eluted by increasing ion strength or pH change. According to the chemistry, SPs in IEX are

classified as strong/weak cation IEX and strong/weak anion IEX. SPs remain charged across the whole pH range in strong IEX while SPs are only charged within a certain pH range. As only ionic analytes are analyzed, IEX has a higher tolerance for matrix, which is beneficial in bioanalysis. Additionally, columns for IEX could be treated with harsh chemical solvents (e.g., KOH, H_2SO_4) for cleaning and regeneration. The limitation for IEX to be coupled to the MS detector is the high concentration of ions, which is not MS compactible. To realize desalting, an ion suppressor was used prior to MS [74–76]. A makeup flow of organic solvent was reported to increase the sensitivity significantly. Recently, with the development of multidimensional LC, the desalting could also be done in the last LC dimension.

3.5. Chiral chromatography

Chiral chromatography is the method of choice for enantiomer separation, which is a large and challenging research field related to biology, analytical chemistry, and drug development. Historically, there are two main approaches: 1) pre-column derivatization with chiral reagent (indirect way), followed by achiral separation. This approach requires high purity for the chiral derivatization reagent. Possible racemization and variation in reaction make it less attractive in bioanalysis, especially in large-scale studies in metabolomics/lipidomics. 2) Chiral MP or chiral SP (CSP) (direct approach) [77]. The CSP approach is widely investigated and applied as it avoids chiral reagent consumption in chiral MP methods. Currently, there are many CSPs available on the market, including macromolecular selectors (e.g., polysaccharides, proteins, synthetic polymers), macrocyclic selectors (e.g., cyclodextrins, macrocyclic antibiotics, chiral crown ethers), and small molecule selector (e.g., donor-acceptor type, chiral ion-exchanger, ligand exchanger). Polysaccharide-based CSPs are the most popular due to their column stability, column capacity, and reproducibility [78]. CSPs can also be classified into coated and immobilized types, among which the former type is more flexible in the choice of selectors and the latter type has a wider choice in solvents for MP. Chiral chromatography has been reported in metabolomics/lipidomics addressing enantiomer separation [79,80]. Recently, chiral chromatography was found to be useful in achiral isomer separation. In this study,

different chiral columns were tested to separate regioisomers of lipids. The multiple interaction sites of CSPs are capable of providing different selectivity, which is complementary to other LC modes.

3.6. Column and system technology

Apart from SP, the column technique plays a critical role in separation performance as well. To describe the mechanism of peak broadening in chromatography, the Van Deemter equation (Eq. 1) below was introduced in 1956 [81,82]. The plate count can be calculated afterward (Eq. 2).

$$\text{Eq. 1} \quad H = A + \frac{B}{u} + Cu$$

$$\text{Eq. 2} \quad N = \frac{L}{H}$$

Where H is the height equivalent to the theoretical plate (the plate height), A-term is eddy-diffusion and flow distribution, B-term is longitudinal diffusion, C-term is resistance to mass transfer, L is the column length, and N is the plate count. According to the equations above, optimal performance (highest N value) is obtained with reduced A-, B-, and C-term. In order to achieve that, efforts in column technologies were made, including particle size [83], particle type [84,85], and column dimensions [86,87]. Smaller particles generate flatter curves, which permit higher flow rates while maintaining resolution performance. Based on this background, sub-2-micron particles (< 2 µm) were used for the LC column, which was named ultraperformance LC (UHPLC). At the same time, backpressure from the column increases significantly with decreasing particle size (see Eq. 3).

$$\text{Eq. 3} \quad \Delta Pcol = \frac{\Phi \eta \mathrm{Lv}}{d_p^2}$$

Where ΔP is the pressure drop, η is fluid viscosity, L is the column length, v is the flow velocity, d_p is the particle diameter, and $\boldsymbol{\Phi}$ is the permeability of the packed particle bed. Therefore, the whole LC instrumentation was upgraded to stand higher pressure. Apart from fully porous particle (FPP), another particle type: superficial porous particle (SPP), also known as core-shell particles is also of interest. They consist of a nonporous core and a thin porous layer with a typical size of 2.6 µm. They can provide comparable performance to sub 2 µm particles

with lower backpressure. In this study, columns packed with both two particle types were used for optimal separation performance. Additionally, targeted phosphorylated analytes are negatively charged and prone to stick to stainless steel, which is the main material in LCMS instruments and LC columns. The undesired absorption leads to a series of analytical issues, including significant carryover, low recovery, bad peak shape, etc. Although PEEK material as housing material could eliminate these problems to some extent, applications of columns in PEEK are limited due to the low-pressure limit. To analyze these challenging analytes, the treatment of metal materials in LC instrumentation and columns was investigated. Improved peak shape and carryover were achieved with the hybrid organic-inorganic surface technology. Following this strategy, some bio-inert LC systems, as well as LC columns are available on the market. They can be promising for phosphorylated compounds without chemical derivatization [88,89].

4. Mass spectrometry for metabolomics and lipidomics

Over the recent decades, there has been significant development in MS-related techniques and instrumentation, which provides high resolving power and high sensitivity [90–92]. In MS, analytes are typically ionized in the ion source, then separated according to their mass-to-charge ratio (m/z) in the mass analyzer, followed by detection in the detector. Mass with optional fragmentation from MS can provide elemental and structural information. Nowadays, MS has become the most widely adopted technique for metabolomics/lipidomics study.

4.1. MS instrumentation

4.1.1. Ion source

As the first step of MS analysis, the analytes must be converted into gas-phase ionized species. In GC-MS, EI is the most common ionization mode by which high energy is applied via metal filament in a high vacuum. In LCMS, ionization and solvent removal should occur under atmospheric pressure conditions. Therefore, so-called soft ionization techniques are developed, among which ESI [93] and atmospheric pressure chemical ionization (APCI) [94] are commonly used.

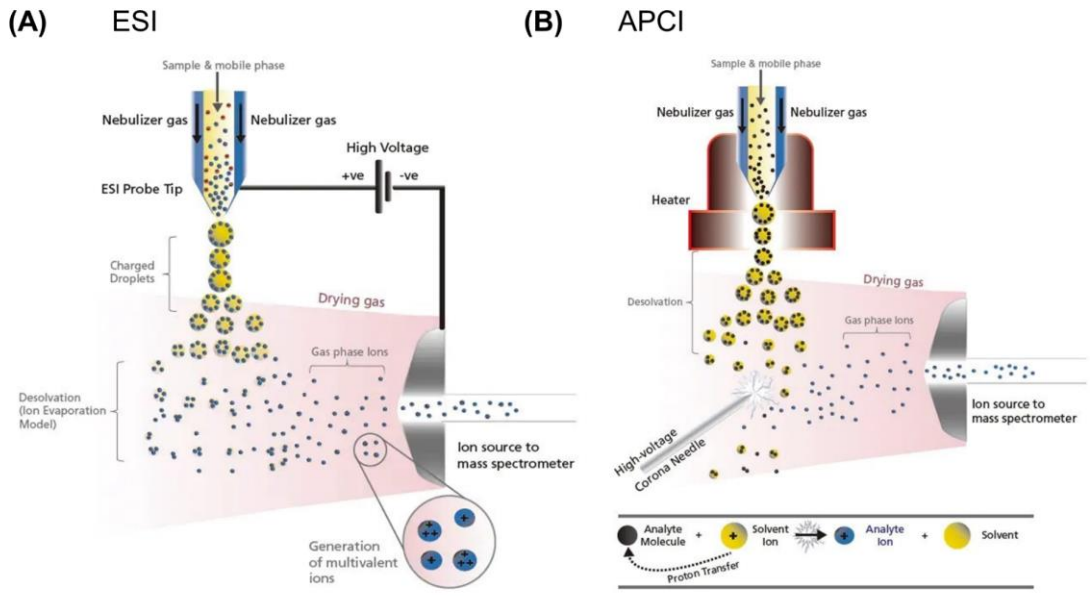

Figure VIII-13 Typical configuration and proposed ionization mechanism in (A) ESI and (B) APCI.

The typical configuration and proposed ionization mechanism of ESI are shown in Figure VIII-13A. LC flow (typical 1-1000 µL/min) containing analytes passes through the spray needle applied with high voltage electricity. The Charged droplets are surrounded by nebulizing gas and heating/drying gas, which accelerate solvent evaporation. Surface charge of droplets increases during this process. Coulombic fission occurs when the mutual repulsive force of the charges exceeds the liquid surface tension. Smaller droplets are generated by repeated abovementioned evaporation and fission. Gas-phase ions are eventually formed to enter the mass spectrometer. Multiply charged ions can be generated in ESI for large molecules with several ionizable sites (e.g., protein), which allows those analytes to be analyzed in a mass analyzer with a limited m/z range. ESI is suitable for a wide range of compounds with moderate to high polarity. For compounds with low to medium polarity, APCI is suitable and can tolerate better salts in the elute. As shown in Figure VIII-13B, the flow is sprayed into a heater with gas. The solvent molecules are ionized by the corona discharge needle. The ionization occurs after proton transfer between solvent ions and sample molecules (via ion-molecule reaction). Due to high energy during the process, APCI does not have the tendency to form multiply-charged ions like in ESI. In this study, ESI was used for the ionization technique for most methods.

In some methods, APCI was used together with ESI to realize embedded calibration in the analytical sequence.

4.1.2. Mass analyzer

The gas-phase ions are sorted in mass analyzers according to their m/z values. There are several mass analyzers available for ESI-LC-MS in bioanalysis. As listed in Table VIII-4, different mass analyzers vary significantly in performance in terms of resolution power, mass range, scan speed, sensitivity, capability of tandem MS analysis and linear dynamic range.

Table VIII-4 Involved MS analysers in this study.

MS analyser	Quadrupole	Ion trap	Time of flight
Mass resolution	unit or higher	unit	10000
Mass accuracy	100 ppm at m/z 1000	100 ppm	2–50 ppm
Mass range	up to 4000	2000	unlimited
Linear dynamic range	10^5	10^2–10^5	10^4
Scan speed	~ second	~ second	~ millisecond
Cost	low to moderate	low	moderate to high

In this study, two triple quadrupole systems (QqQ, API4000 and QTRAP4500 from Sciex) and one quadrupole time of flight (QTOF, TripleTOF5600+ from Sciex) system were used. Involved mass analyzers including quadrupole, linear ion trap, and time-of-flight are discussed below.

4.1.2.1. Quadrupole

Quadrupole is the most widely adopted mass analyzer due to its wide linear dynamic range, high sensitivity, low cost, small size, and ease of automation. The typical structure and scan principle are illustrated in Figure VIII-14A. A combination of radiofrequency (RF) and direct current (DC) is applied to four electrodes. A specific electromagnetic field was created to determine the trajectory of ions with a corresponding m/z value. Therefore, by increasing RF and DC while keeping the ratio of these two parameters constant, ions of different m/z values can pass through the quadrupole sequentially.

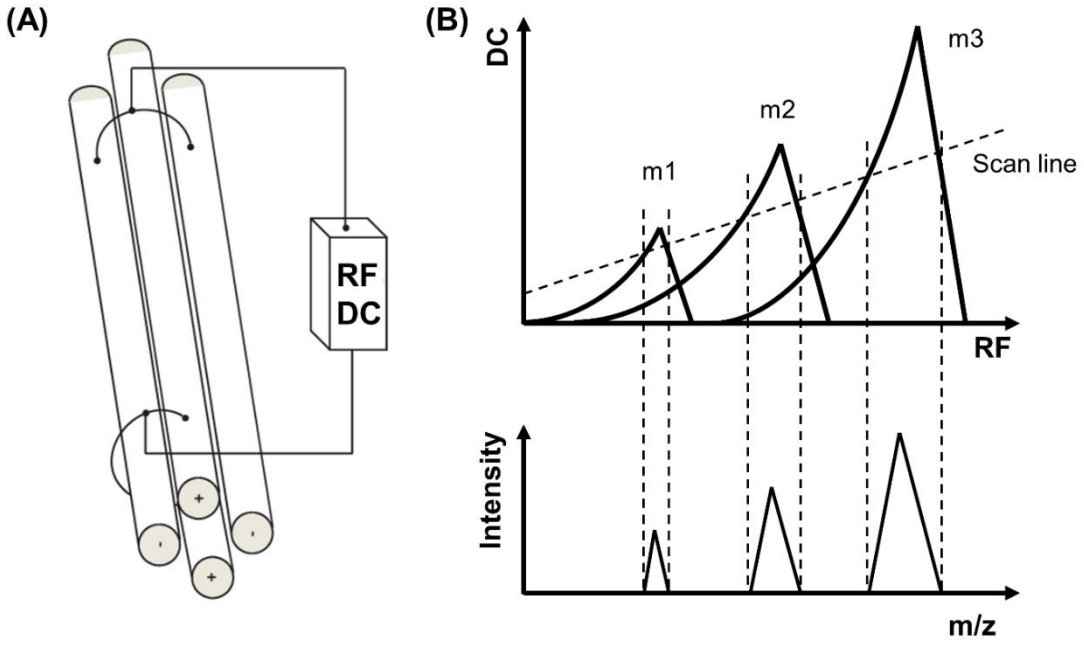

Figure VIII-14 Configuration and principle of quadrupole MS analyser.

As indicated in Figure VIII-14B, different m/z have distinct stable areas in the quadrupole. The offset and slope (or gain) of the scan line are two parameters that can be used to tune the MS performance regarding resolution and sensitivity. The area bisected by the scan line reflects the total amount of ions passing through the quadrupole. Therefore, increasing the offset and slope leads to increased resolution and decreased sensitivity. The opposite is also true. In practice, mass peak width ranges from 0.6 to 0.8 is a good compromise between resolution and sensitivity. In some applications, these parameters can also be adjusted to improve resolution or sensitivity for target masses. Additionally, quadrupole is commonly used as ion guide and collision cell in tandem MS. When quadrupole is used as ion guide transporting ions, it is operated without DC (RF only mode) and ions of a broad range of m/z can pass through. When an inert gas (e.g., nitrogen) and collision energy (CE) is applied, ions can be fragmented, which is termed collision-induced dissociation (CID). The multiple roles of the quadrupole make it suitable to be used in combination with several quadrupoles or other mass analyzers (e.g., QqQ, QTOF).

4.1.2.2. Linear ion trap

Unlike the 3D ion trap, the linear ion trap is a quadrupole ion trap operated as the 2D device. Opposite to that in the quadrupole mass filter, unstable ions are detected in the linear ion trap. The unstable ions are selectively ejected by changing alternating current (AC). Compared to the 3D ion trap, the linear ion trap showed advantages of wider dynamic range and higher sensitivity. Linear ion trap is robust, inexpensive, small in size and excellent in MS^n analysis. When integrated into QqQ, the QTRAP system from Sciex for example, linear ion trap provides extra functions regarding better resolution and sensitivity. However, there is an inherent limitation for ion trap: low mass cut-off, which is also known as the one-third rule. Fragments with m/z values less than 30% of the m/z value of the precursor cannot be effectively trapped.

4.1.2.3. Time-of-flight

Time-of-flight mass (TOF) MS was introduced in the 1940s and commercialized in the 1950s [91]. TOF MS resolves ions with different m/z values by measuring their flying time. Ions are accelerated by an electric field (E) before entering a field-free tube. Ideally, all ions are with equal kinetic energy (KE), and the relationship between m/z value and velocity could be obtained from the below equations (Eq. 5 - Where e is the charge of an electron, V is the voltage, z is the number of charges, m is the mass, and v is the velocity. These equations indicate that with a given KE, smaller ions have larger velocity, which exactly happens in TOF MS. Smaller mass flies faster than larger ones.):

Eq. 4 $KE = zeV$

Eq. 5 $KE = \frac{1}{2}mv^2$

Eq. 6 $zeV = \frac{1}{2}mv^2$

Eq. 7 $\frac{m}{z} = \frac{2eV}{v^2}$

Where e is the charge of an electron, V is the voltage, z is the number of charges, m is the mass, and v is the velocity. These equations indicate that with a given KE, smaller ions have larger velocity, which exactly happens in TOF MS. Smaller mass flies faster than larger ones.

Eq. 8 $v = L/t$

Eq. 9 $\frac{m}{z} = \frac{2eVt^2}{L^2}$

Compared to velocity measurement, it is much easier to measure the flight time (t) of ions at the detector. Velocity could be obtained by dividing tube length (L) by the flight time. Eventually, m/z can be obtained from flight time. With the same principle above, there are several configurations of TOF MS: linear type, reflection type, and orthogonal type, which are illustrated in Figure VIII-15.

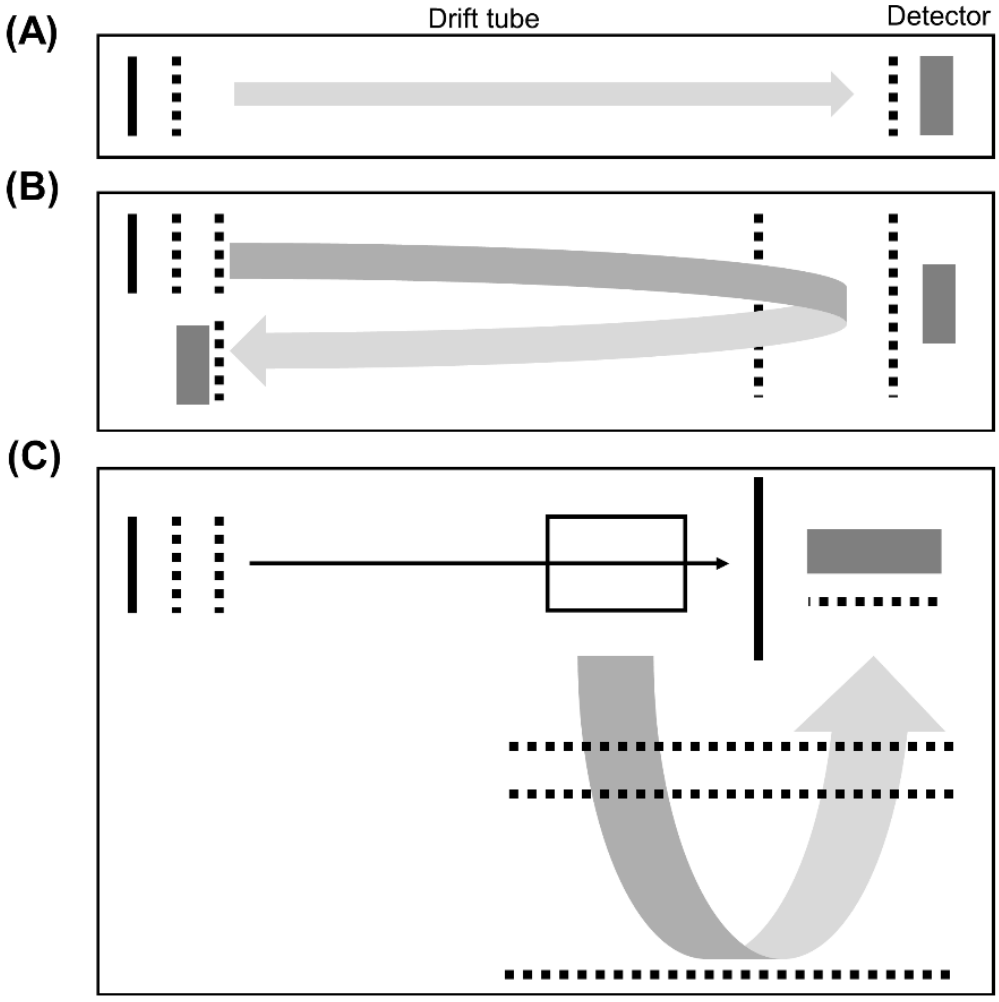

Figure VIII-15 Different types of TOF-MS configurations.

4.1.3. Detector

The detector is the last part of MS. After separated in mass analyzers, ions arrive at the detector by passing by or hitting on the surface, which generates a current

signal. Different detectors have advantages and disadvantages. Table VIII-5 summarizes some commonly used detectors in MS instruments. For TOF MS, two main types of the detectors analog-to-digital converter (ADC) and time-to-digital converter (TDC) are used. ADC is simply a data recorder and records arrived ions at a fixed interval. TDC count the arrived ions when a discriminator is triggered by ions at a certain signal level. When compared to each other, ADC has a wider dynamic range, especially in high ion currents, while TDC is superior in resolution across the whole mass range.

Table VIII-5 Commonly used MS detectors.

Detector type	Advantages	Disadvantages
Faraday cup	Robustness, stable sensitivity, and good for measuring ion transmission	Low amplification (~10)
Scintillation counter	Extremely robust, long lifetime (>5 yrs), good sensitivity ($\sim 10^6$)	Sensitive to light
Electron multiplier (EM)	Fast response, good sensitivity ($\sim 10^6$)	Short lifetime (1–2 yrs)
High-energy dynodes w/EM	Increased sensitivity for measuring high mass	May shorten lifetime of EM
Array	Fast response, good sensitivity, simultaneous detection	Low resolution (~0.2 amu), expensive, short lifetime (<1 yr)
FT-MS (Orbitrap)	Mass analyzer serves as the detector of high resolution	Used only for the specific instruments

4.2. MS experiments and analytical strategies

As different mass analyzers have different functions, different MS experiments can be performed in tandem MS, in which multiple MS analyzers are coupled. In this section, commonly performed MS experiments are discussed

On the low-resolution (LR) MS systems, quadrupoles are coupled in series. Scan types of a QqQ instrument are summarized in Table VIII-6. The second quadrupole (Q2) can be optionally operated in fragmentation mode. When Q1 and Q3 are operated in the scan, selected ion monitoring (SIM), and ion guide

(RF only) mode, different MS experiments can be performed for different purposes. Especially, if the Q3 is a linear ion trap (QTRAP system from Sciex), ions can be trapped before being scanned out, which brings improved sensitivity. Unlike fragmentation and isolation in the ion trap, QTRAP does not suffer from the one-third rule. On the QTRAP system, additional MS experiments can be performed. For example, an enhanced product ion (EPI) scan can be used to generate MS2 spectra of high quality.

Table VIII-6 Scan mode in triple quadrupole MS instrument.

Scan mode	Q1	Q2	Q3
Q1 scan	scan	Ion transmission	Ion transmission
Q3 scan	Ion transmission	Ion transmission	scan
Selected reaction monitor (SRM)	selected ion	Fragmentation	selected ion
Product ion scan (MS2)	selected ion	Fragmentation	scan
Precursor ion scan	scan	Fragmentation	selected ion
Neutral loss scan (NLS)	scan	Fragmentation	scan

In high-resolution (HR) MS systems, when quadrupoles are coupled to an HR-MS analyzer, tandem MS analysis can be performed with high resolution power. The system consists of two quadrupoles and one TOF MS. Different scan types are listed in Figure VIII-16. When MS1 and MS2 analyses are carried out. Usually, the TOF MS scan in MS1 serves as the survey scan, followed by dependent or independent MS2 analysis. The former way is named data-dependent acquisition (DDA, also known as information-dependent acquisition, IDA). The precursors are detected and sorted in MS1. MS2 analysis is triggered by ions that meet specific criteria. The latter way is termed data-independent acquisition (DIA), in which MS2 is performed regardless of results at the MS1 level. The MS2 spectra are the mixture of fragments of multiple precursors. Thus, the spectra from the DIA technique require deconvolution to reconstruct.

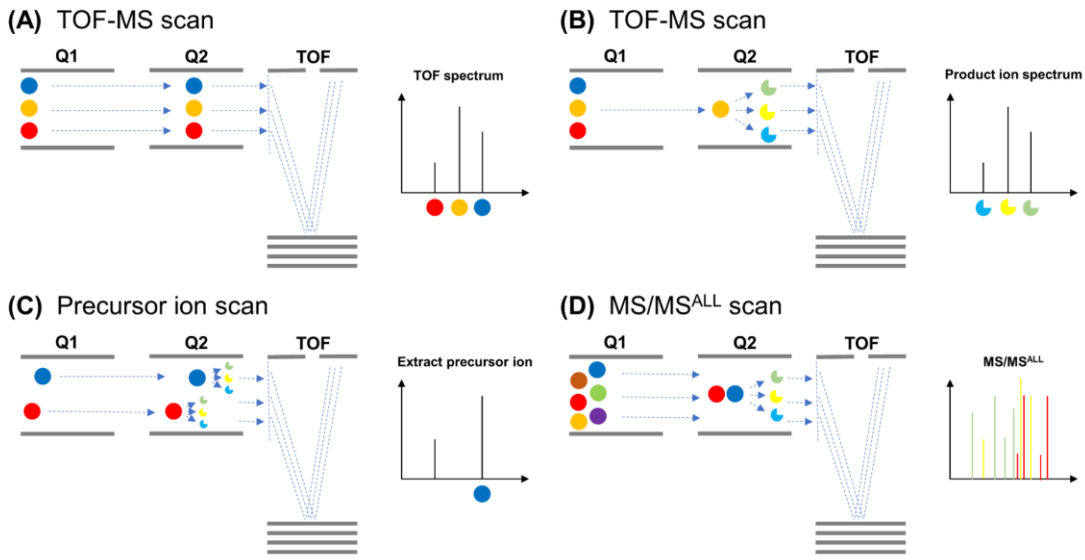

Figure VIII-16 Scan modes in TOF MS instrument.

5. Data processing in metabolomics and lipidomics

To generate a hypothesis, typical metabolomics, and lipidomics study starts with untargeted experiments, in which usually HR-MS is used. Untargeted experiments can provide a comprehensive overview of metabolites/lipids in the metabolism. Holding the hypothesis or prior biological knowledge, targeted experiments (usually LR-MS is used) are performed for better quantification performance. Unlike straightforward targeted data, processing untargeted data remains challenging nowadays and is an active research field in bioinformatics research. Raw data obtained from LC-MS is a gold mine with metabolomics and lipidomics information. Data processing workflow consists of pre-processing of raw data, identification, quantification, statistical analysis, and biological interpretation.

In the pre-processing stage, raw data is converted into a matrix of MS features. To realize this, raw data is optionally converted and imported into software, including XCMS [95–97], MZmine [98], OpenMS [99]. This software performs sequential steps of noise filtering and baseline correction, peak detection and deconvolution, alignment, and normalization. Identification then is carried out with the MS features obtained. Identification can significantly reduce data complexity. It has been well recognized that the MS library contains information on exact mass, isotopic pattern, retention time, fragments, etc. is of great help in identification.

As summarized in Table VIII-7, the currently available MS libraries are large in size and are still growing. Quantification steps are performed to give relative or absolute concentration information, which is further used for statistical analysis. Results are then evaluated together with biological background and experimental design for the biological interpretation.

Table VIII-7 Summary of most used MS databases in metabolomics/lipidomics.

Database	Advantages	Disadvantages
HMDB [12]	Public Mass spectral data on ~9500 chemical standards Spectral data are downloadable	Mixed collision energies and instrument types
METLIN [100]	Public Curated mass spectral data on >13,000 chemical standards Over 63,500 high-resolution MS/MS spectra	Only Q-TOF data Spectral data are not downloadable
LipidSearch [101]	Over 1.5 million lipid ions and their predicted fragment ions Includes lipid adduct ions and MSn fingerprints Data are stored in XML files	Commercial license required Developed for Orbitrap technology In silico generated MS/MS library Overlap with LipidBlast is unclear
LipidBlast [102]	Over 200,000 tandem mass spectra covering 25 lipid classes Publicly available Spectral data are downloadable	In silico generated library using heuristic modeling of tandem mass spectra - “One-third rule” limitation: developed with mostly ion-trap tandem mass spectra - Does not allow batch search of precursor ions - Overlap with LipidSearch unclear
LipidMaps [103]	Over 40,000 unique lipid structures - Spectral data are downloadable	MS/MS spectra only predicted in negative or positive ionization mode MS/MS spectra only available for one adduct per lipid
mzCloud [104]	Public Highly curated MS/MS and MSn spectral information Spectral peaks are structurally annotated	Low number of metabolites Spectral data are not downloadable Only Orbitrap spectra
Wiley 10th [105]	Largest mass spectral library commercially available 719,000 spectra (>950,000 spectra if combined with NIST 14) Over 638,000 compounds (>760,000 compounds if combined with NIST 14) Compatible with most instrument manufacturers	Commercial license required Only 70 eV EI mass spectra Beyond metabolomic applications
MaConDa [106]	Public database of ~200 contaminants in mass spectrometry Theoretical and experimental spectral records detected across several MS platforms Downloadable	Has no MS/MS data

MassBank [107]	Public Mass spectra from different MS setups Approximately 19,000 MS1 and 28,000 MS2 and MSn spectra Spectral data are downloadable	Not sufficiently curated
NIST 14 [108]	234,284 ESI MS/MS spectra of 9344 chemical standards Large number of MS/MS spectra from adducts MS/MS spectra recorded using multiple high- and low-resolution instruments Curated collection of 276,259 EI mass spectra from 242,477 unique compounds 387,463 measured Kovats or Lee retention index information from 82,337 chemical standards	Commercial license - Lack of additional identifiers to external database resources
GMD [17]	Public Over 2500 EI mass spectra and retention index information Spectral data are downloadable	Data derived primarily from plant materials
FiehnLib [18]	Over 2200 EI and retention indices for >1000 metabolites	Commercial license with Agilent Technologies and LECO Corporation Data derived primarily from plant materials
ReSpect [109]	Public More than 9000 MS/MS spectra corresponding to >3600 metabolites: ~38% literature data, ~12% Q-TOF MS/MS, ~50% QqQ MS/MS Merged spectra (same as MassBank) Curated record data Downloadable	Only Q-TOF and QqQ MS data Mainly phytochemicals (plant metabolomics) High degree of redundancy with MassBank
GNPS [110]	Public 8853 MS/MS spectra MS/MS of adducts MS/MS of unidentified structures Downloadable	Very few spectra in negative ionization Limited spectrum information No spectral clean-up/noise removal “Gold standard” is not comparable with reference databases

6. List of figures.

7. List of tables.

8. References.

(1) Collins, S. L.; Koo, I.; Peters, J. M.; Smith, P. B.; Patterson, A. D. Current Challenges and Recent Developments in Mass Spectrometry–Based Metabolomics. *Annu. Rev. Anal. Chem.* **2021**, *14* (1), 467–487. https://doi.org/10.1146/annurev-anchem-091620-015205.

(2) Liu, X.; Locasale, J. W. Metabolomics: A Primer. *Trends Biochem. Sci.* **2017**, *42* (4), 274–284. https://doi.org/10.1016/j.tibs.2017.01.004.

(3) Domenick, T. M.; Gill, E. L.; Vedam-Mai, V.; Yost, R. A. Mass Spectrometry-Based Cellular Metabolomics: Current Approaches, Applications, and Future Directions. *Anal. Chem.* **2021**, *93* (1), 546–566. https://doi.org/10.1021/acs.analchem.0c04363.

(4) Wishart, D. S. Advances in Metabolite Identification. *Bioanalysis* **2011**, *3* (15), 1769–1782. https://doi.org/10.4155/bio.11.155.

(5) Guitton, Y.; Tremblay-Franco, M.; Le Corguillé, G.; Martin, J. F.; Pétéra, M.; Roger-Mele, P.; Delabrière, A.; Goulitquer, S.; Monsoor, M.; Duperier, C.; et al. Create, Run, Share, Publish, and Reference Your LC–MS, FIA–MS, GC–MS, and NMR Data Analysis Workflows with the Workflow4Metabolomics 3.0 Galaxy Online Infrastructure for Metabolomics. *Int. J. Biochem. Cell Biol.* **2017**, *93* (June), 89–101. https://doi.org/10.1016/j.biocel.2017.07.002.

(6) Hansen, A. L.; Kupče, R.; Li, D. W.; Bruschweiler-Li, L.; Wang, C.; Brüschweiler, R. 2D NMR-Based Metabolomics with HSQC/TOCSY NOAH Supersequences. *Anal. Chem.* **2021**, *93* (15), 6112–6119. https://doi.org/10.1021/acs.analchem.0c05205.

(7) Emwas, A. H.; Roy, R.; McKay, R. T.; Tenori, L.; Saccenti, E.; Nagana Gowda, G. A.; Raftery, D.; Alahmari, F.; Jaremko, L.; Jaremko, M.; et al. Nmr Spectroscopy for Metabolomics Research. *Metabolites*. 2019. https://doi.org/10.3390/metabo9070123.

(8) Feizi, N.; Hashemi-Nasab, F. S.; Golpelichi, F.; Saburouh, N.; Parastar, H. Recent Trends in Application of Chemometric Methods for GC-MS and GC×GC-MS-Based Metabolomic Studies. *TrAC Trends Anal. Chem.* **2021**,

138, 116239. https://doi.org/https://doi.org/10.1016/j.trac.2021.116239.
(9) Rey-Stolle, F.; Dudzik, D.; Gonzalez-Riano, C.; Fernández-García, M.; Alonso-Herranz, V.; Rojo, D.; Barbas, C.; García, A. Low and High Resolution Gas Chromatography-Mass Spectrometry for Untargeted Metabolomics: A Tutorial. *Anal. Chim. Acta* **2022**, *1210*, 339043. https://doi.org/https://doi.org/10.1016/j.aca.2021.339043.
(10) Roca, M.; Alcoriza, M. I.; Garcia-Cañaveras, J. C.; Lahoz, A. Reviewing the Metabolome Coverage Provided by LC-MS: Focus on Sample Preparation and Chromatography-A Tutorial. *Anal. Chim. Acta* **2021**, *1147*, 38–55. https://doi.org/10.1016/j.aca.2020.12.025.
(11) Zhou, B.; Xiao, J. F.; Tuli, L.; Ressom, H. W. LC-MS-Based Metabolomics. *Mol. Biosyst.* **2012**, *8* (2), 470–481.
(12) Wishart, D. S.; Feunang, Y. D.; Marcu, A.; Guo, A. C.; Liang, K.; Vázquez-Fresno, R.; Sajed, T.; Johnson, D.; Li, C.; Karu, N. HMDB 4.0: The Human Metabolome Database for 2018. *Nucleic Acids Res.* **2018**, *46* (D1), D608–D617.
(13) Horai, H.; Arita, M.; Kanaya, S.; Nihei, Y.; Ikeda, T.; Suwa, K.; Ojima, Y.; Tanaka, K.; Tanaka, S.; Aoshima, K.; et al. MassBank: A Public Repository for Sharing Mass Spectral Data for Life Sciences. *J. Mass Spectrom.* **2010**, *45* (7), 703–714. https://doi.org/10.1002/jms.1777.
(14) Brown, M.; Dunn, W. B.; Dobson, P.; Patel, Y.; Winder, C. L.; Francis-Mcintyre, S.; Begley, P.; Carroll, K.; Broadhurst, D.; Tseng, A.; et al. Mass Spectrometry Tools and Metabolite-Specific Databases for Molecular Identification in Metabolomics. *Analyst* **2009**, *134* (7), 1322–1332. https://doi.org/10.1039/b901179j.
(15) Guijas, C.; Montenegro-Burke, J. R.; Domingo-Almenara, X.; Palermo, A.; Warth, B.; Hermann, G.; Koellensperger, G.; Huan, T.; Uritboonthai, W.; Aisporna, A. E.; et al. METLIN: A Technology Platform for Identifying Knowns and Unknowns. *Anal. Chem.* **2018**, *90* (5), 3156–3164. https://doi.org/10.1021/acs.analchem.7b04424.
(16) Montenegro-Burke, J. R.; Guijas, C.; Siuzdak, G. METLIN: A Tandem Mass Spectral Library of Standards. *Methods Mol. Biol.* **2020**, *2104*, 149–163. https://doi.org/10.1007/978-1-0716-0239-3_9.
(17) Hummel, J.; Selbig, J.; Walther, D.; Kopka, J. The Golm Metabolome Database: A Database for GC-MS Based Metabolite Profiling. In *Metabolomics*; Springer, 2007; pp 75–95.
(18) Kind, T.; Wohlgemuth, G.; Lee, D. Y.; Lu, Y.; Palazoglu, M.; Shahbaz, S.; Fiehn, O. FiehnLib: Mass Spectral and Retention Index Libraries for Metabolomics Based on Quadrupole and Time-of-Flight Gas Chromatography/Mass Spectrometry. *Anal. Chem.* **2009**, *81* (24), 10038–10048.
(19) Sisco, E.; Moorthy, A. S.; Watt, L. M. Creation and Release of an Updated NIST DART-MS Forensics Database. *J. Am. Soc. Mass Spectrom.* **2021**, *32* (3), 685–689. https://doi.org/10.1021/jasms.0c00416.
(20) Heller, S. The History of the NIST/EPA/NIH Mass Spectral Database. *Today's Chem. Work* **1999**, *8* (2), 45–46.
(21) Kanehisa, M.; Goto, S. KEGG: Kyoto Encyclopedia of Genes and Genomes. *Nucleic Acids Res.* **2000**, *28* (1), 27–30.
(22) Caspi, R.; Billington, R.; Keseler, I. M.; Kothari, A.; Krummenacker, M.; Midford, P. E.; Ong, W. K.; Paley, S.; Subhraveti, P.; Karp, P. D. The MetaCyc Database of Metabolic Pathways and Enzymes-a 2019 Update. *Nucleic Acids Res.* **2020**, *48* (D1), D455–D453. https://doi.org/10.1093/nar/gkz862.
(23) Zamboni, N.; Fendt, S.-M.; Rühl, M.; Sauer, U. 13 C-Based Metabolic Flux Analysis. *Nat. Protoc.* **2009**, *4* (6), 878–892.
(24) Liebisch, G.; Fahy, E.; Aoki, J.; Dennis, E. A.; Durand, T.; Ejsing, C. S.;

Fedorova, M.; Feussner, I.; Griffiths, W. J.; Köfeler, H.; et al. Update on LIPID MAPS Classification, Nomenclature, and Shorthand Notation for MS-Derived Lipid Structures. *J. Lipid Res.* **2020**, *61* (12), 1539–1555. https://doi.org/10.1194/jlr.S120001025.

(25) O'Donnell, V. B.; Dennis, E. A.; Wakelam, M. J. O.; Subramaniam, S. LIPID MAPS: Serving the next Generation of Lipid Researchers with Tools, Resources, Data, and Training. *Sci. Signal.* **2019**, *12* (563), eaaw2964. https://doi.org/10.1126/scisignal.aaw2964.

(26) Han, X.; Gross, R. W. Global Analyses of Cellular Lipidomes Directly from Crude Extracts of Biological Samples by ESI Mass Spectrometry: A Bridge to Lipidomics. *J. Lipid Res.* **2003**, *44* (6), 1071–1079. https://doi.org/10.1194/jlr.R300004-JLR200.

(27) Züllig, T.; Trötzmüller, M.; Köfeler, H. C. Lipidomics from Sample Preparation to Data Analysis: A Primer. *Anal. Bioanal. Chem.* **2020**, *412* (10), 2191–2209. https://doi.org/10.1007/s00216-019-02241-y.

(28) Raghothama, K. G. Phosphate Transport and Signaling. *Curr. Opin. Plant Biol.* **2000**, *3* (3), 182–187. https://doi.org/10.1016/S1369-5266(00)00062-5.

(29) Vuppada, R. K.; Hansen, C. R.; Strickland, K. A. P.; Kelly, K. M.; McCleary, W. R. Phosphate Signaling through Alternate Conformations of the PstSCAB Phosphate Transporter. *BMC Microbiol.* **2018**, *18* (1), 1–9. https://doi.org/10.1186/s12866-017-1126-z.

(30) Koobs, D. H. Phosphate Mediation of the Crabtree and Pasteur Effects. *Science (80-.).* **1972**, *178* (4057), 127–133. https://doi.org/10.1126/science.178.4057.127.

(31) Kamerlin, S. C. L.; Sharma, P. K.; Prasad, R. B.; Warshel, A. Why Nature Really Chose Phosphate. *Q. Rev. Biophys.* **2013**, *46* (1), 1–132. https://doi.org/10.1017/S0033583512000157.

(32) Westheimer, F. H. Nature Chose Phosphates The Role of Phosphates The Importance of Being Ionized. *Science* **1987**, *235* (1), 1173–1178.

(33) Monteil, P. A Study of Coenzyme A Metabolism and Function in Mammalian Cells A Study of Coenzyme A Metabolism and Function in Mammalian Cells Pascale Monteil. UCL (University College London) 2013.

(34) Trefely, S.; Lovell, C. D.; Snyder, N. W.; Wellen, K. E. Compartmentalised Acyl-CoA Metabolism and Roles in Chromatin Regulation. *Mol. Metab.* **2020**, *38*, 100941. https://doi.org/10.1016/j.molmet.2020.01.005.

(35) O'Donnell, V. B.; Murphy, R. C.; Watson, S. P. Platelet Lipidomics: Modern Day Perspective on Lipid Discovery and Characterization in Platelets. *Circ. Res.* **2014**, *114* (7), 1185–1203. https://doi.org/10.1161/CIRCRESAHA.114.301597.

(36) Dickson, E. J.; Hille, B. Understanding Phosphoinositides: Rare, Dynamic, and Essential Membrane Phospholipids. *Biochem. J.* **2019**, *476* (1), 1–23. https://doi.org/10.1042/BCJ20180022.

(37) Di Paolo, G.; De Camilli, P. Phosphoinositides in Cell Regulation and Membrane Dynamics. *Nature* **2006**, *443* (7112), 651–657. https://doi.org/10.1038/nature05185.

(38) Dickson, E. J. Recent Advances in Understanding Phosphoinositide Signaling in the Nervous System [Version 1; Referees: 3 Approved]. *F1000Research* **2019**, *8*. https://doi.org/10.12688/f1000research.16679.1.

(39) Schink, K. O.; Tan, K. W.; Stenmark, H. Phosphoinositides in Control of Membrane Dynamics. *Annu. Rev. Cell Dev. Biol.* **2016**, *32*, 143–171. https://doi.org/10.1146/annurev-cellbio-111315-125349.

(40) Fruman, D. A.; Rommel, C. PI3K and Cancer: Lessons, Challenges and Opportunities. *Nat. Rev. Drug Discov.* **2014**, *13* (2), 140–156. https://doi.org/10.1038/nrd4204.

(41) Mayer, I. A.; Arteaga, C. L. The PI3K/AKT Pathway as a Target for Cancer

Treatment. *Annu. Rev. Med.* **2016**, *67*, 11–28. https://doi.org/10.1146/annurev-med-062913-051343.
(42) Vanhaesebroeck, B.; Perry, M. W. D.; Brown, J. R.; André, F.; Okkenhaug, K. PI3K Inhibitors Are Finally Coming of Age. *Nat. Rev. Drug Discov.* **2021**, *20* (10), 741–769. https://doi.org/10.1038/s41573-021-00209-1.
(43) Hisatsune, C.; Nakamura, K.; Kuroda, Y.; Nakamura, T.; Mikoshiba, K. Amplification of Ca2+ Signaling by Diacylglycerol-Mediated Inositol 1,4,5-Trisphosphate Production. *J. Biol. Chem.* **2005**, *280* (12), 11723–11730. https://doi.org/10.1074/jbc.M409535200.
(44) Berridge, M. J. Inositol Trisphosphate and Diacylglycerol: Two Interacting Second Messengers. *ISI Atlas Sci. Pharmacol.* **1987**, *1* (2), 91–97. https://doi.org/10.1146/annurev.biochem.56.1.159.
(45) Mujalli, A.; Chicanne, G.; Bertrand-Michel, J.; Viars, F.; Stephens, L.; Hawkins, P.; Viaud, J.; Gaits-Iacovoni, F.; Severin, S.; Gratacap, M. P.; et al. Profiling of Phosphoinositide Molecular Species in Human and Mouse Platelets Identifies New Species Increasing Following Stimulation. *Biochim. Biophys. Acta - Mol. Cell Biol. Lipids* **2018**, *1863* (9), 1121–1131. https://doi.org/10.1016/j.bbalip.2018.06.009.
(46) Bozelli, J. C.; Epand, R. M. Specificity of Acyl Chain Composition of Phosphatidylinositols. *Proteomics* **2019**, *19* (18), 1900138. https://doi.org/10.1002/pmic.201900138.
(47) Barneda, D.; Cosulich, S.; Stephens, L.; Hawkins, P. How Is the Acyl Chain Composition of Phosphoinositides Created and Does It Matter? *Biochem. Soc. Trans.* **2019**, *47* (5), 1291–1305. https://doi.org/10.1042/BST20190205.
(48) Chatree, S.; Thongmaen, N.; Tantivejkul, K.; Sitticharoon, C.; Vucenik, I. Role of Inositols and Inositol Phosphates in Energy Metabolism. *Molecules* . 2020. https://doi.org/10.3390/molecules25215079.
(49) Bennett, M.; Onnebo, S. M. N.; Azevedo, C.; Saiardi, A. Inositol Pyrophosphates: Metabolism and Signaling. *Cell. Mol. Life Sci.* **2006**, *63* (5), 552–564. https://doi.org/10.1007/s00018-005-5446-z.
(50) Szijgyarto, Z.; Garedew, A.; Azevedo, C.; Saiardi, A. Influence of Inositol Pyrophosphates on Cellular Energy Dynamics. *Science (80-.).* **2011**, *334* (6057), 802–805. https://doi.org/10.1126/science.1211908.
(51) Malek, C.; Wawrzyniak, A. M.; Koch, P.; Lüchtenborg, C.; Hessenberger, M.; Sachsenheimer, T.; Jang, W.; Bruegger, B.; Haucke, V. Inositol Triphosphate-Triggered Calcium Release Blocks Lipid Exchange at Endoplasmic Reticulum-Golgi Contact Sites. *Nat. Commun.* **2020**, No. 2021, 1–15. https://doi.org/10.21203/rs.3.rs-35925/v1.
(52) Noor, E.; Eden, E.; Milo, R.; Alon, U. Central Carbon Metabolism as a Minimal Biochemical Walk between Precursors for Biomass and Energy. *Mol. Cell* **2010**, *39* (5), 809–820.
(53) Litwack, G. Glycolysis and Gluconeogenesis. *Hum. Biochem.* **2018**, 183–198. https://doi.org/10.1016/b978-0-12-383864-3.00008-9.
(54) Hamanaka, R. B.; Chandel, N. S. Warburg Effect and Redox Balance. *Science (80-.).* **2011**, *334* (6060), 1219–1220.
(55) Vander Heiden, M. G.; Cantley, L. C.; Thompson, C. B. Understanding the Warburg Effect: The Metabolic Requirements of Cell Proliferation. *Science (80-.).* **2009**, *324* (5930), 1029–1033.
(56) Zheng, J. I. E. Energy Metabolism of Cancer: Glycolysis versus Oxidative Phosphorylation. *Oncol. Lett.* **2012**, *4* (6), 1151–1157.
(57) Liebisch, G.; Ahrends, R.; Arita, M.; Arita, M.; Bowden, J. A.; Ejsing, C. S.; Griffiths, W. J.; Holčapek, M.; Köfeler, H.; Mitchell, T. W.; et al. Lipidomics Needs More Standardization. *Nat. Metab.* **2019**, *1* (8), 745–747. https://doi.org/10.1038/s42255-019-0094-z.
(58) D'Hondt, E.; Martín-Juárez, J.; Bolado, S.; Kasperoviciene, J.; Koreiviene,

J.; Sulcius, S.; Elst, K.; Bastiaens, L. Cell Disruption Technologies. *Microalgae-Based Biofuels Bioprod. From Feed. Cultiv. to End-Products* **2017**, 133–154. https://doi.org/10.1016/B978-0-08-101023-5.00006-6.
(59) FOLCH, J.; LEES, M.; SLOANE STANLEY, G. H. A Simple Method for the Isolation and Purification of Total Lipides from Animal Tissues. *J. Biol. Chem.* **1957**, *226* (1), 497–509. https://doi.org/10.1016/s0021-9258(18)64849-5.
(60) Bligh, E. G.; Dyer, W. J. A Rapid Method of Total Lipid Extraction and Purification. *Can. J. Biochem. Physiol.* **1959**, *37* (8), 911–917.
(61) Matyash, V.; Liebisch, G.; Kurzchalia, T. V.; Shevchenko, A.; Schwudke, D. Lipid Extraction by Methyl-Terf-Butyl Ether for High-Throughput Lipidomics. *J. Lipid Res.* **2008**, *49* (5), 1137–1146. https://doi.org/10.1194/jlr.D700041-JLR200.
(62) Leitner, A. Phosphopeptide Enrichment Using Metal Oxide Affinity Chromatography. *TrAC Trends Anal. Chem.* **2010**, *29* (2), 177–185. https://doi.org/https://doi.org/10.1016/j.trac.2009.08.007.
(63) Connor, P. A.; McQuillan, A. J. Phosphate Adsorption onto TiO2 from Aqueous Solutions: An in Situ Internal Reflection Infrared Spectroscopic Study. *Langmuir* **1999**, *15* (8), 2916–2921. https://doi.org/10.1021/la980894p.
(64) Huang, T.; Armbruster, M. R.; Coulton, J. B.; Edwards, J. L. Chemical Tagging in Mass Spectrometry for Systems Biology. *Anal. Chem.* **2019**, *91* (1), 109–125. https://doi.org/10.1021/acs.analchem.8b04951.
(65) Zhang, T. Y.; Li, S.; Zhu, Q. F.; Wang, Q.; Hussain, D.; Feng, Y. Q. Derivatization for Liquid Chromatography-Electrospray Ionization-Mass Spectrometry Analysis of Small-Molecular Weight Compounds. *TrAC - Trends Anal. Chem.* **2019**, *119*. https://doi.org/10.1016/j.trac.2019.07.019.
(66) Žuvela, P.; Skoczylas, M.; Jay Liu, J.; Baczek, T.; Kaliszan, R.; Wong, M. W.; Buszewski, B. Column Characterization and Selection Systems in Reversed-Phase High-Performance Liquid Chromatography. *Chem. Rev.* **2019**, *119* (6), 3674–3729. https://doi.org/10.1021/acs.chemrev.8b00246.
(67) Lange, M.; Ni, Z.; Criscuolo, A.; Fedorova, M. Liquid Chromatography Techniques in Lipidomics Research. *Chromatographia* **2019**, *82* (1), 77–100. https://doi.org/10.1007/s10337-018-3656-4.
(68) Marchand, D. H.; Croes, K.; Dolan, J. W.; Snyder, L. R. Column Selectivity in Reversed-Phase Liquid Chromatography: VII. Cyanopropyl Columns. *J. Chromatogr. A* **2005**, *1062* (1), 57–64. https://doi.org/10.1016/j.chroma.2004.11.015.
(69) Aicheler, F.; Li, J.; Hoene, M.; Lehmann, R.; Xu, G.; Kohlbacher, O. Retention Time Prediction Improves Identification in Nontargeted Lipidomics Approaches. *Anal. Chem.* **2015**, *87* (15), 7698–7704. https://doi.org/10.1021/acs.analchem.5b01139.
(70) Ovčačíková, M.; Lísa, M.; Cífková, E.; Holčapek, M. Retention Behavior of Lipids in Reversed-Phase Ultrahigh-Performance Liquid Chromatography-Electrospray Ionization Mass Spectrometry. *J. Chromatogr. A* **2016**, *1450*, 76–85. https://doi.org/10.1016/j.chroma.2016.04.082.
(71) White, J. B.; Trim, P. J.; Salagaras, T.; Long, A.; Psaltis, P. J.; Verjans, J. W.; Snel, M. F. Equivalent Carbon Number and Interclass Retention Time Conversion Enhance Lipid Identification in Untargeted Clinical Lipidomics. *Anal. Chem.* **2022**. https://doi.org/10.1021/acs.analchem.1c03770.
(72) Pesek, J. J.; Matyska, M. T.; Boysen, R. I.; Yang, Y.; Hearn, M. T. W. Aqueous Normal-Phase Chromatography Using Silica-Hydride-Based Stationary Phases. *TrAC - Trends Anal. Chem.* **2013**, *42*, 64–73. https://doi.org/10.1016/j.trac.2012.09.016.
(73) Cui, L.; Lu, H.; Lee, Y. H. Challenges and Emergent Solutions for LC-MS/MS Based Untargeted Metabolomics in Diseases. *Mass Spectrom.*

Rev. **2018**, *37* (6), 772–792.
(74) Cheung, H. Y. F.; Coman, C.; Westhoff, P.; Manke, M.; Sickmann, A.; Borst, O.; Gawaz, M.; Watson, S. P.; Heemskerk, J. W. M.; Ahrends, R. Targeted Phosphoinositides Analysis Using High-Performance Ion Chromatography-Coupled Selected Reaction Monitoring Mass Spectrometry. *J. Proteome Res.* **2021**, 1–6. https://doi.org/10.1021/acs.jproteome.1c00017.
(75) Haddad, P. R.; Jackson, P. E.; Shaw, M. J. Developments in Suppressor Technology for Inorganic Ion Analysis by Ion Chromatography Using Conductivity Detection. *J. Chromatogr. A* **2003**, *1000* (1–2), 725–742. https://doi.org/10.1016/S0021-9673(02)01999-4.
(76) Saari-Nordhaus, R.; Anderson, J. M. Recent Advances in Ion Chromatography Suppressor Improve Anion Separation and Detection. *J. Chromatogr. A* **2002**, *956* (1–2), 15–22. https://doi.org/10.1016/S0021-9673(01)01515-1.
(77) Lämmerhofer, M. Chiral Recognition by Enantioselective Liquid Chromatography: Mechanisms and Modern Chiral Stationary Phases. *J. Chromatogr. A* **2010**, *1217* (6), 814–856. https://doi.org/10.1016/j.chroma.2009.10.022.
(78) Chankvetadze, B. Recent Trends in Preparation, Investigation and Application of Polysaccharide-Based Chiral Stationary Phases for Separation of Enantiomers in High-Performance Liquid Chromatography. *TrAC - Trends in Analytical Chemistry*. Elsevier January 1, 2020, p 115709. https://doi.org/10.1016/j.trac.2019.115709.
(79) Cebo, M.; Fu, X.; Gawaz, M.; Chatterjee, M.; Lämmerhofer, M. Enantioselective Ultra-High Performance Liquid Chromatography-Tandem Mass Spectrometry Method Based on Sub-2µm Particle Polysaccharide Column for Chiral Separation of Oxylipins and Its Application for the Analysis of Autoxidized Fatty Acids and Platelet R. *J. Chromatogr. A* **2020**, *1624*, 461206. https://doi.org/10.1016/j.chroma.2020.461206.
(80) Calderón, C.; Lämmerhofer, M. Enantioselective Metabolomics by Liquid Chromatography-Mass Spectrometry. *J. Pharm. Biomed. Anal.* **2022**, *207*, 114430. https://doi.org/10.1016/j.jpba.2021.114430.
(81) Gritti, F.; Guiochon, G. The van Deemter Equation: Assumptions, Limits, and Adjustment to Modern High Performance Liquid Chromatography. *J. Chromatogr. A* **2013**, *1302*, 1–13. https://doi.org/10.1016/j.chroma.2013.06.032.
(82) Klinkenberg, A.; Zuiderweg, F. J. Longitudinal Diffusion and Resistance to Mass Transfer as Causes of Nonideality in Chromatography. *Chem. Eng. Sci.* **1956**, *5* (6), 271–289. https://doi.org/10.1016/0009-2509(56)80003-1.
(83) Mazzeo, J. R.; D. Neue, U.; Kele, M.; Plumb, R. S. Advancing LC Performance with Smaller Particles and Higher Pressure. ACS Publications 2005.
(84) Ismail, O. H.; Pasti, L.; Ciogli, A.; Villani, C.; Kocergin, J.; Anderson, S.; Gasparrini, F.; Cavazzini, A.; Catani, M. Pirkle-Type Chiral Stationary Phase on Core–Shell and Fully Porous Particles: Are Superficially Porous Particles Always the Better Choice toward Ultrafast High-Performance Enantioseparations? *J. Chromatogr. A* **2016**, *1466*, 96–104. https://doi.org/10.1016/j.chroma.2016.09.001.
(85) Spudeit, D. A.; Dolzan, M. D.; Breitbach, Z. S.; Barber, W. E.; Micke, G. A.; Armstrong, D. W. Superficially Porous Particles vs. Fully Porous Particles for Bonded High Performance Liquid Chromatographic Chiral Stationary Phases: Isopropyl Cyclofructan 6. *J. Chromatogr. A* **2014**, *1363*, 89–95. https://doi.org/10.1016/j.chroma.2014.08.022.
(86) Shen, Y.; Moore, R. J.; Zhao, R.; Blonder, J.; Auberry, D. L.; Masselon, C.; Paša-Tolić, L.; Hixson, K. K.; Auberry, K. J.; Smith, R. D. High-Efficiency

on-Line Solid-Phase Extraction Coupling to 15-150-Mm-i.d. Column Liquid Chromatography for Proteomic Analysis. *Anal. Chem.* **2003**, *75* (14), 3596–3605. https://doi.org/10.1021/ac0300690.
(87) Desmet, G.; Eeltink, S. Fundamentals for LC Miniaturization. *Anal. Chem.* **2013**, *85* (2), 543–556. https://doi.org/10.1021/ac303317c.
(88) Delano, M.; Walter, T. H.; Lauber, M. A.; Gilar, M.; Jung, M. C.; Nguyen, J. M.; Boissel, C.; Patel, A. V.; Bates-Harrison, A.; Wyndham, K. D. Using Hybrid Organic-Inorganic Surface Technology to Mitigate Analyte Interactions with Metal Surfaces in UHPLC. *Anal. Chem.* **2021**, *93* (14), 5773–5781. https://doi.org/10.1021/acs.analchem.0c05203.
(89) Plumb, R. S.; Gethings, L. A.; King, A.; Mullin, L. G.; Maker, G.; Trengove, R.; Wilson, I. D. Hybrid Organic/Inorganic Hybrid Surface Technology for Increasing the Performance of LC/MS(MS)-Based Drug Metabolite Identification Studies: Application to Gefitinib and Metabolites in Mouse Plasma and Urine. *J. Pharm. Biomed. Anal.* **2021**, *200*, 114076. https://doi.org/10.1016/j.jpba.2021.114076.
(90) Kanu, A. B.; Dwivedi, P.; Tam, M.; Matz, L.; Hill Jr, H. H. Ion Mobility–Mass Spectrometry. *J. mass Spectrom.* **2008**, *43* (1), 1–22.
(91) Chernushevich, I. V; Loboda, A. V; Thomson, B. A. An Introduction to Quadrupole–Time-of-Flight Mass Spectrometry. *J. Mass Spectrom.* **2001**, *36* (8), 849–865. https://doi.org/https://doi.org/10.1002/jms.207.
(92) Perry, R. H.; Cooks, R. G.; Noll, R. J. Orbitrap Mass Spectrometry: Instrumentation, Ion Motion and Applications. *Mass Spectrom. Rev.* **2008**, *27* (6), 661–699. https://doi.org/https://doi.org/10.1002/mas.20186.
(93) Wilm, M. Principles of Electrospray Ionization. *Mol. Cell. Proteomics* **2011**, *10* (7), M111.009407. https://doi.org/10.1074/mcp.M111.009407.
(94) Byrdwell, W. C. Atmospheric Pressure Chemical Ionization Mass Spectrometry for Analysis of Lipids. *Lipids* **2001**, *36* (4), 327–346. https://doi.org/10.1007/s11745-001-0725-5.
(95) Smith, C. A.; Want, E. J.; O'Maille, G.; Abagyan, R.; Siuzdak, G. XCMS: Processing Mass Spectrometry Data for Metabolite Profiling Using Nonlinear Peak Alignment, Matching, and Identification. *Anal. Chem.* **2006**, *78* (3), 779–787. https://doi.org/10.1021/ac051437y.
(96) Smith, C. A.; Want, E. J.; O'Maille, G.; Abagyan, R.; Siuzdak, G. XCMS: Processing Mass Spectrometry Data for Metabolite Profiling Using Nonlinear Peak Alignment, Matching, and Identification. *Anal. Chem.* **2006**, *78* (3), 779–787. https://doi.org/10.1021/ac051437y.
(97) Tautenhahn, R.; Patti, G. J.; Rinehart, D.; Siuzdak, G. XCMS Online: A Web-Based Platform to Process Untargeted Metabolomic Data. *Anal. Chem.* **2012**, *84* (11), 5035–5039. https://doi.org/10.1021/ac300698c.
(98) Pluskal, T.; Castillo, S.; Villar-Briones, A.; Orešič, M. MZmine 2: Modular Framework for Processing, Visualizing, and Analyzing Mass Spectrometry-Based Molecular Profile Data. *BMC Bioinformatics* **2010**, *11* (1), 395. https://doi.org/10.1186/1471-2105-11-395.
(99) Röst, H. L.; Sachsenberg, T.; Aiche, S.; Bielow, C.; Weisser, H.; Aicheler, F.; Andreotti, S.; Ehrlich, H. C.; Gutenbrunner, P.; Kenar, E.; et al. OpenMS: A Flexible Open-Source Software Platform for Mass Spectrometry Data Analysis. *Nat. Methods* **2016**, *13* (9), 741–748. https://doi.org/10.1038/nmeth.3959.
(100) Smith, C. A.; O'Maille, G.; Want, E. J.; Qin, C.; Trauger, S. A.; Brandon, T. R.; Custodio, D. E.; Abagyan, R.; Siuzdak, G. METLIN: A Metabolite Mass Spectral Database. *Ther. Drug Monit.* **2005**, *27* (6), 747–751.
(101) Scientific, T. LipidSearchTM Software https://www.thermofisher.com/de/de/home/industrial/mass-spectrometry/liquid-chromatography-mass-spectrometry-lc-ms/lc-ms-software/multi-omics-data-analysis/lipid-search-software.html.

(102) Kind, T.; Liu, K.-H.; Lee, D. Y.; DeFelice, B.; Meissen, J. K.; Fiehn, O. LipidBlast in Silico Tandem Mass Spectrometry Database for Lipid Identification. *Nat. Methods* **2013**, *10* (8), 755–758.
(103) Fahy, E.; Sud, M.; Cotter, D.; Subramaniam, S. LIPID MAPS Online Tools for Lipid Research. *Nucleic Acids Res.* **2007**, *35* (suppl_2), W606–W612.
(104) HighChem LLC. mzCloud – Advanced Mass Spectral Database https://mzcloud.org/.
(105) Oberacher, H. *Wiley Registry of Tandem Mass Spectral Data, MS for ID*; John Wiley & Sons Inc: Hoboken, NJ, USA, 2012.
(106) Weber, R. J. M.; Li, E.; Bruty, J.; He, S.; Viant, M. R. MaConDa: A Publicly Accessible Mass Spectrometry Contaminants Database. *Bioinformatics* **2012**, *28* (21), 2856–2857.
(107) Horai, H.; Arita, M.; Kanaya, S.; Nihei, Y.; Ikeda, T.; Suwa, K.; Ojima, Y.; Tanaka, K.; Tanaka, S.; Aoshima, K.; et al. MassBank: A Public Repository for Sharing Mass Spectral Data for Life Sciences. *J. Mass Spectrom.* **2010**, *45* (7), 703–714. https://doi.org/10.1002/jms.1777.
(108) National Institute of Standards and Technology. NIST/EPA/NIH Mass Spectral Library https://www.nist.gov/srd/nist-standard-reference-database-1a.
(109) Sawada, Y.; Nakabayashi, R.; Yamada, Y.; Suzuki, M.; Sato, M.; Sakata, A.; Akiyama, K.; Sakurai, T.; Matsuda, F.; Aoki, T.; et al. RIKEN Tandem Mass Spectral Database (ReSpect) for Phytochemicals: A Plant-Specific MS/MS-Based Data Resource and Database. *Phytochemistry* **2012**, *82*, 38–45. https://doi.org/https://doi.org/10.1016/j.phytochem.2012.07.007.
(110) Duncan, K. R.; Crüsemann, M.; Lechner, A.; Sarkar, A.; Li, J.; Ziemert, N.; Wang, M.; Bandeira, N.; Moore, B. S.; Dorrestein, P. C. Molecular Networking and Pattern-Based Genome Mining Improves Discovery of Biosynthetic Gene Clusters and Their Products from Salinispora Species. *Chem. Biol.* **2015**, *22* (4), 460–471.

IX. Objectives of the thesis

The aim of this thesis was to develop new methods of phosphorylated lipids/metabolites by LC-MS/MS. To address the analytical issues airing from phosphate groups, derivatization strategy was developed. Workflow including sample preparation, chromatographic separation, MS detection, and data processing was established and validated accordingly. According to different analytes, my work was divided into the following 4 main projects.

In the first project, a new method was developed for fatty acyl-CoAs with different side chains. Due to diverse fatty acyl compositions, multiple LC methods are required to cover the whole family of fatty acyl-CoAs in chromatography. A methylation strategy was developed to narrow the polarity range, which enables the full coverage with single RP-LC method. The method was validated and applied for clinical samples to look for potential biomarkers of coronary artery disease.

The second study was aimed at the development of a new analysis method of PIPx, which is capable of regioisomer separation and fatty acyl chain coverage. In this study, PIPx was sequentially extracted, methylated for improved extraction efficiency and stability. Immobilized polysaccharide stationary phase was screened and optimized for separation. DIA MS technique was used to acquire full MS2 spectra.

The goal of the 3rd study was to develop a new method of IPx. In the sample preparation, TiO2 was used for extraction. After phosphate methylation, cholesterolether bonded RP column was used to separate I(1,4,5)P3 from other regioisomers.

The aim of the 4th project was to develop a new method of SPx in biological samples. As the proof of concept, SPx in glycolysis was analysed with methylation. PGC column was used for better separation. The method was applied to monitor the glycolysis pathway during platelet activation process.

Apart from method development, other efforts were also made. To support clinical research, method integration strategy was developed to get more information from limited real samples. Modifications of methods were made to meet the requirements of different sample types, including murine platelets, organelle samples.

X. Results and discussion

9. Publication I

Targeted Profiling of Short-, Medium-, and Long-Chain Fatty Acyl-Coenzyme As in Biological Samples by Phosphate Methylation Coupled to Liquid Chromatography–Tandem Mass Spectrometry

Peng Li [a], Meinrad Gawaz [b], Madhumita Chatterjee [b], Michael Lämmerhofer [a]*

[a] Institute of Pharmaceutical Sciences, Pharmaceutical (Bio-)Analysis, University of Tübingen, Tübingen, Germany

[b] Department of Cardiology and Angiology, University Hospital Tübingen, 72076 Tübingen, Germany

Anal. Chem.

Year 2021, Volume 93, Issue 9, Pages 4342–4350

Doi: 10.1021/acs.analchem.1c00664

Graphical Abstract

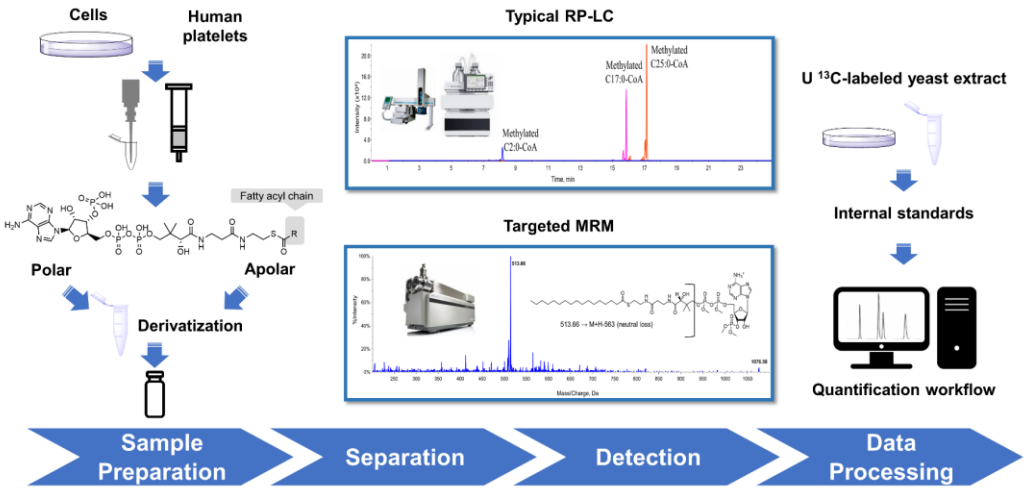

analytical chemistry

pubs.acs.org/ac Article

Targeted Profiling of Short-, Medium-, and Long-Chain Fatty Acyl-Coenzyme As in Biological Samples by Phosphate Methylation Coupled to Liquid Chromatography−Tandem Mass Spectrometry

Peng Li, Meinrad Gawaz, Madhumita Chatterjee, and Michael Lämmerhofer*

Cite This: *Anal. Chem.* 2021, 93, 4342−4350 Read Online

ACCESS | Metrics & More | Article Recommendations | Supporting Information

ABSTRACT: Fatty acyl-coenzyme As (acyl-CoAs) are of central importance in lipid metabolism pathways. Short-chain acyl-CoAs are usually part of metabolomics, and medium- to (very) long-chain acyl-CoAs are focus of lipidomics studies. However, owing to the specific complex and amphiphilic nature contributed by fatty acyl chains and hydrophilic CoA moiety, lipidomic analysis of acyl-CoAs is still challenging, especially in terms of sample preparation and chromatographic coverage. In this work, we propose a derivatization strategy of acyl-CoAs based on phosphate methylation. After derivatization, full coverage (from free CoA to C25:0-CoA) and good peak shape in liquid chromatography were achieved. At the same time, analyte loss due to the high affinity of phosphate groups to glass and metallic surfaces was resolved, which is beneficial for routine analysis in large-scale lipidomics studies. A sample preparation method based on mixed-mode SPE was developed to optimize extraction recoveries and allow optimal integration of the derivatization process in the analytical workflow. LC-MS/MS was performed with targeted data acquisition by SRM transitions, which were constructed based on similar fragmentation rules observed for all methylated acyl-CoAs. To achieve accurate quantification, uniformly ^{13}C-labeled metabolite extract from yeast cells was taken as internal standards. Odd-chain and stable isotope-labeled acyl-CoAs were used as surrogate calibrants in the same matrix. LOQs were between 16.9 nM (short-chain acyl-CoAs) and 4.2 nM (very-long-chain acyl-CoAs). This method was validated in cultured cells and was applied in HeLa cells and human platelets of coronary artery disease patients. It revealed distinct acyl-CoA profiles in HeLa cells and platelets. The results showed that this method can effectively detect acyl-CoAs in biological samples. Considering their central importance in many *de novo* lipid biosynthesis and remodeling processes, this targeted method offers a valid foundation for future lipidomics analysis of acyl-CoA profiles in biological samples, particularly those concerning metabolic syndrome.

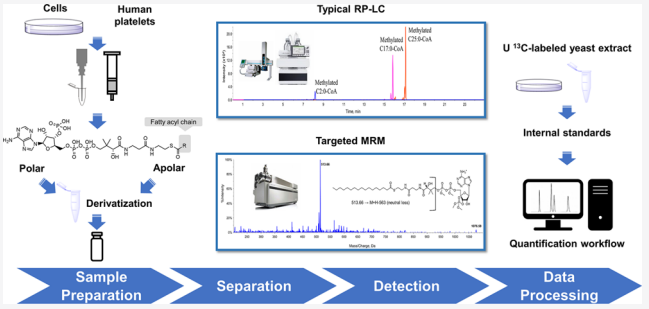

Fatty acyl-coenzyme As (acyl-CoAs) are a kind of fatty acyl lipids (structure shown in Figure 1A) that result from two-step enzymatic reaction of free CoA-SH and fatty acids by thioester bond formation catalyzed by acyl-CoA synthetase (ACS).[1] Fatty acids are converted into acyl-CoAs to enter bioactive enzymatic networks and participate in various metabolic pathways. Acyl-CoAs play vital roles in numerous biological processes, including lipid biosynthesis/remodeling, fatty acid oxidation, mitochondrial dysfunction, and xenobiotic metabolism.[2−5] Considering the key functions of acyl-CoAs in physiological and pathophysiological pathways, it is necessary to have a method for comprehensive profiling of acyl-CoAs in biological samples, particularly those collected from patients with metabolic syndrome and cardiovascular disease. Due to the presence of adenosine group in acyl-CoAs, early methods mainly adopted liquid chromatography coupled with ultraviolet detection (LC-UV), which showed lack in resolution and sensitivity.[6,7] Recently, reversed-phase liquid chromatography−tandem mass spectrometry (RPLC-MS/MS) has been routinely utilized due to the high separation performance of RPLC and the high sensitivity as well as selectivity of tandem MS.[8−12]

Because of different fatty acyl chain compositions, including different chain length, degree of unsaturation, and functional groups, physicochemical properties of acyl-CoAs vary greatly. This has been the bottleneck in the development of comprehensive analytical methods. Due to the high polarity of the CoA residue, short-chain acyl-CoAs require acidic mobile phases to gain better retention in RPLC.[10,11,13,14] On the other hand, long-chain acyl-CoAs show serious peak tailing under these conditions due to too strong retention. Basic

Received: February 11, 2021
Accepted: February 16, 2021
Published: February 23, 2021

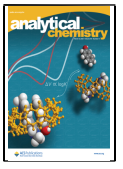

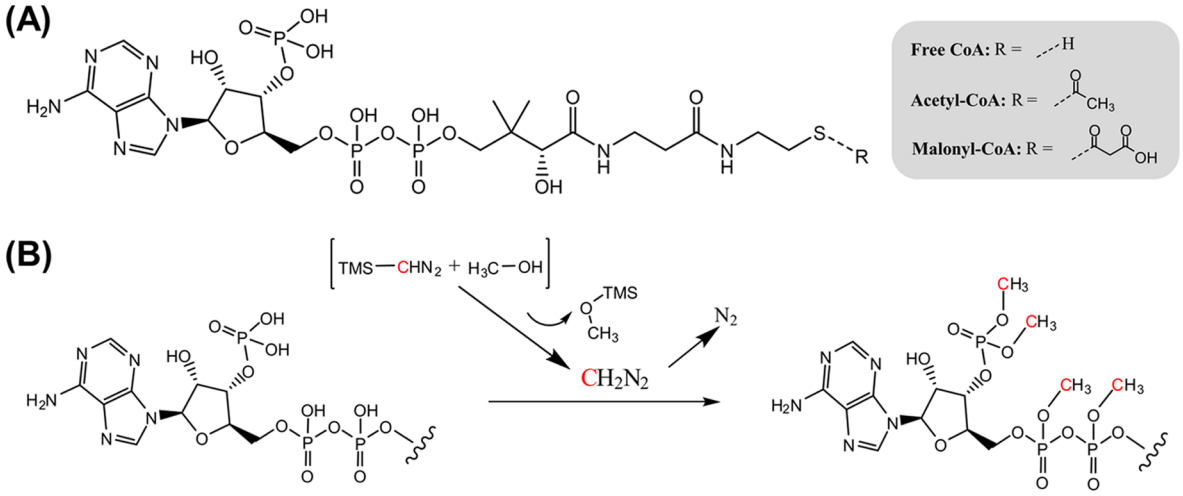

Figure 1. Phosphate methylation mechanism of acyl-CoAs using trimethylsilyl diazomethane.

mobile phases are often used to obtain a better peak shape for long-chain acyl-CoAs.[9,15] Ion pairing reagents were also suggested to improve the separation.[16,17] Unfortunately, satisfactory separation and adequate peak shape could not be obtained simultaneously for both short- and long-chain acyl-CoAs employing a single method. In addition, contamination of MS is a common problem for methods with ion pairing reagents.[16−18] Thus, in the traditional methods mentioned, only a limited range of acyl-CoAs could be simultaneously determined limiting information on the overall metabolic processes.

To combine optimal methods for short-, medium-, and long-chain acyl-CoAs, Wang et al. designed an online 2D-LC high-resolution mass spectrometry (HRMS) platform.[19] During the analytical run, short-chain acyl-CoAs were separated from medium- and long-chain acyl-CoAs in the first dimension. Two parallel columns were employed in the second dimension. Short-chain acyl-CoAs were separated with weakly basic mobile phases, while medium- and long-chain acyl-CoAs were analyzed with strongly basic conditions. Abrankó et al. conducted a comprehensive analysis of acyl-CoAs via two parallel columns, one of which was a hydrophilic interaction liquid chromatography (HILIC) column used for separation of short-chain acyl-CoAs.[20] Although the aforementioned progress has been made, analytical systems consisting of multiple columns are complicated, especially for high-throughout lipidomic research as required for large-scale clinical studies or routine analysis. Besides, problems of signal deterioration (due to dilution effects in the two-step chromatographic process), analytes' stability, and poor sensitivity remained unresolved, which has hampered the development of comprehensive analytical workflows for acyl-CoAs.[20]

In this work, we established a new straightforward approach based on a phosphate methylation methodology to achieve comprehensive profiling of acyl-CoAs. After derivatization, acyl-CoAs of different chain lengths were separated by typical RPLC conditions. Scheduled selected reaction monitoring (sSRM) was adopted for detection. Coverage and sensitivity were improved greatly by analyte methylation, which enabled comprehensive profiling of acyl-CoAs in a single analytical run. To demonstrate the utility of the new method, we analyzed acyl-CoAs in different biological samples, viz., HeLa cells and human platelets.

METHODS

Materials. Fatty acyl-coenzyme A (acyl-CoA) standards, including acetyl Coenzyme A sodium salt (C2:0-CoA), propanoyl Coenzyme A sodium salt (C3:0-CoA), palmitoyl Coenzyme A ammonium salt (C16:0-CoA), palmitoyl-(11,11,12,12-d4) Coenzyme A (C16(d4):0-CoA), heptadecanoyl Coenzyme A ammonium salt (C17:0-CoA), stearoyl Coenzyme A ammonium salt (C18:0-CoA), lignoceroyl Coenzyme A ammonium salt (C24:0-CoA), and pentacosanoyl Coenzyme A ammonium salt (C25:0-CoA) were obtained from Avanti Polar Lipids (Alabaster, AL). Coenzyme A free acid (CoA-SH) and malonyl-CoA (M-CoA) were purchased from Sigma-Aldrich (supplied by Merck, Taufkirchen, Germany). Fully ^{13}C-labeled yeast extract of more than 2×10^9 Pichia pastoris cells (~15 mg; strain CBS 7435) was obtained from ISOtopic Solutions (Vienna, Austria). Standards were dissolved in 50% methanol to give stock solutions of 5 mg/mL except for C16(d4):0-CoA (1 mg/mL). Internal standard solution was prepared by reconstituting dry extract with 2.0 mL of methanol. Solutions were kept at −80 °C until further use.

Acetonitrile, isopropanol, and methanol of Ultra LC-MS grade were supplied by Carl Roth (Karlsruhe, Germany). Ammonium acetate, monopotassium phosphate (KH_2PO_4), trypan blue solution, acetic acid, ammonium hydroxide solution (28.0 - 30.0% NH3 basis), dimethyl sulfoxide (DMSO), and radioimmunoprecipitation assay buffer (RIPA) were purchased from Sigma-Aldrich. Trimethylsilyl diazomethane (TMS-DM) was obtained from Acros Organics (supplied by VWR, Bruchsal, Germany). Water was purified by a Purelab ultrapurification system (ELGA LabWater, Celle, Germany).

Cell Culture. The human cervical HeLa cells adapted to serum-free conditions (AC free, ECACC 08011102) were grown in a humidified incubator at 37 °C with 5% CO_2. Cells were fed with EX-CELL Hela serum-free media (Sigma-Aldrich) with 2 mM L-glutamine (Sigma-Aldrich), 12 U/mL penicillin, and 12 μg/mL streptomycin until the cell density reached around 3×10^6 cells/mL. Cell counting was performed in triplicate with a hemocytometer. Aliquots of 10^7 HeLa cells were transferred into 15 mL falcon tubes and spun down for 5 min at 100*g*. After removing the supernatant, cell pellets were washed twice with ice-cold Dulbecco's

https://dx.doi.org/10.1021/acs.analchem.1c00664
Anal. Chem. 2021, 93, 4342−4350

phosphate-buffered saline (Sigma-Aldrich) with repeated centrifugation. Cell samples were snap-frozen in liquid nitrogen and kept at −80 °C till use.

Human Platelet Isolation. Human platelet samples were from previous studies[21] and were collected from the peripheral blood of donors at the Department of Cardiology and Angiology, University Hospital Tübingen, following a standard protocol, in accordance with ethical guidelines and approved by regional authorities (number 237/2018BO2).

Extraction. Acyl-CoAs were extracted by liquid extraction followed by solid-phase extraction (SPE). Briefly, 80 μL of internal standard solution and 750 μL of acetonitrile/isopropanol (3:1, v/v) were added. Samples were homogenized for 1 min (strength 5, 50% pulse) with a cell disruptor (Branson Sonifier B15, Branson Instruments Co., Stamford). KH_2PO_4 buffer (250 μL, 0.1 M, pH 6.7) was added, and samples were homogenized for another 1 min. After centrifugation (10 min, 1835*g*, 4 °C), the supernatant was acidified by 250 μL of acetic acid and was loaded onto SPE cartridge (Oasis WAX, Waters, Milford, MA), which was previously preconditioned with 1 mL of SPEmix, methanol/water/acetic acid (3:1:1, v/v/v). After washing twice with 1 mL of SPEmix followed by twice 1 mL of 50% (v/v) methanol with a 10 min drying step between. Acyl-CoAs were eluted with 1.5 mL of isopropanol/methanol/3% ammonia (6:3:1, v/v/v) in 0.5 mL aliquots. The samples were dried under nitrogen at R.T. in a Genevac EZ2 system (SP Scientific, Ipswich, U.K.).

Derivatization. Dried extracts were reconstituted with 100 μL of methanol. The upper layer (1 mL) of *tert*-butyl methyl ether/methanol/water (10:3:2.5, v/v/v) and TMS-DM (100 μL, 2 M in hexane) were added. The solutions were gently mixed, and the generated (nitrogen) fume was released for a few seconds. The reaction mixture was shaken for 30 min at room temperature. Then, 5 μL of acetic acid was added to quench the reaction, leading to a visible color change. The samples were dried under N_2 in an evaporator (Genevac EZ-2) and kept at −80°C until analysis. The dried samples were first reconstituted with 50 μL of DMSO. Full recovery of the dried matter was facilitated by sonication and vortexing. H_2O (50 μL) was added, followed by repeated sonication and vortex steps. The samples were centrifuged (at 16 100*g*, 4 °C, for 5 min), and the supernatant was transferred into vials with inserts for LC-MS/MS analysis.

sSRM Analysis with UHPLC-QTRAP MS. Separation was performed on a 1290 Infinity UHPLC system (Agilent Technologies, Waldbronn, Germany) with an ACQUITY UPLC CSH C18 Column (100 mm × 2.1 mm, 1.7 μm, 130 Å) and an ACQUITY UPLC CSH C18 VanGuard precolumn (5 mm × 2.1 mm, 1.7 μm, 130 Å) (Waters, Milford, MA). Mobile phase A was 10 mM ammonium acetate in water. Mobile phase B was methanol. Gradient elution (0.0 min, 10% B; 3 min, 10% B; 16 min, 100% B; 21 min, 100% B; 22 min, 10% B; 25 min, 10% B) was carried out at a flow rate of 0.4 mL/min and a constant column temperature of 50 °C. Injection volume was 20 μL. The first 5 min eluate was diverted into waste to prevent possible contamination of the MS ion source.

Acyl-CoA detection was performed on a QTRAP 4500 mass spectrometer with a Turbo V source (Sciex, Concord, ON, Canada) operated with ESI probe. Data were acquired under the following parameters: collision gas (N_2), 6 psi; curtain gas (N_2), 30 psi; nebulizer gas (zero grade air), 50 psi; heater gas (zero grade air), 50 psi; ion-source voltage, 3500 V (positive mode); and source temperature, 500 °C. An sSRM with a detection window of 30 s around the target retention time was applied for data acquisition. Ion transitions, retention times, and compound dependent parameters for all acyl-CoAs are summarized in Table 1. The total cycle time was 0.6 s, and dwell time was adjusted automatically.

Table 1. Acyl-CoAs Analyzed by This Method and Compound-Specific MS Parameters[a,b]

acyl-CoA	Q1	Q3	RT (min)	DP (V)	CE (V)	CXP (V)
CoA-SH	838.2	275.1	7.84	80	45	20
malonyl	924.2	361.1	8.01	80	45	20
C2:0	866.2	303.1	8.00	80	45	20
C3:0	880.2	317.2	8.77	80	45	20
C4:0	894.2	331.2	9.53	80	45	20
C6:0	922.3	359.2	10.76	80	45	20
C8:0	950.3	387.2	11.50	80	45	20
C10:0	978.3	415.3	13.14	80	50	25
C12:0	1006.4	443.3	14.83	80	50	25
C14:0	1034.4	471.3	15.34	80	50	25
C16:0	1062.4	499.4	15.89	80	50	25
C16(d4):0	1066.5	503.5	15.90	80	50	25
C17:0	1076.4	513.4	16.12	80	50	25
C18:0	1090.4	527.4	16.36	80	50	25
C18:1	1088.4	525.4	16.02	80	50	25
C18:2	1086.4	523.4	15.70	80	50	25
C18:3	1084.4	521.3	15.39	80	50	25
C20:0	1118.5	555.4	16.72	80	55	30
C20:4	1110.4	547.4	15.99	80	55	30
C20:5	1108.4	545.3	15.69	80	55	30
C22:0	1146.5	583.5	17.02	80	55	30
C22:6	1134.4	571.4	15.92	80	55	30
C24:0	1174.5	611.5	17.27	80	55	30
C25:0	1188.6	625.5	17.40	80	55	35
U^{13}C-C2:0	889.3	316.1	8.00	80	45	20
U^{13}C-C16:0	1099.5	526.5	15.89	80	50	25
U^{13}C-C18:0	1129.5	556.5	16.36	80	50	25
U^{13}C-C18:1	1127.5	554.5	16.02	80	50	25
U^{13}C-C22:0	1189.6	616.6	17.02	80	55	30
U^{13}C-C24:0	1219.7	646.6	17.27	80	55	30

[a]RT: retention time, DP: declustering potential, CE: collision energy, CXP: collision cell exit potential. [b]Entrance potential (EP) for all acyl-CoAs was 10 V.

Data Processing. Analyst 1.7 was used in both analytical systems for data acquisition and system control. Commercially available software packages PeakView and MultiQuant were involved in data processing. PeakView 2.2 was used for manual data evaluation and LC-MS performance check by comparing periodically with QC samples. MultiQuant 3.0 was used for peak integration, linear regression, and calculation of concentrations.

RESULTS AND DISCUSSION

Mechanism and Optimization of Derivatization. The analytical challenge for simultaneous short-, medium-, and long-chain fatty acyl-CoAs analysis is related to the wide range of analytes' physicochemical character with high hydrophilicity of short-chain and amphiphilic nature of long-chain CoAs. The most problematic issues of low recoveries and poor chromato-

https://dx.doi.org/10.1021/acs.analchem.1c00664
Anal. Chem. 2021, 93, 4342−4350

graphic performance, however, entirely originate from the phosphate moiety of the ribosyl phosphate residue of CoAs. Hence, we introduced a derivatization strategy to methylate phosphate groups of acyl-CoAs to eliminate its negative charge. TMS-DM was chosen as the derivatizing reagent due to its fast reaction speed, mild conditions, and ease of removing byproducts and excess reagent.[22] TMS-DM was reported to label phospholipids to increase electrospray ionization efficiency.[23,24] The mechanism of methylation of acyl-CoAs is illustrated in Figure 1B. Methanol is a proton provider to form *in situ* diazomethane (CH_2N_2) and CH_3OTMS. Excess TMS-DM is quenched by acetic acid. All of the resultant byproducts during reaction are volatile and can be easily removed by the following evaporation step. Care must be taken as much nitrogen is generated during the derivatization and quenching processes. Therefore, derivatization must be conducted under a well-functioning hood.

Due to the presence of a thioester bond, acyl-CoAs are prone to hydrolysis, posing great challenges to recovery and signal intensity.[25] Thus, the derivatization reaction must be conducted under mild conditions. Different derivatization times were tested at ambient temperature. The data (Figure 2) show that the response of acyl-CoAs reached its maximum between 20 and 30 min. Therefore, 30 min at room temperature was chosen as the optimum condition.

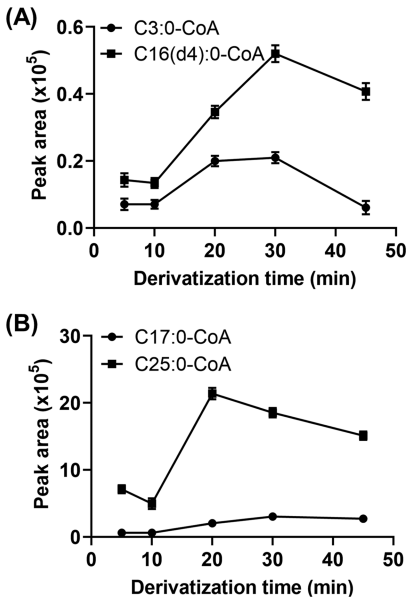

Figure 2. Optimization of derivatization time on peak areas of formed acyl-CoAs (n = 3).

MS Detection of Acyl-CoAs after Methylation. The MS behavior of acyl-CoAs in ESI was well reported previously.[26] To gain better sensitivity, ESI-MS detection of acyl-CoAs was commonly performed in positive-ion mode in spite of a negatively charged free phosphate group since there is only a single abundant precursor ion $[M + H]^+$, while the signal is split into two less abundant precursor ions, viz., $[M - H]^-$ and $[M - 2H]^{2-}$, in the negative mode.

As shown in Figure S1A for nonmethylated C17:0-CoA as an example, the fatty acyl pantetheine ion (m/z 513.7) was the most abundant fragment ion in ESI+ resulting from a neutral loss of 507 Da (3′-phospho-ADP), accompanied by a protonated 3′-phosphate-AMP product ion (m/z 428). The whole family of acyl-CoAs share these fragmentation patterns. Therefore, most published MS/MS methods constructed SRM transitions based on these two ions. As shown in Figure S1B, resulting from a neutral loss of 563 Da (tetra-methylated 3′-phospho-ADP), methylated C17:0-CoA generated only one main fragment in the MS2 level, the same fatty acyl pantetheine ion (m/z 513.7). The accurate masses of precursor and fragment ions were confirmed with high-resolution MS. As shown in Figure 3, methylated C3:0-CoA, C17:0-CoA, and C25:0-CoA have similar fragmentation rules in MS (Triple-TOF method specified in the SI), which could be beneficial for SRM construction and untargeted screening with neutral loss. Later, 10 acyl-CoAs with different chain lengths were tested for their product ion spectra under different collision energies. Utilizing information-dependent acquisition (IDA)-enhanced product ion (EPI) scan mode with QTRAP instrument (method specified in the SI), product ion spectra of high quality were obtained (Figures S2−S11). The results indicate that acyl-CoAs share a similar fragmentation pattern across the whole family after methylation. The charged fatty acyl pantetheine represents the most abundant fragment, while another fragment (m/z 150) came up as a second fragment as CE increased. Under our derivatization conditions, acyl-CoAs-containing carboxylic group (i.e., Malonyl-CoA) and thiol group (i.e., free CoA-SH) are methylated as well.

Chromatographic Improvement after Derivatization. According to different chain lengths, acyl-CoAs exhibit different polarities, which makes simultaneous analysis difficult. Additionally, poor peak shapes of acyl-CoAs (especially for long-chain CoAs) are usually observed even under basic elution conditions. To improve the coverage and peak shape, ion pairing reagents and concentrated buffers are commonly used. However, instrument contamination and signal suppression make them less attractive choices for routine lipidomics analysis. During our preliminary experiments, C2:0-CoA, C17:0-CoA, and C25:0-CoA were tested with typical RP conditions. As shown in Figure 3A,B, the peak shapes of free acyl-CoAs were extremely poor, both with methanol and acetonitrile as organic modifiers. Short-chain CoA (C2:0-CoA) eluted within the dead volume, indicating that acidic conditions should be taken to improve its retention. On the other hand, long-chain CoAs (e.g., C25:0-CoA) could not be eluted efficiently with the screening gradients of Figure 4A,B. Therefore, basic conditions should be employed to weaken its retention. These results showed that acyl-CoAs with different chain lengths favor completely different conditions to gain appropriate retention, which was in accordance with previous reports.

Moreover, during the equilibration phase when the gradient switched back to initial conditions, signals of the analytes were observed, which indicated that acyl-CoAs were stuck somewhere in the instrument or column (memory effect). Being negatively charged, acyl-CoAs are prone to stick to surfaces of glassware and stainless steel. Performance deterioration often occurred after multiple injections. Acidic eluents composed of acetonitrile, water, and formic acid or low quantities of phosphoric acid were used to flush the system. Optionally, neutral washing (i.e., 50% acetonitrile) could be performed to equilibrate the LC system before next injection.

After methylation, acyl-CoAs were converted into corresponding neutral molecules. When tested under a typical RP-LC condition (Figure 4C), methylated acyl-CoAs were separated within a single analytical run. Good peak shapes

https://dx.doi.org/10.1021/acs.analchem.1c00664
Anal. Chem. 2021, 93, 4342−4350

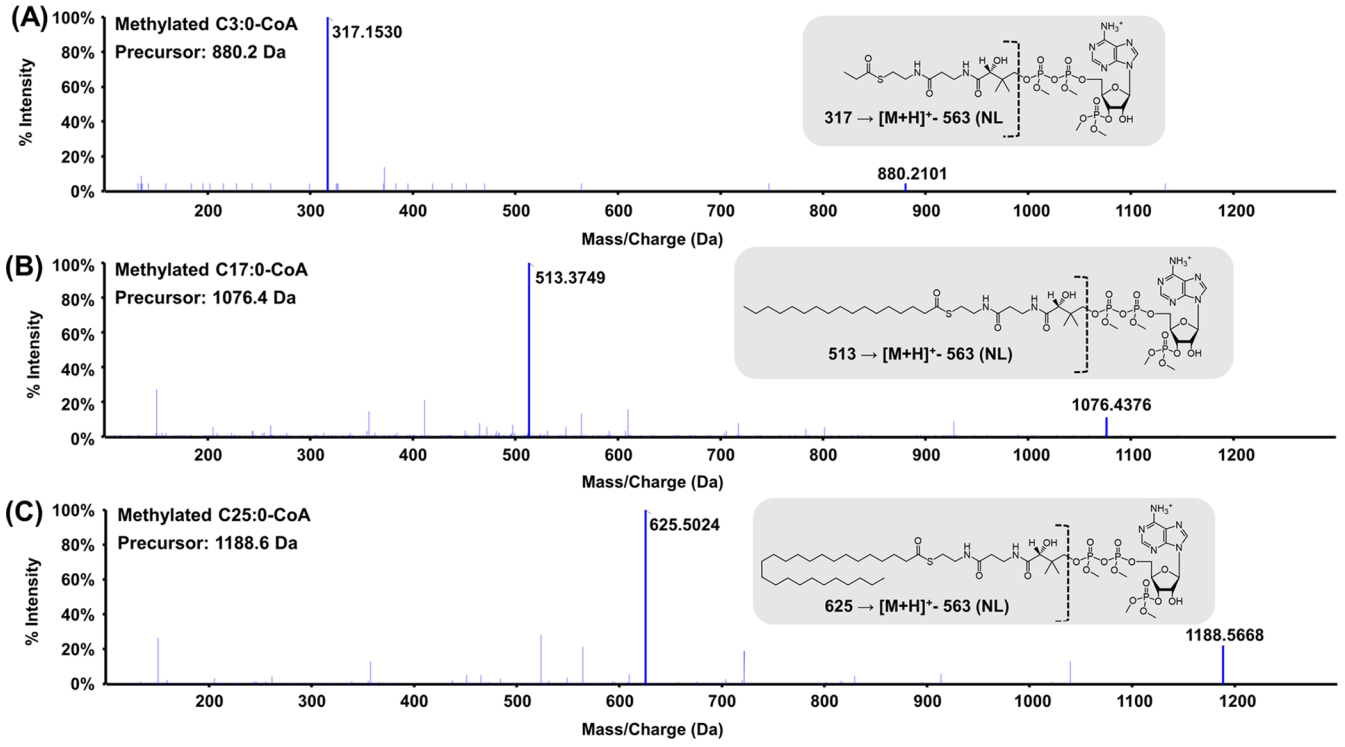

Figure 3. High-resolution product ion spectra of methylated acyl-CoAs with (A) short, (B) long, and (C) very long acyl chains.

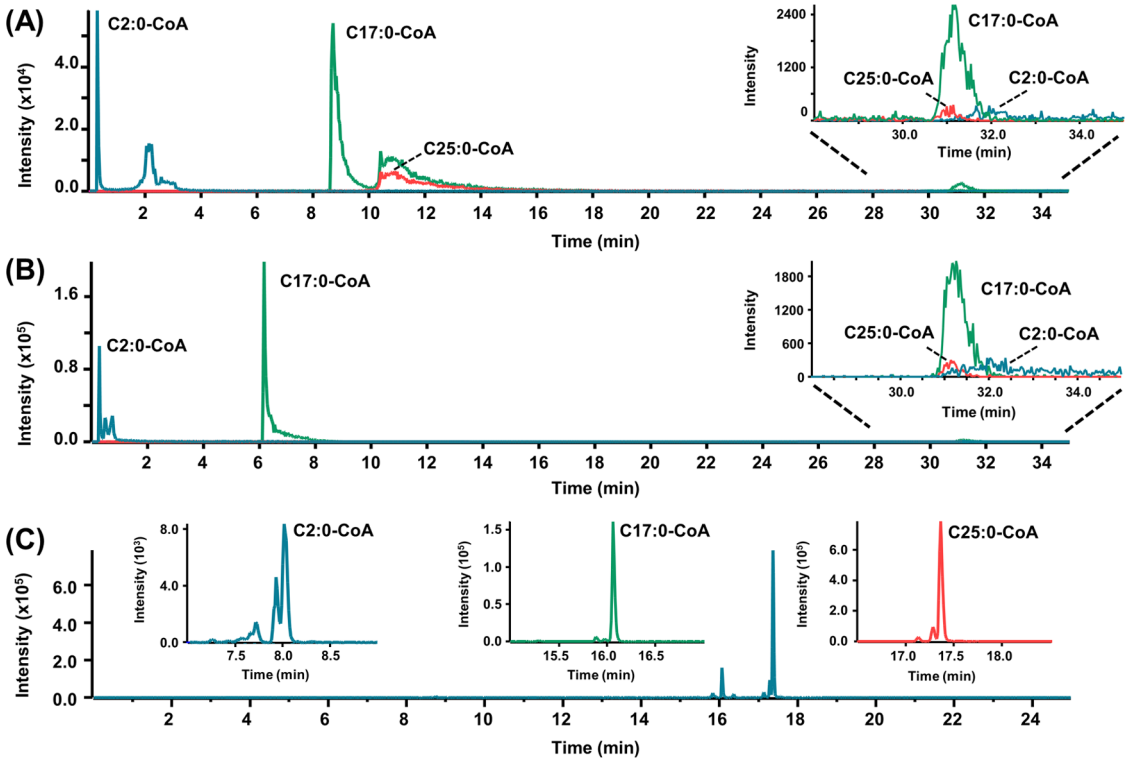

Figure 4. Chromatograms of C2:0-, C17:0-, and C25:0-CoA under the conditions of (A) 10 mM ammonium acetate in water and methanol and (B) 10 mM ammonium acetate in water and acetonitrile. (C) Chromatogram of derivatized (methylated) C3:0-, C17:0-, and C25:0-CoA under the conditions specified in the Methods section.

were obtained. Furthermore, there was no memory effect observed anymore, i.e., no analytes eluted during the reequilibration phase, indicating that carryover and instrument contamination were eliminated. Therefore, an extra washing step after multiple injections was no longer required. Methylated acyl-CoAs exhibit typically a second minor peak, which elutes adjacent to the main peak (see Figure 3C). This isomeric peak is most probably due to a phosphoryl group migration from the 3′ position to the 2′-hydroxy of the ribosyl moiety.

https://dx.doi.org/10.1021/acs.analchem.1c00664
Anal. Chem. 2021, 93, 4342−4350

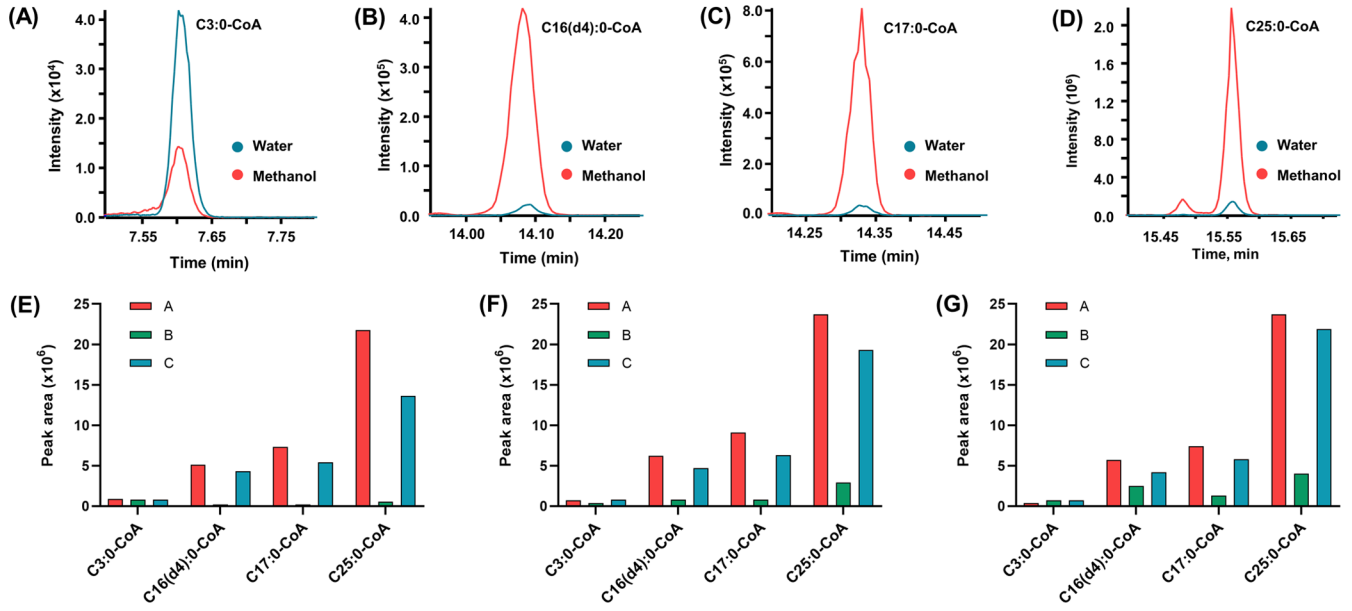

Figure 5. Methylated (A) C3:0-, (B) C16(d4):0-, (C) C17:0-, and (D) C25:0-CoA EICs obtained by the respective reconstitution test with methanol and water. Methylated acyl-CoA reconstitution with (E) 10% (v/v), (F) 20% (v/v), and (G) 50% (v/v) DMSO/water in different reconstitution orders: (A) two steps (DMSO and water); (B) two steps (water and DMSO); (C) one step (DMSO/water mixture).

Sample Preparation. Sample preparation is a critical step for the success of bioanalysis and needs careful attention. It usually starts with homogenization of the samples and ends with reconstitution of the extracted (purified) dried sample extract. Acyl-CoAs are distributed in various subcellular organelles (mitochondria, peroxisomes) besides the cytoplasm; therefore, it is important to disrupt cells thoroughly to release the analytes. This was investigated by a microscopic test using trypan blue as the dye for visualization of nonviable but intact cells. Disrupted cells do not show up under the microscope. As shown in Figure S12, cells with and without membrane could be easily distinguished under the microscope. In negative control (PBS buffer), after staining with trypan blue, complete blue circles were observed, indicating that they have an intact membrane. Radioimmunoprecipitation assay buffer (RIPA buffer) is often used for cell lysis followed by protein extraction and further analysis. Due to incompatibility to MS analysis, RIPA buffer was only used as a positive control here. After lysis with RIPA buffer, HeLa cells could not be observed under a microscope. Different mechanical approaches were tested, including sonication, pellet pestles, and cell disruptor. The results showed that the cell disruptor was the most efficient approach to break the cells, while the pellet pestle could only break the cells partially and required further optimization. Sonication with a sonication bath was not efficient enough for cell disruption. Therefore, homogenization with cell disruptor was taken for further study.

Extraction of acyl-CoAs has been challenging due to their instability and low abundance. The wide polarity range makes comprehensive extraction even more difficult. During our preliminary experiments, a biphasic solvent system composed of chloroform−methanol−water (1:1:0.4, v/v/v) and monophasic solvent systems composed of methanol and methanol/water (1:1, v/v), respectively, were tested (data not shown). Extracts from the aforementioned solvent systems were dried and reconstituted for derivatization. However, weak signals of acyl-CoAs were observed due to interference and matrix effects of coextracted compounds.

According to many reported methods, liquid extraction coupled with SPE has become a commonly accepted solution for acyl-CoA extraction. Quantitative and comprehensive extraction was only achieved with the introduction of weak anion exchange (WAX) 2-(2-pyridyl) ethyl silica.[27] Acyl-CoAs are effectively retained in such SPE cartridge after protonation of the pyridyl-nitrogen by acetic acid-containing buffer. After washing, a neutral buffer was used to elute the analytes. Our derivatization reagent is reactive to carboxylic acids. Even though eluates collected from SPE were dried prior to methylation, residual acetic acid could react with and inactivate TMS-DM. Therefore, we introduced an extra neutral washing step. To fully get rid of acetic acid introduced by SPE, Oasis WAX mixed-mode (WAX and RP) SPE cartridge was used. The cartridge is hydrophilic−lipophilic balanced, which can be dried during extraction. After optimization of all steps (application/washing/elution), an extraction method, which can be directly coupled with the following derivatization process, was obtained (see experimental methods for optimized extraction procedure).

A proper reconstitution solvent for the evaporated SPE product is of utmost importance for redissolution and guaranteeing adequate peak shape in RPLC. During the reconstitution process, at least 80% (v/v) methanol was reported essential to recover long-chain acyl-CoAs in the dry extract.[20] Water and methanol were used to reconstitute methylated acyl-CoA dry extract aliquots. Interestingly, after methylation, acyl-CoAs still differ greatly in polarity. Results (Figure 5A−D) showed that short-chain and long-chain acyl-CoAs favor polar and apolar solvents, respectively, for reconstitution. We then introduced the polar solvent dimethyl sulfoxide (DMSO) to improve recovery for the whole acyl-CoA family. To avoid strong elution strength in the reconstitution solvent, DMSO/water mixtures at ratios of less than 50% were tested in different orders. Results (Figure 5E−G) showed that even with 50% (v/v) DMSO in water, a poor recovery was observed for acyl-CoAs with a long acyl chain when the solvents for reconstitution were added in two

https://dx.doi.org/10.1021/acs.analchem.1c00664
Anal. Chem. 2021, 93, 4342−4350

Table 2. Calibration Curves, LOQs, and LODs of the Four Surrogate Standards

acyl-CoA	C3:0	C16(d4):0	C17:0	C25:0
linear range, nM	22−2248	19−1885	19−1867	8−845
equation[a]	$y = 0.00584x - 0.172$	$y = 0.0267x - 0.925$	$y = 0.0563x - 0.505$	$y = 0.619x + 0.272$
linearity (r)	0.9995	0.9995	0.9970	0.9970
standard error of slope	0.0000959	0.000429	0.00218	0.0279
standard error of y intercept	0.101	0.380	1.91	12.2
LOQ, nM	16.9	9.4	9.3	4.2
LOD, nM	4.6	3.1	2.6	1.2

[a] y (response) is peak area of analyte/peak area of internal standard (U13C-labeled). U13C-labeled C2:0-CoA was taken as internal standard for acyl-CoAs from CoA to C8:0-CoA. Other U13C-labeled acyl-CoA in Table 1 was internal standard for analytes, which has closest Rt.

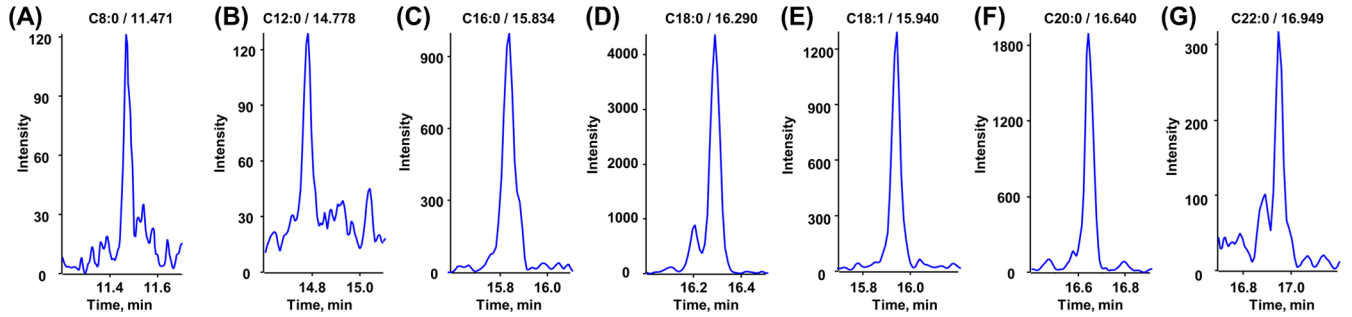

Figure 6. Representative chromatograms (EICs) of acyl-CoAs determined in human platelet sample from a patient with coronary artery disease. Determined concentrations in sample solutions were as follows: (A) C8:0-CoA, 83.1 nM; (B) C12:0-CoA, 37.5 nM; (C) C16:0-CoA, 51.9 nM; (D) C18:0-CoA, 23.0 nM; (E) C18:1-CoA, 18.4 nM; (F) C20:0-CoA, 8.1 nM; and (G) C22:0-CoA, 5.2 nM.

steps starting with water. A two-step reconstitution starting with DMSO followed by dilution with water was found to be a good compromise for acyl-CoAs with different acyl chains. 50% (v/v) DMSO was taken for this method. After optimization, the samples were first dissolved with DMSO, followed by addition of water in a specified volume. Vortexing and sonication were adopted to facilitate the reconstitution process.

Acyl-CoA Profiling in Biological Samples. Internal standards (IS) are essential for LC-MS-based methods due to the need to compensate for sample preparation variations, matrix effects, and variances in ionization efficiencies. Stable isotope-labeled (SIL) analogues are the ideal IS as they have similar analytical properties, can be distinguished by MS, and do not exist in matrix. Unfortunately, SIL ISs are not commercially available for acyl-CoAs. Uniformly ^{13}C-labeled ($U^{13}C$) metabolite extracts were recently introduced as potential IS for metabolic analysis.[11,28−30] As acyl-CoAs from this extract are fully ^{13}C-labeled, there is a low risk of interference at both MS and MS/MS levels. $U^{13}C$ metabolite extract was added into samples before sample preparation, and representative chromatograms of $U^{13}C$-labeled acyl-CoAs are shown in Figure S13. Odd-chain (C3:0-, C17:0-, C25:0-CoA) and deuterated acyl-CoAs (C16(d4):0-CoA) were taken as surrogate calibrants (note: C3:0-CoA was selected herein because it was not found as endogenous CoA in HeLa and human platelets from CAD patients; however, it may appear as an endogenous metabolite in active or inflamed cells, e.g., due to α-oxidation and should be ideally substituted). Extraction recovery and matrix effect were assessed as reported.[31] Data (Table S1) showed that C16(d4):0-CoA and C17:0-CoA suffered from significant matrix effects. This problem remained even with the optimized SPE procedure. Therefore, ISs are mandatory to compensate for matrix effects. After normalization with the aforementioned $U^{13}C$-labeled ISs, satisfying results (Table S2) were obtained (typically 90−115% for the peak area ratio between postextraction spike and standard solution indicating adequate correction of matrix effects). Results (Table S3) showed that the sample preparation has a good recovery (typically 45−70%). Autosampler stability results (Figure S14) showed that methylated acyl-CoAs were stable at least 48 h at 4 °C. Method validation in HeLa cells was carried out according to regulatory guidelines.[32,33] As shown in Table S4, this method was accurate and reliable. As summarized in Table 2, the four-calibration series showed adequate linearity within the specified concentration range. To illustrate its applicability, the method was used to profile acyl-CoAs in HeLa cells and human platelets from coronary artery disease patients. C18:1-CoA was found to be the most abundant acyl-CoA determined by this method in HeLa cells. Results show that HeLa cells and human platelet samples have a significantly different acyl-CoA profile (representative chromatograms of platelet samples are shown in Figure 6 and of HeLa cells in Figure S16) (Figure 7). In a pilot study, a comparison between acyl-CoA profiles of healthy donors (Figure 7B) and coronary artery diseases (CAD) patients (Figure 7C) revealed significant alterations. While the concentrations of the long-chain acyl-CoAs (C16:0, C18:0, C18:1) are comparable in healthy donors and CAD patients, platelets of CAD patients show high levels of medium-chain acyl-CoAs (in particular, C8:0 and C12:0) and in addition detectable quantities of very-long-chain acyl-CoAs (C20:0 and C22:0). They are metabolized in peroxisomes through peroxisomal β-oxidation until they are chain-shortened to C8:0 acyl-CoA.[4] Its further fatty acid oxidation occurs under normal physiological conditions in mitochondria. It seems that a potential alteration in FAO disorder leads to elevated levels of medium-chain acyl-CoAs in the platelets of patients either attributed to age, oxidative status, and disease state.[34] This

https://dx.doi.org/10.1021/acs.analchem.1c00664
Anal. Chem. 2021, 93, 4342−4350

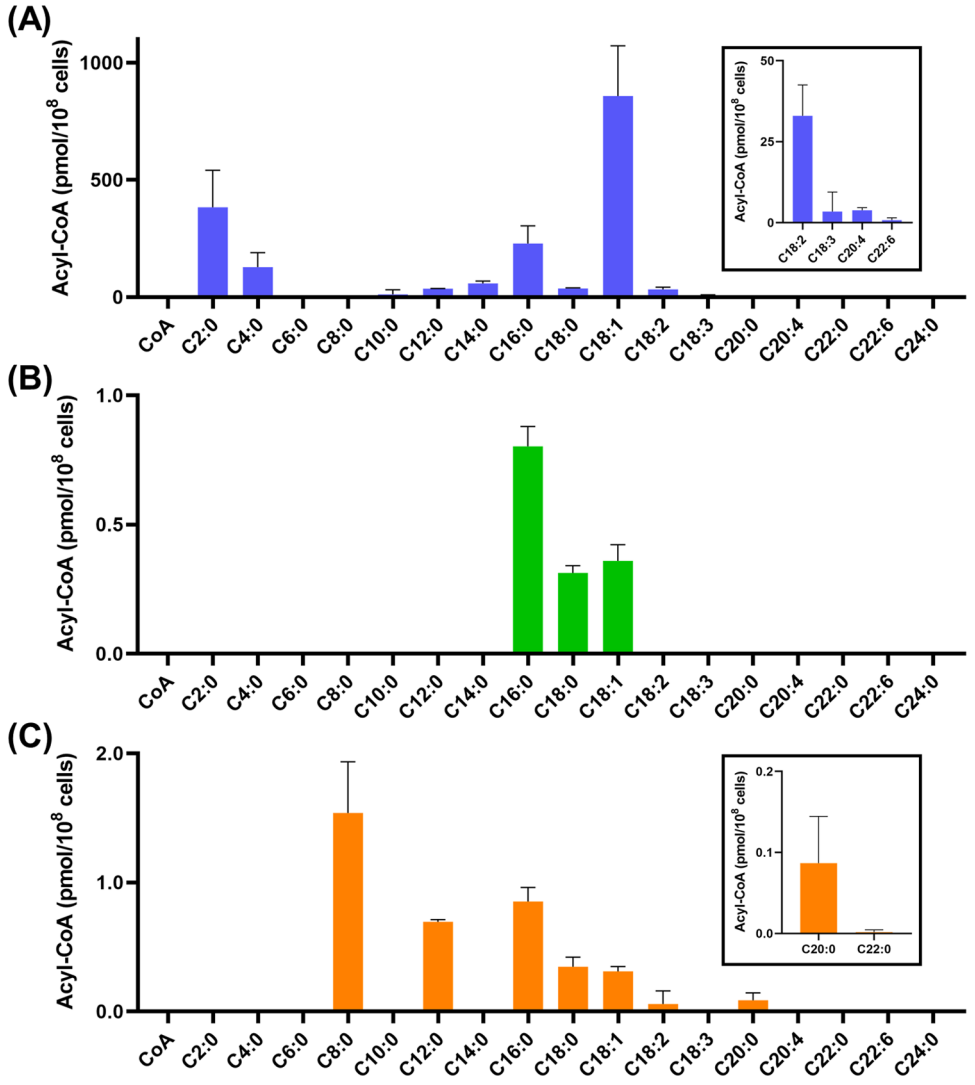

Figure 7. Acyl-CoAs determined in (A) HeLa cells (n = 3 biological replicates). (B) Human platelet sample (n = 3; from three different healthy donors). (C) Human platelet sample (n = 3; from three different patients with coronary artery disease).

aberrant metabolism has also some biochemical and clinical consequences, which are being currently elucidated.

CONCLUSIONS

Lipidomics analysis of acyl-CoAs in biological samples remains challenging due to their diverse acyl chains. Different chain lengths and unsaturation degrees make the development of extraction and chromatographic methods more complicated. The study presented here introduced a derivatization strategy for acyl-CoAs to improve chromatographic performance. Methylated acyl-CoAs were separated within a single RP-LC run with good peak shapes. Meanwhile, there was no need to include washing steps after multiple injections anymore because memory effects could be completely precluded. A mixed-mode SPE sample preparation protocol was developed and optimized accordingly. Uniformly, ^{13}C acyl-CoAs from yeast cells were taken as IS to compensate sample loss and ionization variation. As a proof of concept, this method was applied on cultured HeLa cells and human platelet samples. Acyl-CoAs in biological samples were detected and quantified effectively. Therefore, the developed method will be valuable for routine lipidomic analysis of broad acyl-CoA profiles. In scenarios of clinical analysis, it can help to better understand physiological and pathophysiological pathways involving acyl-CoAs, especially those affected by mitochondrial and peroxisomal dysfunction due to fatty acid oxidation disorders, but are commonly investigated indirectly at the acyl-carnitine level.[34] A direct method for comprehensive acyl-CoAs analysis, however, would be beneficial. In view of this concern, the current method is adapted at present for untargeted acyl-CoA profiling method in biological samples.

ASSOCIATED CONTENT

Supporting Information

The Supporting Information is available free of charge at https://pubs.acs.org/doi/10.1021/acs.analchem.1c00664.

Method information of high-resolution MS and enhanced product ion scan; tables of matrix effect, extraction recovery, and accuracy; comparison of C17:0-CoA product ion spectra before and after methylation; product ion spectra of selected acyl-CoAs with different collision energies; comparison of cell disruption approaches; autosampler stability test; and representa-

https://dx.doi.org/10.1021/acs.analchem.1c00664
Anal. Chem. 2021, 93, 4342−4350

tive chromatograms of internal standards and acyl-CoAs determined in HeLa cells (PDF)

AUTHOR INFORMATION

Corresponding Author

Michael Lämmerhofer − *Institute of Pharmaceutical Sciences, Pharmaceutical (Bio-)Analysis, University of Tübingen, 72076 Tübingen, Germany;* orcid.org/0000-0002-1318-0974; Phone: +49 7071 29 78793; Email: michael.laemmerhofer@uni-tuebingen.de; Fax: +49 7071 29 4565

Authors

Peng Li − *Institute of Pharmaceutical Sciences, Pharmaceutical (Bio-)Analysis, University of Tübingen, 72076 Tübingen, Germany;* orcid.org/0000-0002-4905-3993

Meinrad Gawaz − *Department of Cardiology and Angiology, University Hospital Tübingen, 72076 Tübingen, Germany*

Madhumita Chatterjee − *Department of Cardiology and Angiology, University Hospital Tübingen, 72076 Tübingen, Germany*

Complete contact information is available at: https://pubs.acs.org/10.1021/acs.analchem.1c00664

Author Contributions

M.L. and P.L. designed the study and the analytical method. P.L. performed the experiments and analyzed the data. The manuscript was written through contributions of both authors. M.C. isolated the platelet pellets from blood of human donors and provided the platelet samples for this work. M.G. organized funding through the TRR 240 collaborative research project on platelets.

Notes

The authors declare no competing financial interest.

ACKNOWLEDGMENTS

P.L. gratefully acknowledges the support from the China Scholarship Council (grant number 201807060010). This project was partly funded by the German Research Foundation (DFG, Deutsche Forschungsgemeinschaft), project number 374031971-TRR 240.

REFERENCES

(1) Fahy, E.; Subramaniam, S.; Murphy, R. C.; Nishijima, M.; Raetz, C. R. H.; Shimizu, T.; Spener, F.; Van Meer, G.; Wakelam, M. J. O.; Dennis, E. A. *J. Lipid Res.* **2009**, *50*, S9−S14.

(2) Nochi, Z.; Olsen, R. K. J.; Gregersen, N. *J. Inherited Metab. Dis.* **2017**, *40*, 641−655.

(3) Ellis, J. M.; Li, L. O.; Wu, P.-C.; Koves, T. R.; Ilkayeva, O.; Stevens, R. D.; Watkins, S. M.; Muoio, D. M.; Coleman, R. A. *Cell Metab.* **2010**, *12*, 53−64.

(4) Grevengoed, T. J.; Klett, E. L.; Coleman, R. A. *Annu. Rev. Nutr.* **2014**, *34*, 1−30.

(5) Li, L. O.; Klett, E. L.; Coleman, R. A. *Biochim. Biophys. Acta, Mol. Cell Biol. Lipids* **2010**, *1801*, 246−251.

(6) Deutsch, J.; Grange, E.; Rapoport, S. I.; Purdon, A. D. *Anal. Biochem.* **1994**, *220*, 321−323.

(7) Woldegiorgis, G.; Spennetta, T.; Corkey, B. E.; Williamson, J. R.; Shrago, E. *Anal. Biochem.* **1985**, *150*, 8−12.

(8) Rivera, L. G.; Bartlett, M. G. *Anal. Methods* **2018**, *10*, 5252−5264.

(9) Morin-Rivron, D.; Christinat, N.; Masoodi, M. *Rapid Commun. Mass Spectrom.* **2017**, *31*, 344−350.

(10) Schriewer, A.; Cadenas, C.; Hayen, H. *J. Sep. Sci.* **2017**, *40*, 4303−4310.

(11) Neubauer, S.; Chu, D. B.; Marx, H.; Sauer, M.; Hann, S.; Koellensperger, G. *Anal. Bioanal. Chem.* **2015**, *407*, 6681−6688.

(12) Onorato, J. M.; Chen, L.; Shipkova, P.; Ma, Z.; Azzara, A. V.; Devenny, J. J.; Liang, N.; Haque, T. S.; Cheng, D. *Anal. Bioanal. Chem.* **2010**, *397*, 3137−3142.

(13) Speziale, R.; Montesano, C.; De Leonibus, M. L.; Bonelli, F.; Fezzardi, P.; Beconi, M. G.; Monteagudo, E.; Elbaum, D.; Orsatti, L. *J. Chromatogr. B* **2018**, *1083*, 57−62.

(14) Haynes, C. A.; Allegood, J. C.; Sims, K.; Wang, E. W.; Sullards, M. C.; Merrill, A. H. *J. Lipid Res.* **2008**, *49*, 1113−1125.

(15) Magnes, C.; Sinner, F. M.; Regittnig, W.; Pieber, T. R. *Anal. Chem.* **2005**, *77*, 2889−2894.

(16) Zimmermann, M.; Thormann, V.; Sauer, U.; Zamboni, N. *Anal. Chem.* **2013**, *85*, 8284−8290.

(17) Seifar, R. M.; Ras, C.; Deshmukh, A. T.; Bekers, K. M.; Suarez-Mendez, C. A.; da Cruz, A. L. B.; van Gulik, W. M.; Heijnen, J. J. *J. Chromatogr. A* **2013**, *1311*, 115−120.

(18) Purves, R. W.; Ambrose, S. J.; Clark, S. M.; Stout, J. M.; Page, J. E. *J. Chromatogr. B* **2015**, *980*, 1−7.

(19) Wang, S.; Wang, Z.; Zhou, L.; Shi, X.; Xu, G. *Anal. Chem.* **2017**, *89*, 12902−12908.

(20) Abrankó, L.; Williamson, G.; Gardner, S.; Kerimi, A. *J. Chromatogr. A* **2018**, *1534*, 111−122.

(21) Cebo, M.; Schlotterbeck, J.; Gawaz, M.; Chatterjee, M.; Lämmerhofer, M. *Anal. Chim. Acta* **2020**, *1094*, 57−69.

(22) Oku, N.; Takada, K.; Fuller, R. W.; Wilson, J. A.; Peach, M. L.; Pannell, L. K.; McMahon, J. B.; Gustafson, K. R. *J. Am. Chem. Soc.* **2010**, *132*, 10278−10285.

(23) Clark, J.; Anderson, K. E.; Juvin, V.; Smith, T. S.; Karpe, F.; Wakelam, M. J. O.; Stephens, L. R.; Hawkins, P. T. *Nat. Methods* **2011**, *8*, 267−272.

(24) Lee, J. C.; Byeon, S. K.; Moon, M. H. *Anal. Chem.* **2017**, *89*, 4969−4977.

(25) Yang, X.; Ma, Y.; Li, N.; Cai, H.; Bartlett, M. G. *Anal. Chem.* **2017**, *89*, 813−821.

(26) Magnes, C.; Sinner, F. Liquid Chromatography-Mass Spectrometry of Acyl-CoAs. In *Encyclopedia of Lipidomics*; Wenk, M. R., Ed.; Springer Netherlands: Dordrecht, 2017; pp 1−6.

(27) Minkler, P. E.; Kerner, J.; Ingalls, S. T.; Hoppel, C. L. *Anal. Biochem.* **2008**, *376*, 275−276.

(28) Neubauer, S.; Haberhauer-Troyer, C.; Klavins, K.; Russmayer, H.; Steiger, M. G.; Gasser, B.; Sauer, M.; Mattanovich, D.; Hann, S.; Koellensperger, G. *J. Sep. Sci.* **2012**, *35*, 3091−3105.

(29) Rampler, E.; Coman, C.; Hermann, G.; Sickmann, A.; Ahrends, R.; Koellensperger, G. *Analyst* **2017**, *142*, 1891−1899.

(30) Rampler, E.; Criscuolo, A.; Zeller, M.; El Abiead, Y.; Schoeny, H.; Hermann, G.; Sokol, E.; Cook, K.; Peake, D. A.; Delanghe, B.; et al. *Anal. Chem.* **2018**, *90*, 6494−6501.

(31) Matuszewski, B. K.; Constanzer, M. L.; Chavez-Eng, C. M. *Anal. Chem.* **2003**, *75*, 3019−3030.

(32) Bioanalytical Method Validation Guidance for Industry, FDA, US Department of Health and Human Services 2018. https://www.fda.gov/files/drugs/published/Process-Validation--General-Principles-and-Practices.pdf.

(33) Guideline on bioanalytical method validation, EMA, 2011. https://www.ema.europa.eu/en/documents/scientific-guideline/guideline-bioanalytical-method-validation_en.pdf.

(34) Chatterjee, M.; Rath, D.; Schlotterbeck, J.; Rheinlaender, J.; Walker-Allgaier, B.; Alnaggar, N.; Zdanyte, M.; Muller, I.; Borst, O.; Geisler, T.; et al. *Eur. Heart J.* **2017**, *38*, 1993−2005.

Supporting information

Targeted profiling of short-, medium- and long-chain fatty acyl-Coenzyme As in biological samples by phosphate methylation coupled to liquid chromatography–tandem mass spectrometry

Peng Li[a], Meinrad Gawaz[b], Madhumita Chatterjee[b], Michael Lämmerhofer [a]*

[a] Institute of Pharmaceutical Sciences, Pharmaceutical (Bio-)Analysis, University of Tübingen, Tübingen, Germany

[b] Department of Cardiology and Angiology, University Hospital Tübingen, 72076 Tübingen, Germany

***Author for correspondence:**

Prof. Michael Lämmerhofer
Pharmaceutical (Bio-)Analysis
Institute of Pharmaceutical Sciences
University of Tuebingen
Auf der Morgenstelle 8
72076 Tuebingen, Germany
Tel: +49 7071 29 78793, Fax: +49 7071 29 4565
e-mail: michael.laemmerhofer@uni-tuebingen.de
http://www.bioanalysis.uni-tuebingen.de/

Table of Contents

Text T1. High-resolution MS (TripleTOF) method.

Separation was performed on a 1290 Infinity UHPLC system (Agilent Technologies, Waldbronn, Germany) with a Kinetex C18 column (100 mm × 3.0 mm, 2.6 μm, 100 Å) and a KrudKatcher Ultra HPLC in-line filter (0.5 μm) (Phenomenex, Torrance, CA, USA). Mobile phase A was 10 mM ammonium acetate in water. Mobile phase B was methanol. Gradient elution (0.0 min, 10% B; 2 min, 10% B; 15 min, 100% B; 20 min, 100% B; 21 min, 10% B; 25 min, 10% B) was carried out at a flow rate of 0.8 mL/min and a constant column temperature of 40℃. Injection volume was 20 μL. Derivatization and fragmentation studies of methylated acyl-CoAs were conducted with the above chromatographic system hyphenated to a TripleTOF 5600+ mass spectrometer with a DuoSpray source (Sciex, Concord, ON, Canada) operated with the ESI probe. Ion source parameters were as follows: curtain gas (N2) 25 psi, nebulizer gas (N2) 30 psi; heater gas (N2) 25 psi, ion source voltage +5500 V (positive mode) and source temperature 500 °C. Information dependent acquisition (IDA) product ion scan mode was adopted. Inclusion list was as follow:

Precursor ions, m/z	838.2	924.2	866.2	880.2	1062.4	1066.4	1076.4	1090.4	1174.5	1188.6
Rt, Min	6.89	6.98	6.99	7.61	14.09	14.08	14.32	14.53	15.45	15.56

Text T2. Information dependent acquisition (IDA) - Enhanced product ion scan (EPI) method.

The chromatography part was the same as specified in the method section. Enhanced product ion (EPI) acquisition was performed on a QTRAP 4500 mass spectrometer with a Turbo V source (Sciex) operated with ESI probe. Data acquisition was performed with the following parameters: collision gas (N2) 12, curtain gas (N2) 20 psi, nebulizer gas (zero grade air) 35 psi; heater gas (zero grade air) 35 psi, ion source voltage 3500 V (positive mode) and source temperature 500 °C; scheduled selected reaction monitoring (sSRM) – IDA - EPI was used. The detection window was 30 s around RT. IDA threshold: intensity, 1000; Exclusion time table, Never; Mass tolerance, 250 mDa; Dynamic background subtraction, TRUE. sSRM list was as follows:

Acyl-CoAs	Q1 (m/z)	Q3 (m/z)	Rt (min)	DP (V)	CE (V)	CXP (V)
CoA-SH	838.2	275.1	6.89	80	45	20
Malonyl	924.2	361.1	6.98	80	45	20
C2:0	866.2	303.1	6.99	80	45	20
C3:0	880.2	317.2	7.61	80	45	20
C16:0	1062.4	499.4	14.09	80	50	25
C16(d4):0	1066.5	503.5	14.08	80	50	25
C17:0	1076.4	513.4	14.32	80	50	25
C18:0	1090.4	527.4	14.53	80	50	25
C24:0	1174.5	611.5	15.45	80	55	30
C25:0	1188.6	625.5	15.56	80	55	35

Table S1. Matrix effects of QCs without IS at three different concentration levels in HeLa cells (n=3) (investigated as described in ref. 25 of the main document; comparison of post-extraction spike and standard solution).

Matrix effect, %	C3:0	C16(d4):0	C17:0	C25:0
QC1 (~3 x LLOQ)	75.6 ± 11.3	350.4 ± 10.2	485.3 ± 12.3	154.7 ± 9.4
QC2 (low)	72.4 ± 9.1	317.7 ± 13.7	507.4 ± 8.1	144.3 ± 13.2
QC3 (medium)	81.9 ± 12.4	347.3 ± 11.7	467.4 ± 10.6	137.7 ± 7.3
QC4 (high, ULOQ)	79.7 ± 10.5	316.2 ± 9.6	473.7 ± 13.6	153.7 ± 11.7

Note: Concentrations of QC1, QC2, QC3 and QC4, for C3:0-CoA: 56 nM, 112 nM, 562 nM and 2248 nM; for C16(d4):0-CoA: 23 nM, 94nM, 471 nM and 1885nM; for C17:0-CoA: 23 nM, 93 nM, 467 nM and 1867 nM; for C25:0-CoA: 21 nM, 42 nM, 211 nM and 845 nM.

Table S2. Matrix effects of QCs with IS at three different concentration levels in HeLa cells (n=9) (investigated as described in ref. 25 of the main document but based on peak area ratios of analytes and U13C-labelled IS).

Matrix effect, %	C3:0	C16(d4):0	C17:0	C25:0
QC1 (~3 x LLOQ)	92.6 ± 8.7	103.1 ± 9.2	101.1 ± 6.7	110.4 ± 7.3
QC2 (low)	91.4 ± 11.3	105.7 ± 11.5	102.2 ± 11.3	103.3 ± 7.6
QC3 (medium)	94.3 ± 11.9	97.8 ± 7.9	93.4 ± 12.6	98.7 ± 10.3
QC4 (high, ULOQ)	89.7 ± 8.4	106.4 ± 12.4	106.3 ± 13.4	103.7 ± 13.6

Table S3. Extraction recoveries of QCs at three different concentration levels in HeLa cells (n=9) (investigated as described in ref. 25 of the main document; comparison of post-extraction spike and pre-extraction spike).

Extraction recovery, %	C3:0	C16(d4):0	C17:0	C25:0
QC1 (~3 x LLOQ)	68.3 ± 13.5	64.3 ± 11.5	55.3 ± 6.7	45.1 ± 11.8
QC2 (low)	74.1 ± 11.5	69.1 ± 12.4	56.7 ± 11.4	49.3 ± 8.9
QC3 (medium)	76.1 ± 10.3	71.3 ± 10.6	63.4 ± 13.7	43.4 ± 11.9
QC4 (high, ULOQ)	69.3 ± 9.7	66.8 ± 12.9	61.7 ± 8.3	51.4 ± 14.1

Table S4. Accuracy & precision QCs at three different concentration levels in HeLa cells (n=9).

Accuracy and precision, %	C3:0		C16(d4):0		C17:0		C25:0	
	Intra-day	Inter-day	Intra-day	Inter-day	Intra-day	Inter-day	Intra-day	Inter-day
QC1 (~3 x LLOQ)	91.3 ± 12.1	97.3 ± 10.9	103.1 ± 13.4	109.3 ± 14.3	103.4 ± 9.7	101.1 ± 13.3	107.3 ± 10.3	102.1 ± 9.3
QC2 (low)	97.3 ± 13.7	98.3 ± 13.2	98.3 ± 10.6	103.4 ± 13.2	104.8 ± 10.1	104.4 ± 12.2	103.4 ± 11.6	97.1 ± 8.3
QC3 (medium)	95.1 ± 6.7	96.4 ± 14.8	96.4 ± 9.3	96.7 ± 10.7	96.1 ± 11.5	89.4 ± 14.3	92.1 ± 12.3	96.3 ± 10.1
QC4 (high, ULOQ)	94.3 ± 10.3	91.7 ± 10.7	98.6 ± 12.6	98.3 ± 11.6	98.4 ± 10.9	88.3 ± 12.6	93.4 ± 9.8	95.4 ± 11.8

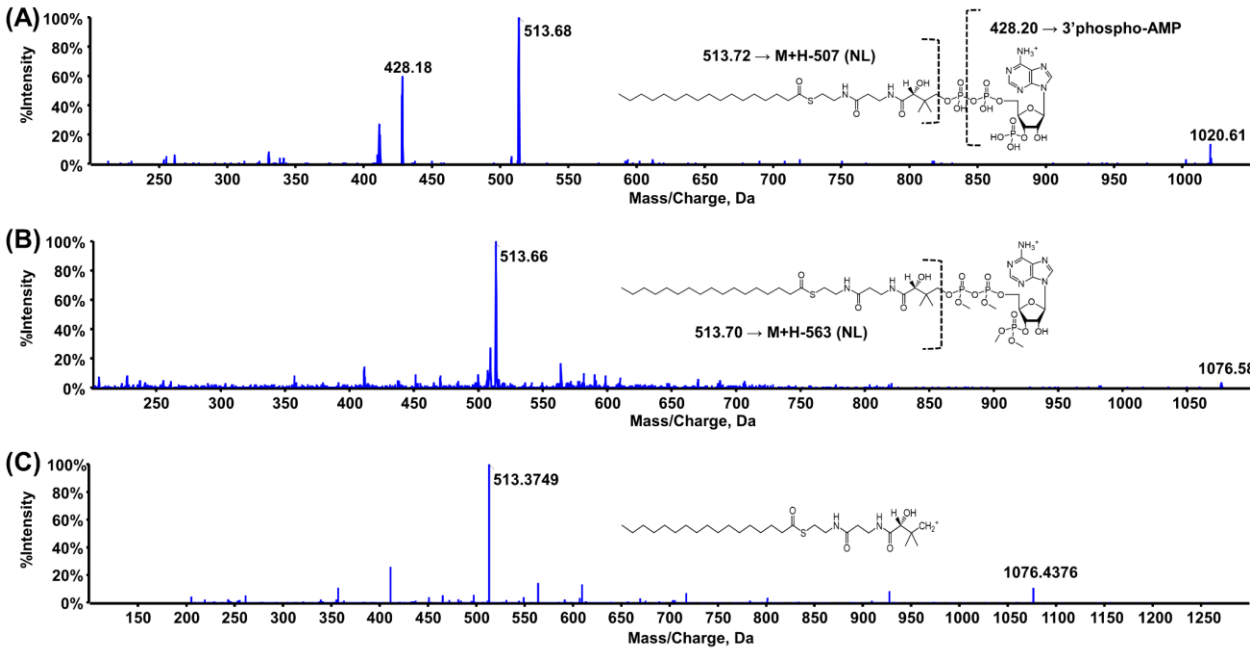

Figure S1. Product ion spectrum (QTRAP) of (A) C17:0-CoA and (B) methylated C17:0-CoA. (C) High resolution (QTOF) product ion spectrum of methylated C17:0-CoA.

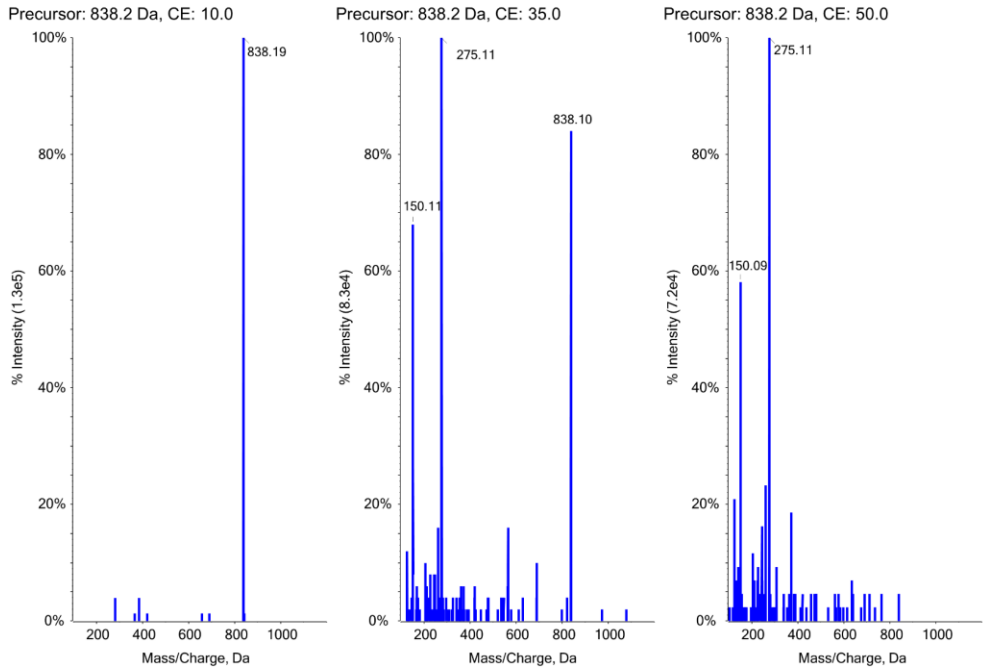

Figure S2. Product ion spectrum (QTRAP) of methylated free CoA under different collision energies.

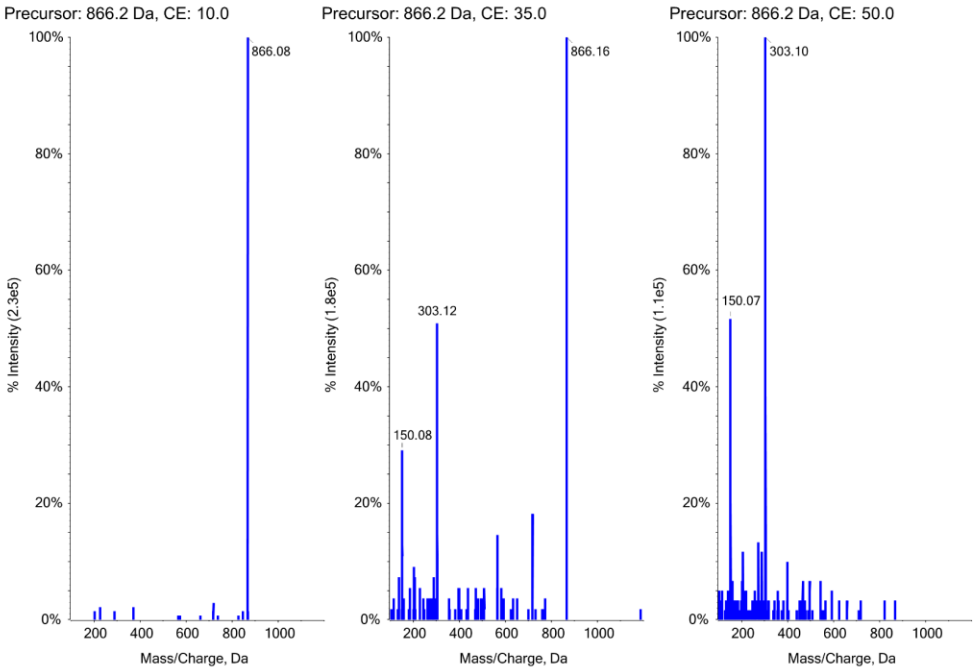

Figure S3. Product ion spectrum (QTRAP) of methylated C2:0-CoA under different collision energies.

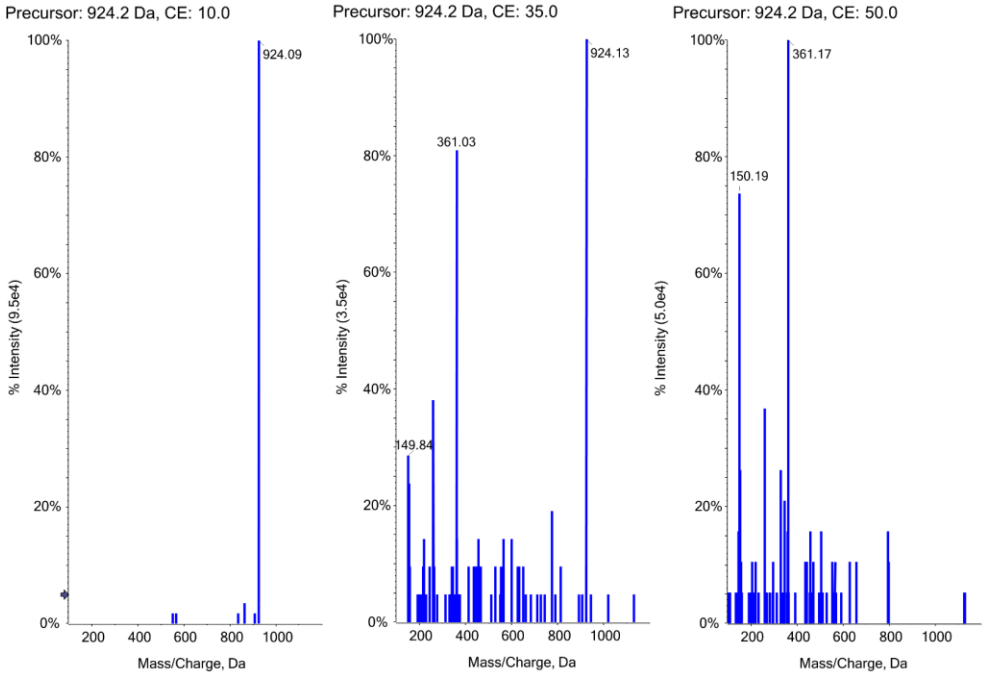

Figure S4. Product ion spectrum (QTRAP) of methylated Malonyl-CoA under different collision energies.

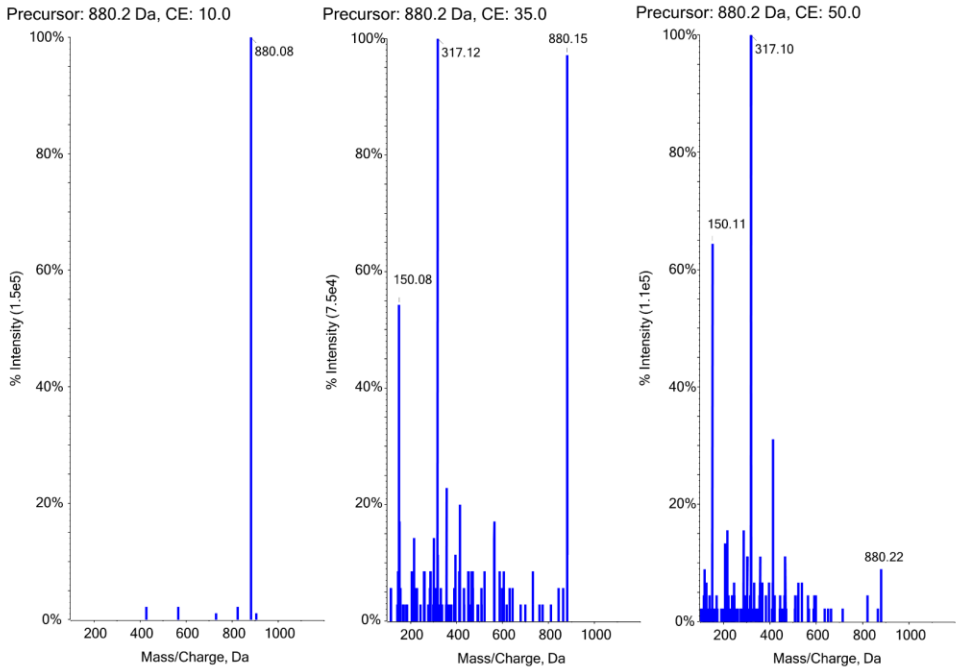

Figure S5. Product ion spectrum (QTRAP) of methylated C3:0-CoA under different collision energies.

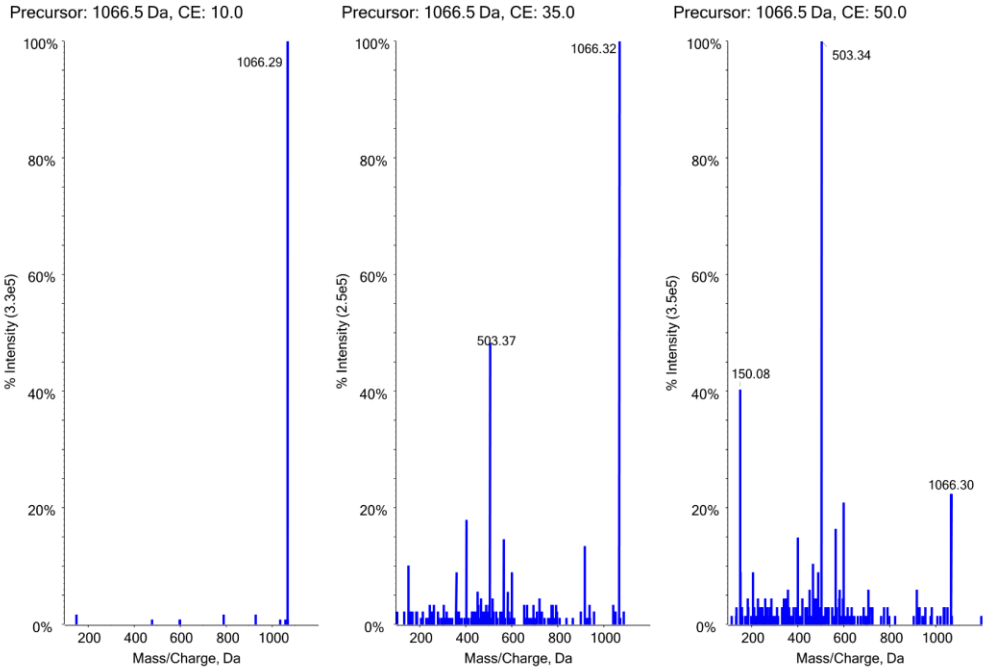

Figure S6. Product ion spectrum (QTRAP) of methylated C16(d4):0-CoA under different collision energies.

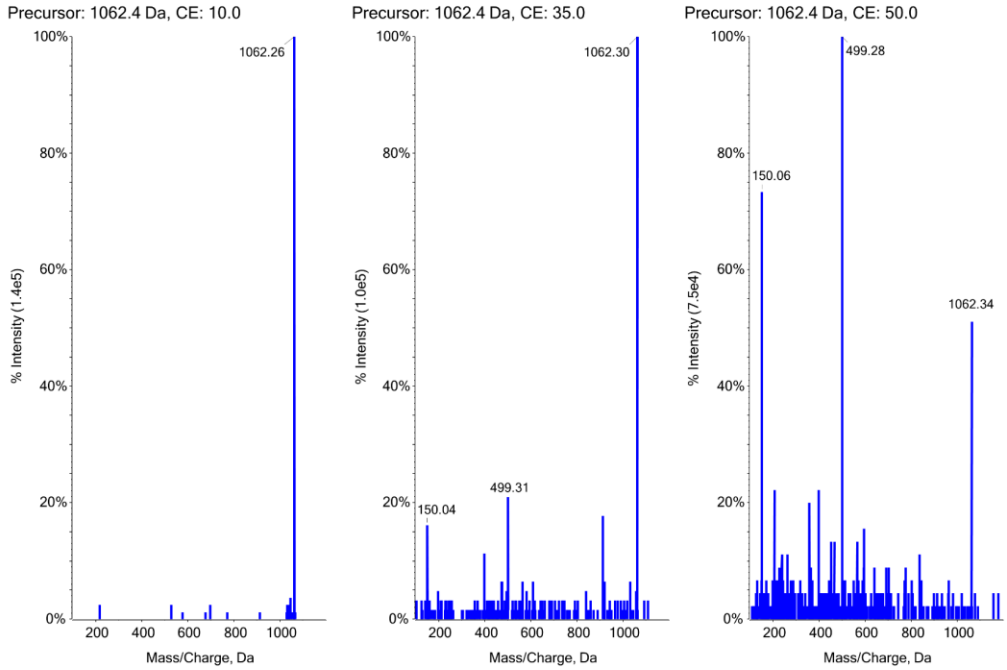

Figure S7. Product ion spectrum (QTRAP) of methylated C16:0-CoA under different collision energies.

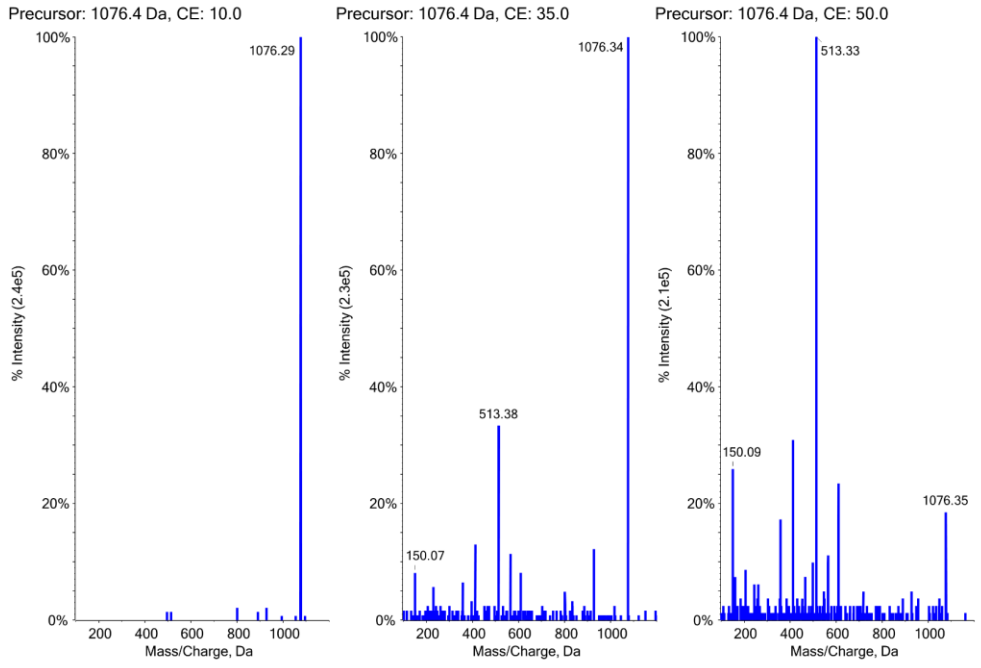

Figure S8. Product ion spectrum (QTRAP) of methylated C17:0-CoA under different collision energies.

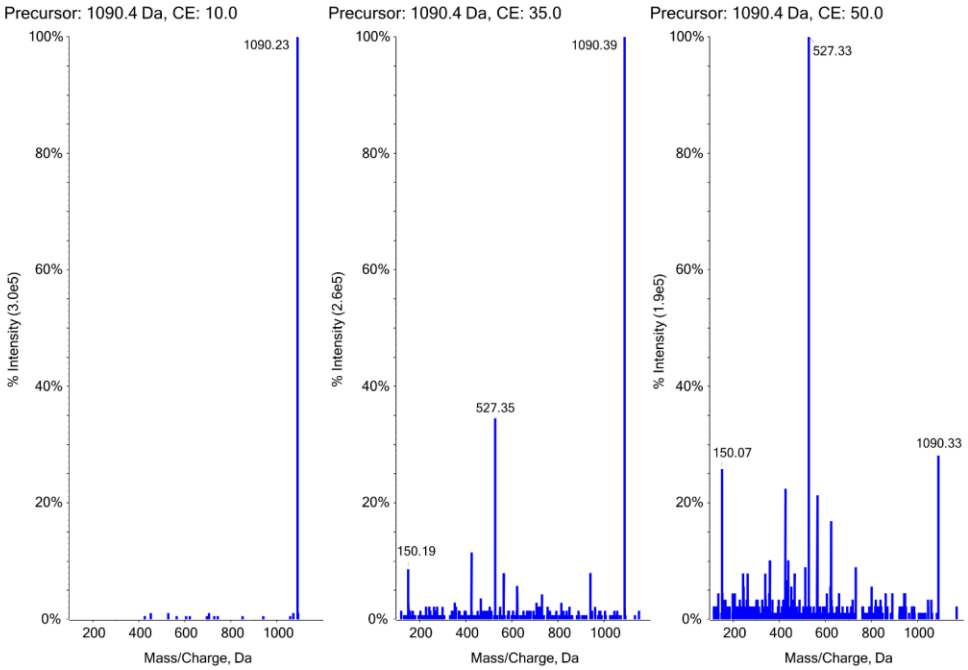

Figure S9. Product ion spectrum (QTRAP) of methylated C18:0-CoA under different collision energies.

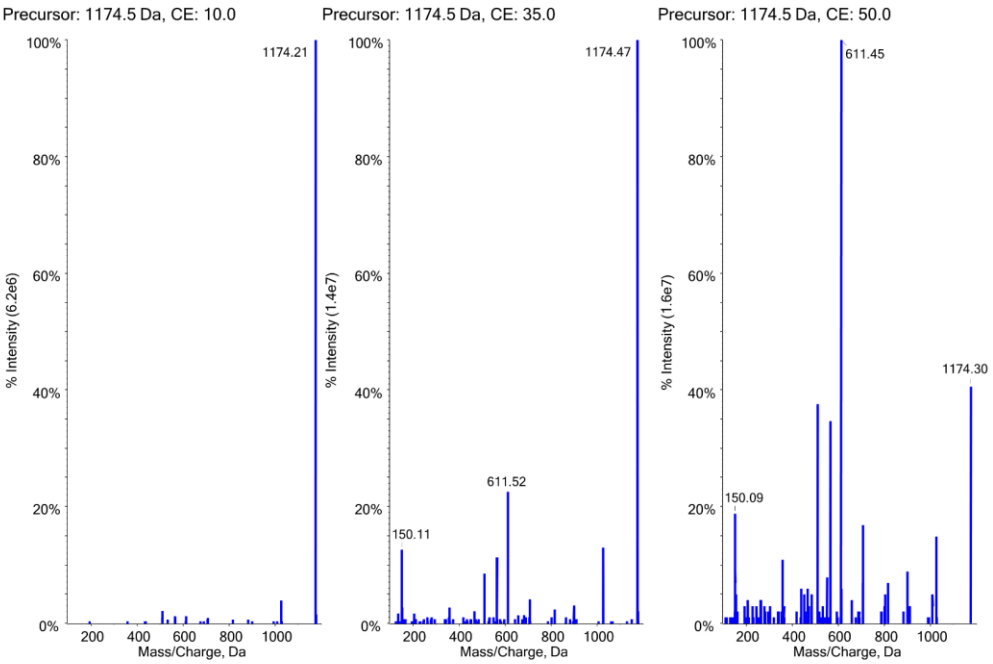

Figure S10. Product ion spectrum (QTRAP) of methylated C24:0-CoA under different collision energies.

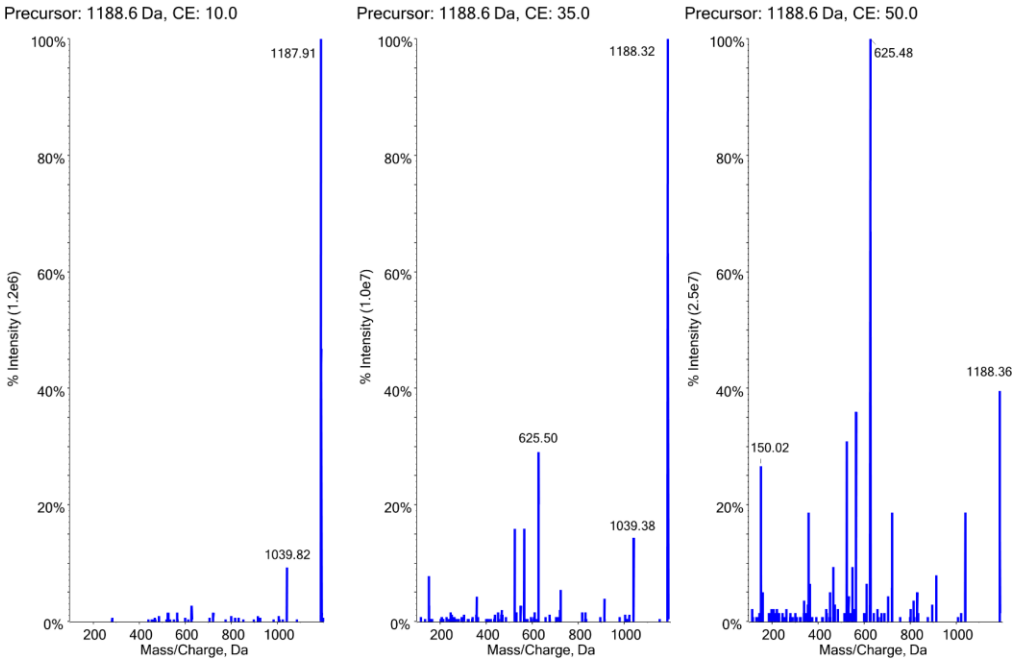

Figure S11. Product ion spectrum (QTRAP) of methylated C25:0-CoA under different collision energies.

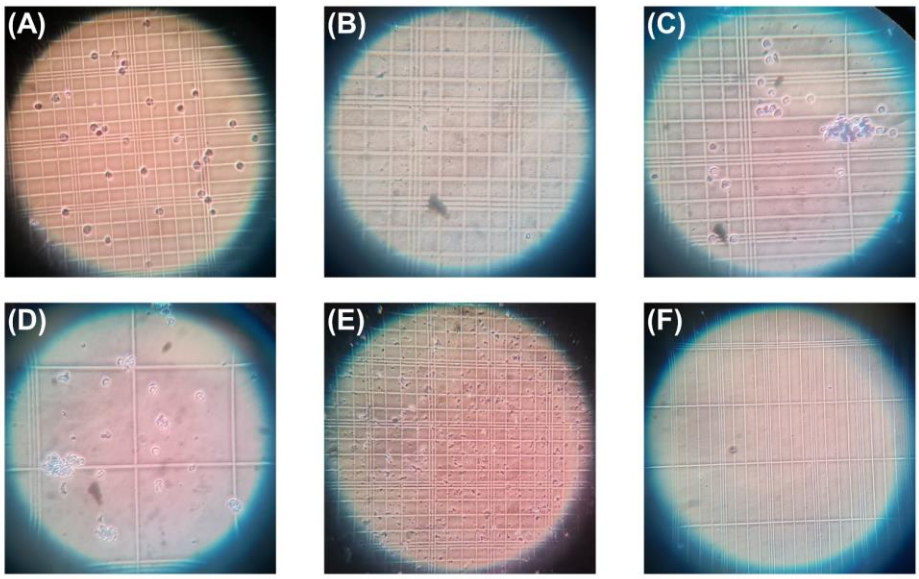

Figure S12. Microscopic test for cell lysis: (A) Negative control, PBS buffer incubation on ice for 5 min; (B) Positive control, RIPA buffer, sonication 30 s with sonication bath; (C) 5 cycles of 1min vortex, 2 min sonication in sonication bath and 1 min vortex; (D) Freeze-thaw, 2 min freeze with liquid nitrogen and 2 min vortex at 4 °C; (E) motor pellet pestle (Kimble®, DWK Life Sciences GmbH, Germany), 2 min maximum strength; (F) cell disruptor (Branson Sonifier B15, Branson Instruments Co., Stamford, USA), 1 min, 50% pulse mode at strength 5.

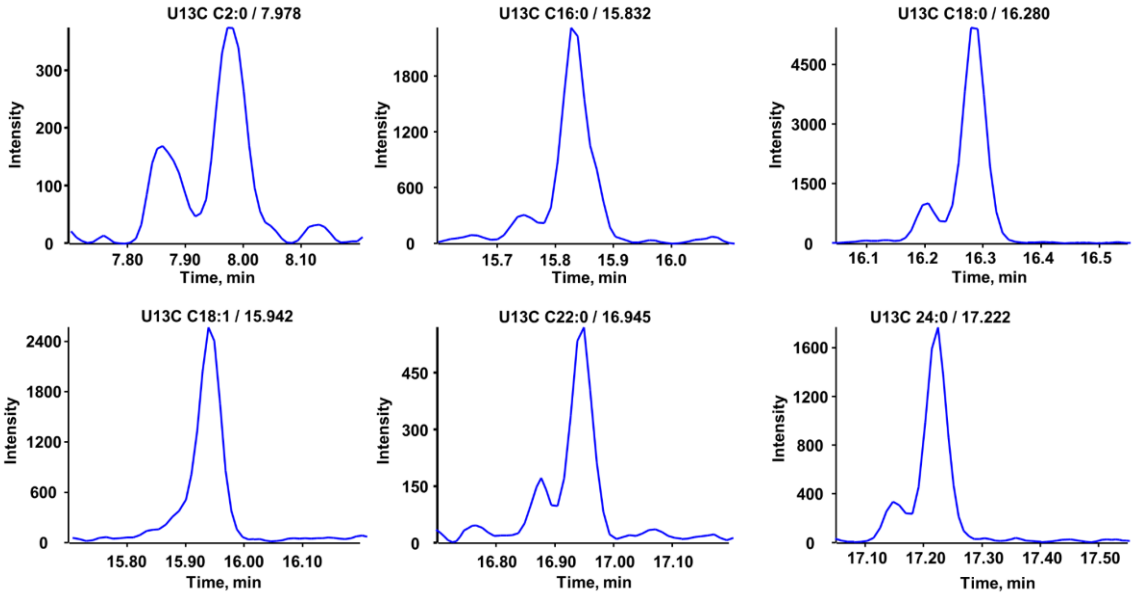

Figure S13. Representative chromatograms (EICs) of U13C labeled acyl-CoAs from yeast extract.

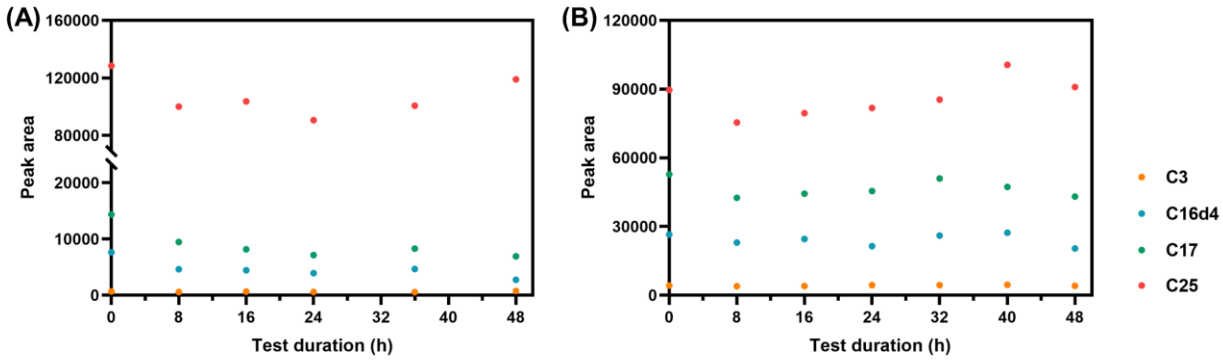

Figure S14. Auto sampler stability test (4 ℃) of methylated acyl-CoAs without (A) or with (B) matrix (HeLa cells).

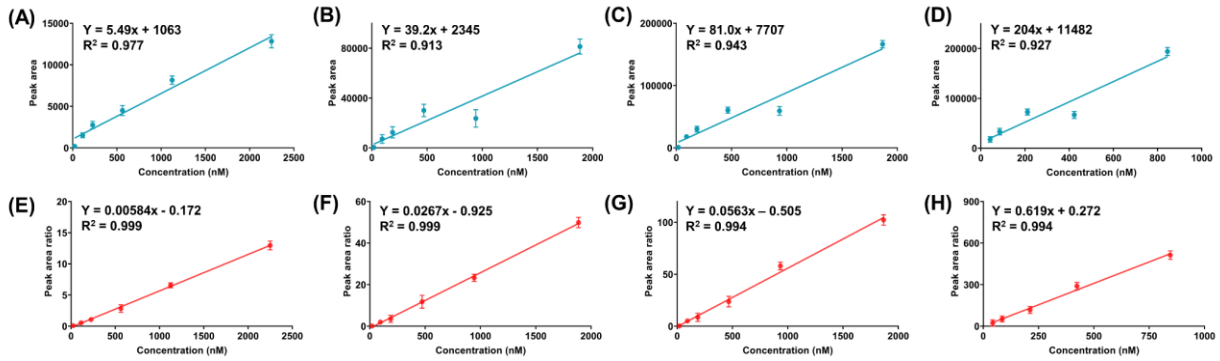

Figure S15. Calibration curves of C3:0 - (A, E), C16(d4):0- (B, E), C17:0- (C, G) and C25:0- (D, H) CoA without (upper row A-D) and with (lower row E-H) U-13C labeled internal standards. Calibration was performed based on peak area ratio of analyte and internal standard. No weighing was used.

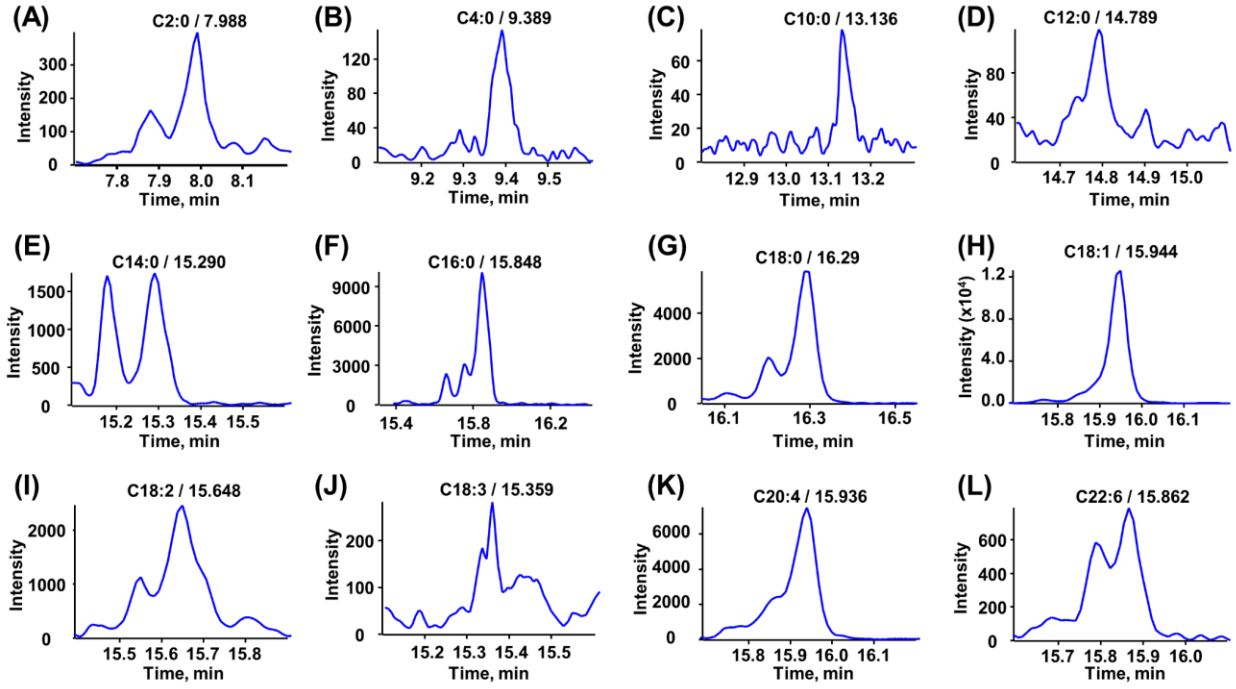

Figure S16. Representative chromatograms (EICs) of Acyl-CoAs determined in HeLa cells. Determined concentration were as follow. (A) C2:0-CoA, 383.3 nM. (B) C4:0-CoA, 127.6 nM. (C) C10:0-CoA, 34.6 nM. (D) C12:0-CoA, 36.3 nM. (E) C14:0-CoA, 58.6 nM. (F) C16:0-CoA, 228.3 nM. (G) C18:0-CoA, 36.7 nM. (H) C18:1-CoA, 857.2 nM. (I) C18:2-CoA, 33.1 nM. (J) C18:3-CoA, 10.4 nM. (K) C20:4-CoA, 55.7 nM. (L) C22:6-CoA, 22.4 nM.

10. Publication II

Isomer Selective Comprehensive Lipidomics Analysis of Phosphoinositides in Biological Samples by Liquid Chromatography with Data Independent Acquisition Tandem Mass Spectrometry

Peng Li, Michael Lämmerhofer *

Institute of Pharmaceutical Sciences, Pharmaceutical (Bio-)Analysis, University of Tübingen, 72076 Tübingen, Germany

Anal. Chem.

Year 2021, Volume 93, Issue 27, Pages 9583-9592

Doi: 10.1021/acs.analchem.1c01751

Graphical Abstract

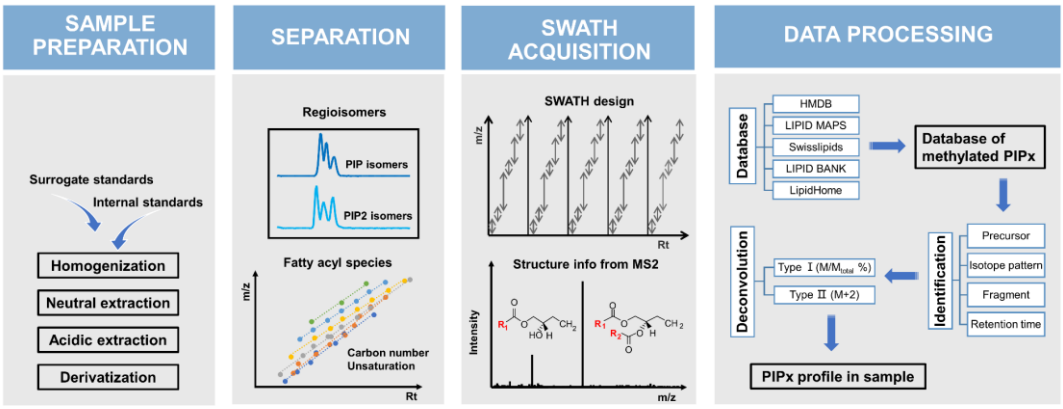

analytical chemistry

pubs.acs.org/ac Article

Isomer Selective Comprehensive Lipidomics Analysis of Phosphoinositides in Biological Samples by Liquid Chromatography with Data Independent Acquisition Tandem Mass Spectrometry

Peng Li and Michael Lämmerhofer*

Cite This: *Anal. Chem.* 2021, 93, 9583−9592 Read Online

ACCESS | Metrics & More | Article Recommendations | Supporting Information

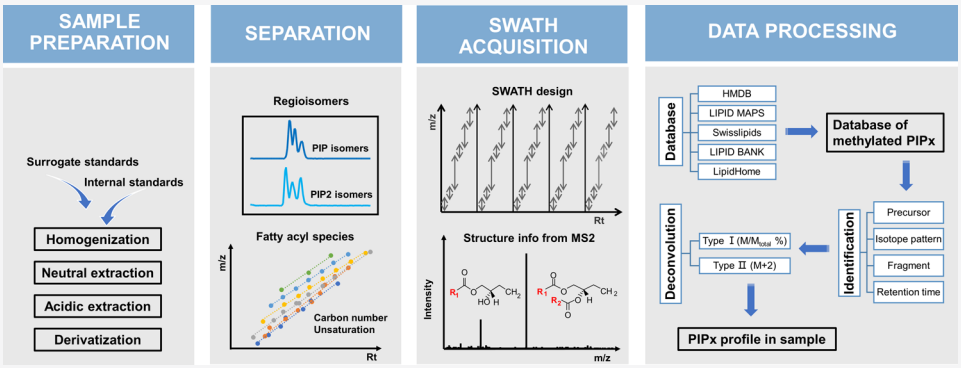

ABSTRACT: Phosphoinositides (PIPx) play central roles in membrane dynamics and signal transduction of key functions like cellular growth, proliferation, differentiation, migration, and adhesion. They are highly regulated through a network of distinct phosphatidylinositol phosphates consisting of seven groups and three regioisomers in two groups (PIP and PIP2), which arise from phosphorylation at 3′, 4′, and 5′ positions of the inositol ring. Numerous studies have revealed the importance of both fatty acyl chains, degree of phosphorylation, and phosphorylation positions under physiological and pathological states. However, a comprehensive analytical method that allows differentiation of all regioisomeric forms with different acyl side chains and degrees of phosphorylation is still lacking. Here, we present an integrated comprehensive workflow of PIPx analysis utilizing a chiral polysaccharide stationary phase coupled with electrospray ionization high-resolution mass spectrometry with a data independent acquisition technique using the SWATH technology. Correspondingly, a targeted data mining strategy in the untargeted comprehensively acquired MS and MS/MS data was developed. This powerful highly selective method gives a full picture of PIPx profiles in biological samples. Herein, we present for the first time the full PIPx profiles of NIST SRM1950 plasma, *Pichia pastoris* lipid extract, and HeLa cell extract, including profile changes upon treatment with potential PI3K inhibitor wortmannin. We also illustrate using this inhibitor that measurements of the PIPx profile averaged over the distinct regioisomers by analytical procedures, which cannot differentiate between the individual PIPx isomers, can easily lead to biased conclusions.

Lipidomics, a sub-discipline of metabolomics, uses analytical techniques to identify and quantify lipids in biological samples.[1] The ultimate goal of lipidomics is to explore underlying mechanisms of lipid metabolism and its (dys)regulation in pathologies and under physiological conditions.[2] As our understanding of lipids as highly dynamic structures with numerous signaling roles matures, the phosphoinositide (PIPx) pathways stand out as a biologically most intriguing, yet analytically extremely challenging metabolic network.[3−5] PIPx are commonly found in eukaryotic cells as low abundant phospholipids. The inter-relationship, conversion pathways, and involved enzymes have been reported previously.[6] Chemically, the family of PIPx is structurally closely related to phosphatidylinositol (PI) (Figure 1A). As shown in Figure 1B, derived from dynamic phosphorylation/dephosphorylation at positions 3′, 4′, and 5′ of the inositol ring of PI, PIPx comprise of seven groups (from the three lipid classes mono-, bis-, and trisphosphates), including phosphatidylinositol-3-phosphate (PI(3)P), phosphatidylinositol-4-phosphate (PI(4)P), phosphatidylinositol-5-phosphate (PI(5)P), phosphatidylinositol-3,4-bisphosphate (PI(3,4)P2), phosphatidylinositol-3,5-bisphosphate (PI(3,5)P2), phosphatidylinositol-4,5-bisphosphate (PI(4,5)P2), and

Received: April 24, 2021
Accepted: June 21, 2021
Published: June 30, 2021

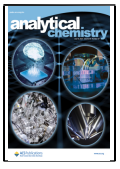

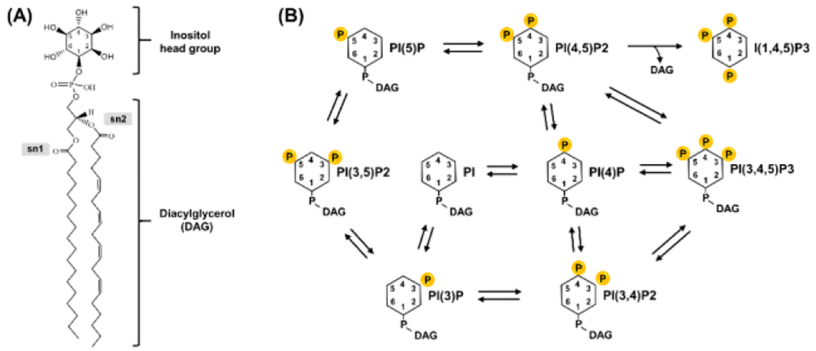

Figure 1. Phosphoinositide structure and metabolic network. (A) Chemical structure of phosphoinositide precursor PI (18:0/20:4 as an example for fatty acyl chains). (B) With reversible phosphorylation at positions 3′, 4′, and 5′ on the inositol ring, a highly dynamic pathway network is formed to regulate cellular processes.

phosphatidylinositol-3,4,5-trisphosphate (PI(3,4,5)P3). The PIPx network regulates a host of cellular activities, such as membrane trafficking, secretion, adhesion, migration, cell survival, and replication.[3−5] Phosphoinositide 3-kinases (PI3K), an enzyme that phosphorylates and activates PI(4,5)-P2 to PI(3,4,5)P3, may become a promising drug target due to its central role in tumor biology.[7−9] There are many ongoing clinical trials of various PI3K inhibitors for several types of cancer.[10,11] Apart from regioisomers on the inositol ring, the fatty acyl profile of PIPx was reported to have specific roles in metabolism.[12−15] Therefore, a lipidomics workflow, which is capable of separating all regioisomers and covering different fatty acyl species, is in great demand.

Although regioisomers on the inositol ring could be separated after chemical deacylation, structure information of fatty acyl chains is missing.[16] Mass spectrometry (MS) was introduced to characterize and measure intact PIPx.[17] Much efforts have been devoted to method development, including ion-pairing and normal phase conditions; satisfactory separation of regioisomers of intact PIP and PIP2 could, however, not be obtained.[18,19] As they are rich in phosphate groups, once extracted, the recovery of the PIPx is a significant problem because they are prone to bind to glassware and stainless steel.[20] Pettitt et al. attempted to alleviate these problems by silanization of all glassware and replacement of steel wherever possible. However, this cannot be complete and undoubtedly affected robustness of the method.[21] Clark et al. showed that TMS-diazomethane could be used to methylate the phosphate groups of PIPx, thus providing a first solution to the issues of stability and sensitivity.[22−24] Based on this derivatization strategy, the methylation pattern was explored and applied to distinguish some regioisomers of PIP and PIP2 except for PI(4)P and PI(5)P.[25] In order to separate regioisomers of PIPx, an ozonolysis procedure was applied to unsaturated PIPx after TMSD derivatization.[26] Although separation of PIP and PIP2 regioisomers could be achieved, sequential derivatization and separate LC methods are required. Additionally, ozonolysis only works on PIPx with double bonds. Most reported methods use specific select reaction monitoring (SRM) and neutral loss scan (NLS) for detection due to coelution of PIPx with the same acyl chain composition, including distinct groups and regioisomers.[27,28] Compared with predefined precursor-fragment transitions and low scan speed in SRM and NLS, data independent acquisition (DIA), such as sequential window acquisition of all theoretical mass spectra (SWATH), has advantages of broad compound coverage, fast acquisition speed, good dynamic range, relatively little method development, and potential of postacquisition data mining. Compared with wide application of SWATH in quantitative proteomics, SWATH analysis of small molecules like lipidomics was less reported.[29]

Here, we established a lipidomics workflow of PIPx. Separation of PIP and PIP2 regioisomers, comprehensive coverage of fatty acyl species, and isotope correction were realized. The workflow was validated and applied to profile PIPx in human plasma, *Pichia pastoris,* and cultured HeLa cells. Furthermore, the selectivity of PI3K inhibitor wortmannin on the PIPx profiles was investigated. We believe that the new workflow has the potential to advance the state of the art for PIPx measurements and could greatly facilitate the study of PIPx under physiological and pathological conditions.

METHODS

Materials. Acetonitrile, methanol (MeOH) of Ultra LC−MS grade, and zirconia/glass beads were supplied by Carl Roth (Karlsruhe, Germany). Ammonium formate, chloroform (CHCl3), methyl tert-butyl ether (MTBE), hydrochloric acid (HCl), and NIST SRM1950 plasma were supplied by Sigma−Aldrich (Saint-Louis, MO, USA). Trimethylsilyl diazomethane (TMSD) was obtained from Acros Chemicals (supplied by VWR, Bruchsal, Germany). Water (H2O) was purified with a Purelab Ultra purification system (ELGA LabWater, Celle, Germany). *Pichia pastoris* cells (strain CBS 7435) were obtained from ISOtopic Solutions (Vienna, Austria).

Odd fatty acyl chain phosphoinositide standards, including 1-heptadecanoyl-2-(5Z,8Z,11Z,14Z-eicosatetraenoyl)-sn-glycero-3-phospho-(1′-myo-inositol) (ammonium salt) (PI 17:0/20:4), 1-heptadecanoyl-2-(5Z,8Z,11Z,14Z-eicosatetraenoyl)-sn-glycero-3-phospho-(1′-myo-inositol-3′-phosphate) (ammonium salt) (PI(3)P 17:0/20:4), 1-heptadecanoyl-2-(5Z,8Z,11Z,14Z-eicosatetraenoyl)-sn-glycero-3-phospho-(1′-myo-inositol-4′-phosphate) (ammonium salt) (PI(4)P 17:0/20:4), 1-heptadecanoyl-2-(5Z,8Z,11Z,14Z-eicosatetraenoyl)-sn-glycero-3-phospho-(1′-myo-inositol-5′-phosphate) (ammonium salt) (PI(5)P 17:0/20:4), 1-heptadecanoyl-2-(5Z,8Z,11Z,14Z-eicosatetraenoyl)-sn-glycero-3-phospho-(1′-myo-inositol-3′,4′-bisphosphate) (ammonium salt) (PI(3,4)P2 17:0/20:4), 1-heptadecanoyl-2-(5Z,8Z,11Z,14Z-eicosatetraenoyl)-sn-glycero-3-phospho-(1′-myo-inositol-4′,5′-bisphosphate) (ammonium salt) (PI(4,5)P2 17:0/20:4), 1-heptadecanoyl-2-(5Z,8Z,11Z,14Z-eicosatetraenoyl)-sn-glycero-3-phospho-(1′-myo-inositol-3′,5′-bisphosphate) (ammonium salt)

https://doi.org/10.1021/acs.analchem.1c01751
Anal. Chem. 2021, 93, 9583−9592

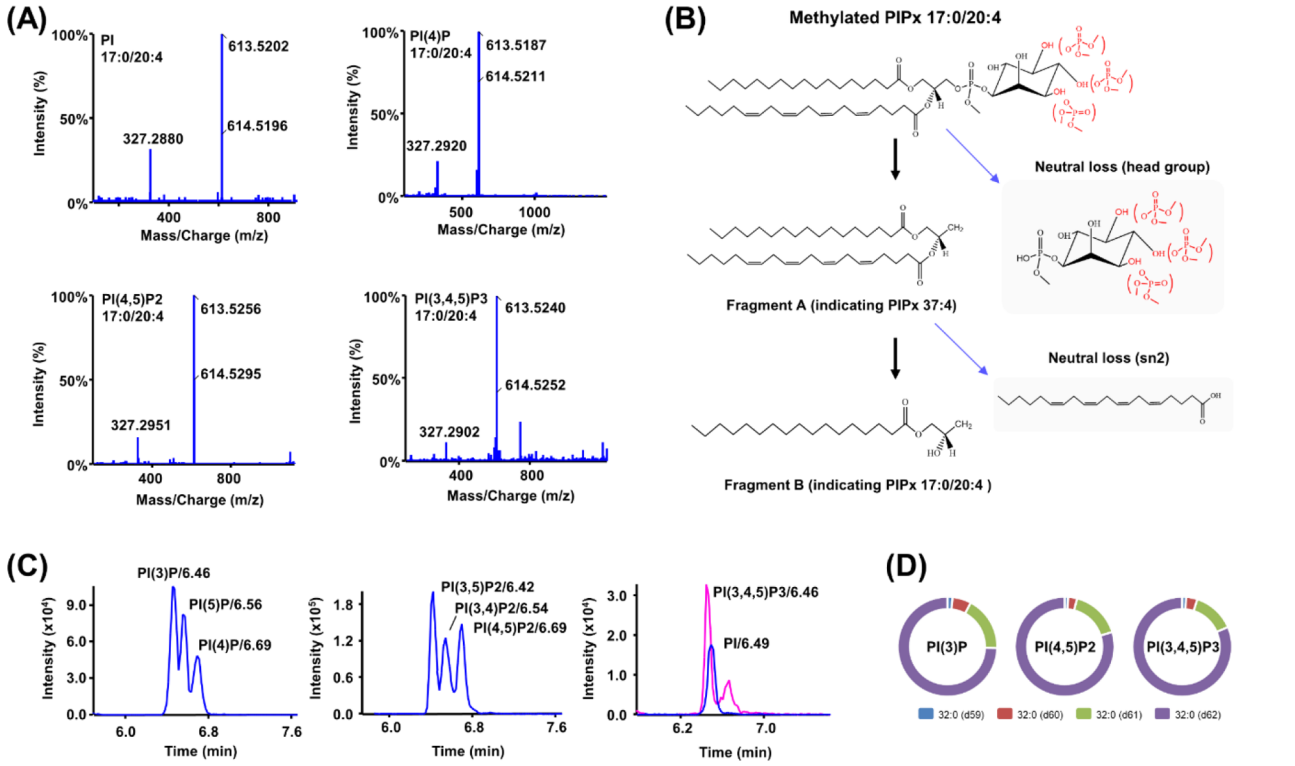

Figure 2. LC-ESI-MS analysis of methylated PIPx. (A) Product ion spectra of PI, PI(4)P, PI(4,5)P2, and PI(3,4,5)P3 with the same fatty acyl chains 17:0/20:4. (B) Reaction scheme of PIPx fragmentation behavior in positive ionization mode. Along with two neutral losses (methylated head group and sn2 fatty acyl), two characteristic fragments (A and B) were observed, providing information of the fatty acyl composition. (C) Chromatograms of PIP 17:0/20:4 regioisomers (left), PIP2 17:0/20:4 regioisomers (middle), and overlay of PI 17:0/20:4 and PI(3,4,5)P3 17:0/20:4 (right). (D) Characterization of stale isotope-labeled standards PI(3)P 16:0/16:0-d62, PI(4,5)P2 16:0/16:0-d62, and PI(3,4,5)P3 16:0/16:0-d62. After comprehensive analysis, standards were found to be mixtures of claimed PIPx with different deuterium degrees in C16:0 fatty acyl chains at the sn1 and sn2 positions (d1-d62), among which fully deuterated forms (d62) account for more than 74%.

(PI(3,5)P2 17:0/20:4), and 1-heptadecanoyl-2-(5Z,8Z,11Z,14Z-eicosatetraenoyl)-sn-glycero-3-phospho-(1′-myo-inositol-3′,4′,5′-trisphosphate) (ammonium salt) (PI-(3,4,5)P3 17:0/20:4), were obtained from Avanti Polar Lipids (Alabaster, AL, USA). Deuterated fatty acyl chain phosphoinositide standards, including 1,2-dipalmitoyl-sn-glycero-3-phospho-(1′-myo-inositol-3′-phosphate)-d62 (ammonium salt) (PI(3)P 16:0/16:0-d62), 1,2-dipalmitoyl-sn-glycero-3-phospho-(1′-myo-inositol-4′,5′-bisphosphate)-d62 (ammonium salt) (PI(4,5)P2 16:0/16:0-d62), and 1,2-dipalmitoyl-sn-glycero-3-phospho-(1′-myo-inositol-3′,4′,5′-trisphosphate)-d62 (ammonium salt) (PI(3,4,5) P316:0/16:0-d62), were purchased from Cayman Chemical (Ann Arbor, Michigan, USA). Odd fatty acyl chain standards were taken as surrogate calibration standards, while deuterated fatty acyl chain phosphoinositide standards were used as internal standards for the respective PIPx group. Surrogate calibration standards and internal standards were dissolved in CHCl3/MeOH/H2O (25:25:1, v/v/v) to give stock solutions of 100 and 25 μg/mL, respectively, except for PI 17:0/20:4 (which was supplied as 10 μg/mL methanol solution).

Preparation of HeLa Cells. The human cervical HeLa cells adapted to serum free conditions (AC free, ECACC 08011102) were grown in a humidified incubator at 37 °C with 5% CO2. Cells were fed with EX-CELL HeLa serum free media (Sigma Aldrich) with 2 mM L-glutamine (Sigma Aldrich), 12 unit/mL penicillin, and 12 μg/mL streptomycin until the cell density reached around 2 × 10^6 cells/mL. Cell counting was performed in triplicate with a hemocytometer. Aliquots of 10^6 HeLa cells were transferred into 2 mL homogenization tubes and spun down (100 g, 5 min at 4 °C). After removing the supernatant, cell pellets were washed twice with ice cold Dulbecco's Phosphate Buffered Saline (Sigma Aldrich) with repeated centrifugation. Cell samples were snap frozen in liquid nitrogen and kept at −80 °C till use.

PIPx Extraction. The desired samples were filled into homogenization tubes (e.g., 100 μL of plasma, 10^6 HeLa cells, or 50 mg of biomass of *Pichia pastoris*). Surrogate standards and internal standards were added prior to sample preparation. After adding 1.0 mL of prechilled CHCl3/MeOH (1:2, v/v) and 0.15 g of zirconia/glass beads, the samples were homogenized (6800 rpm, 1 min at 4 °C, 10 × 10 s, pause 30 s) with Precellys Evolution with Cryolys Evolution using dry ice cooling (Bertin Technologies, France). The samples were then spun down for 5 min (16,100 g at 4 °C). The supernatant was carefully removed. The residues were resuspended in 1365 μL of prechilled MTBE/MeOH/2 N HCl (200:60:13, v/v/v). The samples were homogenized at 4 °C for another 1 min, and 250 μL of 0.1 N HCl was added. The samples were vortexed at 4 °C for 5 min. After centrifugation (16,100 g, 5 min at 4 °C), the upper layer was transferred into fresh tubes and 500 μL of 0.01 N HCl was added. The upper layer was collected for phosphate methylation after 30 s vortexing at 4 °C followed by centrifugation (16,100 g, 5 min at 4 °C).

Phosphate Methylation. TMSD solution (50 μL; 2 M) was added to the PIPx extract from above. The samples were allowed to stand for 10 min at room temperature after brief

https://doi.org/10.1021/acs.analchem.1c01751
Anal. Chem. 2021, 93, 9583−9592

vortexing and fume release. The derivatization was quenched using 5 μL of glacial acetic acid. Methylated PIPx were washed twice with 500 μL of MeOH/H2O (1/1, v/v), including vortexing and centrifugation (16,100 g, 5 min at 4 °C). The samples were dried under N2 in an evaporator (Genevac EZ-2). After reconstitution with 50 μL of MeOH, facilitated by vortexing and sonication, the samples were submitted for LC−MS analysis.

SWATH Acquisition with UHPLC-TripleTOF MS. Chromatographic separation was performed using a 1290 Infinity UHPLC system (Agilent Technologies, Santa Clara, CA, USA) with a Daicel Chiralpak IB-U column (100 mm × 3.0 mm, 1.6 μm) and a KrudKatcher Ultra HPLC in-line filter (0.5 μm) (Phenomenex, Torrance, CA, USA). Mobile phases A and B were 10 mM ammonium formate in water and methanol, respectively. The gradient elution (0.0 min, 50% B; 5 min, 90% B; 10 min, 95% B; 10.1 min, 100% B; 12 min, 100% B; 12.1 min, 50% B; 15 min, 50% B) was carried out at a flow rate of 0.5 mL/min and a constant column temperature of 40 °C. Injection volume was 5 μL. MS detection was conducted with the above chromatographic system hyphenated to a TripleTOF 5600+ mass spectrometer with a DuoSpray source (Sciex, Framingham, MA, USA) operated with an ESI probe. Ion source parameters were as follows: curtain gas (N_2) 30 psi, nebulizer gas (zero grade air) 40 psi; heater gas (zero grade air) 50 psi, ion source voltage +3500 V (positive mode), and source temperature 500 °C. Sequential window acquisition of all theoretical fragment ion mass spectra (SWATH) experiments was performed to obtain comprehensive MS/MS data. Detailed information of SWATH windows can be found in Table S1.

Data Processing. Analyst 1.7 was used in both analytical systems for data acquisition and system control. Commercially available software packages PeakView (MasterView included) and MultiQuant (Sciex, Framingham, MA, USA) were involved in data processing. PeakView 2.2 was used for manual data evaluation and LC−MS performance check by comparing periodically with QC samples. MasterView 1.1 was used for identification. MultiQuant 3.0 was used for peak integration, linear regression, and concentration calculation. Statistical analysis and visualization were performed with R language.

RESULTS AND DISCUSSION

Development of a Comprehensive Workflow for PIPx Profiling. The challenges of PIPx determination by LC−MS mainly arise from the phosphate groups on the inositol ring. In-source fragmentation resulting in loss of phosphate moieties is usually inevitable in direct LC−MS measurements.[18] Due to a reactive phosphoester bond and rich negative charge, PIPx is prone to hydrolysis and phosphate migration, respectively, once isolated from cells or the biological matrix. This problem can be solved by derivatization of the phosphate groups with TMSD. Yet, this phosphate methylation does not alleviate the isomer selectivity problem of RPLC. The goal of this study was therefore to develop a method that also allows one to distinguish PIPx regioisomers. Initially, we examined the product ion spectra of PIPx with the same fatty acyl chains (17:0/20:4) in different groups, including PI, PI(4)P, PI(4,5)P2, and PI(3,4,5)P3. In positive mode (Figure 2A), methylated PIPx of different groups exhibited a similar fragmentation pattern. As illustrated in Figure 2B, after a neutral loss of methylated inositol phosphate, DAG species (glycerol backbone with fatty acyl chains) is the most abundant fragment (fragment A), which indicates the sum composition of the fatty acyl chains. The second fragment (fragment B) shows up when the collision energy is increased. Corresponding to results published before, fragment B is a charged glycerol backbone with a fatty acyl chain in the sn1 position.[30] These two fragments, along with the corresponding precursor ion, were then selected for identification, and both the precursor and fragment A were considered for quantification in MS1 and MS2 levels, respectively. Regioisomers of PIP (PI(3)P and PI(5)P) and PIP2 (PI(3,4)P2 and PI(3,5)P2) were subjected to derivatization followed by their MS2 spectral study. As illustrated in Figure S1, similar fragmentation behaviors were observed without characteristic fragments for the different isomers. A lower ionization efficiency in negative mode was observed compared to that in positive mode. As reported previously, fragments with one and two fatty acyl chains obtained from PIPx by loss of methylated inositol phosphates were found (Figure S2).[25] Therefore, positive ESI mode was adopted in the following workflow development. As shown in Figures S3 and S4, a flow injection method (TOF negative mode) was established to measure the original PIPx. Single charged and double charged ions were taken for further measurements of PIP and PIP2 and PIP3, respectively (in-source fragmentation was observed, data not shown). Methylation efficiency (Table S2) could be obtained from comparison of PIPx response before and after methylation. As summarized in Figure S5, methylation efficiency decreases from PIP to PIP3, and PI(3,5)P2 stands out among PIP2 regioisomers, while there is no significant difference observed for PIP regioisomers. These observations indicate that space resistance plays an important role in methylation efficiency, which could even override the increase of phosphate numbers.

Data acquisition was done by the SWATH technology. SWATH is a DIA technique, which collects MS2 data without bias for fragmentation of only the most abundant analytes (e.g., top 5) and allows for quantifiable signals not only at MS1 but MS2 as well, thus holding great potential for metabolomics and lipidomics study.[29] Precursors isolated within the specified MS range of the same SWATH window (typically intermediate width of 20−30 *m/z* units) are cofragmented. Hence, the direct relation of the fragment ions to their precursor ions is lost and must be re-established by a deconvolution approach. After deconvolution by grouping together matching chromatographic profiles of MS1 data in TOF-MS and MS2 data in SWATH windows (yielding peak groups), multidimensional data including precursor *m/z* values, precursor isotopic patterns, and fragments can be used for confident identification. Postacquisition data processing becomes possible along with flexible choices of data for quantification, which is favorable for comprehensive profiling the PIPx classes. At the same time, SWATH windows should be well designed to avoid two assay specificity problems. If quantification is conducted in the MS2 level, precursors from the same SWATH window, which generate the same fragment, cannot be distinguished by MS. For this reason, PIPx species from different classes but identical diacylglycerol residue are fragmented in distinct SWATH windows, which is ensured if they are narrower than 108 Da. If fragment B was selected for quantification, extremely narrow windows (e.g., 1 Da) would be required to distinguish the PIPx differing only in one double bond in the sn2 position (e.g., PIPx 18:0/20:4 and PIPx 18:0/20:3).

https://doi.org/10.1021/acs.analchem.1c01751
Anal. Chem. 2021, 93, 9583−9592

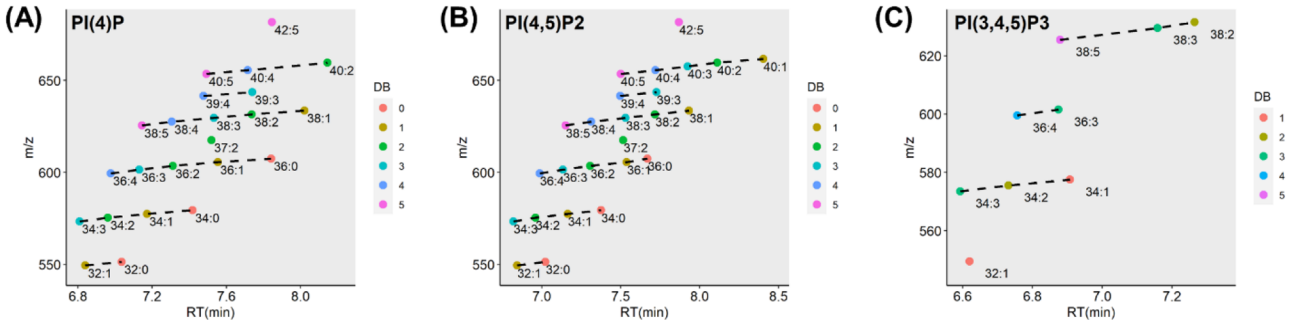

Figure 3. Feature plots of (A) PI(4)P, (B) PI(4,5)P2, and (C) PI(3,4,5)P3 in cultured HeLa cells.

Hence, in this work, quantitation was based on fragment A or the precursor ion, whatever is more selective or more sensitive, along with additional fatty acyl chain assignment from fragment B for full lipid species annotation. Detailed SWATH information is given in Table S1. Due to flexibility of the SWATH technique, another SWATH design (Table S2) is also recommended to have a wider coverage and better selectivity. By distributing accumulation time for varied SWATH windows, a wide mass range with narrower windows for PIPx species is obtained. In this untargeted approach, different SWATH methods with collision energy (CE) ranging from 30 to 105 V were tested (Figure S6). When different fragments are taken for quantification, the CE value should be optimized accordingly to ensure the maximum sensitivity. As a best compromise, a CE of 50 V was selected to gain more sensitivity for polyphosphorylated PIPx.

Since precursor and fragment ions are not paired directly, if quantitation on the MS2 level in SWATH is desired, another specificity problem arising from in-source fragmentation should be considered. Intact PIPx are prone to fragment within the ion source.[18] For evaluating the risk for in-source fragmentation after methylation, single PIPx (different groups and isomers) were methylated and measured. As illustrated in Figure S7, when extracted ion chromatograms of PI were generated, no peaks were found in PIP2 and PIP3 samples, while peaks in PI(3)P, PI(4)P, and PI(5)P samples have the same retention times (Rts) as the PI standard rather than Rts of the corresponding PIPs (as expected for the corresponding in-source fragments). No PIP peaks were observed in the PIP3 sample, while peaks found in PI(3,4)P2, PI(3,5)P2, and PI(4,5)P2 samples have the same Rts as the PIP Regio isomers rather than the PIP2 regioisomers. Also, PIP2 peaks found in the PIP3 sample matched Rts of PIP2 regioisomers rather than those of PIP3. These EIC peaks extracted are supposed to be impurities in the standards rather than in-source fragments. These results indicate there is low risk of in-source fragmentation after methylation in this method.

Regioisomer Separation with a Chiral Column. With the introduction of the TMSD derivatization strategy, much progress has been made regarding PIPx analysis, including stable isotope labeling derivatization,[28] methylation pattern recognition,[25] and fatty acyl chain profiling.[13,14] However, regioisomer separation has still been the bottleneck. Starting from TMSD derivatization, a reversed-phase approach was tested. As shown in Figure S8A, PIPx with the same fatty acyl chain (17:0/20:4) but of different groups from PI to PIP3 all coeluted. Additionally, regioisomers from the same group (PIP and PIP2) also coeluted (shown in Figure S8B,C, respectively). These results indicate that there is little selectivity with the typical RP mechanism.

A chiral column approach was then explored using polysaccharide chiral stationary phases. As shown in Figure S9, four chiral columns based on the chiral selector from two groups were tested (cellulose carbamate-based Chiralpak IB-U, IC-U and amylose carbamate-based Chiralpak IA-U, IG-U). From the obtained chromatograms with a linear screening gradient, it became evident that the cellulose-based columns have a better selectivity for PIPx regioisomers than the amylose-based ones. With an IC-U column, the PIP2 regioisomers could be nicely separated, but PI(4)P and PI(5)P coeluted even after optimization (data not shown). Interestingly, some single PIPx standards exhibited two peaks, for example, PI(3,4)P2 and PIP3 on IC-U. They might result from different stereoisomers of the inositol ring[31,32] but needs further elucidation. IB-U was selected for further method development. LC conditions were optimized to realize adequate separation of PIPx regioisomers within one run. As shown in Figure 2C, PIPx with the same fatty acyl chains but different degrees of phosphorylation exhibit an overlapping elution pattern across the different groups. However, they can be distinguished by MS owing to their distinct precursor ion *m/z* and fragments in distinct SWATH windows. This intergroup pattern is also found for other fatty acyl species from real samples. Typically, PI, PI(3)P, PI(3,5)P2, and PIP3 overlap in retention time, while PI(5)P and PI(4)P overlap with PI(3,4)P2 and PI(4,5)P2, respectively. Additionally, the retention time of PIPx in the same group increases with the carbon number and decreases with double bonds (Figure 3; Figure S10). Based upon identification from standards along with highly abundant PIPx in samples, the above-mentioned intra- and inter-group retention patterns could be utilized to construct a retention time network, which could be conveniently used for confirmation of PIPx identification in the complex sample matrix.

Acidified Extraction with Internal Standards (ISs). Many solvent extraction systems have been reported for lipid extraction. Among them, Folch,[33] Bligh and Dyer[34] and Matyash[35] methods were widely adopted in lipidomics study. All methods involve water, methanol, and chloroform or methyl tert-butyl ether (MTBE) to form two layers, from which the organic phase is taken for lipid analysis. Compared to chloroform-based methods (Folch and Bligh and Dyer), the MTBE-based method has the advantage of low toxicity and simplified phase collection (upper layer for collection and protein residues at the bottom). Therefore, the MTBE method was selected as the start for method development. Due to multiple phosphate moieties, PIPx are prone to bind to

https://doi.org/10.1021/acs.analchem.1c01751
Anal. Chem. 2021, 93, 9583−9592

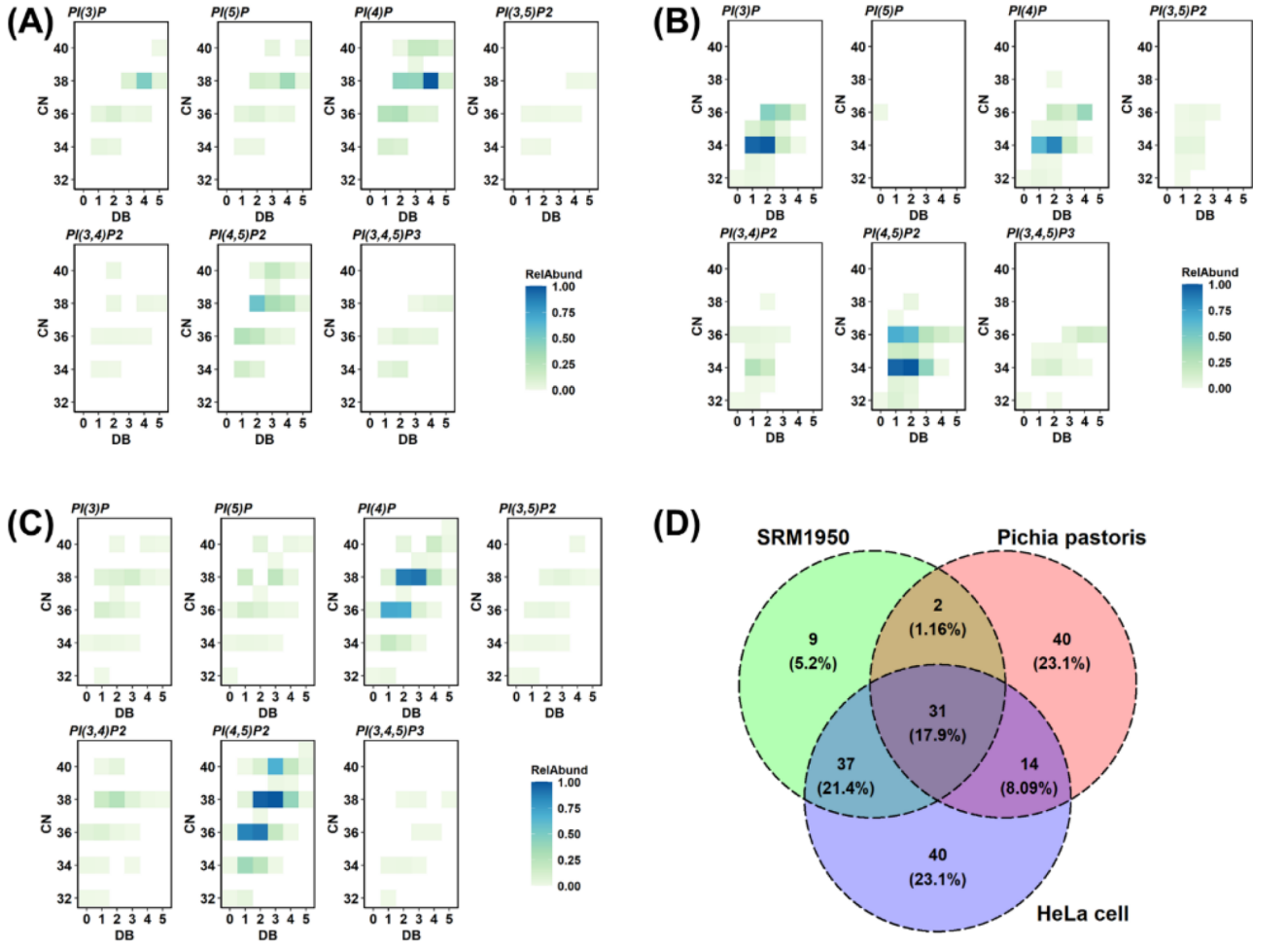

Figure 4. PIPx profiles in different biological samples. (A) PIPx profile in NIST SRM1950 plasma. 18:0/20:4 was the most abundant fatty acyl configuration and molecular lipid species. PI(4)P and PI(4,5)P2 were the most abundant regioisomers in PIP and PIP2 groups, respectively. (B) PIPx profile in *Pichia pastoris*. 34:2 was the most abundant molecular lipid species. PI(3)P and PI(4,5)P2 were the most abundant regioisomers in PIP and PIP2 groups, respectively. (C) PIPx profile in cultured HeLa cells. 18:0/20:3 is the most abundant fatty acyl configuration and molecular lipid species. PI(4)P and PI(4,5)P2 were the most abundant regioisomers in PIP and PIP2 groups, respectively. (D) Overview of PIPx profiles in different samples. Cultured HeLa cells, human plasma, and *Pichia pastoris* have distinct profiles.

proteins in samples. The addition of acid was reported to suppress ionization of phosphates of PIPx in order to improve extraction efficiency. Two extraction strategies were tested in human plasma and cultured HeLa cells: (i) acidic extraction and (ii) neutral extraction followed by acidic extraction. The results (Figure S11) indicate that removal of neutral lipids prior to acidic extraction of PIPx improves the extraction efficiency and thus the signal intensity of PIPx. Superiority of the two-step approach with inclusion of a neutral extraction step becomes more significant for PIPx with more phosphorylations. Meanwhile, extraction recovery of PI was around 20% (data not shown) with neutral removal. There is significant PI loss during neutral extraction. As the PI group is covered by the general untargeted lipidomics method in our lab, the two-step approach with acidified extraction after neutral extraction was selected for further studies, and PIs were no longer included in these measurements. During optimization, homogenization of the residue after neutral extraction was found to be critical for obtaining good extraction recoveries of PIPx. A high-throughput homogenizer (Precellys) was included at this step for sample preparation to make this extraction method more robust and efficient. In order to accurately quantitate analytes with LC−MS, appropriate ISs are required to compensate for sample losses during extraction, matrix effects, and injection variations. Corresponding stable isotope-labeled (SIL) compounds are ideal as ISs due to their absence in the sample matrix and readily distinguishable mass shift in MS. However, SIL standards are not always commercially available and quality of synthetic lipid standards is always a concern. Three SIL PIPx (PI(3)P 16:0/16:0-d62, PI(4,5)P2 16:0/16:0-d62, and PI(3,4,5)P3 16:0/16:0-d62) were tested as IS candidates. These standards were claimed to have deuteration purities more than 99%. However, the distribution of PIPx from d1 to d62 was unknown and not certified in these standards. Therefore, we applied our method first to characterize these three SIL standards. As summarized in Figure 2D and Table S4, PIPx-d62 were found to be more than 70%. PIPx with d0-d58 were not detected. We spiked the three SIL PIPx into the samples at a nominal concentration of 200 ng/mL as ISs across this study (chromatograms shown in Figure S12). No interferences from standards with less deuteration were observed.

Data Processing Workflow. After untargeted measurements with the LC-SWATH method, a targeted data mining strategy was performed. First, an in-house database of methylated PIPx was created based on entries from available

https://doi.org/10.1021/acs.analchem.1c01751
Anal. Chem. 2021, 93, 9583−9592

online databases, including SwissLipids,[36] LIPID MAPS,[37] etc. The product ions of the different PIPx were computed according to the above-described fragmentation pattern. The retention time network was added according to intra- and inter-group retention patterns based on homology series. Then, identification was performed with the MasterView module in vendor software PeakView. The precursor, isotope pattern, fragment, and retention time were taken together to give confident identification. Identified PIPx were directly exported into MultiQuant for quantitation. To improve accuracy of quantitation, two types of isotope correction were performed. As shown in Figure S13, within the same group, M + 2 interferences from PIPx with one more double bond were subtracted (type II isotope correction). Type one correction was carried out to compensate for different ratios between the monoisotopic signal and sum of all isotope signals with different carbon numbers. Finally, PIPx profiles in samples were obtained according to IS normalization and surrogate calibrants (PIPx 17:0/20:4).

Before being applied for biological samples, this method was assessed for its performance by validation. The sample preparation part was evaluated according to the strategy reported elsewhere.[38] Two distinct sample matrices were tested: human plasma and cultured HeLa cells. As shown in Tables S5 and S6 and Figures S14 and 15, limits of quantitation (LOQs) of PIPx in both sample types were established between 8.5 and 10.5 nM. Extraction recoveries of PIPx in both sample types were above 50% (data listed in Tables S7 and S11). Matrix effects could be effectively compensated by ISs (Tables S8, S9, S12, and S13). Therefore, satisfactory process efficiency was achieved (Tables S10 and S14). The whole method was validated according to FDA guidelines with some modifications. Four concentration levels were tested for accuracy and precision. The data (Tables S15 and S16) showed that the method is accurate and precise for PIPx profiling in biological samples. As an example, representative chromatograms of surrogate standards at LOQs in HeLa cell are shown in Figure S16. To further explore the flexibility of postacquisition data processing of the SWATH method, different SWATH window widths were tested. As shown in Figures S16 and S17, less possible interference was observed with narrower SWATH windows. Both the precursor and fragment A could be utilized for quantitation and utilized for intra-assay confirmation (similar to qualifier/quantifier ion transitions in SRM). As shown in Tables S17−20, when the precursor was taken, the sensitivity was compromised for a better assay specificity with current acquisition parameters.

PIPx Profile in NIST SRM1950 Plasma. To standardize the reported data and to assess the method performance within the community, reference materials such as human plasma reference material (NIST SRM1950) have been utilized in metabolomics and lipidomics studies. General metabolites and the lipid profile in NIST SRM1950 have been reported as a useful benchmark. However, the PIPx profile and regioisomer distribution, respectively, have not been investigated before. Hence, we determined the complete PIPx profile in NIST SRM1950 plasma samples in three replicates (estimated concentrations listed in Table S21). As shown in Figure 4A, PI(4)P and PI(4,5)P2 were found to be the most abundant isomers in PIP and PIP2 groups, respectively. Interestingly, PI(3)P 38:4 was found to be 50% as abundant as PI(4)P 38:4, the PIP which was considered to be dominant among the isomers. With regard to fatty acyl chains, 38:4 was, in accordance with previous reports, the most abundant species. Owing to comprehensive MS2 spectra obtained in SWATH (Figure S18), PI(4)P 18:0/20:4 and PI(4,5)P2 18:0/20:4 could be identified by their characteristic fragments.

PIPx Profile in *Pichia pastoris*. Lipidomics and metabolomics studies in yeast cells have gained more and more interest these days.[39] *Pichia pastoris* belongs to methylotrophic yeast. As a successful expression system, it has been widely used in biochemical research and industrial biotechnology. However, its PIPx profile has not been reported yet. After determination of *Pichia pastoris* samples, a comprehensive overview of the PIPx profile was obtained (Figure 4B and Table S22). PIPx in *Pichia pastoris* were found with shorter fatty acyl chains, among which 34:2 and 34:1 were the most abundant species followed by 36:2 and 36:1. Interestingly, as indicated in Figure S19, PI(4)P 34:2 was identified to be PI(4)P 16:0/18:2 and PI(4)P 18:1/16:2, while PI(4,5)P2 was identified as 16:0/18:2 and 18:2/16:0. This inconformity of fatty acyl composition between PIP and PIP2 may indicate preference of different fatty acyl chains. The dominant species 38:4 found in plasma and HeLa cells was of much less abundance in *Pichia pastoris*. Additionally, PI(3)P was the most abundant isomer in the PIP group rather than PI(4)P in mammals. On the other hand, PI(4,5)P2 still stands out in the PIP2 group as the dominant regioisomer like that in mammal samples.

PIPx Profile in Cultured HeLa Cells. As one of the most important intracellular pathways, a phospsphatidylinositol-3-kinase (PI3K)/AKT/mammalian target of rapamycin (mTOR) signaling pathway is found to be dysregulated in most human cancers. Therefore, a lot of efforts have been made to target PI3K/AKT/mTOR for cancer therapy. Our method is supposed to offer a new straightforward insight into the PIPx network. This method was applied to cultured HeLa cells (estimated concentrations listed in Table S23). As shown in Figure 4C, the HeLa cell has a wide distribution in fatty acyl compositions (carbon number from 32 to 42, unsaturation from 0 to 5). C38:4 and C38:3 were found to be the most abundant followed by C36:2 and C36:1. At the same time, regioisomers of PI(4)P and PI(4,5)P2 dominate in their groups, respectively. As can be seen from Figure 4C and Figure S20, PI(4)P 38:3 and PI(4,5)P2 38:3 stand out in the whole PIPx profile, which could be further identified as 18:0/20:3 for their acyl chains. Acyl chains of C18:0 and C20:4 were reported to be enriched in mammal cells in sn1 and sn2 positions, respectively. This enrichment could be achieved via de novo synthesis and acyl chain remodeling. As data indicated (Figure S21), in cultured HeLa cells, PIPx 38:4 were further identified as PIPx 18:1/20:3, revealing a significant, high abundance of the acyl chain of 18:1. Our previous research of fatty acyl coenzyme As (acyl CoA) showed that 18:1 CoA is the dominant acyl composition in HeLa cells.[40] There is a correlation between the acyl CoA profile and PIPx profile, which is expectable, as acyl CoAs are incorporated into phospholipids by de novo synthesis and remodeling of PIPx.

To further explore the applicability, we utilized this method to determine the PIPx profile of HeLa cells after treatment with PI3K inhibitor wortmannin. Wortmannin is a fungal metabolite, which was identified as a potential and selective PI3K inhibitor. After being treated with three concentration levels (A, B, and C), HeLa cells were harvested, quenched, and processed for PIPx measurements, as described above. As

https://doi.org/10.1021/acs.analchem.1c01751
Anal. Chem. 2021, 93, 9583−9592

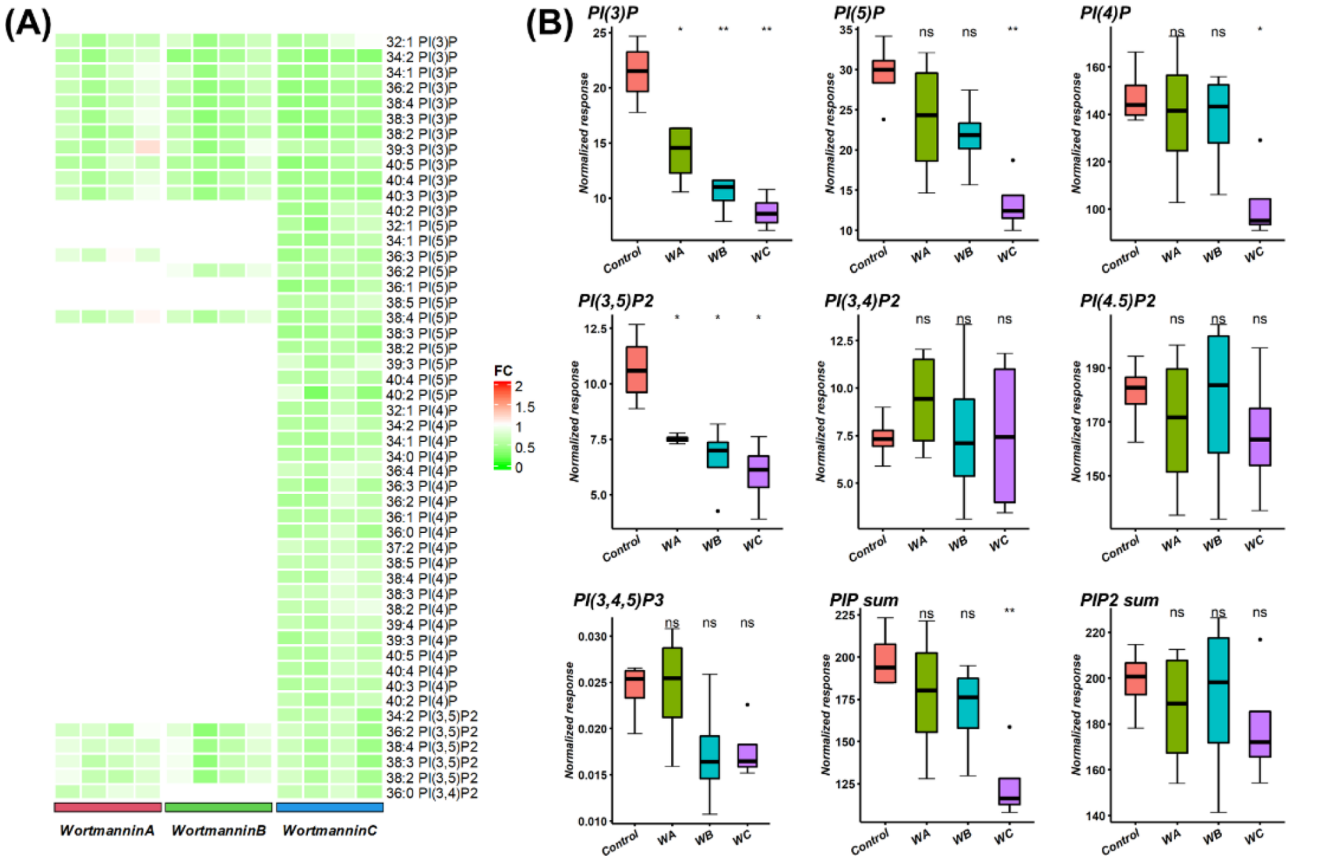

Figure 5. PIPx profile of cultured HeLa cells (n = 4 each) upon treatment with PI3K inhibitor wortmannin at three concentration levels A, B, and C. (A) Heatmap for comparison of PIPx fold change (FC), which showed a significant change (adjusted p value ≤0.05) after treatment of wortmannin. (B) Boxplot of PIPx 18:0/20:3 after treatment of wortmannin. Significance levels are *p < 0.05 and **p < 0.01. PIP sum and PIP2 sum refer to the sum of respective regioisomers. Wortmannin concentrations in groups: control, 0 (DMSO with the same volume); A, 23.3 nM in DMSO; B, 233 nM in DMSO; C, 2330 nM in DMSO.

illustrated in Figure 5, compared with the control group, HeLa cells treated with wortmannin had a significantly lower response for PI(3)P 18:0/20:3 even in the lowest tested concentration group A. At this concentration, no statistically significant downregulation of PI(5)P 18:0/20:3 and PI(4)P 18:0/20:3 was observed, which confirmed the selective inhibition of PI3K over the other two kinases (PI4K and PI5K). With the increased concentration of wortmannin, PI(3)P 18:0/20:3 exhibited a dose dependent decrease, while PI(5)P 18:0/20:3 and PI(4)P 18:0/20:3 showed significant downregulation in the highest concentration group C only. Interestingly, among PIP2 18:0/20:3 isomers, only PI(3,5)P2 concentrations were significantly lowered upon treatment with the inhibitor, which could be due to the much higher abundance of PI(4)P than PI(3)P and PI(5)P. To better show the importance of isomer separation and determination, sums of PIP and PIP2 isomers were also compared between groups. The effect of treatment with the inhibitor was dominated by the most abundant isomers (PI(4)P and PI(4,5)P2). Differences for the other isomers described above were masked. Therefore, our isomer-selective method could be used to monitor PIPx profile changes upon drug treatment more representatively, which indicates its great potential to be integrated as a part of the drug screening method.

CONCLUSIONS

As rare but central membrane lipids, phosphoinositides (PIPx) are interconverted by phosphorylation/dephosphorylation on the inositol ring and consist of a highly regulated network controlled by phosphoinositide-metabolizing enzymes. However, the in-depth study of biomolecular mechanisms of phosphoinositides has been greatly limited by lack of sensitive and isomer-selective analytical methods for their comprehensive coverage. In this work, a comprehensive analytical workflow for lipidomics analysis of PIPx was established for the first time. In this method, isomer-selective separation was coupled with DIA using the SWATH acquisition technique to provide a full picture of PIPx. Starting from a two-step extraction approach followed by phosphate methylation, application of fully ESI-MS compatible liquid chromatography with a polysaccharide-type chiral column enabled full separation of regioisomers of intact PIPx. Characteristic intra- and inter-group elution patterns were observed: (i) Within the PIPx group, for steric reasons, the elution order of regioisomers follows the retention preference 3′ < 5′ < 4′ phosphoinositol head group. It can be rationalized by steric interactions. Steric hindrance for insertion into the cleft formed by the adjacent 2-, 3-, and 6-(3,5-dimethylphenylcarbamate) residues of each glucose unit of the cellulose polymer might be the least for the 4′-phosphorylated PIPx and is less for the 5′-phosphoinositol derivative than the 3′-phosphoinositol analogue, which has the sterically unfavorable axial 2-hydroxy

https://doi.org/10.1021/acs.analchem.1c01751
Anal. Chem. 2021, 93, 9583−9592

substituent next to it. Accordingly, we see an elution order of regioisomers for PIP following PI(3)P<PI(5)P<PI(4)P. The same effect seems to drive the intragroup elution orders for the PIP2 phosphoinositides. The regioisomer with the two more favorable positions elutes last, and the one with the two most unfavorable positions elutes first; hence, PI(3,5)P2 < PI(3,4)-P2 < PI(4,5)P2. (ii) There is little between group retention shift for PIP and PIP2, while PIP3 seems sterically excluded from interaction in the clefts of the pendant 3,5-dimethylphenylcarbamate moieties. Assay specificity arises from their different precursor ion *m/z* values and fragmentation in different SWATH windows. (iii) Aforementioned intragroup and intergroup elution patterns were conserved throughout the distinct fatty acyl side chains, which themselves followed the typical homology principle of RP-type separations. With each additional methylene group, a regular retention increment was added and each double bond brought about a constant shift to earlier elution time as also observed in common RPLC. These regular elution patterns were then utilized to improve identification confidence. The DIA SWATH technique was applied to acquire untargeted comprehensive MS and MS/MS data from samples. Information about the fatty acyl chain composition as well as their sn1/sn2 position was provided at the MS2 level in the SWATH windows. The targeted data mining strategy was applied with an in-house generated library.

Quantitation in the biological sample matrix was achieved with group specific ISs and surrogate calibrators. Application in different biological samples not only revealed the practical applicability of this method but also led to some interesting findings. Overall, PIPx in mammal samples NIST SRM1950 plasma and cultured HeLa cells have a similar distribution in the fatty acyl chain composition, while *Pichia pastoris* enriched shorter fatty acyl chains. Although holding the same sum composition (C38:4), PIPx 18:0/20:4 was found in NIST SRM1950, while PIPx 18:1/20:3 was determined in cultured HeLa cells. In principle, C18:0 and C20:4 acyl chains are enriched at sn1 and sn2 positions, respectively, in mammal cells. It was reported that this specific enrichment of C38:4 in immortalized cell lines could be lost, but the mechanisms behind are still unclear.[13]

Determination of cellular acyl CoA and PIPx profiles could give more insight into how acyl compositions correlate in cells in the future. When it comes to regioisomers, PI(3)P 18:0/20:4 was found to account for a decent portion in NIST SRM1950 plasma. However, PI(4)P 18:0/20:4 takes absolute predominance in terms of abundance within the PIP group. In *Pichia pastoris*, PI(3)P was found to be the most abundant instead of PI(4)P in the HeLa cell and NIST SRM1950 plasma. Our method is able to serve as a quality control method for PIPx regioisomer standard production. Finally, this method was used to monitor PIPx profile changes after treatment with the potential PI3K inhibitor wortmannin. The results showed that this method can determine PIPx profile changes upon treatment with PI3K inhibitors and holds great potential to be integrated as part of drug screening platforms.

■ ASSOCIATED CONTENT

Supporting Information

The Supporting Information is available free of charge at https://pubs.acs.org/doi/10.1021/acs.analchem.1c01751.

Detailed information of SWATH, tables of method evaluation and validation, product ion spectra referred in the main document, summary figure of column screen, elution pattern, isotope correction, calibration curves, chromatograms of PIPx at LOQs, representative PIPx detected in samples, and estimated concentrations of PIPx identified in NIST SRM1950 plasma, *Pichia pastoris,* and cultured HeLa cells (pdf)

■ AUTHOR INFORMATION

Corresponding Author

Michael Lämmerhofer − *Institute of Pharmaceutical Sciences, Pharmaceutical (Bio-)Analysis, University of Tübingen, Tübingen 72076, Germany;* orcid.org/0000-0002-1318-0974; Phone: +497071 29 78793; Email: michael.laemmerhofer@uni-tuebingen.de; Fax: +49 7071 29 4565

Author

Peng Li − *Institute of Pharmaceutical Sciences, Pharmaceutical (Bio-)Analysis, University of Tübingen, Tübingen 72076, Germany;* orcid.org/0000-0002-4905-3993

Complete contact information is available at: https://pubs.acs.org/10.1021/acs.analchem.1c01751

Author Contributions

P.L. and M.L conceptualized the method, and P.L. performed all experiments, analyzed the data, and wrote the manuscript with input from M.L.

Notes

The authors declare no competing financial interest.

■ ACKNOWLEDGMENTS

P.L. gratefully acknowledges the support from the China Scholarship Council (grant number 201807060010). M.L. acknowledges the support by the German Research Foundation (DFG, Deutsche Forschungsgemeinschaft), project number 374031971-TRR 240.

■ REFERENCES

(1) Han, X.; Gross, R. W. *J. Lipid Res.* **2003**, *44*, 1071−1079.
(2) Yang, K.; Han, X. *Trends Biochem. Sci.* **2016**, *41*, 954−969.
(3) Di Paolo, G.; De Camilli, P. *Nature* **2006**, *443*, 651−657.
(4) Dickson, E. J. *F1000Research* **2019**, *8*, 278.
(5) Schink, K. O.; Tan, K. W.; Stenmark, H. *Annu. Rev. Cell Dev. Biol.* **2016**, *32*, 143−171.
(6) O'Donnell, V. B.; Murphy, R. C.; Watson, S. P. *Circ. Res.* **2014**, *114*, 1185−1203.
(7) Fruman, D. A.; Chiu, H.; Hopkins, B. D.; Bagrodia, S.; Cantley, L. C.; Abraham, R. T. *Cell* **2017**, *170*, 605−635.
(8) Fruman, D. A.; Rommel, C. *Nat. Rev. Drug Discov.* **2014**, *13*, 140−156.
(9) Phan, T. K.; Bindra, G. K.; Williams, S. A.; Poon, I. K. H.; Hulett, M. D. *Trends Pharmacol. Sci.* **2019**, *40*, 866−882.
(10) De Santis, M. C.; Gulluni, F.; Campa, C. C.; Martini, M.; Hirsch, E. *Biochim. Biophys. Acta − Rev. Cancer* **2019**, *1871*, 361−366.
(11) Yang, J.; Nie, J.; Ma, X.; Wei, Y.; Peng, Y.; Wei, X. *Mol. Cancer* **2019**, *18*, 26−28.
(12) Bozelli, J. C.; Epand, R. M. *Proteomics* **2019**, *19*, No. e1900138.
(13) Traynor-Kaplan, A.; Kruse, M.; Dickson, E. J.; Dai, G.; Vivas, O.; Yu, H.; Whittington, D.; Hille, B. *Biochim. Biophys. Acta-Mol. Cell Biol. Lipids* **2017**, *1862*, 513−522.
(14) Mujalli, A.; Chicanne, G.; Bertrand-Michel, J.; Viars, F.; Stephens, L.; Hawkins, P.; Viaud, J.; Gaits-Iacovoni, F.; Severin, S.; Gratacap, M. P.; et al. *Biochim. Biophys. Acta-Mol. Cell Biol. Lipids* **2018**, *1863*, 1121−1131.

(15) Ni, Z.; Milic, I.; Fedorova, M. *Anal. Bioanal. Chem.* **2015**, *407*, 5161−5173.
(16) Kiefer, S.; Rogger, J.; Melone, A.; Mertz, A. C.; Koryakina, A.; Hamburger, M.; Küenzi, P. *J. Pharm. Biomed. Anal.* **2010**, *53*, 552−558.
(17) Wenk, M. R.; Lucast, L.; Di Paolo, G.; Romanelli, A. J.; Suchy, S. F.; Nussbaum, R. L.; Cline, G. W.; Shulman, G. I.; McMurray, W.; De Camilli, P. *Nat. Biotechnol.* **2003**, *21*, 813−817.
(18) Bui, H. H.; Sanders, P. E.; Bodenmiller, D.; Kuo, M. S.; Donoho, G. P.; Fischl, A. S. *Anal. Biochem.* **2018**, *547*, 66−76.
(19) Pettitt, T. R.; Dove, S. K.; Lubben, A.; Calaminus, S. D. J.; Wakelam, M. J. O. *J. Lipid Res.* **2006**, *47*, 1588−1596.
(20) Wakelam, M. J. O.; Clark, J. *Biochim. Biophys. Acta-Mol. Cell Biol. Lipids* **2011**, *1811*, 758−762.
(21) Pettitt, T. R. Phosphoinositide Analysis by Liquid Chromatography-Mass Spectrometry. In *Methods in molecular biology (Clifton, N.J.)*; Barker, C. J., Ed.; Humana Press: Totowa, NJ, 2010; Vol. *645*, pp. 203−217. DOI: 10.1007/978-1-60327-175-2_13.
(22) Clark, J.; Anderson, K. E.; Juvin, V.; Smith, T. S.; Karpe, F.; Wakelam, M. J. O.; Stephens, L. R.; Hawkins, P. T. *Nat. Methods* **2011**, *8*, 267−272.
(23) Kielkowska, A.; Niewczas, I.; Anderson, K. E.; Durrant, T. N.; Clark, J.; Stephens, L. R.; Hawkins, P. T. *Adv. Biol. Regul.* **2014**, *54*, 131−141.
(24) Lee, J. C.; Byeon, S. K.; Moon, M. H. *Anal. Chem.* **2017**, *89*, 4969−4977.
(25) Wang, C.; Palavicini, J. P.; Wang, M.; Chen, L.; Yang, K.; Crawford, P. A.; Han, X. *Anal. Chem.* **2016**, *88*, 12137−12144.
(26) Malek, M.; Kielkowska, A.; Chessa, T.; Anderson, K. E.; Barneda, D.; Pir, P.; Nakanishi, H.; Eguchi, S.; Koizumi, A.; Sasaki, J.; et al. *Mol. Cell* **2017**, *68*, 566−580.e10.
(27) Mücksch, F.; Citir, M.; Lüchtenborg, C.; Glass, B.; Traynor-Kaplan, A.; Schultz, C.; Brügger, B.; Kräusslich, H. G. *Sci. Rep.* **2019**, *9*, 17661.
(28) Cai, T.; Shu, Q.; Hou, J.; Liu, P.; Niu, L.; Guo, X.; Liu, C. C.; Yang, F. *Anal. Chem.* **2015**, *87*, 513−521.
(29) Bonner, R.; Hopfgartner, G. *TrAC-Trends Anal. Chem.* **2019**, *120*, 115278.
(30) Kim, S. H.; Song, H. E.; Kim, S. J.; Woo, D. C.; Chang, S.; Choi, W. G.; Kim, M. J.; Back, S. H.; Yoo, H. J. *J. Lipid Res.* **2017**, *58*, 469−478.
(31) Bruzik, K. S.; Hakeem, A. A.; Tsai, M. D. *Biochemistry* **1994**, *33*, 8367−8374.
(32) Bruzik, K. S.; Morocho, A. M.; Jhon, D. Y.; Rhee, S. G.; Tsai, M. D. *Biochemistry* **1992**, *31*, 5183−5193.
(33) Folch, J.; Lees, M.; Stanley, G. H. S. *J. Biol. Chem.* **1957**, *226*, 497−509.
(34) Bligh, E. G.; Dyer, W. J. *Can. J. Biochem. Physiol.* **1959**, *37*, 911−917.
(35) Matyash, V.; Liebisch, G.; Kurzchalia, T. V.; Shevchenko, A.; Schwudke, D. *J. Lipid Res.* **2008**, *49*, 1137−1146.
(36) Aimo, L.; Liechti, R.; Hyka-Nouspikel, N.; Niknejad, A.; Gleizes, A.; Götz, L.; Kuznetsov, D.; David, F. P. A.; Van Der Goot, F. G.; Riezman, H.; et al. *Bioinformatics* **2015**, *31*, 2860−2866.
(37) Fahy, E.; Subramaniam, S.; Murphy, R. C.; Nishijima, M.; Raetz, C. R. H.; Shimizu, T.; Spener, F.; Van Meer, G.; Wakelam, M. J. O.; Dennis, E. A. *J. Lipid Res.* **2009**, *50*, S9−S14.
(38) Matuszewski, B. K.; Constanzer, M. L.; Chavez-Eng, C. M. *Anal. Chem.* **2003**, *75*, 3019−3030.
(39) Rampler, E.; Coman, C.; Hermann, G.; Sickmann, A.; Ahrends, R.; Koellensperger, G. *Analyst* **2017**, *142*, 1891−1899.
(40) Li, P.; Gawaz, M.; Chatterjee, M.; Lämmerhofer, M. *Anal. Chem.* **2021**, *93*, 4342.

https://doi.org/10.1021/acs.analchem.1c01751
Anal. Chem. 2021, 93, 9583−9592

Supporting information

Isomer selective comprehensive lipidomics analysis of phosphoinositides in biological samples by liquid chromatography with data independent acquisition tandem mass spectrometry

Peng Li, Michael Lämmerhofer*

Institute of Pharmaceutical Sciences, Pharmaceutical (Bio-)Analysis, University of Tübingen, Auf der Morgenstelle 8, 72076 Tübingen, Germany

***Authors for correspondence:**

Prof. Michael Lämmerhofer
Pharmaceutical (Bio-)Analysis
Institute of Pharmaceutical Sciences
University of Tuebingen
Auf der Morgenstelle 8
72076 Tuebingen, Germany
T +49 7071 29 78793, F +49 7071 29 4565
e-mail: michael.laemmerhofer@uni-tuebingen.de
http://www.bioanalysis.uni-tuebingen.de/

Content

Table S1 | SWATH window parameters in this study (screening design with wider windows)

Exp Index	Experiment type	Start mass (Da)	Stop mass (Da)	CE (V)	CES (V)	Accumulation time (ms)
1	TOFMS	100	1500	10	0	200
2	SWATH	550	580	50	0	30
3	SWATH	579	610	50	0	30
4	SWATH	609	640	50	0	30
5	SWATH	639	670	50	0	30
6	SWATH	669	700	50	0	30
7	SWATH	699	730	50	0	30
8	SWATH	729	760	50	0	30
9	SWATH	759	790	50	0	30
10	SWATH	789	820	50	0	30
11	SWATH	819	850	50	0	30
12	SWATH	849	880	50	0	30
13	SWATH	879	910	50	0	30
14	SWATH	909	940	50	0	30
15	SWATH	939	970	50	0	30
16	SWATH	969	1000	50	0	30
17	SWATH	999	1030	50	0	30
18	SWATH	1029	1060	50	0	30
19	SWATH	1059	1090	50	0	30
20	SWATH	1089	1120	50	0	30
21	SWATH	1119	1150	50	0	30
22	SWATH	1149	1180	50	0	30
23	SWATH	1179	1210	50	0	30
24	SWATH	1209	1240	50	0	30
25	SWATH	1239	1250	50	0	30

The extracted peaks of PIPx have peak widths around 0.17 min. The cycle time is 970 ms, which ensures around 12 data points across the peaks.

Table S2 | Methylation efficiency data for PIPx 17:0/20:4

Methylation efficiency, %	PI(3)P	PI(4)P	PI(5)P	PI(3,4)P2	PI(3,5)P2	PI(4,5)P2	PI(3,4,5)P2
Replicate 1	99.5 ± 0.1	99.3 ± 0.2	99.7 ± 0.1	90.7 ± 0.8	93.7 ± 0.6	89.4 ± 0.7	86.7 ± 1.2
Replicate 2	99.6 ± 0.1	99.4 ± 0.3	99.4 ± 0.4	91.0 ± 0.4	94.1 ± 0.2	89.8 ± 0.6	86.2 ± 1.5
Replicate 3	99.6 ± 0.1	99.6 ± 0.1	99.3 ± 0.3	90.2 ± 1.0	94.1 ± 0.3	89.6 ± 0.5	85.8 ± 1.9

Replicates prepared with single standards of PIPx 17:0/20:4, then measured in triplicates.

Table S3 | Optimized SWATH parameters with refined, narrower window size

Exp Index	Experiment type	Start mass (Da)	Stop mass (Da)	CE (V)	CES (V)	Accumulation time (ms)
1	TOFMS	100	1500	10	0	200
2	SWATH	50	300	50	0	20
3	SWATH	299	549	50	0	20
4	SWATH	548	748	50	0	20
5	SWATH	747	849	50	0	20
6	SWATH	848	860	50	0	20
7	SWATH	859	871	50	0	20
8	SWATH	870	882	50	0	20
9	SWATH	881	893	50	0	20
10	SWATH	892	904	50	0	20
11	SWATH	903	915	50	0	20
12	SWATH	914	926	50	0	20
13	SWATH	925	937	50	0	20
14	SWATH	936	948	50	0	20
15	SWATH	947	959	50	0	20
16	SWATH	958	970	50	0	20
17	SWATH	969	981	50	0	20
18	SWATH	980	992	50	0	20
19	SWATH	991	1003	50	0	20
20	SWATH	1002	1014	50	0	20
21	SWATH	1013	1025	50	0	20
22	SWATH	1024	1036	50	0	20
23	SWATH	1035	1047	50	0	20
24	SWATH	1046	1058	50	0	20
25	SWATH	1057	1069	50	0	20
26	SWATH	1068	1080	50	0	20
27	SWATH	1079	1091	50	0	20
28	SWATH	1090	1102	50	0	20
29	SWATH	1101	1113	50	0	20
30	SWATH	1112	1124	50	0	20
31	SWATH	1123	1135	50	0	20
32	SWATH	1134	1146	50	0	20
33	SWATH	1145	1157	50	0	20
34	SWATH	1156	1168	50	0	20
35	SWATH	1167	1179	50	0	20
36	SWATH	1178	1190	50	0	20
37	SWATH	1189	1201	50	0	20
38	SWATH	1200	1212	50	0	20
39	SWATH	1211	1223	50	0	20
40	SWATH	1222	1234	50	0	20
41	SWATH	1233	1245	50	0	20
42	SWATH	1244	1250	50	0	20

The cycle time is 1020 ms, which ensures around 10 data points across the peaks.

Table S4 | Characterization of deuterated PIPx standards

PIPx 32:0 (d1-d62), %	d0 - d58	d59	d60	d61	d62
PI(3)P	ND	1.7 ± 0.4	6.1 ± 1.5	17.7 ± 3.2	74.6 ± 4.1
PI(4,5)P2	ND	1.1 ± 0.3	2.9 ± 0.7	16.2 ± 4.6	79.8 ± 5.3
PI(3,4,5)P3	ND	1.3 ± 0.4	3.6 ± 1.0	13.7 ± 2.7	81.4 ± 3.5

ND, not detected.

Table S5 | Linearity and sensitivity of PIPx 17:0/20:4 in human plasma

PIPx in Plasma	Concentration range, nM	Linear equation	r	LOQ, nM
PI(3)P	10.1 - 1013.0	y = 0.0697x + 0.0581	0.9963	10.1
PI(5)P	10.1 - 1013.0	y = 0.0603x + 0.0663	0.9959	10.1
PI(4)P	10.1 - 1013.0	y = 0.0649x + 0.0792	0.9944	10.1
PI(3,5)P2	9.2 - 922.4	y = 0.2357x + 0.1559	0.9941	9.2
PI(3,4)P2	9.2 - 922.4	y = 0.2351x - 0.0460	0.9980	9.2
PI(4,5)P2	9.2 - 922.4	y = 0.2515x + 0.5885	0.9917	9.2
PI(3,4,5)P3	8.5 - 846.6	y = 0.0030x - 0.0001	0.9964	8.5

Table S6 | Linearity and sensitivity of PIPx 17:0/20:4 in HeLa cells

PIPx in HeLa	Concentration range, nM	Linear equation	r	LOQ, nM
PI(3)P	10.1 - 1013.0	y = 0.1122x - 0.0122	0.9963	10.1
PI(5)P	10.1 - 1013.0	y = 0.1311x - 0.0412	0.9959	10.1
PI(4)P	10.1 - 1013.0	y = 0.1497x - 0.0044	0.9944	10.1
PI(3,5)P2	9.2 - 922.4	y = 0.1932x + 0.1209	0.9941	9.2
PI(3,4)P2	9.2 - 922.4	y = 0.1542x - 0.1163	0.9980	9.2
PI(4,5)P2	9.2 - 922.4	y = 0.2116x + 0.1676	0.9917	9.2
PI(3,4,5)P3	8.5 - 846.6	y = 0.0025x - 0.0008	0.9964	8.5

Table S7 | Extraction recovery results of PIPx 17:0/20:4 in human plasma

ER, %	PI(3)P	PI(4)P	PI(5)P	PI(3,4)P2	PI(3,5)P2	PI(4,5)P2	PI(3,4,5)P3
QC1	55.1 ± 11.8	52.8 ± 6.6	53.0 ± 9.4	56.2 ± 10.5	66.5 ± 11.1	65.7 ± 10.8	67.3 ± 11.1
QC2	63.6 ± 8.4	52.0 ± 7.2	52.4 ± 10.2	52.3 ± 5.2	62.0 ± 9.1	61.8 ± 4.8	65.8 ± 9.1
QC3	56.1 ± 7.7	58.1 ± 9.5	59.6 ± 11.1	59.1 ± 7.4	63.1 ± 6.2	66.4 ± 7.5	64.7 ± 7.5
QC4	53.0 ± 5.6	64.1 ± 10.3	50.7 ± 9.7	60.1 ± 10.7	68.9 ± 5.7	62.6 ± 9.1	66.6 ± 5.3

Concentrations of surrogate standards for QC levels: QC1 (~3x LLOQ), QC2 (low), QC3 (medium), QC4 (high). For PIP were 50.7 nM, 101.3 nM, 506.5 nM and 1013.0 nM respectively. For PIP2 were 46.1 nM, 92.2 nM, 461.2 nM and 922.4 nM respectively. For PIP3 were 42.3 nM, 84.7 nM, 423.3 nM and 866.6 nM respectively.

Table S8 | Matrix effect results of PIPx 17:0/20:4 without internal standards in human plasma (n=9)

ME, %	PI(3)P	PI(4)P	PI(5)P	PI(3,4)P2	PI(3,5)P2	PI(4,5)P2	PI(3,4,5)P3
QC1	148.8 ± 13.8	100.9 ± 20.8	121.3 ± 15.1	130.4 ± 6.7	124.1 ± 8.5	75.6 ± 6.2	261.4 ± 16.8
QC2	127.5 ± 29.6	77.1 ± 30.6	102.2 ± 32.0	93.6 ± 30.9	94.7 ± 37.7	78.2 ± 11.7	162.1 ± 49.2
QC3	84.4 ± 22.1	60.5 ± 30.4	66.2 ± 33.8	75.1 ± 28.8	67.7 ± 43.6	57.3 ± 16.8	123.1 ± 52.1
QC4	94.2 ± 20.3	63.9 ± 19.3	76.3 ± 25.8	53.6 ± 25.2	73.8 ± 40.6	75.5 ± 17.5	109.8 ± 8.3

Concentrations of surrogate standards for QC levels were the same as table S4.

Table S9 | Matrix effect results of PIPx 17:0/20:4 with internal standards in human plasma (n=9)

ME, %	PI(3)P	PI(4)P	PI(5)P	PI(3,4)P2	PI(3,5)P2	PI(4,5)P2	PI(3,4,5)P3
QC1	103.9 ± 5.7	95.7 ± 7.4	99.2 ± 5.2	93.4 ± 9.6	91.5 ± 9.9	103.4 ± 5.8	93.4 ± 5.8
QC2	98.6 ± 9.3	96.2 ± 3.4	90.3 ± 7.8	93.2 ± 7.1	105.2 ± 11.3	100.6 ± 8.4	90.6 ± 8.4
QC3	102.8 ± 5.8	93.8 ± 8.9	97.6 ± 10.5	95.2 ± 8.4	94.2 ± 8.1	101.8 ± 9.6	91.0 ± 9.6
QC4	101.8 ± 6.1	93.6 ± 7.8	91.7 ± 8.1	97.9 ± 12.1	96.8 ± 8.8	100.9 ± 9.9	90.9 ± 9.9

Concentrations of surrogate standards for QC levels were the same as table S4.

Table S10 | Process efficiency of PIPx 17:0/20:4 in human plasma (n=9)

PE, %	PI(3)P	PI(4)P	PI(5)P	PI(3,4)P2	PI(3,5)P2	PI(4,5)P2	PI(3,4,5)P3
QC1	56.8 ± 10.9	50.5 ± 8.4	52.6 ± 9.3	52.5 ± 11.6	60.8 ± 10.6	67.7 ± 13.4	62.9 ± 8.4
QC2	62.7 ± 8.1	50.0 ± 9.4	47.3 ± 10.4	48.7 ± 10.8	65.1 ± 5.7	61.8 ± 11.6	59.6 ± 6.9
QC3	57.2 ± 9.8	54.5 ± 10.5	58.2 ± 6.4	56.3 ± 8.4	59.4 ± 6.8	67.1 ± 6.7	58.9 ± 7.4
QC4	53.5 ± 11.5	60.0 ± 6.7	46.5 ± 5.4	58.8 ± 6.7	66.7 ± 11.9	62.6 ± 8.4	60.5 ± 10.8

Concentrations of surrogate standards for QC levels were the same as table S4.

Table S11 | Extraction recovery results of PIPx17:0/20:4in HeLa cells (n=9)

ER, %	PI(3)P	PI(4)P	PI(5)P	PI(3,4)P2	PI(3,5)P2	PI(4,5)P2	PI(3,4,5)P3
QC1	50.9 ± 4.4	54.6 ± 3.3	52.2 ± 4.6	69.2 ± 11.9	68.0 ± 9.8	67.4 ± 10.3	69.2 ± 1.2
QC2	49.4 ± 2.0	60.0 ± 12.8	56.4 ± 11.3	63.3 ± 14.2	70.5 ± 11.0	70.0 ± 10.9	64.7 ± 10.0
QC3	50.6 ± 3.4	62.6 ± 13.2	54.0 ± 12.2	62.7 ± 13.5	67.3 ± 8.4	68.8 ± 9.2	60.4 ± 11.8
QC4	52.9 ± 2.9	67.9 ± 12.6	55.8 ± 11.7	67.8 ± 11.0	66.5 ± 8.8	68.0 ± 10.4	63.4 ± 9.8

Concentrations of surrogate standards for QC levels were the same as table S4.

Table S12 | Matrix effect results of PIPx 17:0/20:4 without internal standards in HeLa cells (n=9)

ME, %	PI(3)P	PI(4)P	PI(5)P	PI(3,4)P2	PI(3,5)P2	PI(4,5)P2	PI(3,4,5)P3
QC1	111.8 ± 9.6	153.1 ± 26.6	145.8 ± 3.4	147.1 ± 3.5	151.7 ± 29.8	136.2 ± 32.1	127.3 ± 6.5
QC2	114.9 ± 13.7	120.7 ± 27.9	138.4 ± 9.7	117.9 ± 21.1	118.1 ± 25.7	109.6 ± 18.4	111.6 ± 9.8
QC3	88.1 ± 13.9	89.8 ± 27.1	96.6 ± 6.8	125.5 ± 20.3	102.8 ± 22.7	116.7 ± 17.9	114.7 ± 6.9
QC4	93.7 ± 19.6	85.1 ± 11.7	90.8 ± 12.1	100.9 ± 5.5	94.6 ± 43.5	114.1 ± 24.6	108.7 ± 5.2

Concentrations of surrogate standards for QC levels were the same as table S4.

Table S13 | Matrix effect results of PIPx 17:0/20:4 with internal standards in HeLa cells (n=9)

ME, %	PI(3)P	PI(4)P	PI(5)P	PI(3,4)P2	PI(3,5)P2	PI(4,5)P2	PI(3,4,5)P3
QC1	95.5 ± 4.8	95.7 ± 2.2	99.9 ± 6.7	92.1 ± 11.9	89.4 ± 8.3	96.3 ± 10.2	87.7 ± 5.4
QC2	96.3 ± 1.2	92.5 ± 2.5	97.9 ± 2.1	97.7 ± 3.3	93.6 ± 2.5	98.1 ± 2.2	93.4 ± 6.4
QC3	95.7 ± 0.8	93.9 ± 0.5	93.8 ± 0.4	92.6 ± 2.4	93.9 ± 1.4	91.6 ± 1.9	91.1 ± 7.8
QC4	91.7 ± 4.2	89.4 ± 4.8	89.6 ± 5.0	88.1 ± 10.3	87.9 ± 6.3	90.1 ± 5.3	89.5 ± 2.7

Concentrations of surrogate standards for QC levels were the same as table S4.

Table S14 | Process efficiency of PIPx in HeLa cells (n=9)

PE, %	PI(3)P	PI(4)P	PI(5)P	PI(3,4)P2	PI(3,5)P2	PI(4,5)P2	PI(3,4,5)P3
QC1	48.6 ± 7.1	52.3 ± 5.2	52.1 ± 5.2	63.7 ± 10.5	60.8 ± 8.7	64.9 ± 10.6	60.7 ± 3.1
QC2	47.6 ± 6.2	55.5 ± 10.4	55.2 ± 10.4	61.8 ± 8.6	66.0 ± 5.6	68.7 ± 8.3	60.4 ± 10.4
QC3	48.4 ± 8.4	58.8 ± 11.9	50.7 ± 12.4	58.1 ± 6.8	63.2 ± 6.7	63.0 ± 6.8	55.0 ± 10.6
QC4	48.5 ± 9.5	60.7 ± 8.3	50.0 ± 10.1	59.7 ± 10.8	58.5 ± 5.9	61.3 ± 9.7	56.7 ± 9.4

Concentrations of surrogate standards for QC levels were the same as table S4.

Table S15 | Intra-batch accuracy and precision of PIPx 17:0/20:4 in plasma (n=9)

Accuracy and Precision, %	PI(3)P	PI(4)P	PI(5)P	PI(3,4)P2	PI(3,5)P2	PI(4,5)P2	PI(3,4,5)P3
QC1	87.6 ± 13.4	88.9 ± 13.9	86.7 ± 13.4	86.9 ± 6.1	87.9 ± 4.9	86.5 ± 4.2	88.6 ± 10.8
QC2	90.8 ± 4.4	108.1 ± 12.2	86.4 ± 5.2	105.3 ± 6.3	110.4 ± 7.2	109.9 ± 7.7	92.0 ± 11.1
QC3	113.4 ± 11.8	105.4 ± 5.9	106.9 ± 14.8	113.8 ± 10.8	97.4 ± 9.1	105.5 ± 11.1	113.9 ± 6.0
QC4	98.6 ± 6.5	103.5 ± 6.1	99.9 ± 6.8	99.8 ± 7.9	101.3 ± 8.2	100.2 ± 7.6	108.2 ± 8.7

Concentrations of surrogate standards for QC levels were the same as table S4.

Table S16 | Intra-batch accuracy and precision of PIPx 17:0/20:4 in HeLa cells (n=9)

Accuracy and Precision, %	PI(3)P	PI(4)P	PI(5)P	PI(3,4)P2	PI(3,5)P2	PI(4,5)P2	PI(3,4,5)P3
QC1	100.0 ± 11.6	85.9 ± 13.8	95.8 ± 14.7	89.9 ± 11.8	94.5 ± 13.7	91.5 ± 8.3	92.8 ± 10.3
QC2	113.8 ± 8.3	87.5 ± 6.6	109.1 ± 11.2	106.2 ± 4.4	105.9 ± 2.7	104.5 ± 4.1	91.1 ± 9.5
QC3	98.5 ± 10.2	96.1 ± 2.5	98.0 ± 8.2	108.8 ± 7.5	113.3 ± 11.7	91.4 ± 12.5	110.6 ± 13.1
QC4	102.4 ± 6.1	93.5 ± 7.2	102.5 ± 5.1	95.2 ± 7.8	100.3 ± 5.9	98.4 ± 5.2	103.5 ± 6.7

Concentrations of surrogate standards for QC levels were the same as table S4.

Table S17 | Linearity and sensitivity of PIPx 17:0/20:4 in HeLa cells based on precursor

PIPx in HeLa	Concentration range, nM	Linear equation	r	LOQ, nM
PI(3)P	50.5 - 1013.0	y = 0.01150x + 0.17202	0.9883	50.5
PI(5)P	50.5 - 1013.0	y = 0.01273x + 0.14406	0.9878	50.5
PI(4)P	50.5 - 1013.0	y = 0.00548x + 0.07722	0.9761	50.5
PI(3,5)P2	46.0 - 922.4	y = 0.01562x + 0.02666	0.9936	46.0
PI(3,4)P2	46.0 - 922.4	y = 0.01075x - 0.02273	0.9932	46.0
PI(4,5)P2	46.0 - 922.4	y = 0.01041x - 0.03517	0.9929	46.0
PI(3,4,5)P3	42.5 - 846.6	y = 0.00078x - 0.00324	0.9714	42.5

Table S18 | Intra-batch accuracy and precision of PIPx 17:0/20:4 in HeLa cells based on precursor (n=9)

Accuracy and Precision, %	PI(3)P	PI(4)P	PI(5)P	PI(3,4)P2	PI(3,5)P2	PI(4,5)P2	PI(3,4,5)P3
QC1	91.6 ± 18.2	89.9 ± 10.5	90.5 ± 18.4	96.2 ± 9.0	94.0 ± 9.0	98.8 ± 17.1	97.0 ± 7.7
QC2	102.7 ± 9.7	101 ± 14.6	102.4 ± 6.5	105.3 ± 7.4	108.0 ± 10.0	102.6 ± 2.8	101.1 ± 9.7
QC3	114.8 ± 12.6	105.2 ± 12.0	111.8 ± 6.4	97.9 ± 11.0	98.2 ± 13.6	99.5 ± 10.1	96.9 ± 12.2
QC4	100.3 ± 11.9	97.8 ± 9.3	97.8 ± 7.4	101.0 ± 11.4	103.1 ± 5.4	103.8 ± 11.3	105.2 ± 11.4

Concentrations of surrogate standards for QC levels were the same as table S4.

Table S19 | Linearity and sensitivity of PIPx 17:0/20:4 in plasma based on precursor

PIPx in HeLa	Concentration range, nM	Linear equation	r	LOQ, nM
PI(3)P	50.5 - 1013.0	y = 0.00377x + 0.16107	0.9937	50.5
PI(5)P	50.5 - 1013.0	y = 0.00303x + 0.04981	0.9950	50.5
PI(4)P	50.5 - 1013.0	y = 0.00109x + 0.09848	0.9865	50.5
PI(3,5)P2	46.0 - 922.4	y = 0.01383x - 0.03344	0.9948	46.0
PI(3,4)P2	46.0 - 922.4	y = 0.01229x - 0.06463	0.9938	46.0
PI(4,5)P2	46.0 - 922.4	y = 0.01180x + 0.06554	0.9993	46.0
PI(3,4,5)P3	42.5 - 846.6	y = 0.00109x + 0.00281	0.9742	42.5

Table S20 | Intra-batch accuracy and precision of PIPx 17:0/20:4 in plasma based on precursor (n=9)

Accuracy and Precision, %	PI(3)P	PI(4)P	PI(5)P	PI(3,4)P2	PI(3,5)P2	PI(4,5)P2	PI(3,4,5)P3
QC1	102.7 ± 6.5	90.8 ± 18.1	89.5 ± 8.6	96.5 ± 10.0	103.3 ± 3.9	100.3 ± 17.5	111.6 ± 12.2
QC2	103.8 ± 8.2	112.5 ± 9.3	104.3 ± 14.4	99.2 ± 10.7	100.9 ± 10.4	99.5 ± 4.1	88.0 ± 12.1
QC3	113.0 ± 7.1	115.8 ± 8.8	103.5 ± 11.7	106.8 ± 10.4	104.3 ± 2.1	102.6 ± 5.8	108.8 ± 23.5
QC4	97.6 ± 13.1	99.1 ± 7.7	98.8 ± 14.7	102.5 ± 6.6	101.0 ± 12.2	103.2 ± 8.9	96.5 ± 15.1

Concentrations of surrogate standards for QC levels were the same as table S4.

Table S21 | Estimated concentration of PIPx in NIST SRM1950 plasma (n= 3, technical replicates)

Nr.	PIPx	Formula	Methylated Formula	Fragment A [DAG]+	Rt, min	Conc., pmol/100 µL plasma
1	PI(3)P 34:1	C43H82O16P2	C46H88O16P2	577.51904	6.84	2.2 ± 0.2
2	PI(3)P 34:2	C43H80O16P2	C46H86O16P2	575.50339	6.69	1.7 ± 0.3
3	PI(3)P 36:1	C45H86O16P2	C48H92O16P2	605.55034	7.18	2.5 ± 0.7
4	PI(3)P 36:2	C45H84O16P2	C48H90O16P2	603.53469	7.03	4.9 ± 0.4
5	PI(3)P 36:3	C45H82O16P2	C48H88O16P2	601.51904	6.83	1.4 ± 0.1
6	PI(3)P 36:4	C45H80O16P2	C48H86O16P2	599.50339	6.70	1.9 ± 0.2
7	PI(3)P 38:3	C47H86O16P2	C50H92O16P2	629.55034	7.17	4.6 ± 1.1
8	PI(3)P 38:4	C47H84O16P2	C50H90O16P2	627.53469	7.02	20.8 ± 2.1
9	PI(3)P 38:5	C47H82O16P2	C50H88O16P2	625.51904	6.88	3.3 ± 0.3
10	PI(3)P 40:5	C49H86O16P2	C52H92O16P2	653.55034	7.28	0.9 ± 0.1
11	PI(5)P 34:1	C43H82O16P2	C46H88O16P2	577.51904	6.96	1.1 ± 0.2
12	PI(5)P 34:2	C43H80O16P2	C46H86O16P2	575.50339	6.79	1.0 ± 0.2
13	PI(5)P 36:1	C45H86O16P2	C48H92O16P2	605.55034	7.31	2.4 ± 0.9
14	PI(5)P 36:2	C45H84O16P2	C48H90O16P2	603.53469	7.13	3.5 ± 0.3
15	PI(5)P 36:3	C45H82O16P2	C48H88O16P2	601.51904	6.91	1 ± 0.2
16	PI(5)P 36:4	C45H80O16P2	C48H86O16P2	599.50339	6.77	1.5 ± 0.3
17	PI(5)P 38:2	C47H88O16P2	C50H94O16P2	631.56599	7.56	5.7 ± 5.5
18	PI(5)P 38:3	C47H86O16P2	C50H92O16P2	629.55034	7.35	4.7 ± 2.5
19	PI(5)P 38:4	C47H84O16P2	C50H90O16P2	627.53469	7.20	14.8 ± 2.2
20	PI(5)P 38:5	C47H82O16P2	C50H88O16P2	625.51904	6.97	1.8 ± 0.3
21	PI(5)P 40:3	C49H90O16P2	C52H96O16P2	657.58164	7.73	2.1 ± 1.5
22	PI(5)P 40:5	C49H86O16P2	C52H92O16P2	653.55034	7.42	1.6 ± 0.4
23	PI(4)P 34:1	C43H82O16P2	C46H88O16P2	577.51904	7.13	5.3 ± 1.8
24	PI(4)P 34:2	C43H80O16P2	C46H86O16P2	575.50339	6.96	4.3 ± 0.9
25	PI(4)P 36:1	C45H86O16P2	C48H92O16P2	605.55034	7.52	12.1 ± 6.4
26	PI(4)P 36:2	C45H84O16P2	C48H90O16P2	603.53469	7.31	13 ± 5.1
27	PI(4)P 36:3	C45H82O16P2	C48H88O16P2	601.51904	7.11	3.5 ± 0.9
28	PI(4)P 36:4	C45H80O16P2	C48H86O16P2	599.50339	6.96	3.2 ± 0.4
29	PI(4)P 38:2	C47H88O16P2	C50H94O16P2	631.56599	7.70	18.8 ± 14
30	PI(4)P 38:3	C47H86O16P2	C50H92O16P2	629.55034	7.50	18.3 ± 9.1
31	PI(4)P 38:4	C47H84O16P2	C50H90O16P2	627.53469	7.33	43.6 ± 3.6
32	PI(4)P 38:5	C47H82O16P2	C50H88O16P2	625.51904	7.13	4.8 ± 0.4
33	PI(4)P 39:3	C48H88O16P2	C51H94O16P2	643.56599	7.68	1.4 ± 1.2
34	PI(4)P 40:2	C49H92O16P2	C52H98O16P2	659.59729	8.11	1.1 ± 0.8
35	PI(4)P 40:3	C49H90O16P2	C52H96O16P2	657.58164	7.89	8.7 ± 6.4
36	PI(4)P 40:4	C49H88O16P2	C52H94O16P2	655.56599	7.70	8.4 ± 3.4
37	PI(4)P 40:5	C49H86O16P2	C52H92O16P2	653.55034	7.54	3.3 ± 0.3
38	PI(3,5)P2 34:1	C43H83O19P3	C48H93O19P3	577.51904	6.75	0.8 ± 0.2
39	PI(3,5)P2 34:2	C43H81O19P3	C48H91O19P3	575.50339	6.59	1.0 ± 0.2
40	PI(3,5)P2 36:1	C45H87O19P3	C50H97O19P3	605.55034	7.07	0.9 ± 0.4
41	PI(3,5)P2 36:2	C45H85O19P3	C50H95O19P3	603.53469	6.90	1.5 ± 0.5
42	PI(3,5)P2 36:3	C45H83O19P3	C50H93O19P3	601.51904	6.74	0.5 ± 0.1
43	PI(3,5)P2 36:4	C45H81O19P3	C50H91O19P3	599.50339	6.60	0.6 ± 0.1
44	PI(3,5)P2 38:4	C47H85O19P3	C52H95O19P3	627.53469	6.92	1.6 ± 0.4
45	PI(3,5)P2 38:5	C47H83O19P3	C52H93O19P3	625.51904	6.87	1.2 ± 0.3
46	PI(3,4)P2 34:1	C43H83O19P3	C48H93O19P3	577.51904	6.94	1.5 ± 0.2

47	PI(3,4)P2 34:2	C43H81O19P3	C48H91O19P3	575.50339	6.81	1.1 ± 0.5
48	PI(3,4)P2 36:1	C45H87O19P3	C50H97O19P3	605.55034	7.28	1.6 ± 0.6
49	PI(3,4)P2 36:2	C45H85O19P3	C50H95O19P3	603.53469	7.10	1.9 ± 0.6
50	PI(3,4)P2 36:3	C45H83O19P3	C50H93O19P3	601.51904	6.96	1.2 ± 0.4
51	PI(3,4)P2 36:4	C45H81O19P3	C50H91O19P3	599.50339	6.74	1.1 ± 0.1
52	PI(3,4)P2 38:2	C47H89O19P3	C52H99O19P3	631.56599	7.49	4.0 ± 2.5
53	PI(3,4)P2 38:4	C47H85O19P3	C52H95O19P3	627.53469	7.10	2.8 ± 0.3
54	PI(3,4)P2 38:5	C47H83O19P3	C52H93O19P3	625.51904	6.93	1.7 ± 0.3
55	PI(3,4)P2 40:2	C49H93O19P3	C54H103O19P3	659.59729	7.88	4.4 ± 3.1
56	PI(4,5)P2 34:1	C43H83O19P3	C48H93O19P3	577.51904	7.13	4.2 ± 2.2
57	PI(4,5)P2 34:2	C43H81O19P3	C48H91O19P3	575.50339	6.95	2.2 ± 0.9
58	PI(4,5)P2 36:1	C45H87O19P3	C50H97O19P3	605.55034	7.50	8.0 ± 5.0
59	PI(4,5)P2 36:2	C45H85O19P3	C50H95O19P3	603.53469	7.28	6.3 ± 3.8
60	PI(4,5)P2 36:3	C45H83O19P3	C50H93O19P3	601.51904	7.10	1.8 ± 0.6
61	PI(4,5)P2 36:4	C45H81O19P3	C50H91O19P3	599.50339	6.96	1.0 ± 0.1
62	PI(4,5)P2 38:2	C47H89O19P3	C52H99O19P3	631.56599	7.68	16.0 ± 10.2
63	PI(4,5)P2 38:3	C47H87O19P3	C52H97O19P3	629.55034	7.49	9.4 ± 5.3
64	PI(4,5)P2 38:4	C47H85O19P3	C52H95O19P3	627.53469	7.32	7.7 ± 0.8
65	PI(4,5)P2 38:5	C47H83O19P3	C52H93O19P3	625.51904	7.13	1.4 ± 0.1
66	PI(4,5)P2 39:3	C48H89O19P3	C53H99O19P3	643.56599	7.68	1.1 ± 0.6
67	PI(4,5)P2 40:2	C49H93O19P3	C54H103O19P3	659.59729	8.07	1.3 ± 0.7
68	PI(4,5)P2 40:3	C49H91O19P3	C54H101O19P3	657.58164	7.88	6.0 ± 4.2
69	PI(4,5)P2 40:4	C49H89O19P3	C54H99O19P3	655.56599	7.69	3.2 ± 1.6
70	PI(4,5)P2 40:5	C49H87O19P3	C54H97O19P3	653.55034	7.53	0.8 ± 0.1
71	PI(3,4,5)P3 34:1	C43H84O22P4	C50H98O22P4	577.51904	6.71	0.8 ± 0.6
72	PI(3,4,5)P3 34:2	C43H82O22P4	C50H96O22P4	575.50339	6.58	1.3 ± 0.8
73	PI(3,4,5)P3 36:2	C45H86O22P4	C52H100O22P4	603.53469	6.90	1.0 ± 0.7
74	PI(3,4,5)P3 36:3	C45H84O22P4	C52H98O22P4	601.51904	6.73	0.5 ± 0.4
75	PI(3,4,5)P3 36:4	C45H82O22P4	C52H96O22P4	599.50339	6.57	0.5 ± 0.4
76	PI(3,4,5)P3 38:4	C47H86O22P4	C54H100O22P4	627.53469	7.04	0.6 ± 0.4
77	PI(3,4,5)P3 38:5	C47H84O22P4	C54H98O22P4	625.51904	6.90	0.8 ± 0.5

MS tolerance was set 10 ppm. Retention time window was set 0.4 min.

Table S22 | Estimated concentration of PIPx in *pichia pastoris* (n= 3, biological replicates)

Nr.	PIPx	Formula	Methylated Formula	Fragment A [DAG]+	Rt, min	Conc., pmol/50mg biomass
1	PI(3)P 32:0	C41H80O16P2	C44H86O16P2	551.50339	6.79	1.5 ± 0.3
2	PI(3)P 32:1	C41H78O16P2	C44H84O16P2	549.48774	6.57	10.1 ± 2.0
3	PI(3)P 32:2	C41H76O16P2	C44H82O16P2	547.47209	6.44	4.6 ± 0.7
4	PI(3)P 33:1	C42H80O16P2	C45H86O16P2	563.50339	6.70	16.4 ± 4.1
5	PI(3)P 33:2	C42H78O16P2	C45H84O16P2	561.48774	6.58	6.3 ± 1.5
6	PI(3)P 34:1	C43H82O16P2	C46H88O16P2	577.51904	6.84	323.9 ± 27.2
7	PI(3)P 34:2	C43H80O16P2	C46H86O16P2	575.50339	6.71	336 ± 12.5
8	PI(3)P 34:3	C43H78O16P2	C46H84O16P2	573.48774	6.61	55.4 ± 13.5
9	PI(3)P 34:4	C43H76O16P2	C46H82O16P2	571.47209	6.46	2.0 ± 0.6
10	PI(3)P 35:1	C44H84O16P2	C47H90O16P2	591.53469	7.00	33.6 ± 9.7
11	PI(3)P 35:2	C44H82O16P2	C47H88O16P2	589.51904	6.86	66.0 ± 18.1
12	PI(3)P 35:3	C44H80O16P2	C47H86O16P2	587.50339	6.70	9.2 ± 1.8
13	PI(3)P 36:2	C45H84O16P2	C48H90O16P2	603.53469	7.00	157.8 ± 47.4

14	PI(3)P 36:3	C45H82O16P2	C48H88O16P2	601.51904	6.82	126.4 ± 38.6
15	PI(3)P 36:4	C45H80O16P2	C48H86O16P2	599.50339	6.71	44.7 ± 9.2
16	PI(4)P 32:0	C41H80O16P2	C44H86O16P2	551.50339	7.05	0.3 ± 0.1
17	PI(4)P 32:1	C41H78O16P2	C44H84O16P2	549.48774	6.81	12.1 ± 3.2
18	PI(4)P 32:2	C41H76O16P2	C44H82O16P2	547.47209	6.68	4.4 ± 0.9
19	PI(4)P 33:1	C42H80O16P2	C45H86O16P2	563.50339	6.97	2.8 ± 0.2
20	PI(4)P 33:2	C42H78O16P2	C45H84O16P2	561.48774	6.83	1.9 ± 0.3
21	PI(4)P 34:1	C43H82O16P2	C46H88O16P2	577.51904	7.12	225.0 ± 22.1
22	PI(4)P 34:2	C43H80O16P2	C46H86O16P2	575.50339	6.96	300.6 ± 34.3
23	PI(4)P 34:3	C43H78O16P2	C46H84O16P2	573.48774	6.85	60.1 ± 14.1
24	PI(4)P 34:4	C43H76O16P2	C46H82O16P2	571.47209	6.69	1.9 ± 0.4
25	PI(4)P 35:1	C44H84O16P2	C47H90O16P2	591.53469	7.34	4.6 ± 0.2
26	PI(4)P 35:2	C44H82O16P2	C47H88O16P2	589.51904	7.16	6.3 ± 0.5
27	PI(4)P 35:3	C44H80O16P2	C47H86O16P2	587.50339	6.93	3.9 ± 0.9
28	PI(4)P 36:2	C45H84O16P2	C48H90O16P2	603.53469	7.31	65.8 ± 13.7
29	PI(4)P 36:3	C45H82O16P2	C48H88O16P2	601.51904	7.09	40.3 ± 8.8
30	PI(4)P 36:4	C45H80O16P2	C48H86O16P2	599.50339	6.93	138.7 ± 33.2
31	PI(4)P 38:2	C47H88O16P2	C50H94O16P2	631.56599	7.70	1.0 ± 0.2
32	PI(5)P 36:0	C45H88O16P2	C48H94O16P2	607.56599	7.52	4.0 ± 1.0
33	PI(3,5)P2 32:1	C41H79O19P3	C46H89O19P3	549.48774	6.51	0.3 ± 0.1
34	PI(3,5)P2 33:1	C42H81O19P3	C47H91O19P3	563.50339	6.65	0.4 ± 0.0
35	PI(3,5)P2 33:2	C42H79O19P3	C47H89O19P3	561.48774	6.53	0.2 ± 0.0
36	PI(3,5)P2 34:1	C43H83O19P3	C48H93O19P3	577.51904	6.79	15.5 ± 4.2
37	PI(3,5)P2 34:2	C43H81O19P3	C48H91O19P3	575.50339	6.66	14.9 ± 3.5
38	PI(3,5)P2 35:1	C44H85O19P3	C49H95O19P3	591.53469	6.90	1.5 ± 0.4
39	PI(3,5)P2 35:2	C44H83O19P3	C49H93O19P3	589.51904	6.80	2.0 ± 0.5
40	PI(3,5)P2 36:1	C45H87O19P3	C50H97O19P3	605.55034	7.07	2.7 ± 0.6
41	PI(3,5)P2 36:2	C45H85O19P3	C50H95O19P3	603.53469	6.92	5.9 ± 1.2
42	PI(3,5)P2 36:3	C45H83O19P3	C50H93O19P3	601.51904	6.77	2.8 ± 0.5
43	PI(3,4)P2 32:0	C41H81O19P3	C46H91O19P3	551.50339	6.82	0.9 ± 0.3
44	PI(3,4)P2 32:1	C41H79O19P3	C46H89O19P3	549.48774	6.68	2.0 ± 0.4
45	PI(3,4)P2 33:1	C42H81O19P3	C47H91O19P3	563.50339	6.82	2.6 ± 1.0
46	PI(3,4)P2 33:2	C42H79O19P3	C47H89O19P3	561.48774	6.66	0.6 ± 0.1
47	PI(3,4)P2 34:1	C43H83O19P3	C48H93O19P3	577.51904	6.98	94.4 ± 22.4
48	PI(3,4)P2 34:2	C43H81O19P3	C48H91O19P3	575.50339	6.82	55.7 ± 22.8
49	PI(3,4)P2 35:1	C44H85O19P3	C49H95O19P3	591.53469	7.17	5.1 ± 2.3
50	PI(3,4)P2 35:2	C44H83O19P3	C49H93O19P3	589.51904	6.92	2.7 ± 0.4
51	PI(3,4)P2 36:0	C45H89O19P3	C50H99O19P3	607.56599	7.53	14.4 ± 4.7
52	PI(3,4)P2 36:1	C45H87O19P3	C50H97O19P3	605.55034	7.32	14.3 ± 5.5
53	PI(3,4)P2 36:2	C45H85O19P3	C50H95O19P3	603.53469	7.11	9.2 ± 2.4
54	PI(3,4)P2 36:3	C45H83O19P3	C50H93O19P3	601.51904	6.94	5.4 ± 1.1
55	PI(3,4)P2 38:2	C47H89O19P3	C52H99O19P3	631.56599	7.50	1.1 ± 0.0
56	PI(4,5)P2 32:0	C41H81O19P3	C46H91O19P3	551.50339	7.01	0.6 ± 0.2
57	PI(4,5)P2 32:1	C41H79O19P3	C46H89O19P3	549.48774	6.82	6.4 ± 2.0
58	PI(4,5)P2 32:2	C41H77O19P3	C46H87O19P3	547.47209	6.68	2.2 ± 0.5
59	PI(4,5)P2 33:1	C42H81O19P3	C47H91O19P3	563.50339	6.97	4.8 ± 1.5
60	PI(4,5)P2 33:2	C42H79O19P3	C47H89O19P3	561.48774	6.83	3.1 ± 0.8
61	PI(4,5)P2 34:1	C43H83O19P3	C48H93O19P3	577.51904	7.14	62.5 ± 2.5
62	PI(4,5)P2 34:2	C43H81O19P3	C48H91O19P3	575.50339	6.98	65.3 ± 3.5
63	PI(4,5)P2 34:3	C43H79O19P3	C48H89O19P3	573.48774	6.87	28.3 ± 8.1

64	PI(4,5)P2 34:4	C43H77O19P3	C48H87O19P3	571.47209	6.70	1.1 ± 0.2
65	PI(4,5)P2 35:1	C44H85O19P3	C49H95O19P3	591.53469	7.32	10.4 ± 4.1
66	PI(4,5)P2 35:2	C44H83O19P3	C49H93O19P3	589.51904	7.16	11.2 ± 4.1
67	PI(4,5)P2 35:3	C44H81O19P3	C49H91O19P3	587.50339	6.96	2.1 ± 0.4
68	PI(4,5)P2 36:1	C45H87O19P3	C50H97O19P3	605.55034	7.52	44.9 ± 11
69	PI(4,5)P2 36:2	C45H85O19P3	C50H95O19P3	603.53469	7.34	40 ± 10.4
70	PI(4,5)P2 36:3	C45H83O19P3	C50H93O19P3	601.51904	7.12	17.2 ± 4.6
71	PI(4,5)P2 36:4	C45H81O19P3	C50H91O19P3	599.50339	6.96	9.9 ± 2.7
72	PI(4,5)P2 36:5	C45H79O19P3	C50H89O19P3	597.48774	6.85	5.5 ± 1.6
73	PI(4,5)P2 36:6	C45H77O19P3	C50H87O19P3	595.47209	6.75	1.2 ± 0.2
74	PI(4,5)P2 37:1	C46H89O19P3	C51H99O19P3	619.56599	7.72	0.4 ± 0.0
75	PI(4,5)P2 38:2	C47H89O19P3	C52H99O19P3	631.56599	7.69	2.2 ± 0.5
76	PI(3,4,5)P3 34:1	C43H84O22P4	C50H98O22P4	577.51904	6.86	3.7 ± 1.4
77	PI(3,4,5)P3 34:2	C43H82O22P4	C50H96O22P4	575.50339	6.73	5.2 ± 1.8
78	PI(3,4,5)P3 34:3	C43H80O22P4	C50H94O22P4	573.48774	6.53	0.5 ± 0.2
79	PI(3,4,5)P3 35:2	C44H84O22P4	C51H98O22P4	589.51904	6.84	0.3 ± 0.1
80	PI(3,4,5)P3 35:3	C44H82O22P4	C51H96O22P4	587.50339	6.65	0.1 ± 0.1
81	PI(3,4,5)P3 36:3	C45H84O22P4	C52H98O22P4	601.51904	6.81	3.0 ± 0.9
82	PI(3,4,5)P3 36:4	C45H82O22P4	C52H96O22P4	599.50339	6.74	7.1 ± 2.4
83	PI(3,4,5)P3 36:5	C45H80O22P4	C52H94O22P4	597.48774	6.64	5.9 ± 2.0

MS tolerance was set 10 ppm. Retention time window was set 0.4 min.

Table S23 | Estimated concentration of PIPx in cultured HeLa cells (n= 3, biological replicates)

Nr.	PIPx	Formula	Methylated Formula	Fragment A [DAG]+	Rt, min	Conc., pmol/1.0e6 cells
1	PI(3)P 32:1	C41H78O16P2	C44H84O16P2	549.48774	6.58	1.5 ± 0.2
2	PI(3)P 34:0	C43H84O16P2	C46H90O16P2	579.53469	7.00	1.6 ± 0.2
3	PI(3)P 34:1	C43H82O16P2	C46H88O16P2	577.51904	6.88	11.2 ± 0.6
4	PI(3)P 34:2	C43H80O16P2	C46H86O16P2	575.50339	6.69	5.6 ± 0.7
5	PI(3)P 34:3	C43H78O16P2	C46H84O16P2	573.48774	6.55	0.7 ± 0.1
6	PI(3)P 36:1	C45H86O16P2	C48H92O16P2	605.55034	7.25	52.6 ± 6.2
7	PI(3)P 36:2	C45H84O16P2	C48H90O16P2	603.53469	7.00	32.8 ± 3.3
8	PI(3)P 36:3	C45H82O16P2	C48H88O16P2	601.51904	6.85	5.8 ± 0.2
9	PI(3)P 37:2	C46H86O16P2	C49H92O16P2	617.55034	7.19	0.7 ± 0.2
10	PI(3)P 38:1	C47H90O16P2	C50H96O16P2	633.58164	7.65	33.2 ± 8.6
11	PI(3)P 38:2	C47H88O16P2	C50H94O16P2	631.56599	7.36	42.3 ± 3.2
12	PI(3)P 38:3	C47H86O16P2	C50H92O16P2	629.55034	7.21	59.5 ± 5.8
13	PI(3)P 38:4	C47H84O16P2	C50H90O16P2	627.53469	6.99	14.2 ± 1.3
14	PI(3)P 38:5	C47H82O16P2	C50H88O16P2	625.51904	6.88	3.2 ± 0.7
15	PI(3)P 40:2	C49H92O16P2	C52H98O16P2	659.59729	7.74	5.0 ± 0.4
16	PI(3)P 40:4	C49H88O16P2	C52H94O16P2	655.56599	7.33	6.5 ± 0.6
17	PI(3)P 40:5	C49H86O16P2	C52H92O16P2	653.55034	7.15	1.5 ± 0.2
18	PI(5)P 32:0	C41H80O16P2	C44H86O16P2	551.50339	6.85	1.1 ± 0.1
19	PI(5)P 34:0	C43H84O16P2	C46H90O16P2	579.53469	7.17	3.6 ± 0.6
20	PI(5)P 34:1	C43H82O16P2	C46H88O16P2	577.51904	6.99	9.7 ± 0.8
21	PI(5)P 34:2	C43H80O16P2	C46H86O16P2	575.50339	6.82	8.2 ± 0.9
22	PI(5)P 34:3	C43H78O16P2	C46H84O16P2	573.48774	6.65	0.9 ± 0.2
23	PI(5)P 36:0	C45H88O16P2	C48H94O16P2	607.56599	7.56	6.4 ± 2.9

24	PI(5)P 36:1	C45H86O16P2	C48H92O16P2	605.55034	7.34	53.4 ± 9.2
25	PI(5)P 36:2	C45H84O16P2	C48H90O16P2	603.53469	7.14	39.0 ± 2.2
26	PI(5)P 36:3	C45H82O16P2	C48H88O16P2	601.51904	6.97	7.3 ± 0.8
27	PI(5)P 36:4	C45H80O16P2	C48H86O16P2	599.50339	6.77	3.6 ± 0.6
28	PI(5)P 37:2	C46H86O16P2	C49H92O16P2	617.55034	7.34	0.7 ± 0.1
29	PI(5)P 38:1	C47H90O16P2	C50H96O16P2	633.58164	7.74	71.2 ± 43.6
30	PI(5)P 38:3	C47H86O16P2	C50H92O16P2	629.55034	7.35	95.0 ± 18.4
31	PI(5)P 38:4	C47H84O16P2	C50H90O16P2	627.53469	7.11	14.6 ± 1.1
32	PI(5)P 39:3	C48H88O16P2	C51H94O16P2	643.56599	7.57	1.5 ± 0.2
33	PI(5)P 40:2	C49H92O16P2	C52H98O16P2	659.59729	7.95	25.9 ± 1.6
34	PI(5)P 40:4	C49H88O16P2	C52H94O16P2	655.56599	7.50	9.0 ± 1.1
35	PI(5)P 40:5	C49H86O16P2	C52H92O16P2	653.55034	7.31	2.1 ± 0.4
36	PI(4)P 32:0	C41H80O16P2	C44H86O16P2	551.50339	7.04	2.3 ± 0.1
37	PI(4)P 32:1	C41H78O16P2	C44H84O16P2	549.48774	6.84	11.0 ± 1.0
38	PI(4)P 34:0	C43H84O16P2	C46H90O16P2	579.53469	7.42	8.8 ± 0.7
39	PI(4)P 34:1	C43H82O16P2	C46H88O16P2	577.51904	7.17	86.8 ± 2.5
40	PI(4)P 34:2	C43H80O16P2	C46H86O16P2	575.50339	6.96	52.2 ± 1.8
41	PI(4)P 34:3	C43H78O16P2	C46H84O16P2	573.48774	6.81	3.3 ± 0.3
42	PI(4)P 36:0	C45H88O16P2	C48H94O16P2	607.56599	7.84	18.1 ± 3.2
43	PI(4)P 36:1	C45H86O16P2	C48H92O16P2	605.55034	7.55	327.8 ± 22.4
44	PI(4)P 36:2	C45H84O16P2	C48H90O16P2	603.53469	7.31	322.4 ± 17.6
45	PI(4)P 36:3	C45H82O16P2	C48H88O16P2	601.51904	7.13	44.9 ± 3.8
46	PI(4)P 36:4	C45H80O16P2	C48H86O16P2	599.50339	6.98	3.5 ± 0.1
47	PI(4)P 37:2	C46H86O16P2	C49H92O16P2	617.55034	7.52	2.3 ± 0.0
48	PI(4)P 38:1	C47H90O16P2	C50H96O16P2	633.58164	8.02	39.5 ± 6.6
49	PI(4)P 38:2	C47H88O16P2	C50H94O16P2	631.56599	7.74	408.3 ± 55.3
50	PI(4)P 38:3	C47H86O16P2	C50H92O16P2	629.55034	7.53	420.6 ± 30.9
51	PI(4)P 38:4	C47H84O16P2	C50H90O16P2	627.53469	7.31	118.4 ± 10.7
52	PI(4)P 38:5	C47H82O16P2	C50H88O16P2	625.51904	7.14	7.4 ± 0.7
53	PI(4)P 39:3	C48H88O16P2	C51H94O16P2	643.56599	7.74	7.5 ± 0.6
54	PI(4)P 39:4	C48H86O16P2	C51H92O16P2	641.55034	7.48	1.7 ± 0.4
55	PI(4)P 40:2	C49H92O16P2	C52H98O16P2	659.59729	8.14	23.5 ± 1.1
56	PI(4)P 40:4	C49H88O16P2	C52H94O16P2	655.56599	7.72	72.0 ± 3.1
57	PI(4)P 40:5	C49H86O16P2	C52H92O16P2	653.55034	7.49	10.6 ± 0.6
58	PI(4)P 42:5	C51H90O16P2	C54H96O16P2	681.58164	7.85	1.9 ± 0.2
59	PI(3,5)P2 32:0	C41H81O19P3	C46H91O19P3	551.50339	6.65	0.3 ± 0.1
60	PI(3,5)P2 32:1	C41H79O19P3	C46H89O19P3	549.48774	6.53	0.7 ± 0.2
61	PI(3,5)P2 34:0	C43H85O19P3	C48H95O19P3	579.53469	6.97	0.5 ± 0.2
62	PI(3,5)P2 34:1	C43H83O19P3	C48H93O19P3	577.51904	6.79	4.5 ± 0.7
63	PI(3,5)P2 34:2	C43H81O19P3	C48H91O19P3	575.50339	6.63	2.7 ± 0.2
64	PI(3,5)P2 34:3	C43H79O19P3	C48H89O19P3	573.48774	6.52	0.3 ± 0.1
65	PI(3,5)P2 36:1	C45H87O19P3	C50H97O19P3	605.55034	7.09	10.5 ± 1.1
66	PI(3,5)P2 36:2	C45H85O19P3	C50H95O19P3	603.53469	6.90	13.2 ± 1.0
67	PI(3,5)P2 36:3	C45H83O19P3	C50H93O19P3	601.51904	6.78	2.8 ± 0.2
68	PI(3,5)P2 38:2	C47H89O19P3	C52H99O19P3	631.56599	7.24	13.6 ± 1.0
69	PI(3,5)P2 38:3	C47H87O19P3	C52H97O19P3	629.55034	7.09	23.6 ± 1.9
70	PI(3,5)P2 38:4	C47H85O19P3	C52H95O19P3	627.53469	6.91	6.2 ± 1.2
71	PI(3,5)P2 38:5	C47H83O19P3	C52H93O19P3	625.51904	6.76	0.4 ± 0.1
72	PI(3,5)P2 40:4	C49H89O19P3	C54H99O19P3	655.56599	7.22	2.7 ± 0.1
73	PI(3,4)P2 32:0	C41H81O19P3	C46H91O19P3	551.50339	6.84	1.9 ± 0.2

74	PI(3,4)P2 32:1	C41H79O19P3	C46H89O19P3	549.48774	6.67	0.8 ± 0.1
75	PI(3,4)P2 34:0	C43H85O19P3	C48H95O19P3	579.53469	7.17	7.4 ± 0.9
76	PI(3,4)P2 34:1	C43H83O19P3	C48H93O19P3	577.51904	6.96	5.3 ± 0.7
77	PI(3,4)P2 34:3	C43H79O19P3	C48H89O19P3	573.48774	6.65	0.8 ± 0.1
78	PI(3,4)P2 36:0	C45H89O19P3	C50H99O19P3	607.56599	7.55	29.4 ± 3.7
79	PI(3,4)P2 36:1	C45H87O19P3	C50H97O19P3	605.55034	7.31	39.2 ± 12.7
80	PI(3,4)P2 36:2	C45H85O19P3	C50H95O19P3	603.53469	7.13	13.1 ± 4.7
81	PI(3,4)P2 36:3	C45H83O19P3	C50H93O19P3	601.51904	6.93	1.8 ± 0.2
82	PI(3,4)P2 38:1	C47H91O19P3	C52H101O19P3	633.58164	7.72	75.9 ± 8.9
83	PI(3,4)P2 38:2	C47H89O19P3	C52H99O19P3	631.56599	7.53	121.9 ± 5.3
84	PI(3,4)P2 38:3	C47H87O19P3	C52H97O19P3	629.55034	7.29	33.9 ± 10.6
85	PI(3,4)P2 38:4	C47H85O19P3	C52H95O19P3	627.53469	7.14	6.7 ± 2.1
86	PI(3,4)P2 38:5	C47H83O19P3	C52H93O19P3	625.51904	6.88	1.3 ± 0.3
87	PI(3,4)P2 40:1	C49H95O19P3	C54H105O19P3	661.61294	8.12	3.9 ± 0.2
88	PI(3,4)P2 40:2	C49H93O19P3	C54H103O19P3	659.59729	7.92	22.6 ± 3
89	PI(4,5)P2 32:0	C41H81O19P3	C46H91O19P3	551.50339	7.02	0.8 ± 0.1
90	PI(4,5)P2 32:1	C41H79O19P3	C46H89O19P3	549.48774	6.84	4.0 ± 0.2
91	PI(4,5)P2 34:0	C43H85O19P3	C48H95O19P3	579.53469	7.37	1.2 ± 0.1
92	PI(4,5)P2 34:1	C43H83O19P3	C48H93O19P3	577.51904	7.16	31.9 ± 3
93	PI(4,5)P2 34:2	C43H81O19P3	C48H91O19P3	575.50339	6.96	20.4 ± 2.1
94	PI(4,5)P2 34:3	C43H79O19P3	C48H89O19P3	573.48774	6.82	1.2 ± 0.1
95	PI(4,5)P2 36:0	C45H89O19P3	C50H99O19P3	607.56599	7.67	2.4 ± 0.8
96	PI(4,5)P2 36:1	C45H87O19P3	C50H97O19P3	605.55034	7.54	73.6 ± 9.7
97	PI(4,5)P2 36:2	C45H85O19P3	C50H95O19P3	603.53469	7.31	77.1 ± 9.8
98	PI(4,5)P2 36:3	C45H83O19P3	C50H93O19P3	601.51904	7.13	17.1 ± 1.7
99	PI(4,5)P2 36:4	C45H81O19P3	C50H91O19P3	599.50339	6.99	1.3 ± 0.0
100	PI(4,5)P2 37:2	C46H87O19P3	C51H97O19P3	617.55034	7.52	0.8 ± 0.1
101	PI(4,5)P2 38:1	C47H91O19P3	C52H101O19P3	633.58164	7.93	5.9 ± 0.5
102	PI(4,5)P2 38:2	C47H89O19P3	C52H99O19P3	631.56599	7.72	83.0 ± 10.8
103	PI(4,5)P2 38:3	C47H87O19P3	C52H97O19P3	629.55034	7.53	85.7 ± 11.4
104	PI(4,5)P2 38:4	C47H85O19P3	C52H95O19P3	627.53469	7.31	35.2 ± 2.2
105	PI(4,5)P2 38:5	C47H83O19P3	C52H93O19P3	625.51904	7.15	2.3 ± 0.3
106	PI(4,5)P2 39:3	C48H89O19P3	C53H99O19P3	643.56599	7.73	1.9 ± 0.1
107	PI(4,5)P2 39:4	C48H87O19P3	C53H97O19P3	641.55034	7.50	0.6 ± 0.0
108	PI(4,5)P2 40:1	C49H95O19P3	C54H105O19P3	661.61294	8.40	0.6 ± 0.0
109	PI(4,5)P2 40:2	C49H93O19P3	C54H103O19P3	659.59729	8.11	9.4 ± 0.4
110	PI(4,5)P2 40:3	C49H91O19P3	C54H101O19P3	657.58164	7.92	57.9 ± 8.0
111	PI(4,5)P2 40:4	C49H89O19P3	C54H99O19P3	655.56599	7.72	17.3 ± 1.3
112	PI(4,5)P2 40:5	C49H87O19P3	C54H97O19P3	653.55034	7.50	3.1 ± 0.3
113	PI(4,5)P2 42:5	C51H91O19P3	C56H101O19P3	681.58164	7.87	0.7 ± 0.0
114	PI(3,4,5)P3 32:1	C41H80O22P4	C48H94O22P4	549.48774	6.62	0.2 ± 0.1
115	PI(3,4,5)P3 34:1	C43H84O22P4	C50H98O22P4	577.51904	6.91	1.1 ± 0.3
116	PI(3,4,5)P3 34:2	C43H82O22P4	C50H96O22P4	575.50339	6.73	1.2 ± 0.5
117	PI(3,4,5)P3 36:3	C45H84O22P4	C52H98O22P4	601.51904	6.87	0.4 ± 0.1
118	PI(3,4,5)P3 36:4	C45H82O22P4	C52H96O22P4	599.50339	6.76	0.6 ± 0.3
119	PI(3,4,5)P3 38:2	C47H90O22P4	C54H104O22P4	631.56599	7.27	0.2 ± 0.1
120	PI(3,4,5)P3 38:3	C47H88O22P4	C54H102O22P4	629.55034	7.16	0.5 ± 0.2
121	PI(3,4,5)P3 38:5	C47H84O22P4	C54H98O22P4	625.51904	6.88	0.2 ± 0.1

MS tolerance was set 10 ppm. Retention time window was set 0.4 min.

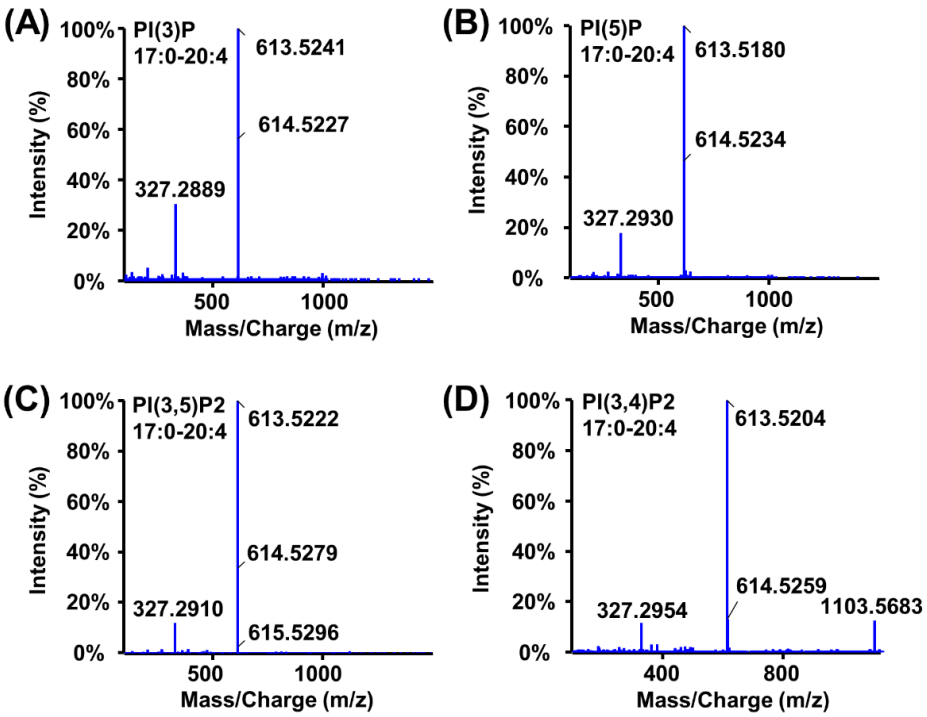

Figure S1 | Product ion spectra of regioisomers of methylated 17:0/20:4 PIP and PIP2 (positive ESI mode). (A) PI(3)P. (B) PI(5)P. (C) PI(3,5)P2. (D) PI(3,4)P2. No extra characteristic fragments besides fragment A and B (described in main document) were found for the different regioisomers.

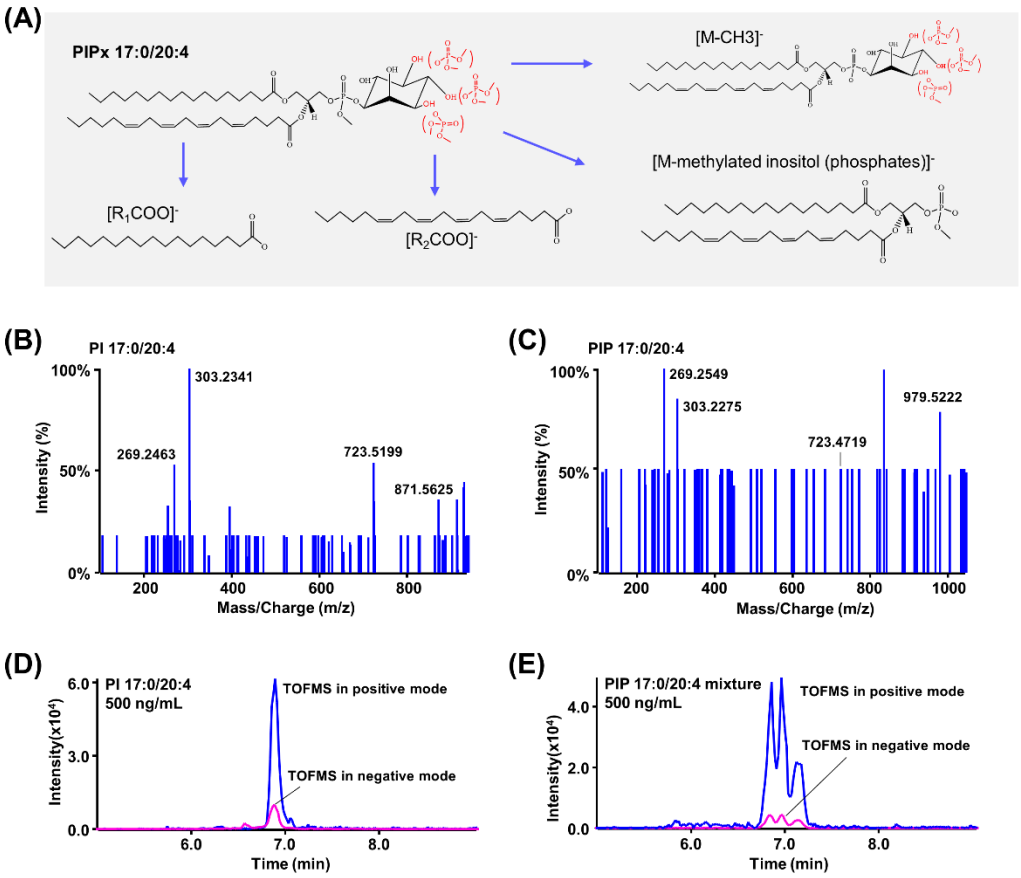

Figure S2 | MS fragmentation in negative ESI mode. (A) Fragmentation reactions of methylated PIPx in negative mode. (B-C) Product ion spectra of 17:0/20:4 PI and PIP. (D-E) Overlap of chromatogram in positive and negative mode. Although fragments arising from fatty acyl chains were observed in negative mode, ionization efficiency was significantly lower compared to that in positive mode. Signals of PIP2 and PIP3 are not shown due to low signal intensity.

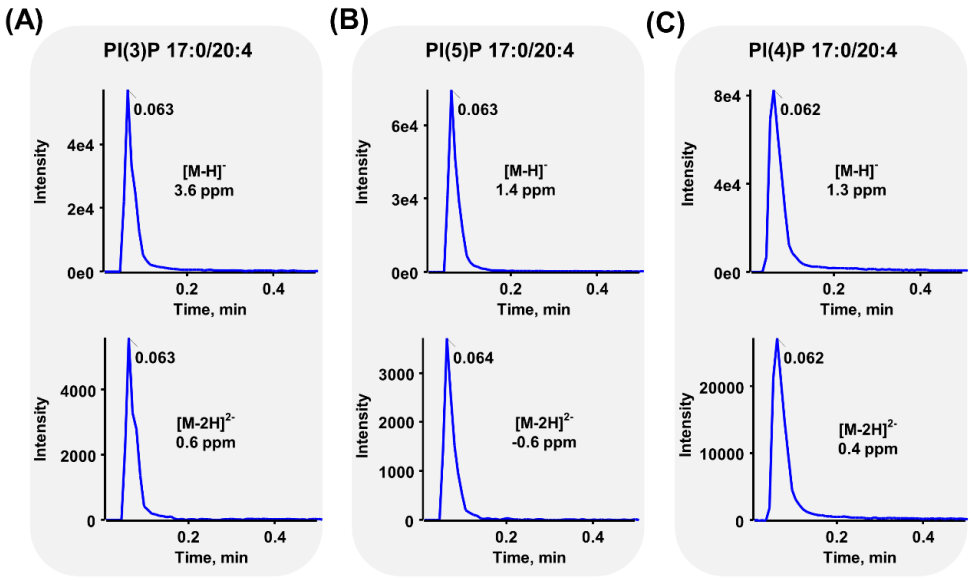

Figure S3 | Flow injection analysis (FIA) results of original PIP 17:0/20:4 regioisomers. Single charge ions were taken for measurement. Mobile phase: 10mM ammonium formate in 50% methanol in water. Flow 0.5 mL/min. MS parameters: TOFMS scan 50 – 1250, negative mode, CUR 30, Gas1 40, Gas2 50, Voltage -3500V, temperature 500 °C, DP -70V, CE -10V, accumulation time 500 ms.

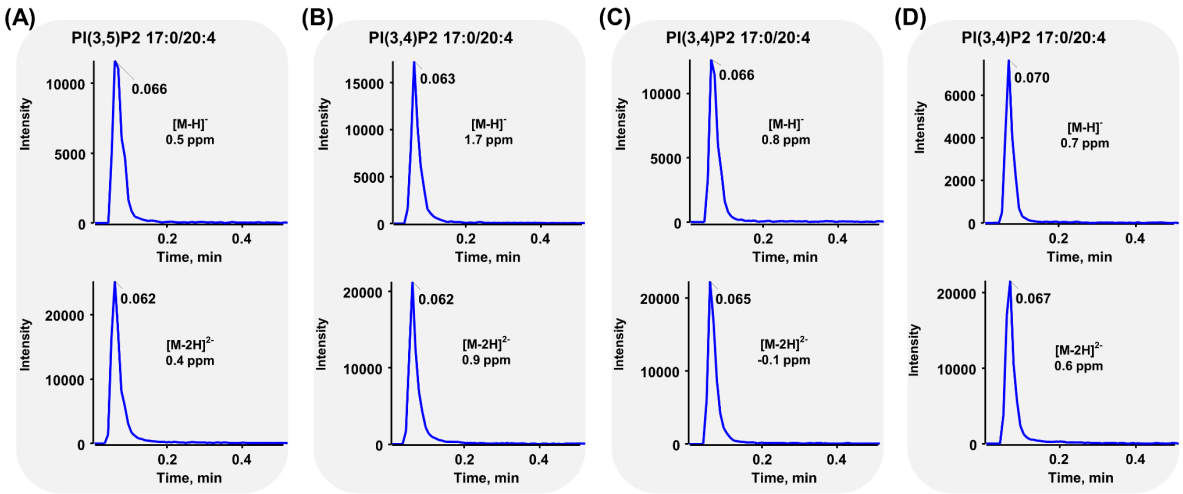

Figure S4 | Flow injection analysis (FIA) results of original PIP2 17:0/20:4 regioisomers and PIP3. Double charged ions were taken for measurement. Mobile phase: 10mM ammonium formate in 50% methanol in water. Flow 0.5 mL/min. MS parameters: TOFMS scan 50 – 1250, negative mode, CUR 30, Gas1 40, Gas2 50, Voltage -3500V, temperature 500 °C, DP -70V, CE -10V, accumulation time 500 ms.

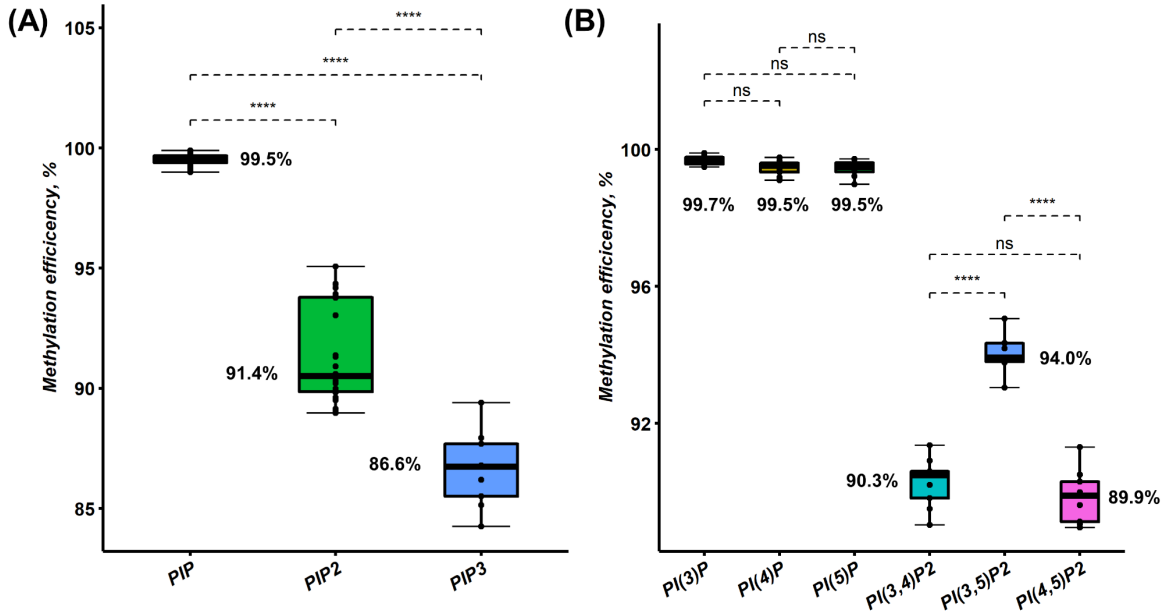

Figure S5 | Methylation efficiency of PIPx 17:0/20:4. Data was acquired using single standards of PIPx. (A) comparison between PIPx with different degrees of phosphorylation (t test, p value adjusted by Bonferroni–Holm method, ns: adjusted p value > 0.05, ****: adjusted p value < 1e-4). Mean value of methylation efficiency was labeled for each group. (B) comparison between PIPx with different regioisomers (t test, p value adjusted by Bonferroni–Holm method, ns: adjusted p value > 0.05, ****: adjusted p value < 1e-4). Mean value of methylation efficiency was labeled for each group.

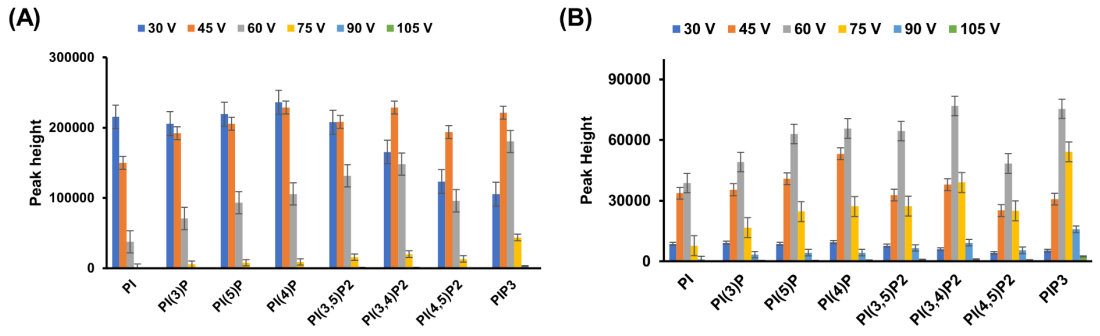

Figure S6 | Optimization of collision energy from 30 V to 105 V. (A) Results of fragment A, optimum around 45 V. (B) Results of fragment B, optimum around 60 V.

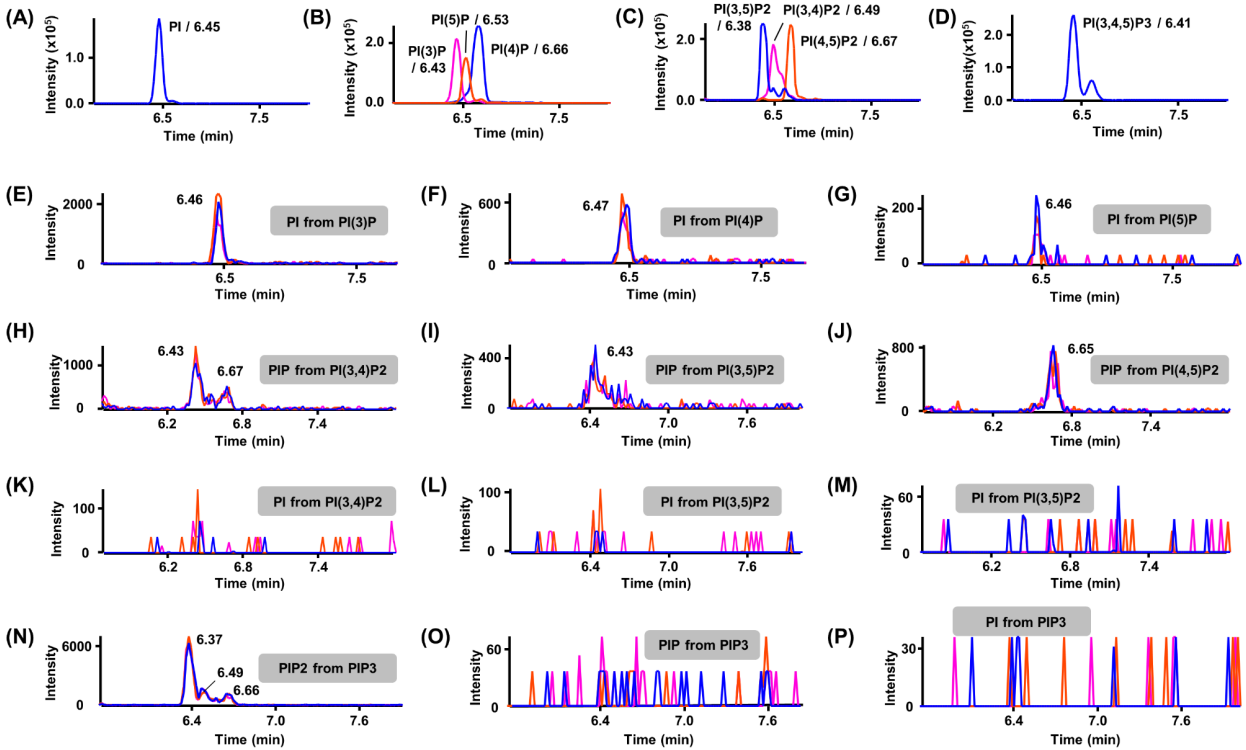

Figure S7 | Evaluation of in source fragmentation risk using 17:0/20:4 PIPx standards with three different declustering potential values. (A-D) Chromatograms of PI, PI(3)P, PI(5)P, PI(4)P, PI(3,5)P2, PI(3,4)P2, PI(4,5)P2 and PI(3,4,5)P3. (E-G) PI extracted from single standard sample of PIP isomers. (H-J) PIP extracted from single standard sample of PIP2 isomers. (K-M) PI extracted from single standard sample of PIP2 isomers. (n-p) PI, PIP and PIP2 extracted from single standard sample of PI(3,4,5)P3. Under varied DP values, there was no significant trend found in intensity of extracted signals. These extracted in source fragmentation signals exhibited the same retention times as PIPx with less phosphates but not of the corresponding samples from which they would originate in case of in-source fragmentation, which indicates these signals stem from impurities rather than in source fragmentation. For example, the PI peak in (E), (F) and (G) elute at 6.46, 6.47, 6.46 min which is the retention time of PI shown in (A), but do not correspond to the retention times of PI(3)P (6.43 min), PI(5)P (6.53 min) and PI(4)P (6.66 min) at which the PI peak would be detected in case of its formation by in-source fragmentation. Likewise, the retention times of PIP measured in PI(3,4)P2 (H) correspond to those of the three PIP constitutional isomers (B) and hence do not originate from in-source fragmentation. The PIP peak in (I) also elutes later than its expected retention at 6.38 min for the in-source fragment from PI(3,5)P2. Since IP(4)P and PI(4,5)P2 both elute at 6.66 and 6.65 min, respectively, it is inadequate for a proof, however, in analogy to (H) and (I) no in-source-fragmentation is expected. No peaks are observed in (K) to (M) and (O) to (P) which means no insource fragmentations for the analytes injected in those examples. The PIP2 peaks in (N) correspond to the PIP2 regioisomers, but not the PIP3 retention time.

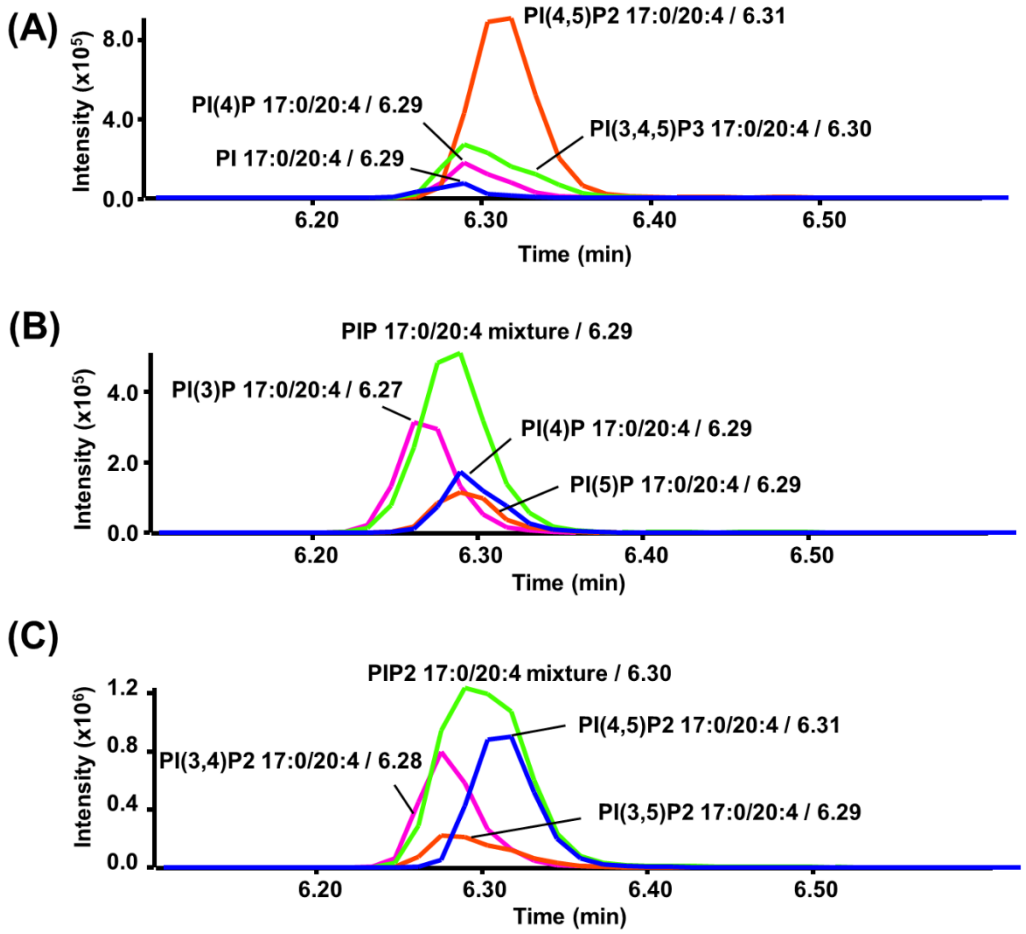

Figure S8 | Selectivity of RPLC. (A) PIPx 17:0/20:4 with different phosphorylation degrees, (B) PIP 17:0/20:4 regioisomer standards and mixture and (C) PIP 17:0/20:4 regioisomer standards and mixture were analyzed. Analysis was conducted on CSH C18 column (1.7 µm, 2.1x100mm) with 10 mM ammonium formate in water and methanol as eluent A and B, respectively. Column temperature and flow rate were 50 °C and 0.5 mL/min. Eluent B was increased from 50% to 100% in 5 min followed by a hold for 7 min. Afterwards, the gradient went back to initial conditions in 1 min and the column equilibrated for 2 min.

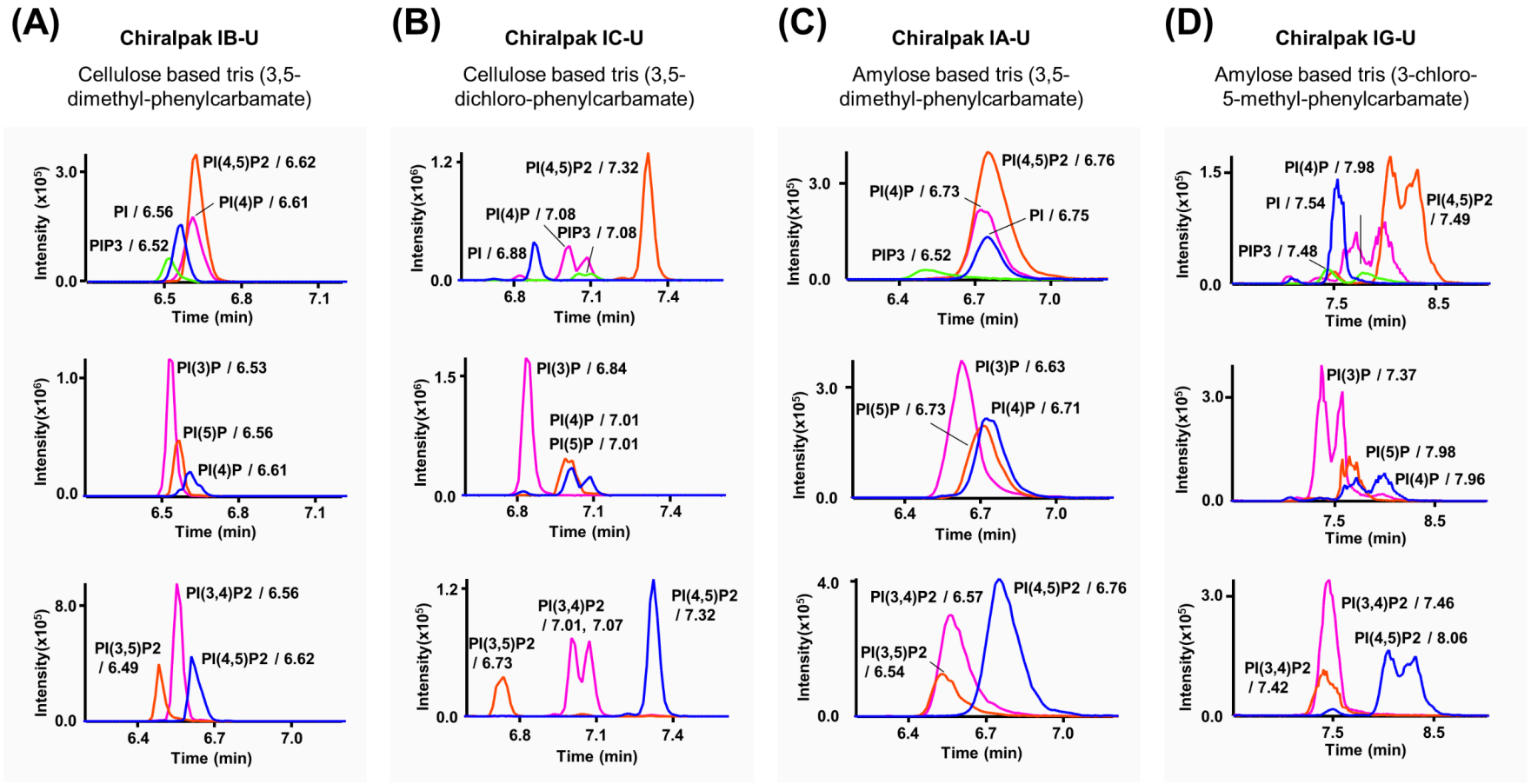

Figure S9 | Column screening with immobilized polysaccharide chiral columns: (A) Chirpak IB-U, (B) Chirpak IC-U, (C) Chirpak IA-U and (D) Chiralpak IG-U. Screening experiments were performed with single PIPx standards and linear gradient. Eluents were 10 mM ammonium formate in water and methanol, respectively, with a flow rate at 0.4 mL/min. Column temperature was consistently at 30 °C. Eluent B started from 20% to 100% in 5 min followed by a hold at 100% B for 7 min. The gradient went back to initial conditions in 1 min and then the column was equilibrated for 2 min.

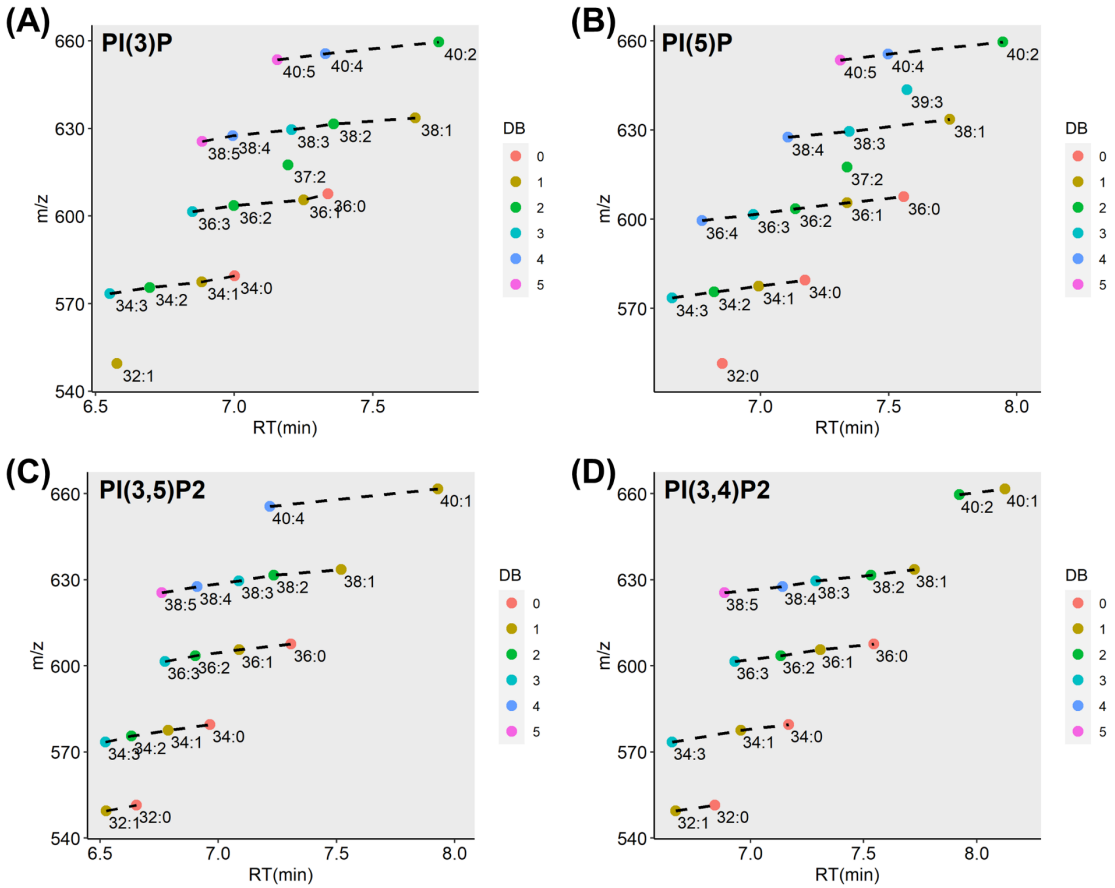

Figure S10 | Intra class retention patterns of PIPx regioisomers.

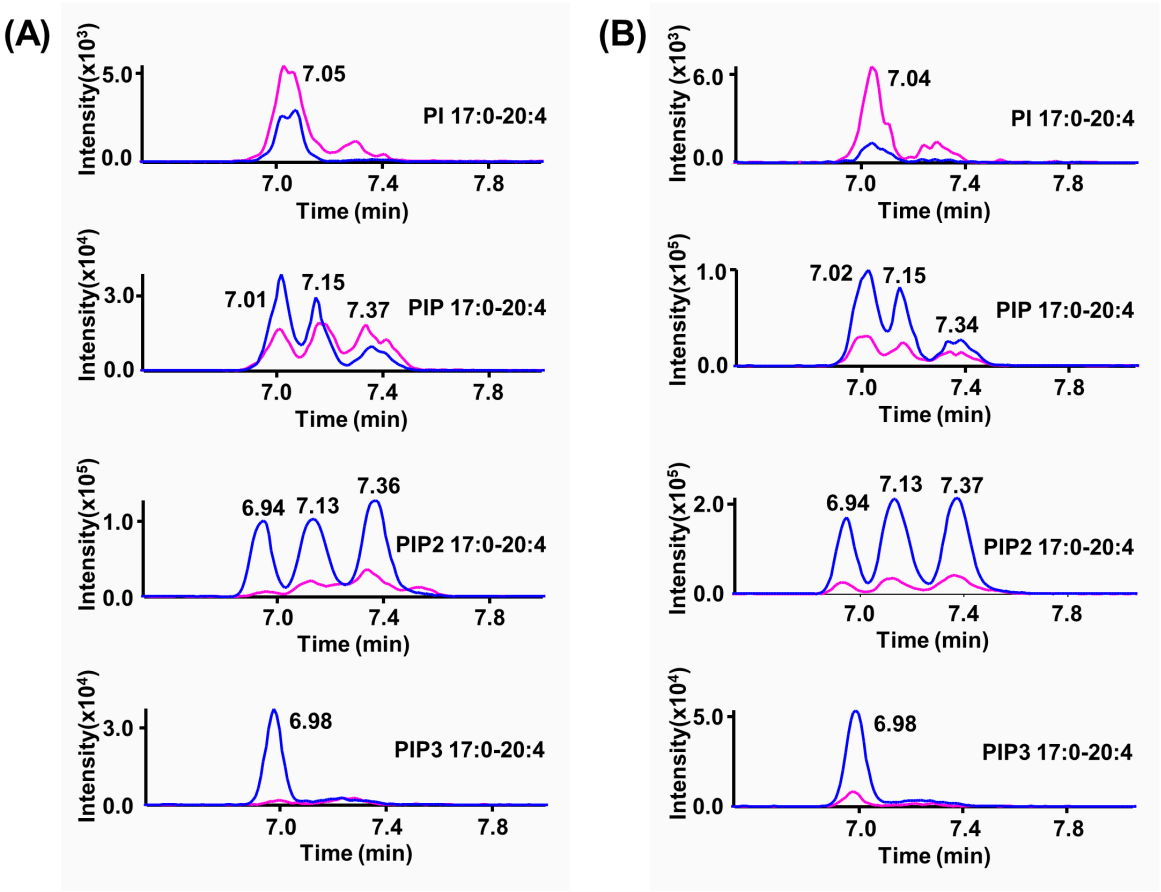

Figure S11 | Extraction protocol comparison in (A) human plasma and (B) cultured HeLa cells. For acidic extraction, the sample was homogenized and extracted with MTBE/MeOH/2N HCl (200:60:13, v/v/v). For the two-step extraction approach, the sample was homogenized and extracted first with CH_3Cl_3/MeOH (1:2, v/v). After removal of the supernatant, the residue was extracted again with MTBE/MeOH/2N HCl (200:60:13, v/v/v). All samples were submitted for methylation and measurement in the same manner. Combined extraction was found to be favorable for PIPx, especially for PIPx with more phosphates.

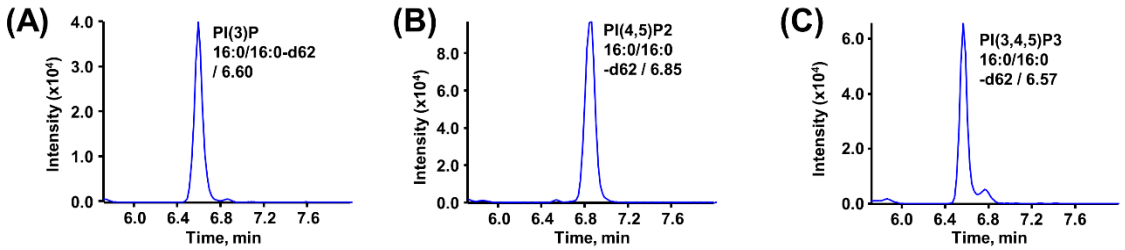

Figure S12 | Chromatograms of stable isotope labeled standards: (A) PI(3)P 16:0/16:0-d62, (B) PI(4,5)P2 16:0/16:0-d62 and (C) PI(3,4,5)P3 16:0/16:0-d62.

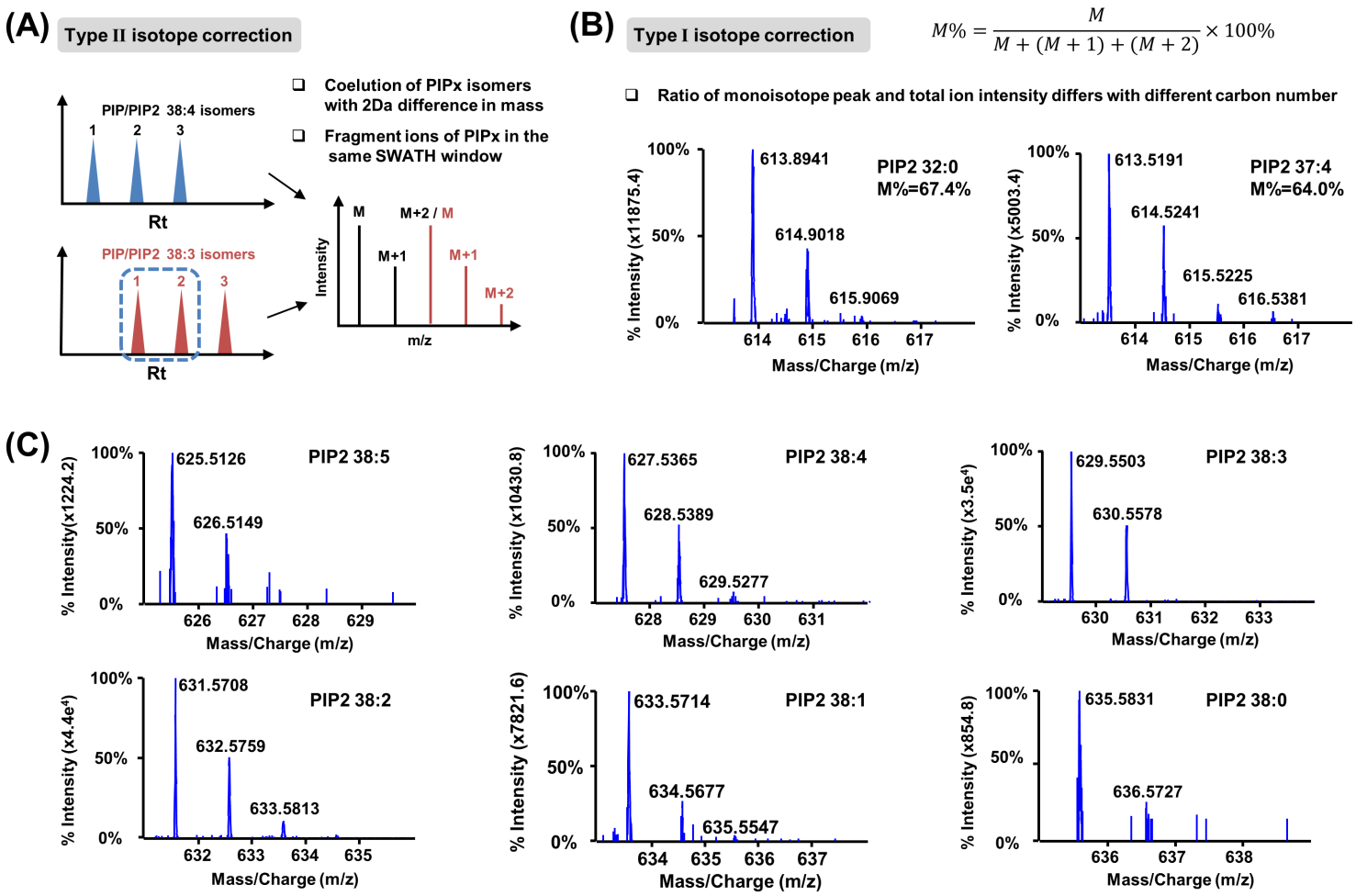

Figure S13 | Isotope corrections. (A) Type I isotope correction caused by coelution and difference only in one unsaturation. (B) Type II isotope correction resulting from ion ratio between monoisotopic peak intensity versus total ion intensity. (C) Representative MS2 spectra of PIP2 in HeLa cells.

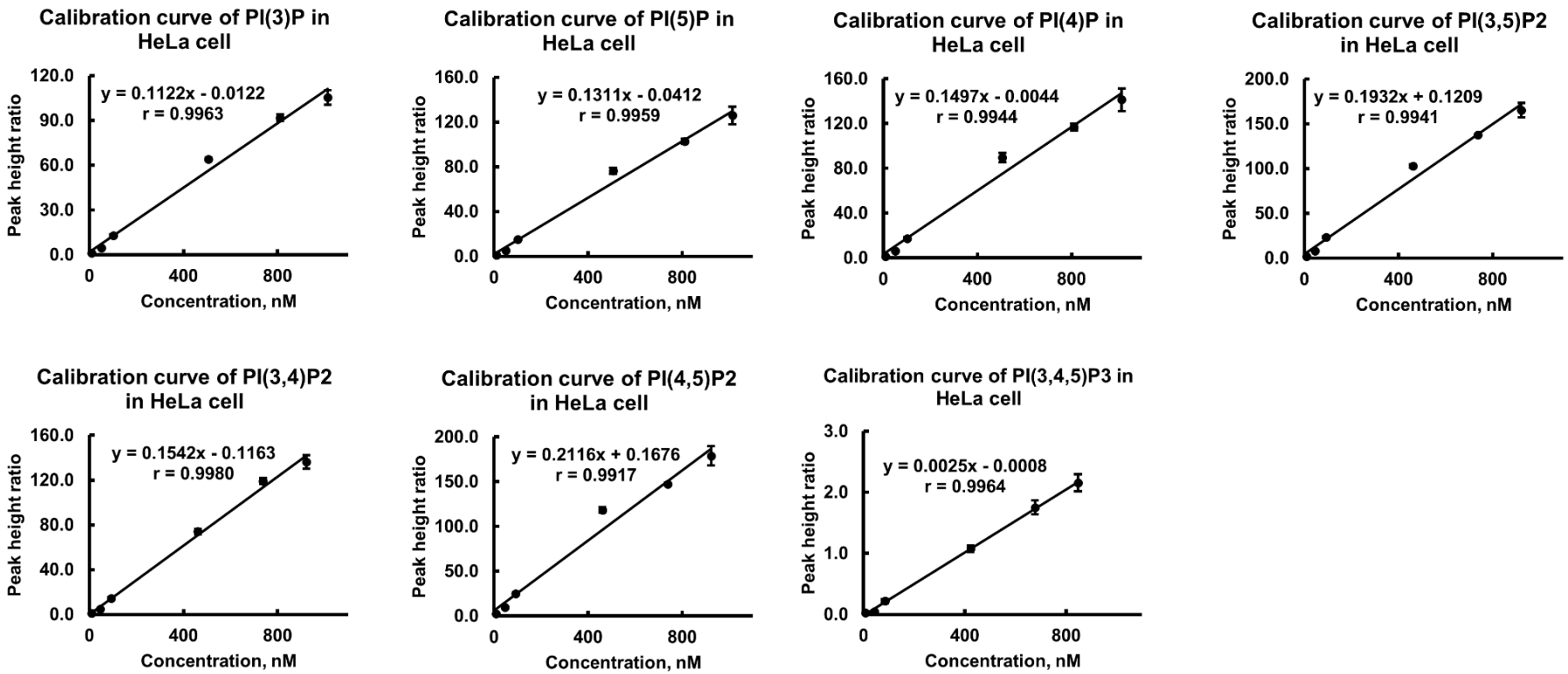

Figure S14 | Calibration curves of PIPx in cultured HeLa cells. Weighting 1/x was used.

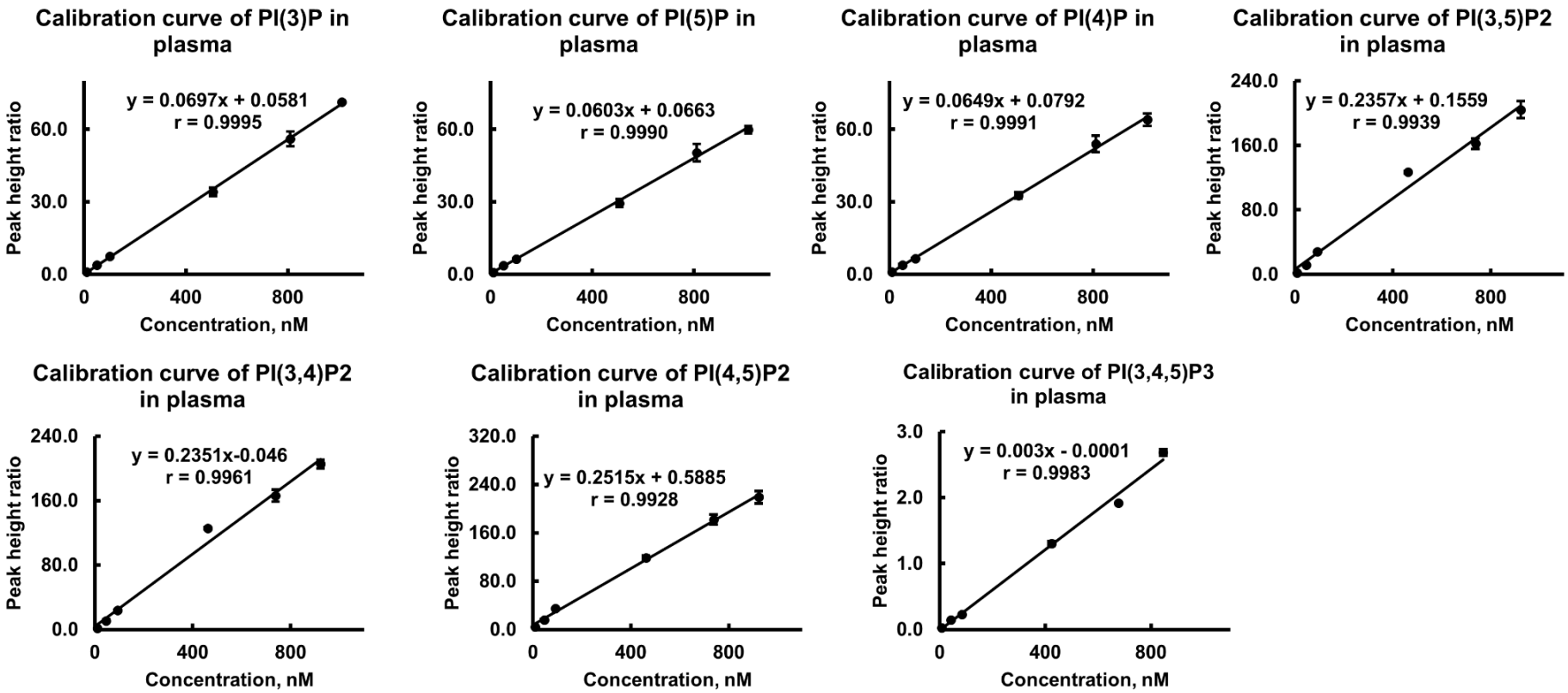

Figure S15 | Calibration curves of PIPx in human plasma. Weighting 1/x was used.

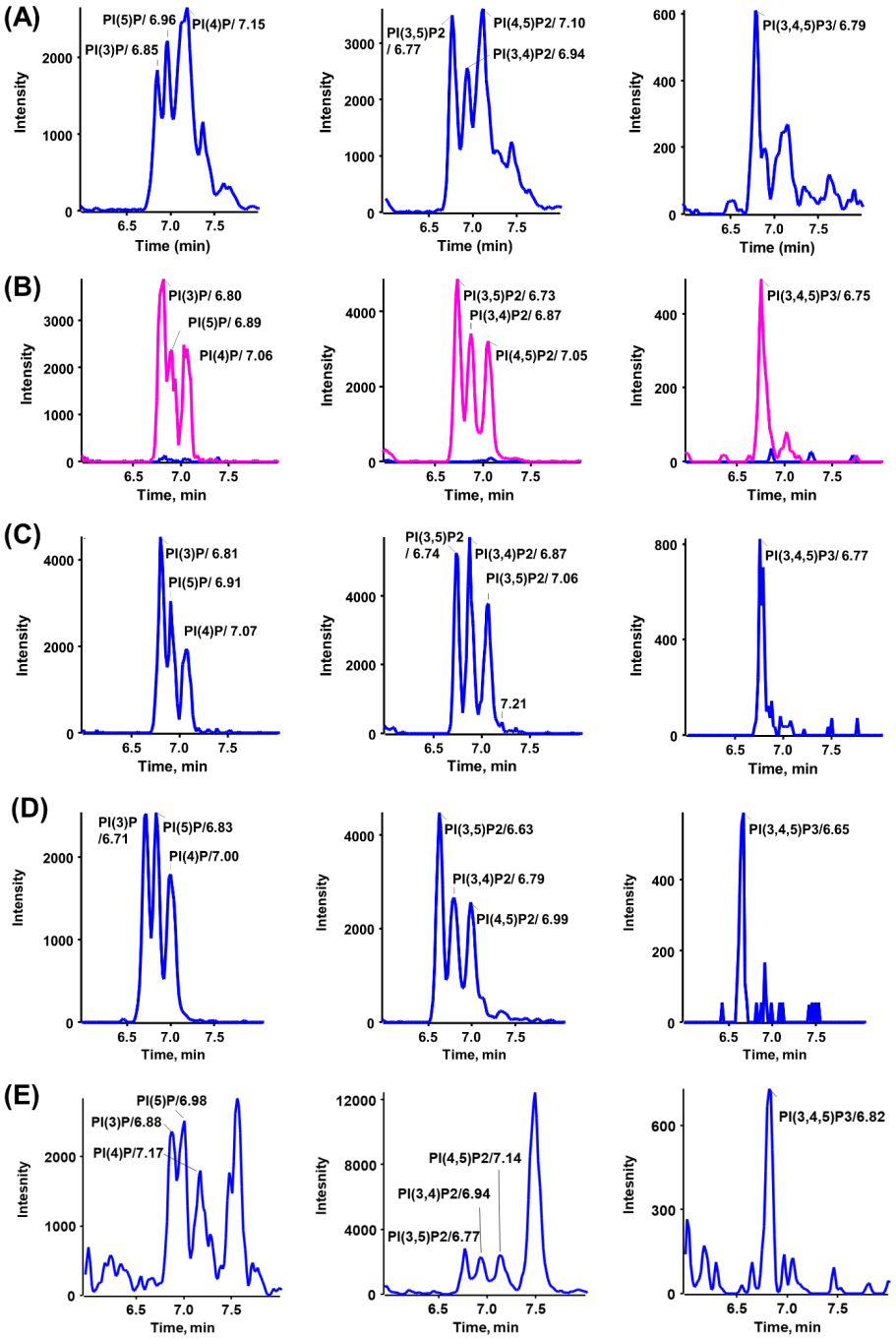

Figure S16 | Representative chromatograms of PIPx 17:0/20:4. (A) Standards spiked at LOQs based on fragment A before extraction in HeLa cell sample. (B) Unspiked sample (blue) with spiked standards (pink) at LOQs based on fragment A, measured with narrowed SWATH window (5Da). (C) Neat standard solution at LOQs based on fragment A measured with narrowed SWATH window (5Da). (D) Standards spiked at LOQs based on fragment A before extraction in HeLa cell sample, measured with recommended SWATH design (as listed in table S3, window width 12Da). (E) Precursor chromatograms spiked at LOQs based on precursor before extraction in HeLa cell sample. LOQs based on fragment A are listed in Table S4. LOQs based on the precursor are listed in Table S15.

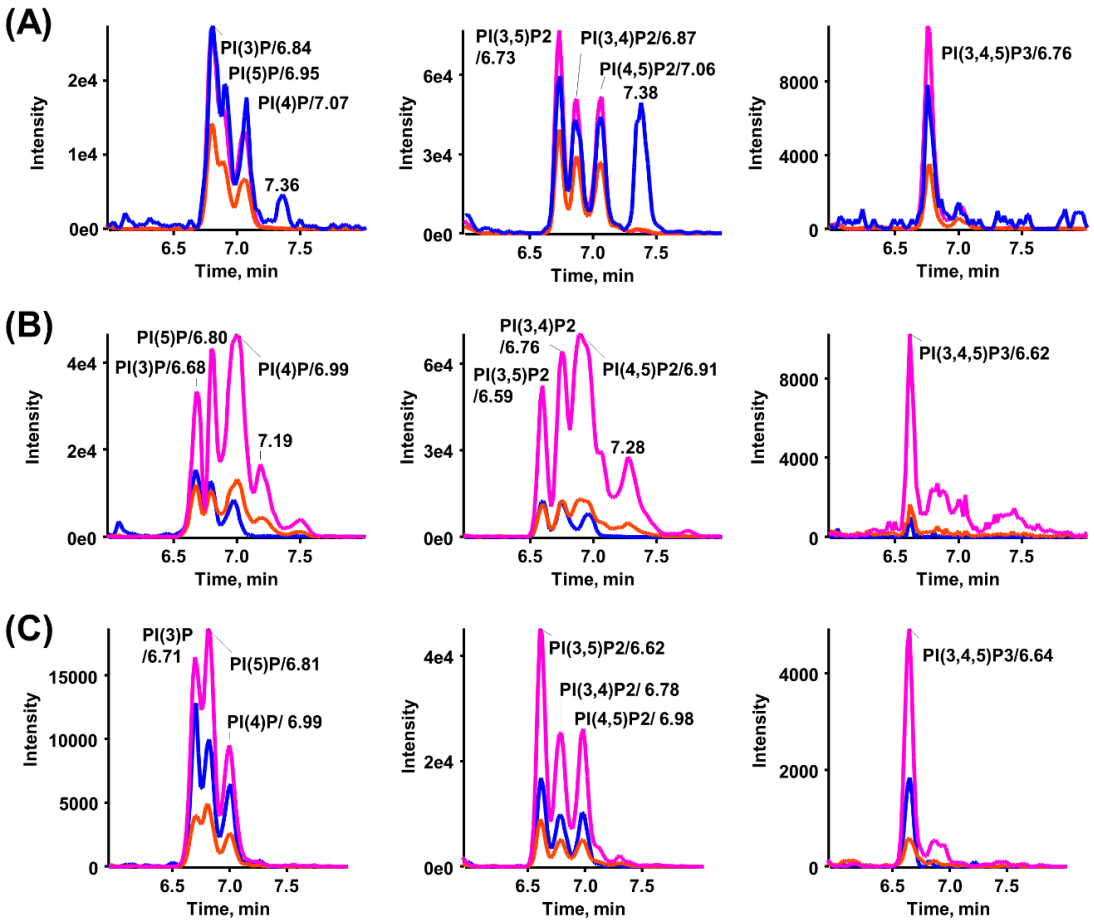

Figure S17 | Comparison of different SWATH widths: (A) 5 Da, (B) 25 Da and (C) 12 Da. PIPx 17:0/20:4 standards were spiked at the same concentration level in the HeLa cells and measured separately with different SWATH width, keeping the cycle time constant at 1s. Due to the comprehensive acquisition by SWATH, we could extract different chromatograms (XIC, blue: precursor, pink: fragment A and red: fragment B). Comparing the retention profiles of different XIC chromatograms, the most suitable signal (tradeoff between specificity and sensitivity) can be taken for further quantitation, e.g. in B) precursor ion (blue) for PIP and PIP2, and fragment ion A (pink) for PIP3. SWATH design in table S3 is recommended for profiling due to the combination of coverage and selectivity.

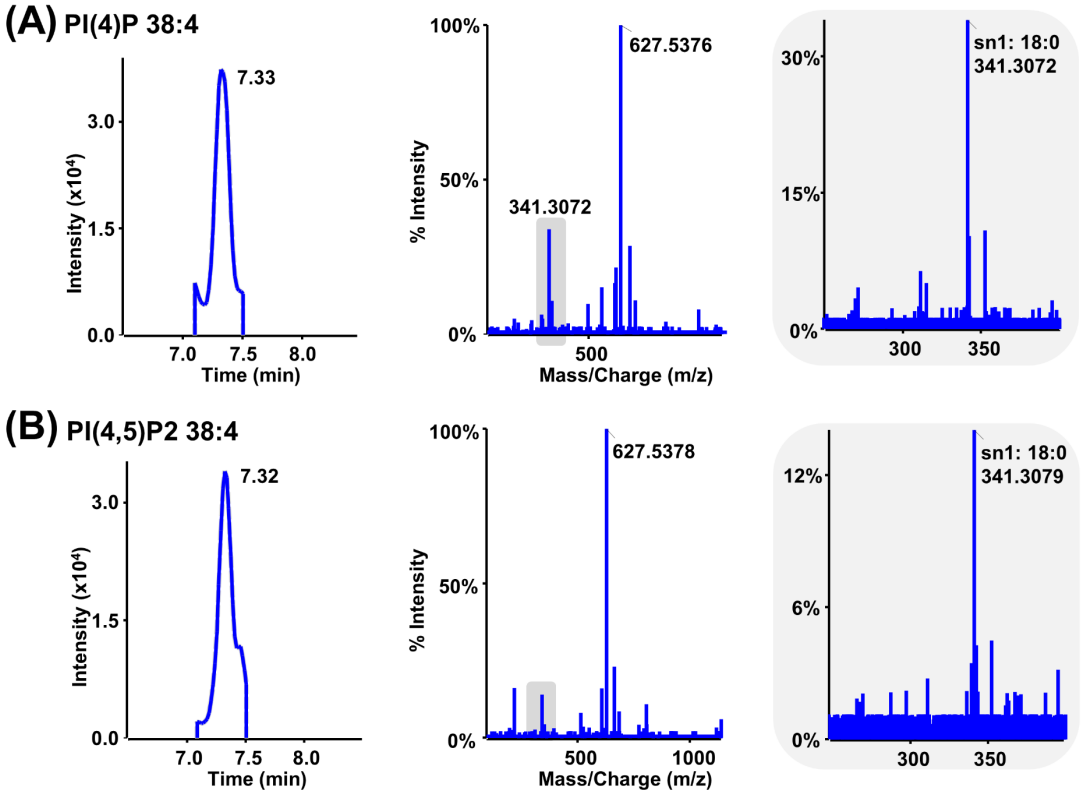

Figure S18 | Representative PIPx in NIST SRM1950. (A) 38:4 PI(4)P was identified as 18:0/20:4 PI(4)P. (B) 38:4 PI(4,5)P2 was identified as 18:0/20:4 PI(4,5)P2. Chromatogram with MS2 spectra were exported from MasterView. The retention time window was 0.4 min. MS2 chromatograms were matched with MS1 chromatograms according to retention time profiles. Background subtraction was performed automatically for corresponding MS2 spectra. Due to incomplete resolution between the regioisomer peaks peak height was used for quantitative analysis which was less effected from partial overlap. Peak cut in peak valley between neighboring peaks.

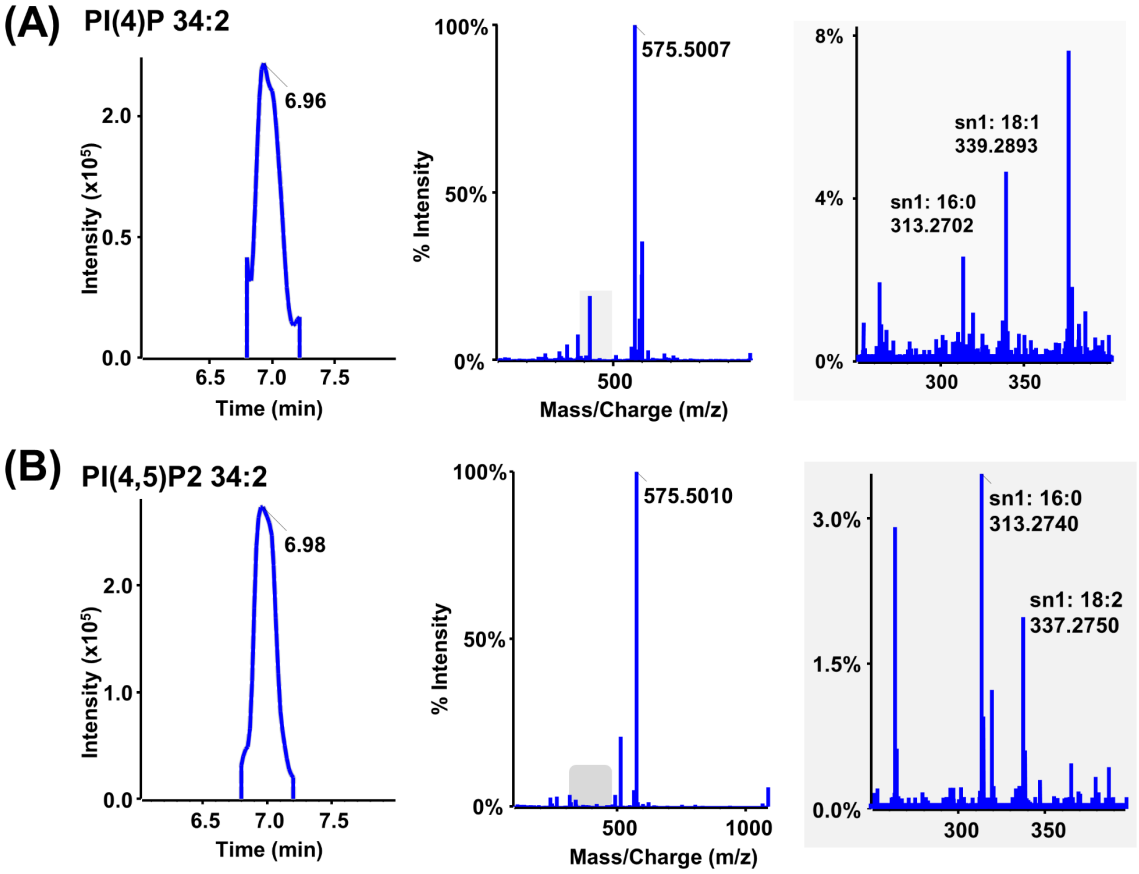

Figure S19 | Representative PIPx in Pichia pastoris. (A) 34:2 PI(4)P was identified as 16:0/18:2 PI(4)P and 18:1/16:1 PI(4)P. (B) 34:2 PI(4,5)P2 was identified as 16:0/18:2 PI(4,5)P2 and 18:2/16:0 PI(4,5)P2. Chromatogram with MS2 spectra were exported from MasterView. The retention time window was 0.4 min. MS2 chromatograms were matched with MS1 chromatograms according to retention time profiles. Background subtraction was performed automatically for corresponding MS2 spectra. Due to incomplete resolution between the regioisomer peaks peak height was used for quantitative analysis which was less effected from partial overlap. Peak cut in peak valley between neighboring peaks.

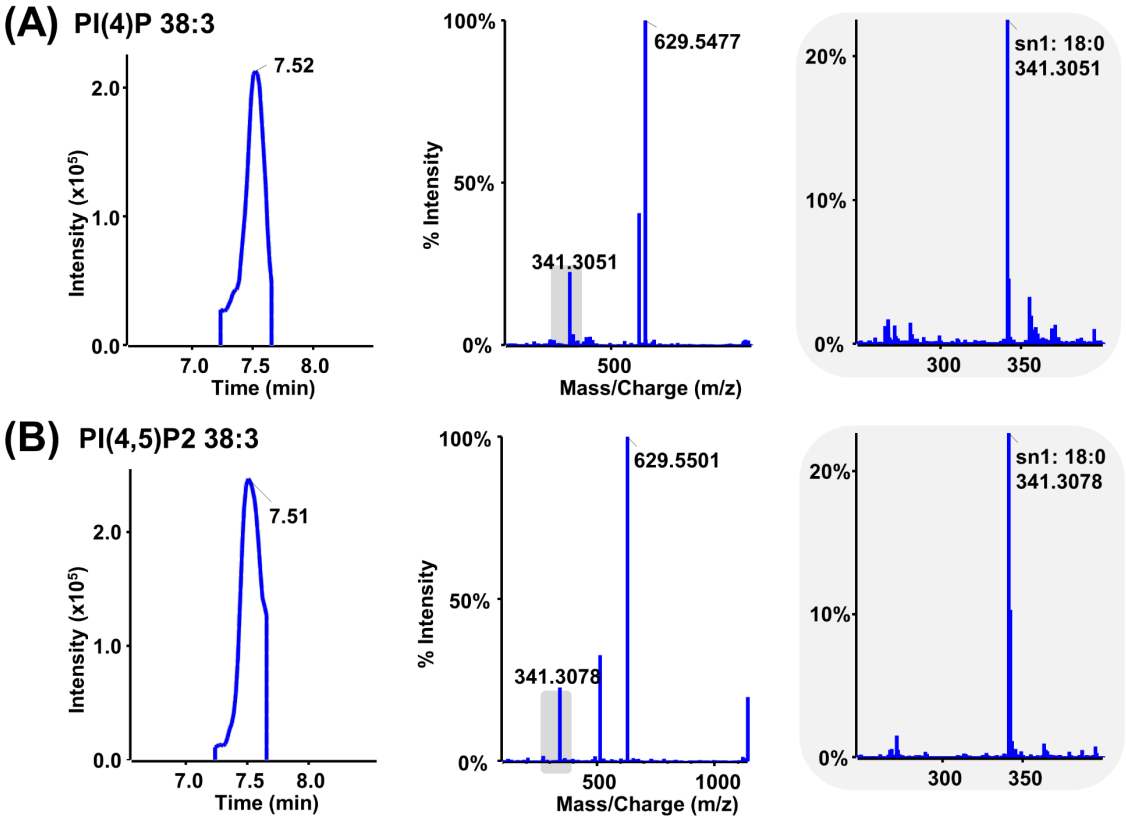

Figure S20 | Representative PIPx in cultured HeLa cells. (A) 38:3 PI(4)P was identified as 18:0/20:3 PI(4)P. (B) 18:3 PI(4,5)P2 was identified as 18:0/20:3 PI(4,5)P2. Chromatogram with MS2 spectra were exported from MasterView. The retention time window was 0.4 min. MS2 chromatograms were matched with MS1 chromatograms according to retention time profiles. Background subtraction was performed automatically for corresponding MS2 spectra. Due to incomplete resolution between the regioisomer peaks peak height was used for quantitative analysis which was less effected from partial overlap. Peak cut in peak valley between neighboring peaks.

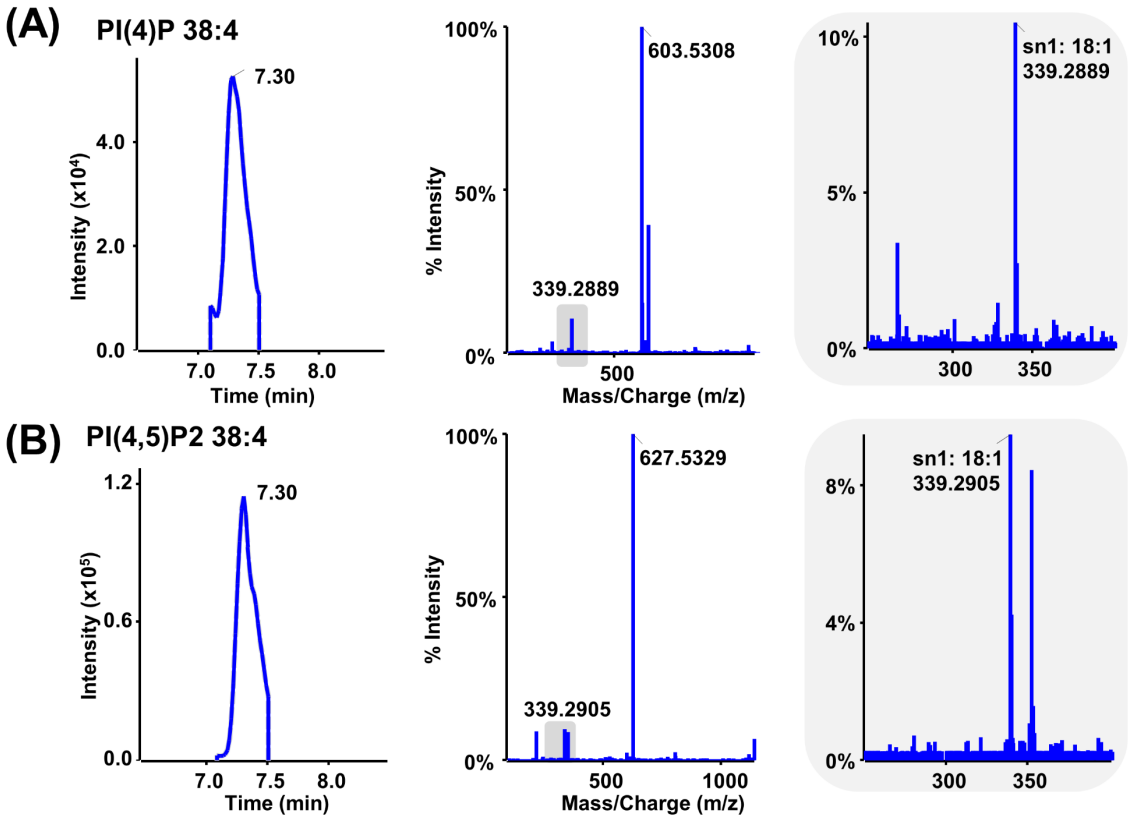

Figure S21 | Representative PIPx in cultured HeLa cells. (A) PI(4)P 38:4 was identified as PI(4)P 18:1/20:3. (B) PI(4,5)P2 38:4 was identified as 18:1/20:4 PI(4,5)P2. Chromatogram with MS2 spectra were exported from MasterView. The retention time window was 0.4 min. MS2 chromatograms were matched with MS1 chromatograms according to retention time profiles. Background subtraction was performed automatically for corresponding MS2 spectra. Due to incomplete resolution between the regioisomer peaks peak height was used for quantitative analysis which was less effected from partial overlap. Peak cut in peak valley between neighboring peaks.

11. Publication III

Isomer-selective analysis of inositol phosphates with differential isotope labelling by phosphate methylation using liquid chromatography with tandem mass spectrometry

Peng Li [a], Meinrad Gawaz [b], Madhumita Chatterjee [b], Michael Lämmerhofer [a*]

[a] Institute of Pharmaceutical Sciences, Pharmaceutical (Bio-)Analysis, University of Tübingen, Tübingen, Germany

[b] Department of Cardiology and Angiology, University Hospital Tübingen, 72076 Tübingen, Germany

Anal. Chim. Acta.

Year 2022, Volume 1191, Pages 339286

Doi: 10.1016/j.aca.2021.339286.

Graphical Abstract

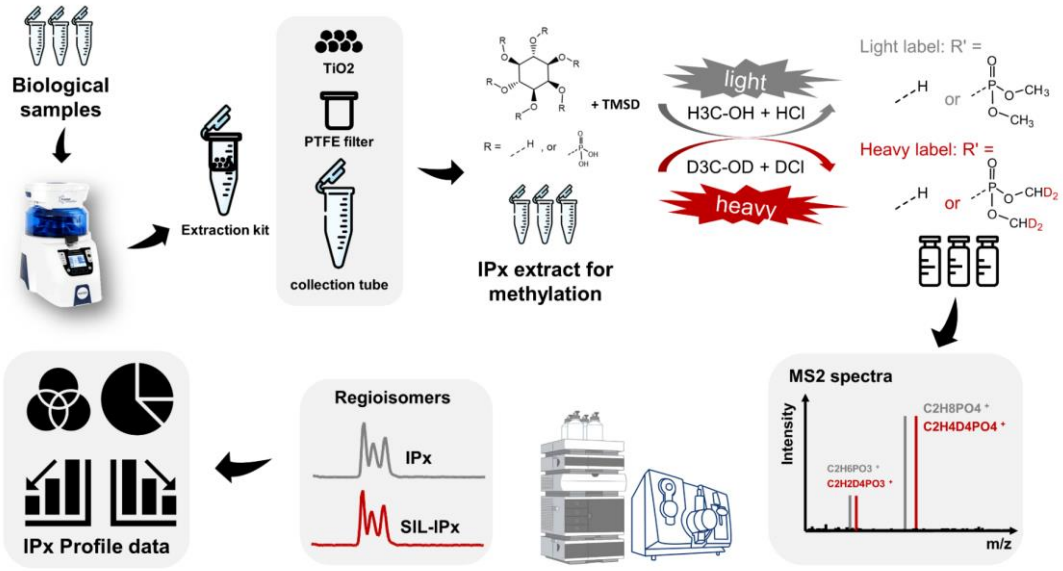

Analytica Chimica Acta xxx (xxxx) xxx

Contents lists available at ScienceDirect

Analytica Chimica Acta

journal homepage: www.elsevier.com/locate/aca

Isomer-selective analysis of inositol phosphates with differential isotope labelling by phosphate methylation using liquid chromatography with tandem mass spectrometry

Peng Li [a], Meinrad Gawaz [b], Madhumita Chatterjee [b], Michael Lämmerhofer [a, *]

[a] Institute of Pharmaceutical Sciences, Pharmaceutical (Bio-)Analysis, University of Tübingen, Tübingen, Germany
[b] Department of Cardiology and Angiology, University Hospital Tübingen, 72076, Tübingen, Germany

HIGHLIGHTS

- Method for inositol phosphate (IPx) signaling network with phosphate methylation.
- RP-UHPLC-MS/MS (using SRM) with core-shell Cholester phase for isomer separation.
- Optimized TiO2-SPE extraction with PTFE filter achieved high extraction yields (>50%).
- Differential isotope labelling by methylation gives access to internal standards.
- Inositol phosphate profile acquired in different biological samples (HeLa, platelets, plasma).

GRAPHICAL ABSTRACT

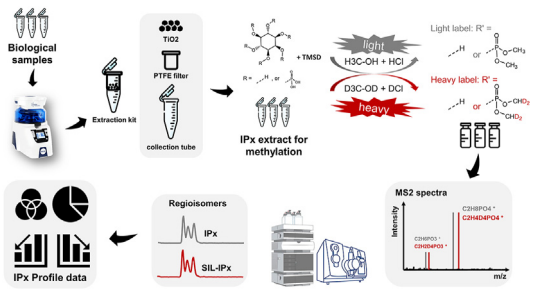

ARTICLE INFO

Article history:
Received 3 September 2021
Received in revised form
8 November 2021
Accepted 14 November 2021
Available online xxx

Keywords:
Inositol phosphate
Metal oxide-based affinity chromatography
Solid-phase extraction
Derivatization
Isotope labeling
Targeted metabolomics

ABSTRACT

Inositol phosphates belong to a family of structurally diverse signaling molecules playing crucial role in Ca^{2+} release from intracellular storage vesicles. There are many possibilities of phosphorylation, including their degree and position. Inositol (1,4,5) trisphosphate has been well recognized as the most important second messenger among this family. It remains a challenge to analyse the entire inositol phosphate metabolite family due to its structural complexity, high polarity, and high phosphate density. In this study, we have established an improved UHPLC-ESI-MS/MS method based on a differential isotope labelling methylation strategy. An SPE extraction kit composed of TiO2 and PTFE filter was employed for sample preparation which provided good extraction performance. Samples were methylated (light label) to neutralize the phosphate groups and give better performance in liquid chromatography. Regioisomers and inositol phosphates differing in their number of phosphate residues were successfully separated after optimization on a core-shell cholesterylether-bonded RP-type column (Cosmocore 2.6Cholester) using methanol as organic modifier. Triple quadrupole MS detection was based on selected reaction monitoring (SRM) acquisition with characteristic fragments. Stable isotope labeling methylation was performed to generate internal standards (heavy label). Limits of quantification from 0.32 to 0.89 pmol on column was achieved. This method was validated to be suitable for inositol phosphate profiling in biological samples. After application in cultured HeLa cells, NIST SRM1950 plasma, and human platelets,

* Corresponding author. Pharmaceutical (Bio-)Analysis, Institute of Pharmaceutical Sciences, University of Tübingen, Auf der Morgenstelle 8, 72076, Tübingen, Germany.
E-mail address: michael.laemmerhofer@uni-tuebingen.de (M. Lämmerhofer).

https://doi.org/10.1016/j.aca.2021.339286

Please cite this article as: P. Li, M. Gawaz, M. Chatterjee *et al.*, Isomer-selective analysis of inositol phosphates with differential isotope labelling by phosphate methylation using liquid chromatography with tandem mass spectrometry, Analytica Chimica Acta, https://doi.org/10.1016/j.aca.2021.339286

distinct inositol profiles were obtained. This newly established method exhibited improved analytical performance, holding the potential to advance the understanding of inositol phosphate signaling.

Abbreviations

IPx	inositol phosphate(s)
IP1	inositol monophosphate
IP2	inositol bisphosphate
IP3	inositol trisphosphate
IP4	inositol tetrakisphosphate
IP5	inositol pentakisphosphate
IP6	inositol hexakisphosphate
IP7	diphosphoinositol pentakisphosphate
IP8	bisdiphosphoinositol tetrakisphosphate
DAG	sn-1,2-diacylglycerol
PP-IPx	inositol pyrophosphate
SAX-LC	strong anion-exchange liquid chromatography
HILIC	hydrophilic interaction liquid chromatography
CE	capillary electrophoresis
SIL,	stable isotope labeled
IS	internal standard
TMSD	(trimethylsilyl)diazomethane
PA	perchloric acid
PIP3	phosphoinositol trisphosphate
IDA-EPI	information dependent acquisition with enhanced product ion scan
DoE	design of experiment
EIC	extracted ion chromatogram
AA	acetic acid
TCA	trichloroacetic acid
MOAC	metal oxide-based affinity chromatography
PTFE	polytetrafluoroethylene

1. Introduction

Myo-inositol (hereafter I) is the predominant and most intensively studied stereoisomer of inositol, a cyclohexane-1,2,3,4,5,6-hexol (structure shown in Fig. 1) [1]. Arising from phosphorylation at hydroxy groups, myo-inositol phosphates (IPx) are formed. The IPx family is diverse due to different positions and number (or both) of phosphorylation. Inositol mono-, bis-, tris-, tetrakis-, pentakis-, and hexakis-phosphate are named according to their phosphorylation degree, abbreviated as IP1, IP2, IP3, IP4, IP5, and IP6. Apart from IP6, IPx (with x < 6) has many possibilities of regioisomers. Among these, I(1,4,5)P3 is found ubiquitously in eukaryotes. I(1,4,5)P3 is generated together with sn-1,2-diacylglycerol (DAG) via phospholipase C - mediated hydrolysis of phosphoinositol-4,5-bisphosphate (PI(4,5)P2). I(1,4,5)P3 is reported to induce calcium release from intracellular stores, which could be

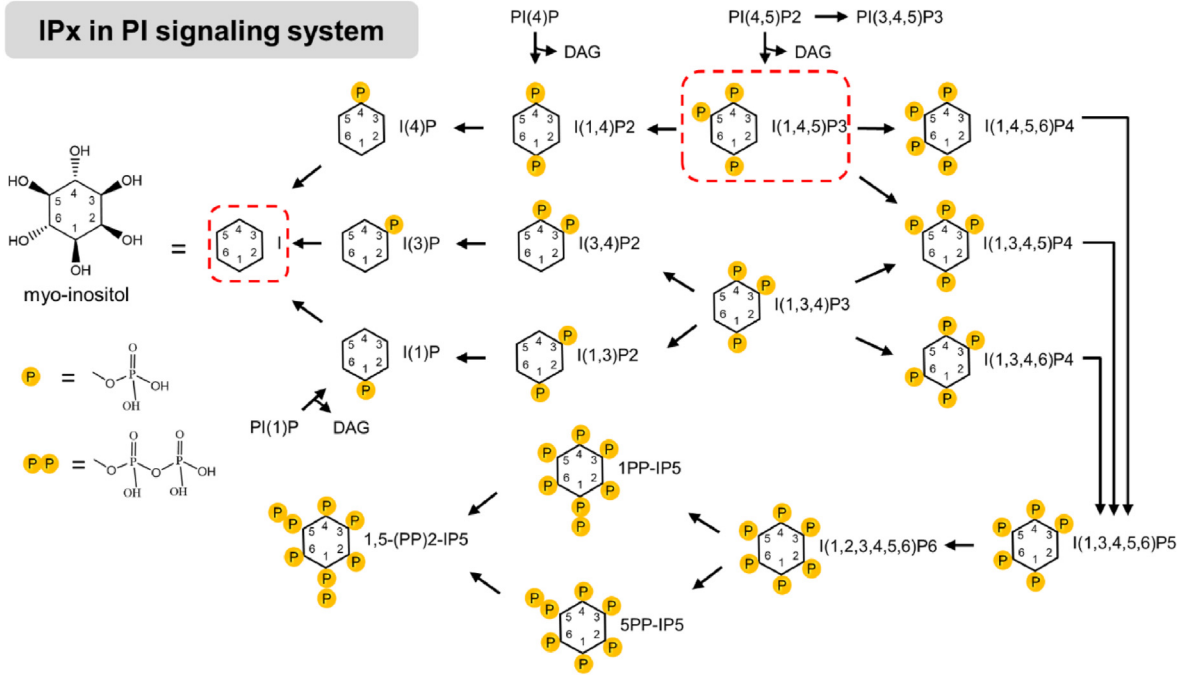

Fig. 1. Inositol and inositol phosphates in phosphoinositol signaling system (inspired by Refs. [4–6]).

terminated by two alternatives: hydrolysis of I(1,4,5)P3 to I(1,4)P2 and phosphorylation of I(1,4,5)P3 to I(1,3,4,5)P4 [2,3]. As shown in Fig. 1, starting from I(1,4,5)P3, a highly complex and regulated metabolic network can be constructed [4–6]. Inositol pyrophosphates (PP-IPx) are formed by further phosphorylation of phosphates of IPx [5,7]. Recently, we have developed a workflow to analyse the phosphoinositide (PIPx) network [8]. For a full understanding of the phosphoinositide pathway, a method to analyse I(1,4,5)P3 as well as the IPx family is required, so as to have a more comprehensive metabolic information.

The analysis of the IPx family in biological samples has been challenging due to its structural complexity, high charge density, instability, and low abundance. Historically, IPx were commonly analyzed by metabolic labelling, followed by strong anion-exchange chromatography (SAX-LC) [9–11]. This approach is sensitive while requires labour- and time-consuming radio labelling as well as specifically equipped laboratory. With the development of mass spectrometry (MS) based metabolomics, LC-MS/MS has been more and more widely adopted due to its sensitivity and selectivity [12]. Highly concentrated and non-volatile buffers that are required for efficient elution from anion-exchangers make it difficult to hyphenate SAX-LC to MS. Further efforts have been directed towards ion pairing reagents and were reported to have improved peak shape and enhanced retention in reversed-phase (RP) LC [13,14]. However, ion suppression is inevitable with ion pairing approach in ESI-MS detection. Moreover, hydrophilic interaction liquid chromatography (HILIC) has increasingly gained interest for polar analytes for metabolomics studies [15,16]. A HILIC approach was established for IP6 and IP7 analysis [17]. Concentrated buffer (300 mM ammonium carbonate, pH 10.5) was involved to obtain minimal peak tailing. IP6 and IP7 were detected in MS with their singly and doubly deprotonated forms. Recently, capillary electrophoresis (CE) MS was reported to separate inositol pyrophosphates with significantly improved separation of regioisomers of PP-IPx, as well as peak shape and sensitivity [18]. In-house synthesized stable isotope labeled (SIL) ($^{13}C_6$) IPx and PP-IPx were used as internal standards. However, I(1,4,5)P3 was not included in the both abovementioned methods. To measure IPx with LC-MS/MS, in-source fragmentation (ISF, i.e. cleavage of phosphate from higher inositol phosphates) is the common problem. For this reason, there is a higher requirement for the separation prior to ESI-MS detection. To compensate matrix effects in real samples, SIL compounds are usually taken as internal standards (IS). The availability of standards as well as internal standards has become the bottleneck for IPx analysis. So far, an isomer-selective and instrument-friendly method for IPx analysis is still missing.

Chemical derivatization is a powerful tool to address challenging analytes (reviewed in Refs. [19–21]). The derivatization approach modifies the chemical structure of the analytes to improve the analytical performance, including sensitivity, separation, stability, and the production of SIL compounds for IS becomes possible. Ideally, derivatization methods should meet the following requirements: (1) high and reproducible yield; (2) minimum generation of by-products; (3) negligible interference from derivatization reagents and by products. Many problems in the analysis of phosphorylated compounds (such as carry over, ISF, problems with too weak (RP) or too strong retention (SAX-LC), etc.) arise from phosphate groups. Therefore, a derivatization strategy targeting phosphate groups is desired. Amidation and diazo reagents were reported for phosphate derivatization. Derivatization with diazomethane and (trimethylsilyl)diazomethane (TMSD) stand out due to their fast reaction speed, mild condition, ease of removal of reagents and by products. Compared with other derivatization reagents, methylation is more appealing as there is less space resistance for complete conversion of multiple phosphates in close proximity such as in IPx [22,23].

Here, we introduce an advanced strategy using differential isotope labelling by phosphate methylation combined with LC-MS/MS for IPx analysis. A corresponding sample preparation method was developed that allows sensitive and selective analysis in biological sample matrix. With differential isotope label methylation, stable isotope labeled IPx were obtained as internal standards. Methylated IPx were analyzed by reversed-phase liquid chromatography with improved analytical performance. The regioisomer of major interest, viz. (1,4,5)P3, was separated for the first time. With this method, we were able to profile IPx (IP1 – IP6) in different biological samples, including human plasma, cultured HeLa cells, and human platelets. This method also enables analysing the IPx profile upon specific compound treatment in cultured HeLa cells in accordance to a targeted pharmacometabolomics approach.

2. Materials and methods

2.1. Materials

Acetonitrile, methanol (MeOH) of Ultra LC-MS grade and zirconia/glass beads were supplied by Carl Roth (Karlsruhe, Germany). Methanol-d4, ammonium hydroxide solution (NH4OH, ~30% NH3 basis), ammonium formate (NH4FA), hydrochloric acid (HCl, ACS reagent, 37%), hydrogen chloride solution (HCl, 3 M in methanol), deuterium chloride solution (DCl, 35% in D2O) and perchloric acid (PA) were supplied by Sigma–Aldrich (Saint-Louis, MO, USA). Trimethylsilyl diazomethane (TMSD, 2 M in hexane) was obtained from Acros Chemicals (supplied by VWR, Bruchsal, Germany). Water (H2O) was purified by a Purelab Ultra purification system (ELGA LabWater, Celle, Germany).

2.2. IPx standards

D-myo-Inositol-1-phosphate sodium salt (I(1)P), D-myo-Inositol-1,3-bisphosphate sodium salt (I(1,3)P2), D-myo-Inositol-1,4-bisphosphate sodium salt (I(1,4)P2), D-myo-Inositol-1,5-bisphosphate sodium salt (I(1,5)P2), D-myo-Inositol-1,3,5-trisphosphate sodium salt (I(1,3,5)P3), D-myo-Inositol-1,3,4,5,6-pentaphosphate ammonium salt (I(1,3,4,5,6)P5), D-myo-Inositol-1,2,3,4,5,6-hexaphosphate sodium salt (myo-IP6), D-chiro-Inositol-1,2,3,4,5,6-hexaphosphate sodium salt (chiro-IP6) and scyllo-Inositol-1,2,3,4,5,6-hexaphosphate sodium salt (scyllo-IP6) were purchased from Cayman Chemical (Ann Arbor, MI, USA). D-myo-Inositol-1,3,4-trisphosphate ammonium salt (I(1,3,4)P3), D-myo-Inositol-1,4,5-trisphosphate ammonium salt (I(1,4,5)P3) and D-myo-Inositol-1,3,4,5-tetraphosphate ammonium salt (I(1,3,4,5)P4) were obtained from Avanti Polar Lipids (Alabaster, AL, USA).

2.3. Sample preparation

2.3.1. Preparation of cultured HeLa cells

The human cervical HeLa cells adapted to serum free conditions (AC free, ECACC 08011102) were grown in a humidified incubator at 37 °C with 5% CO2. Cells were fed with EX-CELL HeLa serum free media (Sigma Aldrich) with 2 mM L-glutamine (Sigma Aldrich), 12 units/mL penicillin and 12 μg/mL streptomycin until the cell density reached around 2×10^6 cells/mL. Cell counting was performed in triplicate with a hemocytometer. Aliquots of 10^7 HeLa cells were transferred into 2 mL homogenization tubes and spun down for 5 min (100 g at 4 °C). After removing the supernatant, cell pellets were washed twice with ice-cold Dulbecco's Phosphate Buffered Saline (Sigma Aldrich) with repeated centrifugation. Cell samples were snap frozen in liquid nitrogen and kept at −80 °C till use.

2.3.2. Human platelet isolation

Human platelet samples were isolated from acid-citrate-dextrose (ACD) anticoagulated (12.5 g sodium citrate, 6.82 g of citric acid, 10 g glucose, 500 mL distilled water, adjusted to pH 4.69 with NaOH) (1:4) blood of healthy volunteers free of cardiovascular risk factors and medications. Washed platelets were isolated as previously described [24–26] and kept under resting condition without subjecting them to further activation. This was done to concentrate on the basal IPx profile of platelets from healthy donors. Briefly blood was centrifuged at 190 g for 20 min without break or acceleration. Platelet-rich plasma (PRP) was collected from the upper 2/3 layer. PRP was diluted with Tyrodes-HEPES buffer (2.5 mM HEPES, 150 mM NaCl, 1 mM KCl, 2.5 mM $NaHCO_3$, 0.36 mM NaH_2PO_4, 5.5 mM glucose, 1 mg/mL BSA, pH 6.5) and centrifuged at 800 g for 10 min without break or acceleration. The platelet pellet thus obtained was suspended in PBS (pH 7.4) supplemented with $CaCl_2$. Platelet count was estimated with Sysmex®. Isolated platelet suspension was snap frozen in liquid nitrogen and kept at −80 °C till use. The study was carried out at the Dept. of Cardiology and Angiology, University Hospital Tübingen, in accordance to ethical guidelines and approved by regional authorities (number 237/2018BO2).

2.3.3. IPx extraction

The extraction was performed as reported before with slight modification [27,28]. Briefly, around 5 mg TiO2 was transferred into centrifuge filter units after consecutive washing with H2O and 1 M PA solution. Samples were filled into homogenization tubes (e.g., 10^7 HeLa cells or 2×10^8 human platelets). After adding 450 μL pre-chilled 1 M PA solution and 0.15 g zirconia/glass beads, samples were homogenized at 4 °C for 10 cycles (10 s per cycle, 6800 rpm, pause 30 s) with Precellys Evolution with Cryolys Evolution using dry ice cooling (Bertin Technologies, France). The samples were then centrifuged for 5 min (16,100 g at 4 °C). The supernatant was transferred into the centrifuge filter units with washed TiO2. After shaking for 15 min (1000 rpm at 4 °C) followed by a centrifugation step (3500 g at 4 °C for 1 min), the filtrate was discarded. Then, 300 μL of 100 mM HCl water solution was added for washing. After shaking (1000 rpm at 4 °C for 1 min) and centrifugation (3500 g at 4 °C for 1 min), the filtrate was discarded. The washing step was repeated once. Two-hundred-microliter 10% (v/v) NH4OH solution was added for elution. After shaking (1000 rpm at 4 °C for 5 min) and centrifugation (3500 g at 4 °C for 1 min), the filtrates were combined and lyophilized prior to methylation.

2.3.4. Differential isotope labeling methylation

Samples and lyophilized IPx standards were reconstituted with 1 mM HCl in MeOH (light label) and 1 mM DCl in MeOH-d4 (heavy label), respectively. Hundred-microliter of 2 M TMSD solution were added. The samples were allowed to stand for 10 min at R.T. after brief vortexing and fume releasing. The derivatization was quenched by addition of 5 μL glacial acetic acid. Samples were dried under N2 in an evaporator (Genevac EZ-2, around 2 h). Internal standard solution was prepared by resuspending heavy labeled standards at 250 ng/mL with MeOH/H2O (1:9, v/v). After reconstitution with 50 μL internal standard solution, facilitated by vortexing and sonication, samples were ready for LC-MS analysis.

2.4. UHPLC-ESI-QqQ-MS/MS analysis with SRM acquisition

Chromatographic separation was performed on a 1290 Infinity UHPLC system (Agilent Technologies, Santa Clara, CA, USA) with a core-shell COSMOCORE 2.6Cholester packed column (2.6 μm, 2.1 mm × 150 mm) (Nascalai Tesque, Kyoto, Japan) equipped with a KrudKatcher Ultra HPLC in-line filter (0.5 μm) (Phenomenex, Torrance, CA, USA). Mobile phase A and B were 10 mM ammonium formate in water and methanol, respectively. The gradient elution (0.0 min, 5% B; 3 min, 5% B; 9 min, 40% B; 10 min, 40% B; 10.1 min, 5% B; 15 min, 5% B) was carried out at a flow rate of 0.4 mL/min and a constant column temperature of 60 °C. Injection volume was 5 μL. MS detection was conducted with the above chromatographic system hyphenated to a QTRAP4500 mass spectrometer with a Turbo V source (Sciex, Framingham, MA, USA) operated with the ESI probe. Ion source parameters were as follows: curtain gas (N2) 30 psi, nebulizer gas (zero grade air) 30 psi; heater gas (zero grade air) 30 psi, ion source voltage +4500 V (positive mode) and source temperature 500 °C. SRM transitions and compound-dependent parameters for analytes and internal standards are summarized in Table 1. The total cycle time was 810 ms.

Table 1
SRM transitions with MS parameters (dt, dwell time; DP, declustering potential; EP, entrance potential; CE, collision energy; CXP, collision cell exit potential).

IPx	Q1	Q3	Dt	DP, V	EP, V	CE, V	CXP, V
IP-1	289.1	127	40	55	10	20	10
IP-2	289.1	109	40	55	10	50	10
IP2-1	397.1	127	40	60	10	25	10
IP2-2	397.1	109	40	60	10	55	10
IP3-1	505.1	127	40	80	10	45	15
IP3-2	505.1	109	40	80	10	80	15
IP4-1	613.1	127	40	90	10	70	15
IP4-2	613.1	109	40	90	10	95	15
IP5-1	721.1	127	40	110	10	80	15
IP5-2	721.1	109	40	110	10	100	15
IP6-1	829.1	127	40	120	10	105	15
IP6-2	829.1	109	40	120	10	130	15
IS IP1	293.1	131	40	55	10	20	10
IS IP2	405.1	131	40	60	10	25	10
IS IP3	517.1	131	40	80	10	45	15
IS IP4	629.1	131	40	90	10	70	15
IS IP5	741.1	113	40	110	10	100	15
IS IP6	853.2	113	40	120	10	130	15

2.5. Data processing

Analyst 1.7 was used for data acquisition and system control. Commercially available software packages PeakView (Master View included) and MultiQuant (Sciex, Framingham, MA, USA) were involved in data processing. PeakView 2.2 was used for manual data evaluation. MultiQuant 3.0 was used for peak integration, linear regression and concentration calculation. Optimization data were processed with MODDE 12.1 (Umetrics AB, Sweden). Statistical analysis and visualization were performed with R language.

3. Results and discussion

3.1. MS behavior of IPx after phosphate methylation

The phosphatidylinositol signaling system is of central importance in many fundamental metabolic processes such as the PI3K-Akt signaling pathway or the calcium signaling pathway downstream of phospholipase C activity. We recently proposed a workflow for the regioisomer-selective comprehensive PIPx analysis in biological samples. Unfortunately, this method does not cover the IPx family, which is however needed for a full understanding of metabolic processes via the phosphatidylinositol signaling pathways, especially knowledge regarding alterations of I(1,4,5)P3 concentrations is fundamental for biological interpretations of processes like platelet activation. Like the PIPx analysis, due to high density of phosphates the analysis of IPx also remains to be similarly challenging. To overcome this problem, we herein developed a

phosphate methylation method to improve its analytical performance for the IPx family.

SRM coupled with mass spectrometry has become the golden standard for targeted metabolomics, which integrates robustness, wide dynamic range, sensitivity, and selectivity [29]. Previously, IPx was usually measured by MS in negative ESI mode. Singly and doubly deprotonated ion forms were reported as precursors while *m*/*z* 97 ($H2PO4^-$) and *m*/*z* 79 ($PO3^-$) were observed as common fragments of the IPx family [17,18,30]. TMSD was first applied for the derivatization of phosphatidylinositol trisphosphate (PIP3) with improved stability and electrospray ionization efficiency [23]. Following this strategy, various methods targeting lipophilic compounds containing phosphate groups were established [31,32]. Unlike phospholipids, methylation of IPx with TMSD is challenging. TMSD is insoluble in water and available in hexane or diethyl ether, while IPx is hydrophilic due to its rich hydroxy and phosphate groups. Therefore, we started our method development by screening for suitable solvent (mixture). Upper layer of *tert*-butyl methyl ether/methanol/water (10:3:2.5, v/v/v), lower layer of chloroform/methanol/water (8:4:3, v/v/v), and methanol were tested for a set of IPx standards including I(1)P, I(1,4)P2, I(1,4,5)P3, and I(1,3,4,5)P4. To increase selectivity, pseudo SRM transitions (Q1 equals to Q3), followed by information-dependent acquisition with enhanced product ion scan (IDA-EPI) was used for measurement (detailed method information can be found in the Supplementary Text S1). Among low response of IPx with the tested solvents (mixtures), methanol stood out with relatively higher response (data not shown). Trimethylsilylation could occur as a competing reaction to methylation. As reported, the presence of strong acid could improve selectivity of methylation over trimethylsilylation [33]. Hydrochloric acid (HCl) was tested as it is volatile to be evaporated after reaction. As shown in Fig. 2, four tested IPx standards exhibited significant signals as compared to derivatization blanks (tests performed in duplicates). In the tested RP-LC condition, retention increased with phosphorylation degree of IPx, which could later be utilized for identification. To address the problem of two peaks arising from I(1)P, further LC optimization was carried out as discussed in the next section. Two common fragments were observed in product ion spectra of methylated IPx standards, which are proposed to arise from methylated phosphates (Fig. 2A, right). Therefore, acidic methanol was chosen as the derivatization solvent for further study.

To optimize derivatization conditions, a design of experiment (DoE) strategy was applied with MODDE software. The experiments

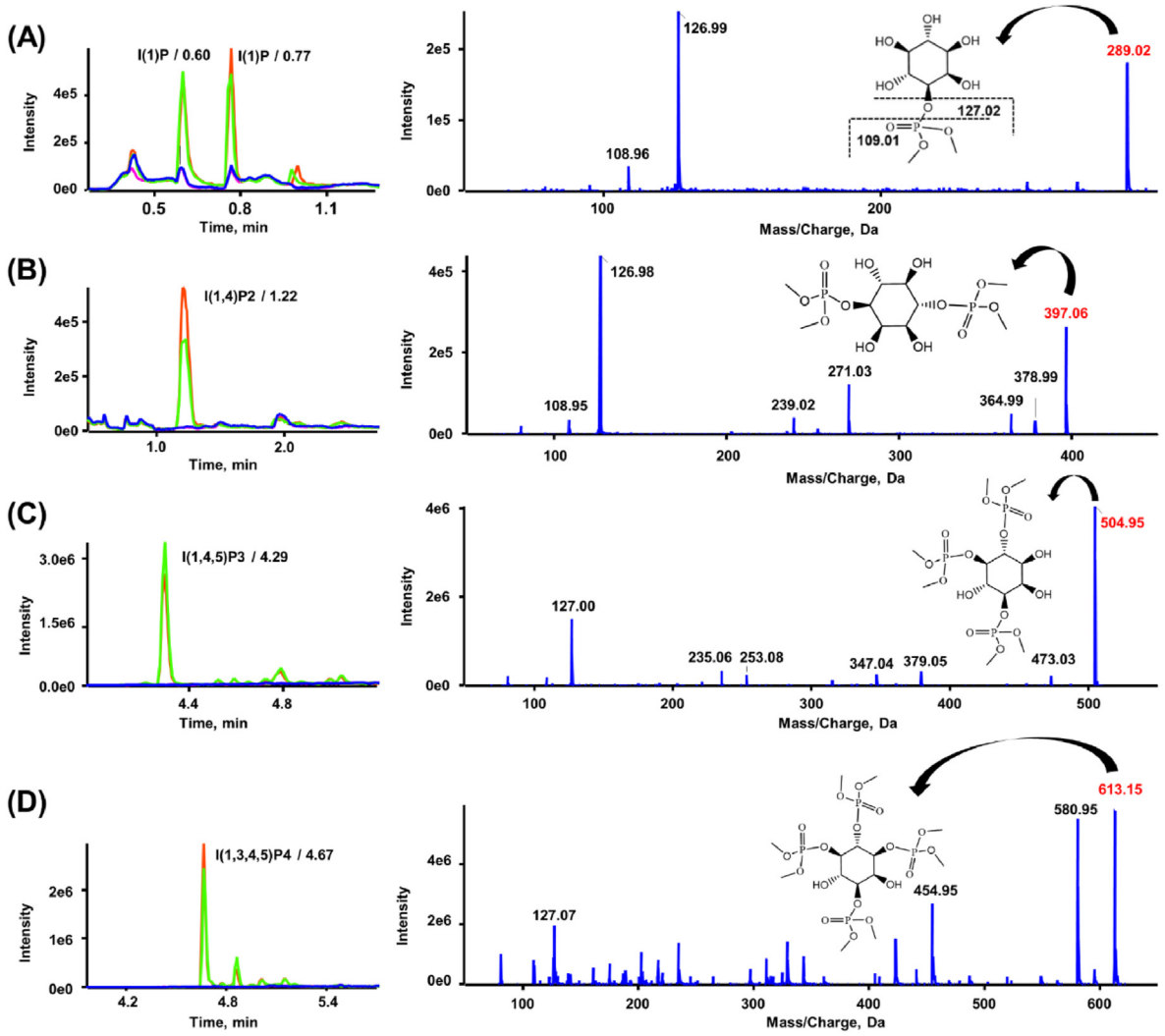

Fig. 2. Chromatograms and corresponding product ion spectra of IPx in LC-IDA-EPI method. (A) I(1)P; (B) I(1,4)P2; (C) I(1,4,5)P3; (D) I(1,3,4,5)P4. LC parameters were: column, ACQUITY CSH C18 (1.7 μm, 2.1 × 100 mm); Mobile phase: 0.1% formic acid in water and acetonitrile respectively; Gradient, linear gradient of acetonitrile from 5% to 100% over 5 min after holding for 3 min at the beginning; Sample solvent: 20% methanol in water.

were carried out at room temperature. Different HCl concentrations, different amount of TMSD, and reaction times were tested. The results are shown by response contour plots under three TMSD amounts (Figs. S1−S3). The optimum reaction duration is from 0 to 30 min for IP1-IP4 standards, which indicates that the derivatization proceeded quite fast under tested conditions. The concentration of HCl should be minimum. HCl could not only catalyze the formation of diazomethane from TMSD but also completely reacted with diazomethane to generate methyl chloride. There was an improvement from 50 μL TMSD to 100−200 μL. Furthermore, TMSD more than 100 μL ensured the reaction mixture to be slightly yellow, which indicates excess of TMSD. Therefore, 100 μL was chosen, together with 1 mM HCl in methanol (prepared with methanolic HCl), 10 min at room temperature, as the optimum derivatization condition. The reaction was quenched by addition of acetic acid. The mixture became transparent after significant nitrogen release. Byproducts and reagents were all volatile. Evaporation and reconstitution were adopted before LC-MS/MS measurement. With this optimized condition, regioisomers of IP2 and IP3 were subjected to high-resolution (HR) MS analysis to look for differential fragments. Detailed method information of HR-MS is available in Supplementary Text S2. Results (Fig. S4) showed that ions with *m*/*z* 127.0160 and *m*/*z* 109.0055 were confirmed to be the main fragments of IPx after methylation. Although some fragments were observed to have differential intensity, it was still challenging to distinguish regioisomers based on these fragments. More standards are required to explore the underlying fragmentation rules for IPx regioisomers. Also, limited by the acquisition speed with the triple quadrupole instrument and the requirement for collecting sufficient data points across the peaks , it is undesirable to use multiple SRM transitions when there are many analytes with ISs. For this reason, more attention was paid to optimize the chromatographic separation to provide adequate selectivity for IPx regioisomers. According to the mechanism of TMSD methylation (illustrated in Fig. S5), heavy label (mass shift of 2 Da per methylation) could be introduced by replacing HCl and methanol with deuterated forms (similar approach as reported in Refs. [31,32]). IP1 − IP4 standards were heavily labeled and measured with HR-MS (results in Fig. S6). Proposed mass shifts were obtained for both fragments (*m*/*z* 131 versus *m*/*z* 127 and *m*/*z* 113 versus *m*/*z* 109 for heavy and light versions, respectively). Thus, a differential methylation strategy was established for IPx, in which samples were lightly labeled while internal standards were heavily labeled. To extend the coverage of this method, more standards, including IP1-IP6, IP2 regioisomers, IP3 regioisomers, were methylated as aforementioned. Direct infusion of methylated single standards of IPx was performed to optimize compound-dependent parameters. Optimized MS parameters are listed in Table 1. As mentioned before, interferences from ISF of higher IPx represent a major problem for IPx in MS detection, which may lead to misidentifications if not adequately separated. Respective IPx standards with different phosphorylation degrees were measured. As shown in Fig. S7, after methylation there was no signal of lower IPx found at the same retention time (Rt) as higher IPx in the corresponding extracted ion chromatograms (EIC). It indicates the risk of ISF in MS detection is negligible after methylation.

3.2. LC analysis of methylated IPx

During preliminary experiments, IPx showed improved peak shape and reasonable retention after methylation. The development of the liquid chromatography method started with a column screening aiming at solving the problem with double peaks of IP1 (owing to peak splitting due to insufficient retention and no refocusing). Furthermore, another goal was to separate the regioisomers of IP2 and IP3, especially focusing on avoidance of interferences with I(1,4,5)P3. To confirm the phenomenon of peak splitting of IP1, methylated IPx was reconstituted with 10% MeOH and analyzed with ACQUITY CSH C18. Ten (10) mM ammonium formate (NH4FA) in water and methanol or 90% acetonitrile were used as mobile phases with the same linear gradient starting from 5% organic eluent. As shown in Fig. S8, I(1)P was confirmed to have split peaks on this column when AcN was used as the organic modifier. On the other hand, regioisomers of IP2 and IP3 were adequately separated under these conditions. With methanol as organic modifier, peak splitting was better but the selectivity between the regioisomers of IP3 (I(1,3,4)P3 and I(1,3,5)P3) was lost. A more hydrophobic C30 stationary phase was tested for stronger retention of IPx. Taking the same screening conditions as before, IPx reconstituted in 100% water, 5% methanol, and 10% methanol were measured. Results showed that there is no selectivity for the regioisomers of IP3. It was noted that peak shape of IP1 became worse as the methanol content in the sample diluent increased from 0% to 10%, while there was no similar effect observed for IP2 to IP4. Therefore, it was concluded that the two peaks of the early eluted IP1 were arising from elution strength mismatch between sample solvent and initial mobile phase composition. To address this problem, columns compatible with 100% aqueous mobile phases were tested. Waters HSS T3 column (Fig. S10) and YMC Triart C18 column (Fig. S11) showed significantly improved peak shape for IP1 when 100% aqueous solvent was taken as sample solvent and mobile phase at the same time. Unfortunately, there was no selectivity observed between the regioisomers I(1,3,5)P3 and I(1,4,5)P3 under all tested conditions on both columns. More LC columns were therefore tested for achieving better peak shape of IP1 and simultaneously maintaining selectivity between reg ioisomers, including chiral columns (data not shown). Among all the LC columns tested, 2.6Cholester column (larger dimension, 4.6 × 250 mm) showed symmetrical peaks for all IPx analytes including IP1 with both methanol and acetonitrile (Fig. S12). Selectivity for regioisomers was obtained with methanol as organic modifier. In order to be utilized for LC-MS/MS approach, a smaller column (2.1 × 150 mm) with the same stationary phase was purchased and used for further optimization.

To improve the robustness of this method, a further test for reconstitution solvent was carried out (Fig. S13). When IPx dissolved in 5%, 10%, and 20% methanol as sample diluent were analyzed, the peak shape got significantly deteriorated at 20% methanol. To leave some space for further extending the method coverage to more lipophilic analytes (due to higher phosphate and methylation degrees) in the future, 10% methanol was chosen as the reconstitution solvent. Finally, as shown in Fig. 3A-F, IPx from IP1 to IP6 were reasonably well eluted and sufficiently separated in this method. Due to faster exchange kinetics in RP-LC than that in ion exchange chromatography, the IPx analytes exhibit improved peak shapes along with shorter measurement time in this method. After methylation, negative charges were neutralized so that the instrument carry over was eliminated. In addition to selectivity of regioisomers, selectivity of three stereoisomers (myo-, scyllo-, and chiro-IP6) was also obtained (Fig. 3G). SIL ISs were produced using the derivatization strategy discussed in the last section. Representative chromatograms are shown in Fig. 3H. Corresponding SIL IS of IPx (with deuterium) has slightly shorter Rt than IPx does, which could be expected in RP-LC. However, the shift is minimal and this strategy can be regarded as best practice currently. The (partial) hydrolysis product of IP6 is a good mixture to show separation performance of the method [30,34−37]. Similarly, a hydrolysis product of IP6 (water, 5 h at 110 °C) was measured. As illustrated in Fig. 4, the whole series of IPx could be generated from IP6 during hydrolysis, together with multiple regioisomers, which could be

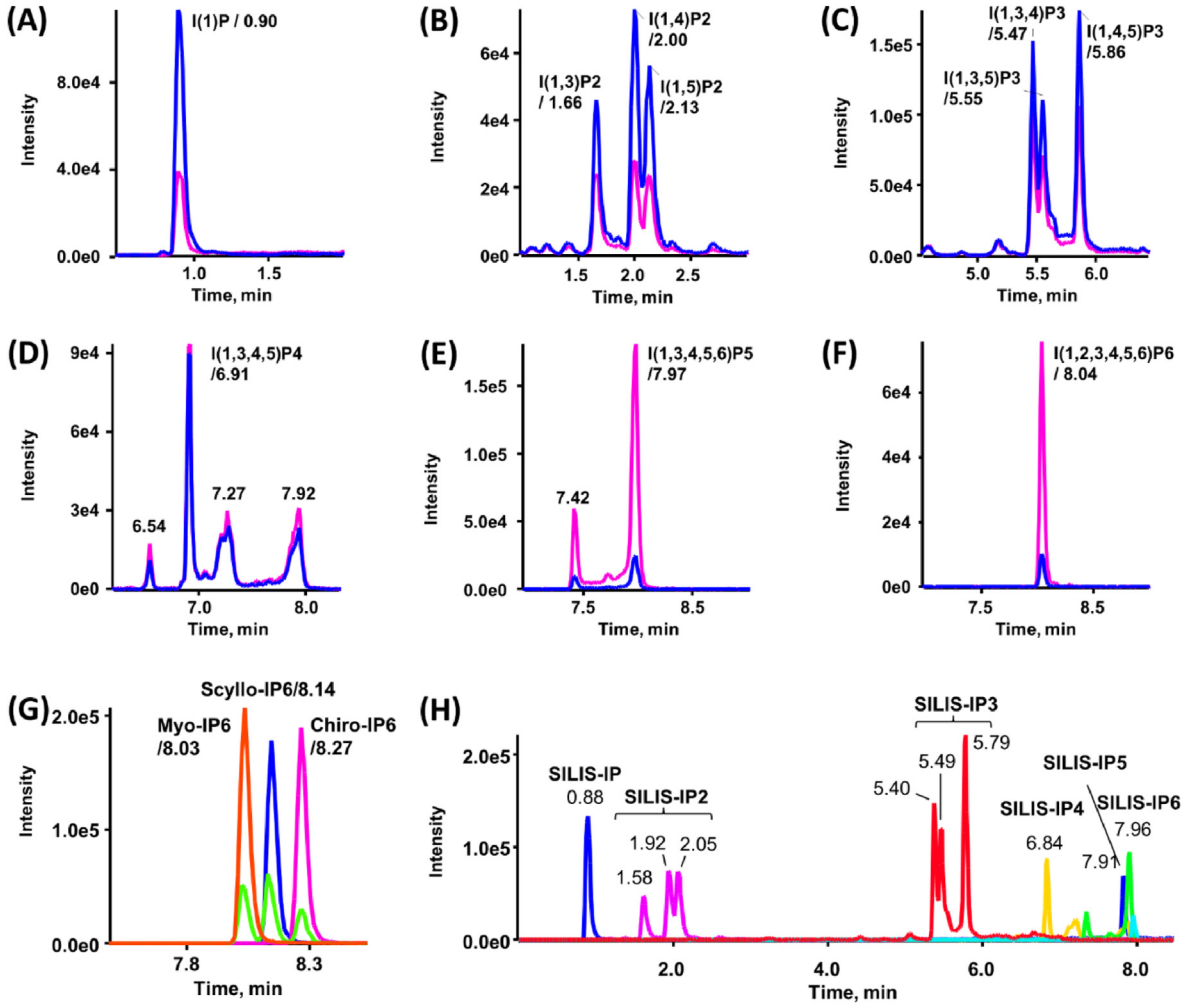

Fig. 3. Chromatograms of targeted analytes and internal standards of IPx in this study (EICs of two SRM transitions for A–G: blue trace, precursor to *m*/*z* 127; pink trace, precursor to *m*/*z* 109. Most abundant SRM transition of isotope labeled IPx for H. All transitions with MS parameters listed in Table 1). (A) I(1)P; (B) Regioisomers of IP2: I(1,3)P2, I(1,4)P2, and I(1,5)P2; (C) Regioisomers of IP3: I(1,3,4)P3, I(1,3,5)P3, and I(1,4,5)P3; (D) I(1,3,4,5)P4; (E) I(1,3,4,5,6)P5; (F) Myo-I(1,2,3,4,5,6)P6; (G) Myo-, scyllo-, and chiro-I(1,2,3,4,5,6)P6. (H) SIL-ISs of IPx obtained with derivatization. The chromatograms were obtained with: Cosmocore 2.6Cholester column (2.6 μm, 2.1 × 150 mm), mobile phase: 10 mM NH4FA in water and methanol (details documented in materials and methods section). (For interpretation of the references to colour in this figure legend, the reader is referred to the Web version of this article.)

confirmed with two overlapped SRM transitions. In conclusion, the regioisomers were separated for the first time by LC-MS/MS. At the same time, SIL ISs were generated for accurate quantitative analysis in complex sample matrix.

3.3. Extraction protocol with TiO2

IPx is prone to bind to proteins in real samples due to their phosphate-rich, highly negatively charged structural moiety. Acid-assisted approaches were reported for extraction of IPx, including acetic acid (AA) [38], hydrochloric acid (HCl) [39–41], trichloroacetic acid (TCA) [42,43], and perchloric acid (PA) [9,44,45]. Herein, cultured HeLa cells were taken for preliminary tests and optimization of sample preparation. HCl- and AA-based liquid extraction methods were carried out. Methylation was performed after evaporation of the extract to dryness (to remove acid introduced for extraction). Low signal intensities and low extraction recoveries were observed for higher IPx. Stronger acidic conditions should be involved to improve extraction yields, which is however harmful for the downstream methylation. Alternatively, a more efficient and easy-to-automate extraction approach should be developed. Metal oxide-based affinity chromatography (MOAC) has been reported for purification of phosphate containing compounds such as phosphopeptides and phosphoproteins [46,47]. Under acidic conditions (pH 2–3), increased selectivity is gained in MOAC as non-specific interactions are minimized [48,49]. Following this principle, a novel extraction protocol based on titanium dioxide (TiO2) was established for IPx and PP-IPx [18,27,28]. A TiO2 protocol, as suggested previously [27,28], was tested without modification. Briefly, IPx standard solutions without sample matrix were treated with PA solution and were loaded to TiO2 for binding. After washing with PA solution twice, analytes were eluted with diluted ammonia. As listed in Table S1, improved extraction recoveries (more than 50%) were obtained with significant matrix effect (20–45%, assessment according to Ref. [50] with modification). Unlike general matrix effect, ion suppression or ion enhancement arising from sample matrix, low signal here was recognized as pseudo matrix effect as it comes from residual acid interference. The residue of PA (introduced in the sample loading and washing steps) in the eluates was found to be responsible for this pseudo matrix effect. HCl at three different concentrations were tested as last washing step. As shown in Table S1, the pseudo matrix effect was observed to improve as the

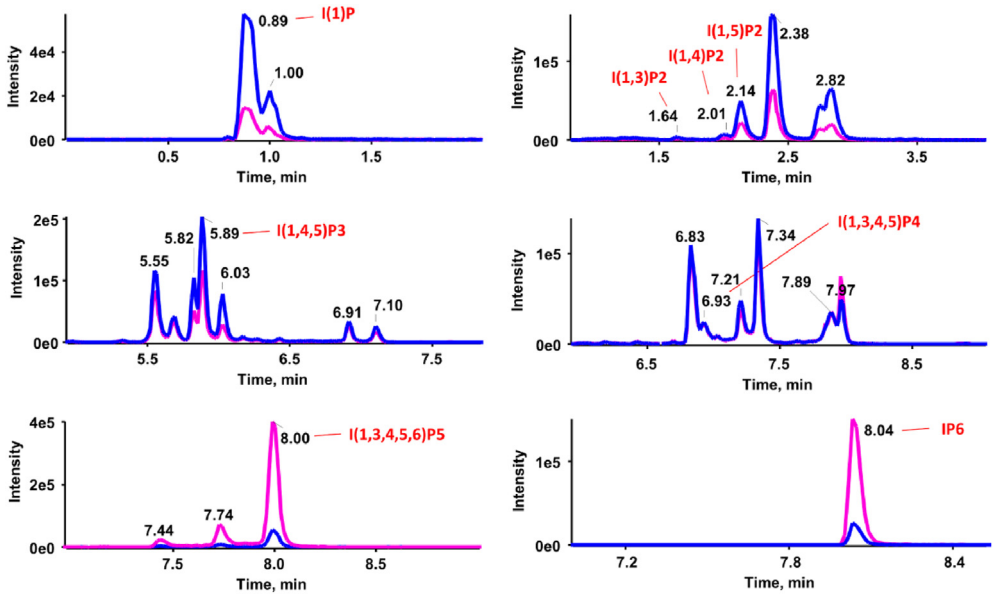

Fig. 4. Hydrolysis products of IP6. Two EICs are shown: blue trace, precursor to *m*/*z* 127 and pink trace, precursor to *m*/*z* 109. (For interpretation of the references to colour in this figure legend, the reader is referred to the Web version of this article.)

HCl concentration increased from 1 mM to 100 mM. Thus, 100 mM HCl was finally taken for the last washing step. After measurement of more samples, a random retention time shift was observed. This problem was corresponding to the pressure increase during analysis, which indicated that small particles of TiO2 were injected into the system. A more sophisticated extraction cartridge was proposed to improve the robustness of this method. As shown in Fig. S14, the advanced cartridge is the combination of centrifuge filter and TiO2 pellets. Hydrophilic polytetrafluoroethylene (PTFE) was chosen as membrane material, because it is durable for strong acid like PA. The sample preparation protocol is shown in Fig. S14, which is efficient and easy-to-automate. Samples were treated with 1 M PA solution for protein precipitation and IPx release from proteins. The supernatant was loaded into the extraction cartridge. Washing was performed with diluted HCl as discussed above. The eluates from these loading and washing steps, obtained after centrifugation with these spin vials, were discarded. The IPx were finally eluted from the TiO2 beads using a pH change induced by diluted ammonia (10%, v/v). The samples were measured after lyophilization followed by methylation. Furthermore, it is worth noting that the extraction cartridge is reusable in principle [28].

3.4. Method validation

Method validation was performed in cultured HeLa cells according to FDA guidelines (with slight modifications), including linearity, limit of quantification (LOQ), precision and accuracy [51]. As shown in Table 2 and Fig. S15, external calibration curves of IPx (peak height ratio to SIL-IS) were constructed with standard solutions at six concentration levels. Satisfying regression coefficients were obtained across the determined concentration range with weighing factor 1/x. Representative EICs of IPx at LOQs were shown in Fig. S16 (estimated signal-to-noise ratios obtained in PeakView). IPx standards were spiked into cultured HeLa cells to get standard addition samples. Standard addition samples at 4 concentration levels were analyzed for intra- and inter-batch accuracy and precision. As listed in Tables S2–S3, this method is accurate (accuracy between 87 and 115%) and precise (within ±15% RSD from replicate measurements in triplicate, n = 3) for IPx analysis. The IS solution was injected repeatedly to test for autosampler stability. Results (Fig. S17) showed that the analytes were stable in the autosampler (4 °C) for more than 72 h. Due to the unavailability of analyte-free sample matrix, calibration was performed with standard solution with SIL-ISs. Evaluation of matrix effect and extraction recovery was carried out using a strategy reported previously, with endogenous amount of IPx subtracted from the blank samples (only ISs spiked) [50]. Matrix effect was obtained via comparison between SIL IS signals in calibration solutions and standard addition sample solutions (Table S4). As it was already shown in preliminary experiments, it is necessary to include ISs due to significant matrix effect.

Currently, there is no consensus of IS amount in LC-MS based

Table 2
Calibration curve of IPx.

IPx	range, ng/mL	linear equation	r	LOQ on column, pmol
I(1)P	50–5000	y = 0.0025291x - 0.011586	0.9985	0.89
I(1,3)P2	50–5000	y = 0.003222x - 0.094437	0.9975	0.65
I(1,4)P2	50–5000	y = 0.0026848x - 0.062403	0.9979	0.65
I(1,5)P2	50–5000	y = 0.0027389x - 0.064495	0.9975	0.65
I(1,3,4)P3	50–5000	y = 0.0036367x - 0.10641	0.9977	0.53
I(1,3,5)P3	50–5000	y = 0.0032788x - 0.092061	0.9949	0.53
I(1,4,5)P3	50–5000	y = 0.0033722x - 0.13519	0.9977	0.53
I(1,3,4,5)P4	50–5000	y = 0.0062857x - 0.2452	0.9955	0.44
I(1,3,4,5,6)P5	50–5000	y = 0.0054363x - 0.18834	0.9971	0.33
I(1,2,3,4,5,6)P6	50–5000	y = 0.004332x - 0.22253	0.9969	0.32

Table 3
IPx profile of different biological samples (n = 3).

Px quantified	I(1)P	I(1,3)P2	I(1,4)P2	I(1,5)P2	I(1,3,4)P3	I(1,3,5)P3	I(1,4,5)P3	I(1,3,4,5)P4	I(1,3,4,5,6)P5	myo-IP6
HeLa cell (pmol/10^7 cells)	432.5 ± 121.5	76.2 ± 20.5	25.0 ± 5.7	114.8 ± 26	16.7 ± 2.1	6.6 ± 1.2	16.2 ± 3.2	9.9 ± 0.6	158.6 ± 19.8	1070.3 ± 153.3
Platelet (pmol/3 × 10^8 cells)	4.9 ± 2.9	ND	0.3 ± 1	0.1 ± 0.3	0.5 ± 0.1	ND	0.5 ± 0.3	ND	0.6 ± 0.1	1.3 ± 0.1
SRM1950 (pmol/200 μL)	7.3 ± 1.3	ND	ND	ND	ND	ND	ND	ND	ND	ND

bioanalysis. A low IS concentration at one-third of upper limit of quantification (ULOQ) is preferred by some authors [52], while a high IS concentration corresponding to 50% ULOQ or even higher than ULOQ is preferred by some other [53,54]. Therefore, the IS concentration should be chosen with consideration of different factors, including cross-signal contribution between IS and analyte, method sensitivity, ion suppression and ion enhancement arising from IS, and linearity of IS [55]. Cross-signal contribution may arise from chemical impurities and isotope interference and have to be avoided. SIL ISs in this study were generated from differential isotope methylation. As shown in Fig. S18, no signal of IPx was observed from SIL IS only sample, which indicate negligible cross contribution here. The optimal IS concentration was determined by other factors. The minimum concentration should be higher than 3 x LLOQ to ensure good accuracy and precision of IS signals. The maximum concentration must not be higher than ULOQ or actually should be a lower concentration. Such high concentrations in the upper concentration range, however, may cause significant ion suppression and ion enhancement, respectively. When it comes to unknown samples, a pilot experiment could be conducted with updated IS concentration estimated by the protein amount in the sample as reported previously. [56]. Another factor to consider is the cost of IS. An appropriate low IS concentration will be preferred when a large cohort of clinical samples has to be investigated. In this study, we picked a lower IS concentration of around 5 x LLOQ. With the compensation of SIL ISs, matrix effects of 90–110% for IPx analytes were obtained being well in the acceptable range for external calibration (Table S5). As shown in Table S6 and Table S7, extraction recovery of 41–62% and process efficiency of 38–61% were obtained in this method for IPx from IP1 to IP6. The SPE extraction method with TiO2 based on the proposed extraction cartridge showed wide extraction recovery for the entire IPx family investigated herein. To sum up, this method turned out to be suitable to profile IPx in biological samples.

3.5. IPx profile in biological samples

This method was applied to profile IPx in different biological samples, including cultured HeLa cells, resting human platelets, and NIST SRM1950 plasma. Identification of IPx was based on two characteristic SRM transitions with the same Rt. Regioisomers of IPx (with x < 6) and stereoisomers of IP6 were annotated using purchased standards (listed in IPx standards section). Only myo-IP6 was detected in three tested samples. As shown in Table 3, and Fig. S19, distinct IPx profiles were observed in different samples. Cultured HeLa cells have a widely distributed IPx profile across the whole family, as well as regioisomers including I(1,4,5)P3. Therefore, HeLa cells could serve as the model cellular system in method development for IPx. I(1,4,5)P3 is well recognized as a second messenger generated after PLC-mediated hydrolysis, which plays an important role in platelet functions. I(1,4,5)P3 in human platelets from healthy donors was successfully separated and determined. This method could be utilized to study platelet activation involving more experimental conditions in the future (e.g. *ex vivo* pharmacometabolomics). The standard reference material (SRM) was often adopted to compare method performance in the

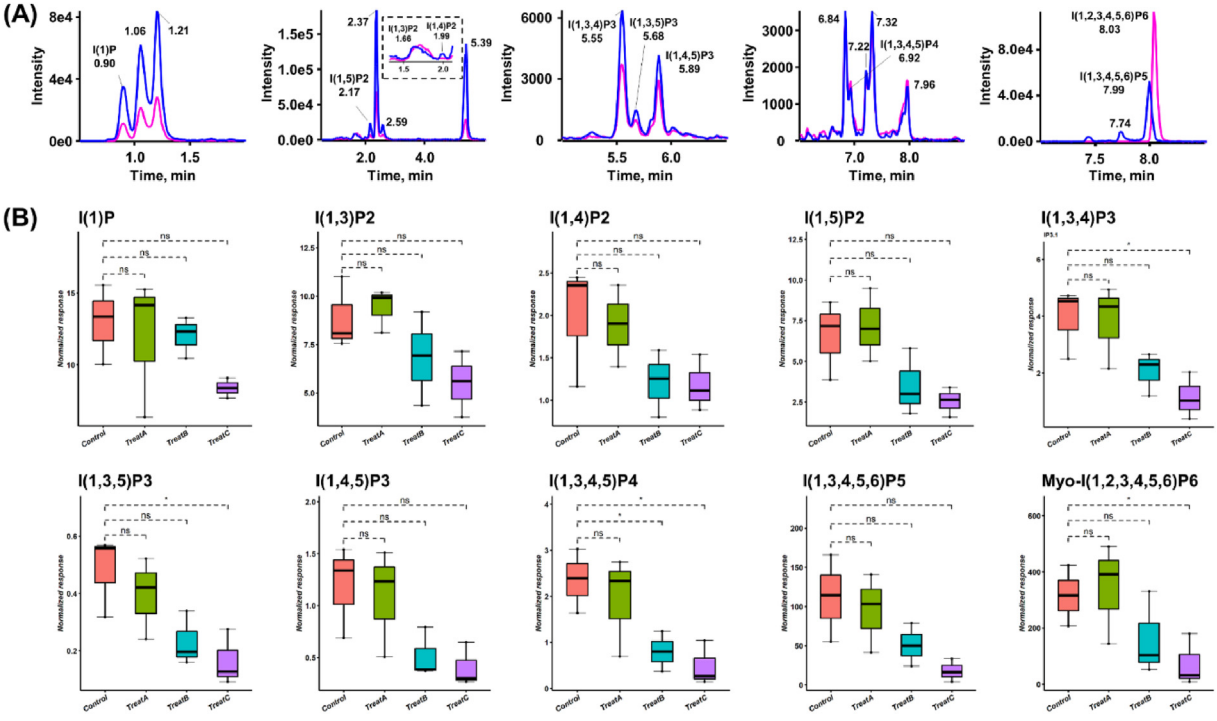

Fig. 5. IPx results in cultured HeLa cells: (A) representative EICs of IPx; (B) IPx profile upon PLC inhibitor treatment. Significance levels are, ns not significant, * p < 0.05.

metabolomics community. Interestingly, only I(1)P was detected in NIST SRM1950 plasma in this method. This is corresponding to the absence of IP6 in human blood as reported before. After incubation for 30 min at 37 °C, no IP6 could be detected even when it was spiked intentionally [27]. Multiple inositol polyphosphate phosphatases are reported to be responsible for the conversion of IP6 into lower IPx [57]. This could be considered as a good indication that phosphatase inhibitors should be considered during sample collection when human blood is involved for IPx study. As the model sample, representative EICs in HeLa cells are shown in Fig. 5A. To further reveal the method performance and applicability for targeted pharmacometabolomics, PLC inhibitor treated HeLa cells were measured. U73122 was reported to inhibit PLC-dependent calcium release [58]. HeLa cells were treated by U73122 at three concentration levels (A, 107.6 nM; B, 1.076 μM; and C, 10.76 μM). After incubation for 10 min at 37 °C, the overall IPx profile was affected by the treatment as shown in Fig. 5B, including I(1,4,5)P3. The down-regulated IPx showed a concentration-dependent effect. These results demonstrate that this established method is suitable for IPx monitoring in biological samples of diverse cellular systems.

4. Conclusions

In this study, an improved method for IPx analysis was established, validated and applied to biological samples, including cultured HeLa cells, NIST SRM1950 plasma and human platelets. With the differential isotope labeling methylation strategy, lightly labeled IPx gave characteristic fragments and improved peak shape. The methylation conditions were systematically optimized by DoE strategy. Regioisomers of IPx, including the most important I(1,4,5)P3, were separated by RP-LC approach for the first time using a core-shell cholesterylether-bonded RP-type column. The hydrolysis products of I(1,2,3,4,5,6)P6 was used to reveal the performance of this method in terms of assay specificity. At the same time, heavily labeled IPx with adequate mass shift (more than 4 Da) was generated as internal standards for quantitative analysis in real samples. Accordingly, a methylation-compatible extraction method was developed. With the extraction cartridge containing TiO2 and PTFE filter, the sample preparation approach was robust, efficient, as well as easy-to-automate. Distinct IPx profiles, including phosphorylation degree and regioisomers, were observed in different biological samples. Changes of IPx profile in HeLa cells induced by a phospholipase C inhibitor was obtained. These results indicate that this established method has improved analytical performance. We believe it could facilitate the study of inositol phosphate metabolism, as well as the PI signaling system.

CRediT authorship contribution statement

Peng Li: Investigation, Methodology, Formal analysis, Data curation, Visualization, Writing – original draft, Writing – review & editing. **Meinrad Gawaz:** Writing – review & editing, Funding acquisition. **Madhumita Chatterjee:** Investigation, Writing – review & editing, Funding acquisition. **Michael Lämmerhofer:** Conceptualization, Methodology, Supervision, Writing – review & editing, Resources, Funding acquisition.

Declaration of competing interest

The authors declare that they have no known competing financial interests or personal relationships that could have appeared to influence the work reported in this paper.

Acknowledgements

P.L. gratefully acknowledges the support from the China Scholarship Council (grant number 201807060010). M.L., M.C., and M.G. acknowledge the support by the German Research Foundation (DFG, Deutsche Forschungsgemeinschaft), project number 374031971-TRR 240.

Appendix A. Supplementary data

Supplementary data to this article can be found online at https://doi.org/10.1016/j.aca.2021.339286.

References

[1] I. Monnard, T. Bénet, R. Jenni, S. Austin, I. Silva-Zolezzi, J.P. Godin, Plasma and urinary inositol isomer profiles measured by UHPLC-MS/MS reveal differences in scyllo-inositol levels between non-pregnant and pregnant women, Anal. Bioanal. Chem. 412 (2020) 7871–7880, https://doi.org/10.1007/s00216-020-02919-8.
[2] J.H. Horne, T. Meyer, Elementary calcium-release units induced by inositol trisphosphate, Science (80-.) 276 (1997) 1690–1693, https://doi.org/10.1126/science.276.5319.1690.
[3] M.J. Berridge, R.F. Irvine, Inositol phosphates and cell signalling, Nature 341 (1989) 197–205, https://doi.org/10.1038/341197a0.
[4] T. Sasaki, S. Takasuga, J. Sasaki, S. Kofuji, S. Eguchi, M. Yamazaki, A. Suzuki, Mammalian phosphoinositide kinases and phosphatases, Prog. Lipid Res. 48 (2009) 307–343, https://doi.org/10.1016/j.plipres.2009.06.001.
[5] S.B. Shears, Diphosphoinositol polyphosphates: metabolic messengers? Mol. Pharmacol. 76 (2009) 236–252, https://doi.org/10.1124/mol.109.055897.
[6] H. Ogata, S. Goto, K. Sato, W. Fujibuchi, H. Bono, M. Kanehisa, KEGG: Kyoto encyclopedia of genes and genomes, Nucleic Acids Res. 27 (1999) 29–34, https://doi.org/10.1093/nar/27.1.29.
[7] S.B. Shears, Inositol pyrophosphates: why so many phosphates? Adv. Biol. Regul. 57 (2015) 203–216.
[8] P. Li, M. Lämmerhofer, Isomer selective comprehensive lipidomics analysis of phosphoinositides in biological samples by liquid chromatography with data independent acquisition tandem mass spectrometry, Anal. Chem. 93 (2021) 9583–9592, https://doi.org/10.1021/acs.analchem.1c01751.
[9] C. Azevedo, A. Saiardi, Extraction and analysis of soluble inositol polyphosphates from yeast, Nat. Protoc. 1 (2006) 2416–2422, https://doi.org/10.1038/nprot.2006.337.
[10] M.S.C. Wilson, A. Saiardi, Importance of radioactive labelling to elucidate inositol polyphosphate signalling, Phosphate Label. Sens. Chem. Biol. (2017) 67–87.
[11] D. Laha, P. Johnen, C. Azevedo, M. Dynowski, M. Weiß, S. Capolicchio, H. Mao, T. Iven, M. Steenbergen, M. Freyer, P. Gaugler, M.K.F. De Campos, N. Zheng, I. Feussner, H.J. Jessen, S.C.M. Van Wees, A. Saiardi, G. Schaaf, VIH2 regulates the synthesis of inositol pyrophosphate InsP8 and jasmonate-dependent defenses in arabidopsis, Plant Cell 27 (2015) 1082–1097, https://doi.org/10.1105/tpc.114.135160.
[12] S.L. Collins, I. Koo, J.M. Peters, P.B. Smith, A.D. Patterson, Current challenges and recent developments in mass spectrometry–based metabolomics, Annu. Rev. Anal. Chem. 14 (2021) 467–487, https://doi.org/10.1146/annurev-anchem-091620-015205.
[13] J. Lehrfeld, High-performance liquid chromatography analysis of phytic acid on a pH-stable, macroporous polymer column, Cereal Chem. 66 (1989) 510–515. http://cat.inist.fr/?aModele=afficheN&cpsidt=6733043.
[14] C. Burbano, M. Muzquiz, A. Osagie, G. Ayet, C. Cuadrado, Determination of phytate and lower inositol phosphates in Spanish legumes by HPLC methodology, Food Chem. 52 (1995) 321–325, https://doi.org/10.1016/0308-8146(95)92831-4.
[15] D. Tang, L. Zou, X. Yin, C.N. Ong, HILIC-MS for metabolomics: an attractive and complementary approach to RPLC-MS, Mass Spectrom. Rev. 35 (2016) 574–600.
[16] H. Gallart-Ayala, I. Konz, F. Mehl, T. Teav, A. Oikonomidi, G. Peyratout, V. van der Velpen, J. Popp, J. Ivanisevic, A global HILIC-MS approach to measure polar human cerebrospinal fluid metabolome: exploring gender-associated variation in a cohort of elderly cognitively healthy subjects, Anal. Chim. Acta 1037 (2018) 327–337, https://doi.org/10.1016/j.aca.2018.04.002.
[17] M. Ito, N. Fujii, C. Wittwer, A. Sasaki, M. Tanaka, T. Bittner, H.J. Jessen, A. Saiardi, S. Takizawa, E. Nagata, Hydrophilic interaction liquid chromatography–tandem mass spectrometry for the quantitative analysis of mammalian-derived inositol poly/pyrophosphates, J. Chromatogr., A 1573 (2018) 87–97, https://doi.org/10.1016/j.chroma.2018.08.061.
[18] D. Qiu, M.S. Wilson, V.B. Eisenbeis, R.K. Harmel, E. Riemer, T.M. Haas, C. Wittwer, N. Jork, C. Gu, S.B. Shears, G. Schaaf, B. Kammerer, D. Fiedler, A. Saiardi, H.J. Jessen, Analysis of inositol phosphate metabolism by capillary electrophoresis electrospray ionization mass spectrometry, Nat. Commun. 11 (2020) 1–12, https://doi.org/10.1038/s41467-020-19928-x.

[19] T.Y. Zhang, S. Li, Q.F. Zhu, Q. Wang, D. Hussain, Y.Q. Feng, Derivatization for liquid chromatography-electrospray ionization-mass spectrometry analysis of small-molecular weight compounds, TrAC Trends Anal. Chem. (Reference Ed.) 119 (2019), https://doi.org/10.1016/j.trac.2019.07.019.
[20] S. Zhao, L. Li, Chemical derivatization in LC-MS-based metabolomics study, TrAC Trends Anal. Chem. (Reference Ed.) 131 (2020) 115988, https://doi.org/10.1016/j.trac.2020.115988.
[21] T. Huang, M.R. Armbruster, J.B. Coulton, J.L. Edwards, Chemical tagging in mass spectrometry for systems biology, Anal. Chem. 91 (2019) 109–125, https://doi.org/10.1021/acs.analchem.8b04951.
[22] H.P. Jiang, J. Xiong, F.L. Liu, C.J. Ma, X.L. Tang, B.F. Yuan, Y.Q. Feng, Modified nucleoside triphosphates exist in mammals, Chem. Sci. 9 (2018) 4160–4167, https://doi.org/10.1039/c7sc05472f.
[23] J. Clark, K.E. Anderson, V. Juvin, T.S. Smith, F. Karpe, M.J.O. Wakelam, L.R. Stephens, P.T. Hawkins, Quantification of PtdInsP3 molecular species in cells and tissues by mass spectrometry, Nat. Methods 8 (2011) 267–272, https://doi.org/10.1038/nmeth.1564.
[24] M. Chatterjee, D. Rath, J. Schlotterbeck, J. Rheinlaender, B. Walker-Allgaier, N. Alnaggar, M. Zdanyte, I. Müller, O. Borst, T. Geisler, T.E. Schäffer, M. Lämmerhofer, M. Gawaz, Regulation of oxidized platelet lipidome: implications for coronary artery disease, Eur. Heart J. 38 (2017) 1993–2005, https://doi.org/10.1093/eurheartj/ehx146.
[25] M. Cebo, C. Calderón Castro, J. Schlotterbeck, M. Gawaz, M. Chatterjee, M. Lämmerhofer, Untargeted UHPLC-ESI-QTOF-MS/MS analysis with targeted feature extraction at precursor and fragment level for profiling of the platelet lipidome with ex vivo thrombin-activation, J. Pharmaceut. Biomed. Anal. 205 (2021) 114301, https://doi.org/10.1016/j.jpba.2021.114301.
[26] T. Harm, A. Bild, K. Dittrich, A. Goldschmied, J. Nestele, M. Chatterjee, X. Fu, K. Kolb, T. Castor, O. Borst, T. Geisler, D. Rath, M. LäMmerhofer, M. Gawaz, Acute coronary syndrome is associated with a substantial change in the platelet lipidome, Cardiovasc. Res. (2021), https://doi.org/10.1093/cvr/cvab238.
[27] M.S.C. Wilson, S.J. Bulley, F. Pisani, R.F. Irvine, A. Saiardi, A novel method for the purification of inositol phosphates from biological samples reveals that no phytate is present in human plasma or urine, Open Biol 5 (2015), https://doi.org/10.1098/rsob.150014.
[28] M. Wilson, A. Saiardi, Inositol phosphates purification using titanium dioxide beads, Bio-Protocol 8 (2018), https://doi.org/10.21769/bioprotoc.2959.
[29] T. Xu, C. Hu, Q. Xuan, G. Xu, Recent advances in analytical strategies for mass spectrometry-based lipidomics, Anal. Chim. Acta 1137 (2020) 156–169, https://doi.org/10.1016/j.aca.2020.09.060.
[30] J.V. Paraskova, C. Jørgensen, K. Reitzel, J. Pettersson, E. Rydin, P.J.R. Sjöberg, Speciation of inositol phosphates in lake sediments by ion-exchange chromatography coupled with mass spectrometry, inductively coupled plasma atomic emission spectroscopy, and 31P NMR spectroscopy, Anal. Chem. 87 (2015) 2672–2677, https://doi.org/10.1021/ac5033484.
[31] F. Wei, X. Wang, H. fang Ma, X. Lv, X. yan Dong, H. Chen, Rapid profiling and quantification of phospholipid molecular species in human plasma based on chemical derivatization coupled with electrospray ionization tandem mass spectrometry, Anal. Chim. Acta 1024 (2018) 101–111, https://doi.org/10.1016/j.aca.2018.04.012.
[32] J.C. Lee, S.K. Byeon, M.H. Moon, Relative quantification of phospholipids based on isotope-labeled methylation by nanoflow ultrahigh performance liquid chromatography-tandem mass spectrometry: enhancement in cardiolipin profiling, Anal. Chem. 89 (2017) 4969–4977, https://doi.org/10.1021/acs.analchem.7b00297.
[33] E. Kühnel, D.D.P. Laffan, G.C. Lloyd-Jones, T. Martínez Del Campo, I.R. Shepperson, J.L. Slaughter, Mechanism of methyl esterification of carboxylic acids by trimethylsilyldiazomethane, Angew. Chem. Int. Ed. 46 (2007) 7075–7078, https://doi.org/10.1002/anie.200702131.
[34] C.P. Shelor, H. Liao, A.F. Kadjo, P.K. Dasgupta, Enigmatic ion-exchange behavior of myo -inositol phosphates, Anal. Chem. 87 (2015) 4851–4855, https://doi.org/10.1021/acs.analchem.5b00351.
[35] Q. Chen, Determination of phytic acid and inositol pentakisphosphates in foods by high-performance ion chromatography, J. Agric. Food Chem. 52 (2004) 4604–4613, https://doi.org/10.1021/jf035294x.
[36] Q.C. Chen, B.W. Li, Separation of phytic acid and other related inositol phosphates by high-performance ion chromatography and its applications, J. Chromatogr., A 1018 (2003) 41–52, https://doi.org/10.1016/j.chroma.2003.08.040.
[37] C. Görgens, S. Guddat, W. Schänzer, M. Thevis, Screening and confirmation of myo-inositol trispyrophosphate (ITPP) in human urine by hydrophilic interaction liquid chromatography high resolution/high accuracy mass spectrometry for doping control purposes, Drug Test. Anal. 6 (2014) 1102–1107, https://doi.org/10.1002/dta.1700.
[38] X. Liu, P.W. Villalta, S.J. Sturla, Simultaneous determination of inositol and inositol phosphates in complex biological matrices: quantitative ion-exchange chromatography/tandem mass spectrometry, Rapid Commun. Mass Spectrom. 23 (2009) 705–712, https://doi.org/10.1002/rcm.3923.
[39] F. Kvasnička, J. Čopíková, R. Ševčík, E. Václavíková, A. Synytsya, K. Vaculová, M. Voldřich, Determination of phytic acid and in ositolphosphates in barley, Electrophoresis 32 (2011) 1090–1093, https://doi.org/10.1002/elps.201000578.
[40] K. Blaabjerg, J. Hansen-Møller, H.D. Poulsen, High-performance ion chromatography method for separation and quantification of inositol phosphates in diets and digesta, J. Chromatogr. B 878 (2010) 347–354, https://doi.org/10.1016/j.jchromb.2009.11.046.
[41] M. Sun, D.P. Jaisi, Distribution of inositol phosphates in animal feed grains and excreta: distinctions among isomers and phosphate oxygen isotope compositions, Plant Soil 430 (2018) 291–305, https://doi.org/10.1007/s11104-018-3723-5.
[42] Y. Sekiguchi, A. Matsunaga, A. Yamamoto, Y. Inoue, Analysis of condensed phosphates in food products by ion chromatography with an on-line hydroxide eluent generator, J. Chromatogr., A 881 (2000) 639–644, https://doi.org/10.1016/S0021-9673(99)01278-9.
[43] A.J. Letcher, M.J. Schell, R.F. Irvine, Do mammals make all their own inositol hexakisphosphate? Biochem. J. 416 (2008) 263–270, https://doi.org/10.1042/BJ20081417.
[44] J.L. Meek, Inositol bis-, tris-, and tetrakis(phosphate)s: analysis in tissues by HPLC, Proc. Natl. Acad. Sci. Unit. States Am. 83 (1986) 4162–4166, https://doi.org/10.1073/pnas.83.12.4162.
[45] A.H. Guse, A. Goldwich, K. Weber, G.W. Mayr, Non-radioactive, isomer-specific inositol phosphate mass determinations: high-performance liquid chromatography-micro-metal-dye detection strongly improves speed and sensitivity of analyses from cells and micro-enzyme assays, J. Chromatogr. B Biomed. Sci. Appl. 672 (1995) 189–198, https://doi.org/10.1016/0378-4347(95)00219-9.
[46] M.W.H. Pinkse, P.M. Uitto, M.J. Hilhorst, B. Ooms, A.J.R. Heck, Selective isolation at the femtomole level of phosphopeptides from proteolytic digests using 2D-NanoLC-ESI-MS/MS and titanium oxide precolumns, Anal. Chem. 76 (2004) 3935–3943, https://doi.org/10.1021/ac0498617.
[47] A. Leitner, Phosphopeptide enrichment using metal oxide affinity chromatography, TrAC Trends Anal. Chem. (Reference Ed.) 29 (2010) 177–185, https://doi.org/10.1016/j.trac.2009.08.007.
[48] P.A. Connor, A.J. McQuillan, Phosphate adsorption onto TiO_2 from aqueous solutions:an in situ internal reflection infrared spectroscopic study, Langmuir 15 (1999) 2916–2921, https://doi.org/10.1021/la980894p.
[49] L. Si-Hung, C. Troyer, T. Causon, S. Hann, Sensitive quantitative analysis of phosphorylated primary metabolites using selective metal oxide enrichment and GC- and IC- MS/MS, Talanta 205 (2019) 120147, https://doi.org/10.1016/j.talanta.2019.120147.
[50] B.K. Matuszewski, M.L. Constanzer, C.M. Chavez-Eng, Strategies for the assessment of matrix effect in quantitative bioanalytical methods based on HPLC-MS/MS, Anal. Chem. 75 (2003) 3019–3030, https://doi.org/10.1021/ac020361s.
[51] F. and D.A. U.S. Department of Health and Human Services, Bioanalytical Method Validation Guidance for Industry 1043, U.S. Dep. Heal. Hum. Serv. Food Drug Adm, 2018, pp. 1–41. https://www.fda.gov/files/drugs/published/Bioanalytical-Method-Validation-Guidance-for-Industry.pdf.
[52] N. Ansermot, S. Rudaz, M. Brawand-Amey, S. Fleury-Souverain, J.-L. Veuthey, C.B. Eap, Validation and long-term evaluation of a modified on-line chiral analytical method for therapeutic drug monitoring of (R, S)-methadone in clinical samples, J. Chromatogr. B 877 (2009) 2301–2307.
[53] R. Bakhtiar, T.K. Majumdar, Tracking problems and possible solutions in the quantitative determination of small molecule drugs and metabolites in biological fluids using liquid chromatography-mass spectrometry, J. Pharmacol. Toxicol. Methods 55 (2007) 227–243, https://doi.org/10.1016/j.vascn.2006.10.002.
[54] L. Cuadros-Rodríguez, M.G. Bagur-González, M. Sánchez-Viñas, A. González-Casado, A.M. Gómez-Sáez, Principles of analytical calibration/quantification for the separation sciences, J. Chromatogr., A 1158 (2007) 33–46, https://doi.org/10.1016/j.chroma.2007.03.030.
[55] A. Tan, K. Awaiye, Use of internal standards in LC-MS bioanalysis, in: Handb. LC-MS Bioanal., John Wiley & Sons Inc., Hoboken, NJ, USA, 2013, pp. 217–227, https://doi.org/10.1002/9781118671276.ch17.
[56] M. Wang, C. Wang, X. Han, Selection of internal standards for accurate quantification of complex lipid species in biological extracts by electrospray ionization mass spectrometry—what, how and why? Mass Spectrom. Rev. 36 (2017) 693–714, https://doi.org/10.1002/mas.21492.
[57] S. Windhorst, H. Lin, C. Blechner, W. Fanick, L. Brandt, M.A. Brehm, G.W. Mayr, Tumour cells can employ extracellular Ins(1,2,3,4,5,6)P6 and multiple inositol-polyphosphate phosphatase 1 (MINPP1) dephosphorylation to improve their proliferation, Biochem. J. 450 (2013) 115–125, https://doi.org/10.1042/BJ20121524.
[58] W. Jin, T.M. Lo, H.H. Loh, S.A. Thayer, U73122 inhibits phospholipase C-dependent calcium mobilization in neuronal cells, Brain Res. 642 (1994) 237–243, https://doi.org/10.1016/0006-8993(94)90927-X.

Supplementary information

Isomer-selective analysis of inositol phosphates with differential isotope labelling by phosphate methylation using liquid chromatography with tandem mass spectrometry

Peng Li [a], Meinrad Gawaz [b], Madhumita Chatterjee [b], Michael Lämmerhofer [a] *

[a] Institute of Pharmaceutical Sciences, Pharmaceutical (Bio-)Analysis, University of Tübingen, Tübingen, Germany

[b] Department of Cardiology and Angiology, University Hospital Tübingen, 72076 Tübingen, Germany

*Author for correspondence:
Prof. Dr. Michael Lämmerhofer
Pharmaceutical (Bio-)Analysis
Institute of Pharmaceutical Sciences
University of Tübingen
Auf der Morgenstelle 8
72076 Tübingen, Germany
T +49 7071 29 78793, F +49 7071 29 4565
e-mail: michael.laemmerhofer@uni-tuebingen.de

Text S1. IDA-EPI method information.

The IDA-EPI was performed on a QTRAP4500 mass spectrometer with a Turbo V source (Sciex, Framingham, MA, USA) operated with the ESI probe, the same instrument as mentioned in the main manuscript. Ion source parameters were as follows: curtain gas (N2) 30 psi, nebulizer gas (zero grade air) 30 psi; heater gas (zero grade air) 30 psi, ion source voltage +4500 V (positive mode) and source temperature 500 °C. Pseudo-SRM transitions were constructed as the survey scan for 4 methylated IPx standards (Q1 = Q3). MS parameters were DP 100, CE 5, CXP 15. Each transition had a dwell time of 20 ms. IDA criteria were selection of one intense peak, intensity 10000 cps, and never exclude target ions. EPI experiment had the same parameters as the SRM except for CE 30 and collision energy at high level. Detection mass range was 50 – 650 Da. The total cycle time was 0.59 ms.

Text S2. HR-MS method information

The HR-MS detection was performed on a TripleTOF 5600+ mass spectrometer with a DuoSpray source (Sciex, Framingham, MA, USA) operated with the ESI probe. Ion source parameters were: curtain gas (N2) 30 psi, nebulizer gas (zero grade air) 30 psi; heater gas (zero grade air) 30 psi, ion source voltage +4500 V (positive mode) and source temperature 500 °C. Sequential window acquisition of all theoretical fragment ion mass spectra (SWATH) experiments were performed to obtain comprehensive MS/MS data. In the TOF scan, MS parameters were: DP 100, CE 10, mass range 50 – 1500, accumulation time 150 ms. SWATH experiments were conducted from 250 – 850 Da. The SWATH window width was 40 Da with accumulation time 20 ms. Other MS parameters were DP 100, CE 30, CES 5. The total cycle time was 500 ms. The instrument was automatically calibrated every 5 samples via calibration delivery system (CDS) using commercial calibration solution. The EIC of precursor was extracted in MasterView software according to chemical formula. Corresponding product ion spectra was obtained after deconvolution in the software according to Rt in chromatography.

Table S1. Extraction recovery and pseudo matrix effect results in preliminary experiments.

Extraction recovery and pseudo-matrix effect, %		IP1	IP2	IP3	IP4
100 mM HCl	ER	22.8	19.1	17.8	25.6
	P-ME	55.4	112.0	108.7	69.8
10 mM HCl	ER	72.7	87.3	80.2	77.0
	P-ME	10.8	16.3	8.6	7.6
1 mM HCl	ER	63.2	45.1	61.8	65.6
	P-ME	7.6	8.0	1.7	1.9

Table S2. Intra-batch accuracy and precision results (in HeLa cell matrix corrected for endogenous levels).

Accuracy and Precision, %	I(1)P	I(1,3)P2	I(1,4)P2	I(1,5)P2	I(1,3,4)P3	I(1,3,5)P3	I(1,4,5)P3	I(1,3,4,5)P4	I(1,3,4,5,6)P5	IP6
QC1(LLOQ)	95.4 ± 21.1	113.6 ± 7.8	114.6 ± 3.9	113.9 ± 1.6	117.3 ± 1.7	107.4 ± 1.8	107.5 ± 4.4	112.3 ± 4.2	111.1 ± 2.8	113.7 ± 3.2
QC2(Low)	92.8 ± 9.7	91.3 ± 5.1	88.0 ± 1.0	91.7 ± 4.8	89.1 ± 4.4	87.6 ± 1.7	96.1 ± 14.4	91.2 ± 3.4	88.4 ± 2.2	90.2 ± 2.4
QC3(Medium)	94.9 ± 7.5	85.6 ± 1.8	95.3 ± 3.1	91.1 ± 5.2	94.2 ± 6.7	98.3 ± 5.4	87.0 ± 1.5	88.1 ± 3.6	87.5 ± 1.8	92.2 ± 3.5
QC4(High)	99.3 ± 2.1	106.6 ± 6.5	102.5 ± 2.5	108 ± 4.2	103.9 ± 7.1	101.1 ± 14.2	107.1 ± 11.6	103.4 ± 14.9	102.3 ± 13.7	102.9 ± 12

Table S3. Inter-batch accuracy and precision results (in HeLa cell matrix corrected for endogenous levels).

Accuracy and Precision, %	I(1)P	I(1,3)P2	I(1,4)P2	I(1,5)P2	I(1,3,4)P3	I(1,3,5)P3	I(1,4,5)P3	I(1,3,4,5)P4	I(1,3,4,5,6)P5	IP6
QC1(LLOQ)	99.4 ± 14.4	113.0 ± 4.5	113.1 ± 5.1	114.3 ± 3.7	112.6 ± 4.7	110.6 ± 4.6	107.5 ± 4.4	110.1 ± 4.1	110.3 ± 4.9	110.3 ± 4.9
QC2(Low)	93.1 ± 9.8	92.0 ± 3.2	87.7 ± 1.3	90.6 ± 3.4	89.3 ± 3.5	89.2 ± 3.0	91.7 ± 8.3	90.0 ± 3.2	89.8 ± 4.2	89.1 ± 2.5
QC3(Medium)	91.4 ± 5.7	87.8 ± 2.6	93.6 ± 4.2	89.3 ± 3.3	92.2 ± 4.0	93.8 ± 6.2	88.6 ± 2.1	90.6 ± 4.8	87.9 ± 2.0	91.8 ± 3.1
QC4(High)	100.2 ± 5.8	106.7 ± 5.9	101.4 ± 8.6	105.7 ± 7.8	105.6 ± 5.6	101.6 ± 9.3	106.4 ± 7.3	104.5 ± 11.2	102.0 ± 11.0	102.0 ± 10.2

Table S4. Matrix effect without internal standards.

Matrix effect, %	SIL-I(1)P	SIL-I(1,3)P2	SIL-I(1,4)P2	SIL-I(1,5)P2	SIL-I(1,3,4)P3	SIL-I(1,3,5)P3	SIL-I(1,4,5)P3	I(1,3,4,5)P4	SIL-I(1,3,4,5,6)P5	SIL-IP6
QC1(Low)	83.1 ± 18.9	159.7 ± 31.7	105.1 ± 29.9	141.3 ± 37.5	163.6 ± 29.6	116.4 ± 17.9	164.1 ± 37.6	60.5 ± 15.2	65 ± 12.8	41 ± 9.8
QC2(Medium)	47 ± 7.5	94.1 ± 4.3	71.3 ± 1.8	90.2 ± 4	78.9 ± 12.1	73.7 ± 4.7	83 ± 5.2	45 ± 10.7	43.7 ± 11.1	29.6 ± 5
QC3(High)	42.8 ± 9.4	95.4 ± 25.1	62.3 ± 11	82.5 ± 9	80 ± 7.4	64.7 ± 4.9	97.6 ± 0.3	36.1 ± 4.3	46.4 ± 5.2	35.7 ± 7.5

Table S5. Matrix effect with internal standards.

Matrix effect, %	I(1)P	I(1,3)P2	I(1,4)P2	I(1,5)P2	I(1,3,4)P3	I(1,3,5)P3	I(1,4,5)P3	I(1,3,4,5)P4	I(1,3,4,5,6)P5	IP6
QC1(Low)	91.7 ± 4.9	89.5 ± 4.7	92.2 ± 1.7	92.8 ± 0.6	90 ± 5	95.4 ± 2.8	94.2 ± 3	105 ± 2.1	105.1 ± 1.9	104.5 ± 4.4
QC2(Medium)	92.9 ± 1.8	94.4 ± 2.2	90.8 ± 1.9	98.1 ± 10.3	91.1 ± 4.2	106.5 ± 2.6	93.9 ± 5.4	92.3 ± 6.5	104.5 ± 4.4	104.6 ± 3.8
QC3(High)	92.6 ± 7.1	99.9 ± 7.1	93.1 ± 5	90.9 ± 4.9	96 ± 3.7	92.1 ± 3.4	98.6 ± 1.9	105.4 ± 4.9	101.2 ± 6.3	108.5 ± 2.8

Table S6. Extraction recovery results.

Extraction recovery, %	I(1)P	I(1,3)P2	I(1,4)P2	I(1,5)P2	I(1,3,4)P3	I(1,3,5)P3	I(1,4,5)P3	I(1,3,4,5)P4	I(1,3,4,5,6)P5	IP6
QC1(Low)	61.8 ± 2.6	54 ± 3.1	50.1 ± 6.5	50.6 ± 2.2	55.6 ± 2.2	57.7 ± 7	55.2 ± 1.7	57.2 ± 1.1	55 ± 3.1	54 ± 2.8
QC2(Medium)	55.2 ± 3.3	60.3 ± 1	56.9 ± 11	48.2 ± 3.7	54.1 ± 8.4	45.2 ± 1.7	56.8 ± 4.2	41.6 ± 4.9	55.4 ± 3.2	51.2 ± 4.5
QC3(High)	61.7 ± 4.6	49.7 ± 3.8	58.4 ± 9.3	54.8 ± 6.1	49.4 ± 3.6	42.8 ± 8.4	50.2 ± 10.2	47.7 ± 5.4	49.5 ± 5.2	55.9 ± 3.3

Table S7. Process efficiency results.

Process efficiency, %	I(1)P	I(1,3)P2	I(1,4)P2	I(1,5)P2	I(1,3,4)P3	I(1,3,5)P3	I(1,4,5)P3	I(1,3,4,5)P4	I(1,3,4,5,6)P5	IP6
QC1(Low)	56.6 ± 0.8	48.3 ± 0.9	46.3 ± 6.6	47.0 ± 2.2	49.9 ± 1.3	55.1 ± 7.8	52.1 ± 3.2	60.1 ± 2.0	57.8 ± 2.5	56.6 ± 5.3
QC2(Medium)	51.3 ± 3.7	56.9 ± 0.5	51.6 ± 9.1	47.1 ± 3.3	49.2 ± 7.3	48.1 ± 2.4	53.5 ± 6.0	38.6 ± 7.0	57.8 ± 3.5	53.6 ± 5.7
QC3(High)	57.1 ± 6	49.8 ± 7.3	54.5 ± 11.3	49.9 ± 6.6	47.4 ± 4.7	39.6 ± 9.3	49.6 ± 11.1	50.3 ± 5.9	49.9 ± 3	60.7 ± 2.7

Figure S1. Methylation optimization results with 50 µL TMSD.

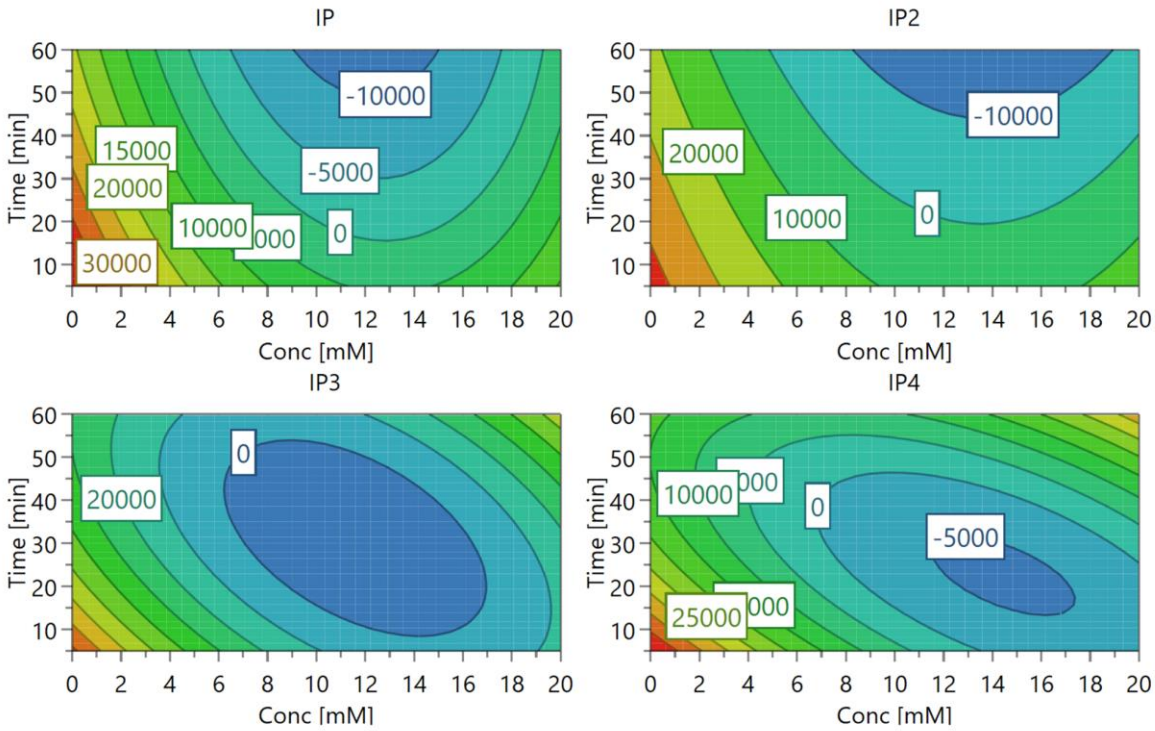

Figure S2. Methylation optimization results with 100 µL TMSD.

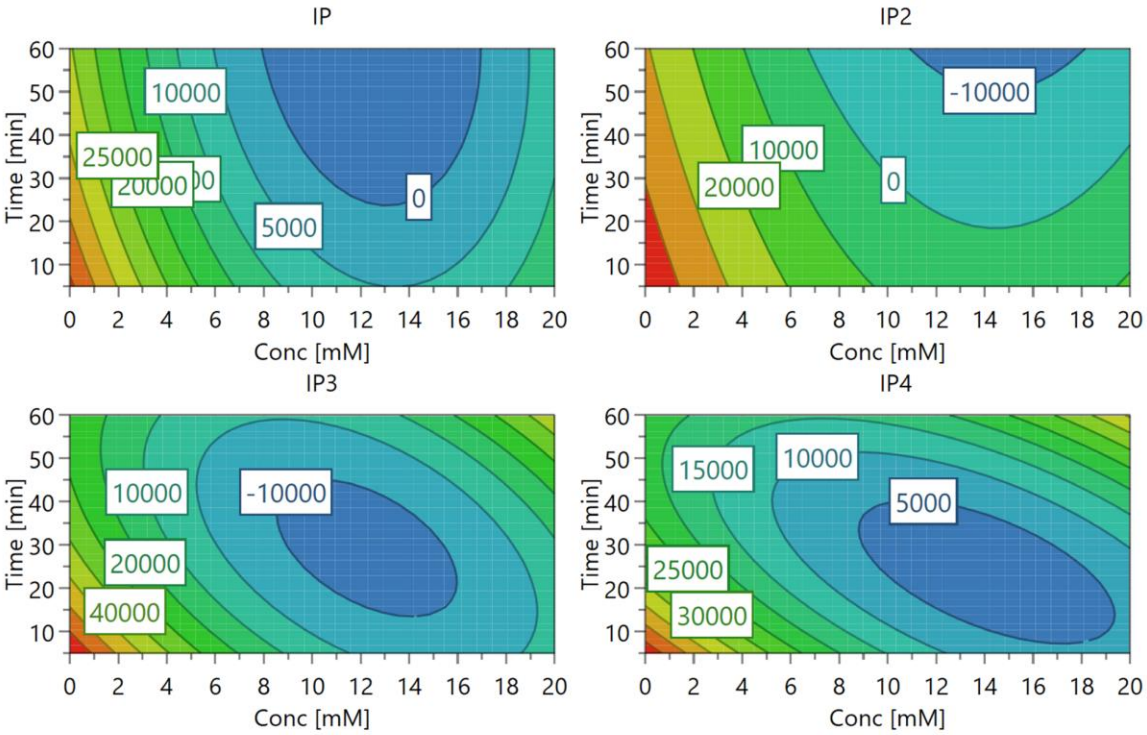

Figure S3. Methylation optimization results with 200 µL TMSD.

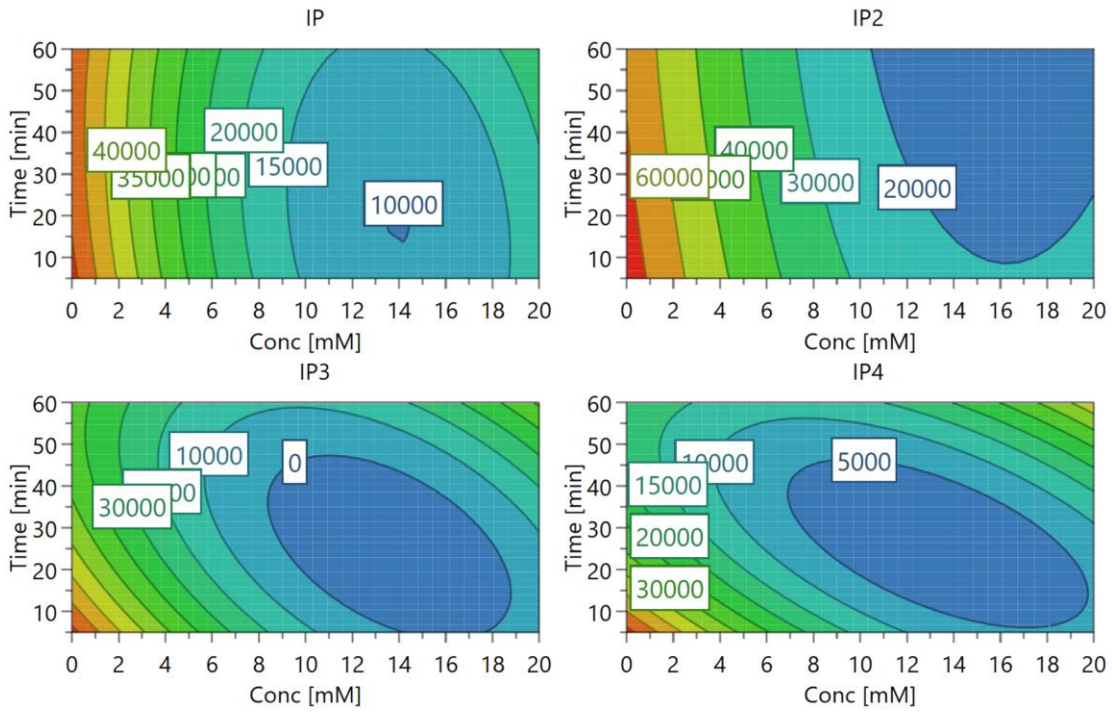

Figure S4. Product ion spectra in high-resolution mass spectrometry.

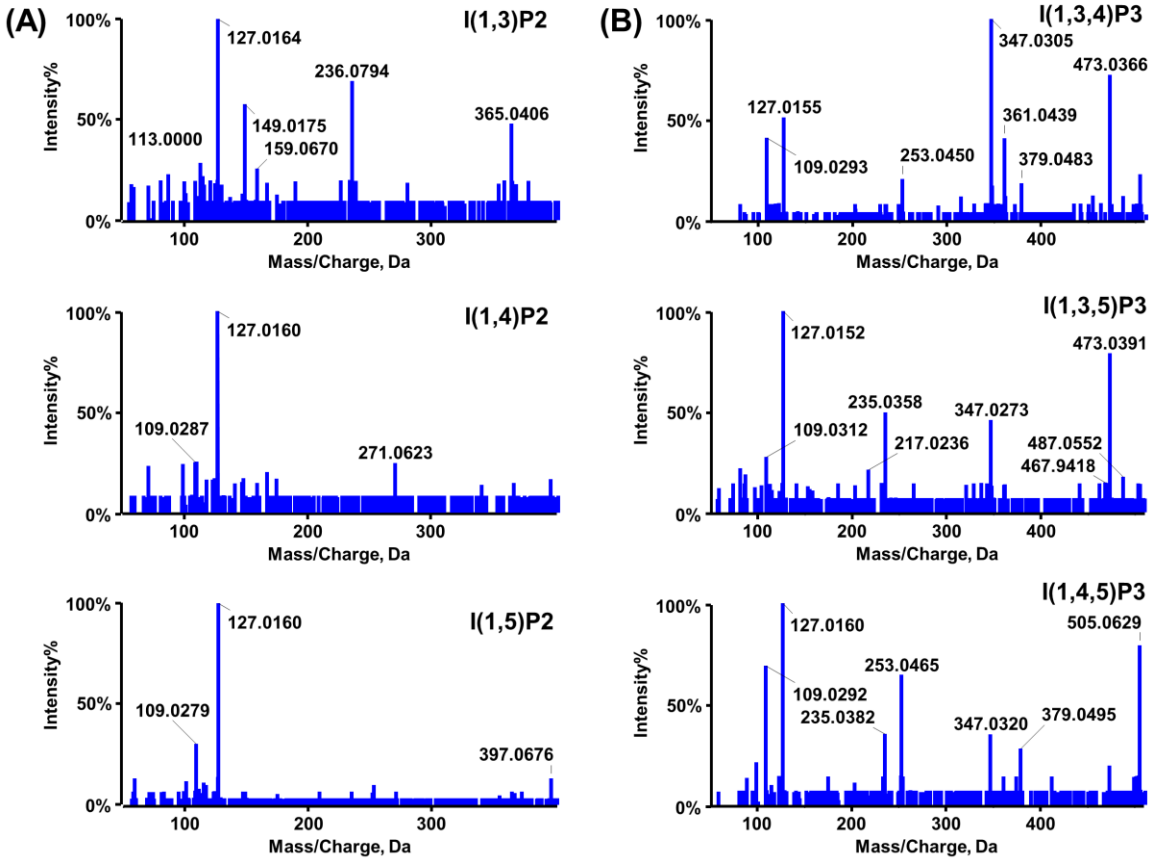

Figure S5. Reaction mechanism of differential isotope labelling methylation of IPx.

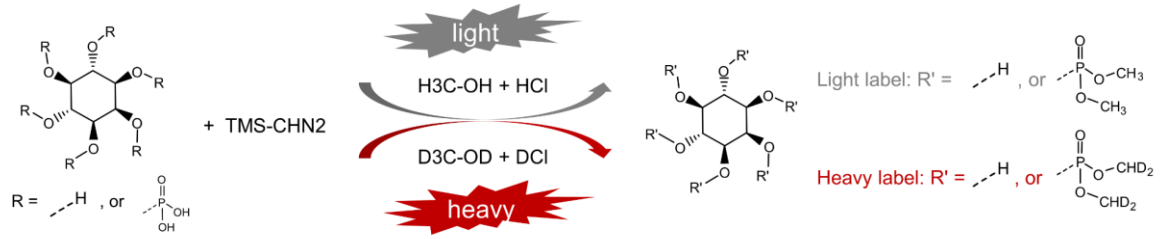

Figure S6. Representative EICs with product ion spectra of heavily labeled IPx standards.

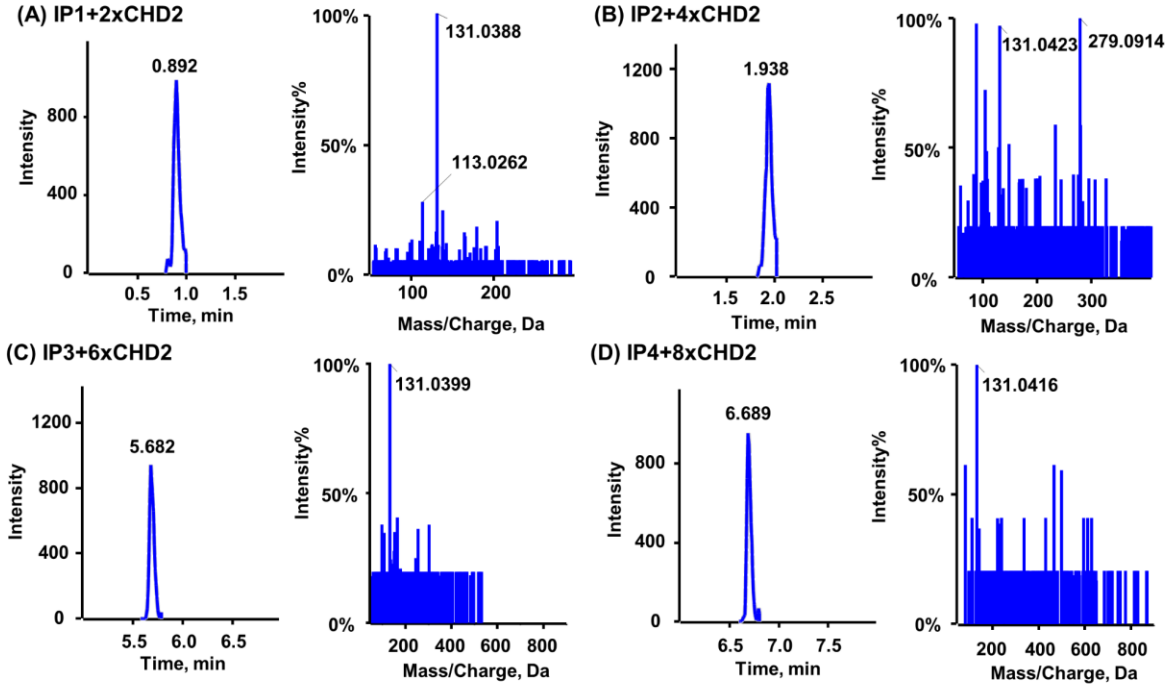

Figure S7. Evaluation of in source fragmentation of IPx after methylation (note, in E the peak for IP5 at tR 7.97 min in the IP6 sample is due to a chemical impurity in IP6 standard).

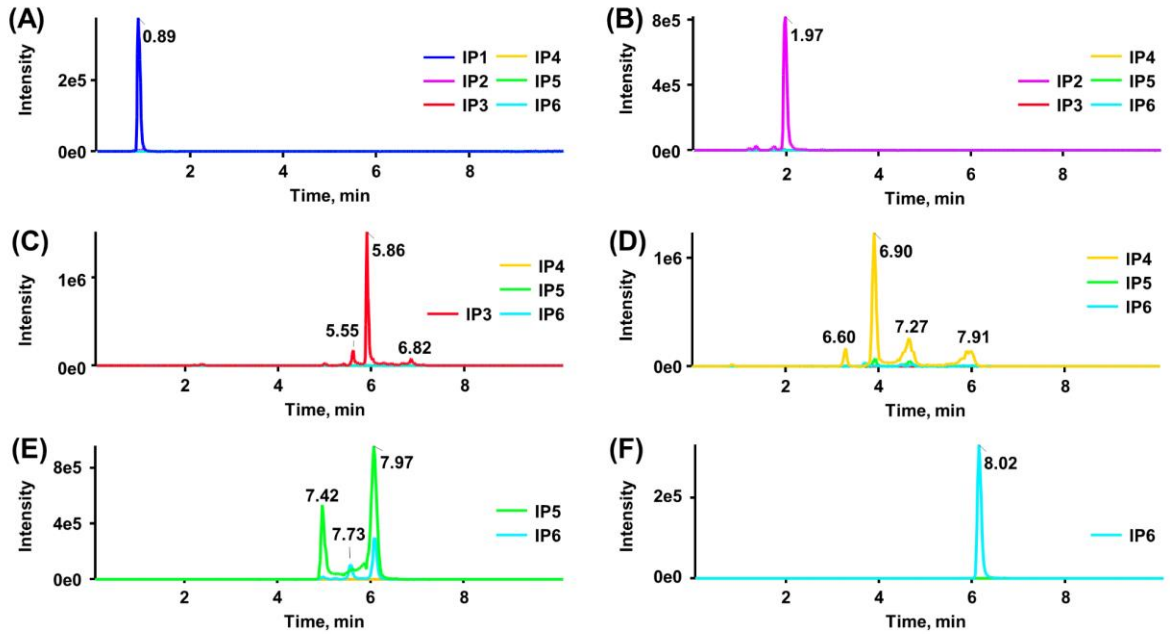

Figure S8. Column screening results on Waters CSH C18 column. Mobile phases used: (A) 10 mM NH4FA in water and methanol; (B) 10 mM NH4FA in water and acetonitrile.

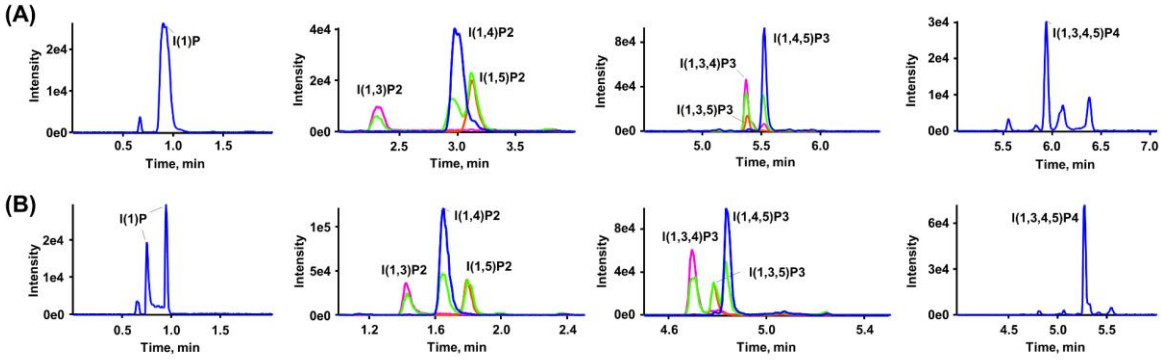

Figure S9. Column screening results on ProntoSIL C30 column. Mobile phases used: (A) 10 mM NH4FA in water and methanol; (B) 10 mM NH4FA in water and acetonitrile.

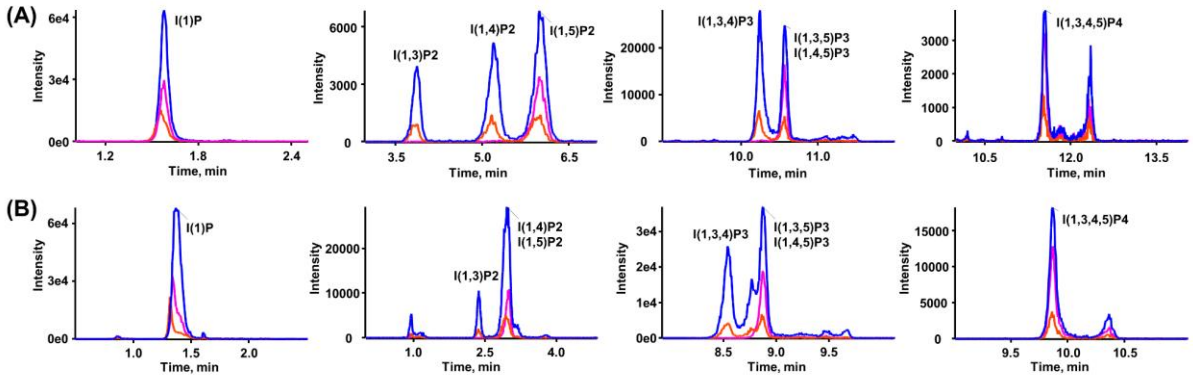

Figure S10. Column screen results on Waters HSS T3 column. Mobile phases used: (A) 10 mM NH4FA in water and methanol; (B) 10 mM NH4FA in water and acetonitrile.

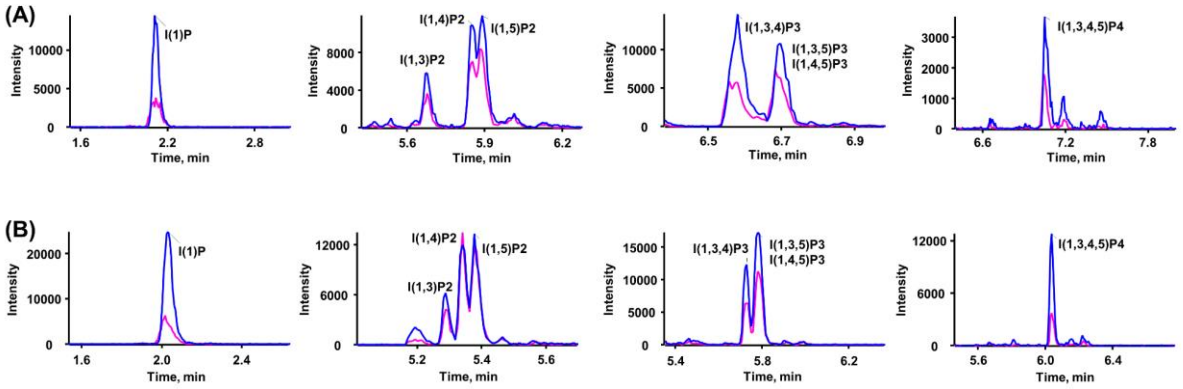

Figure S11. Column screen results on YMC Triart C18 column. Mobile phases used: (A) 10 mM NH4FA in water and methanol; (B) 10 mM NH4FA in water and acetonitrile.

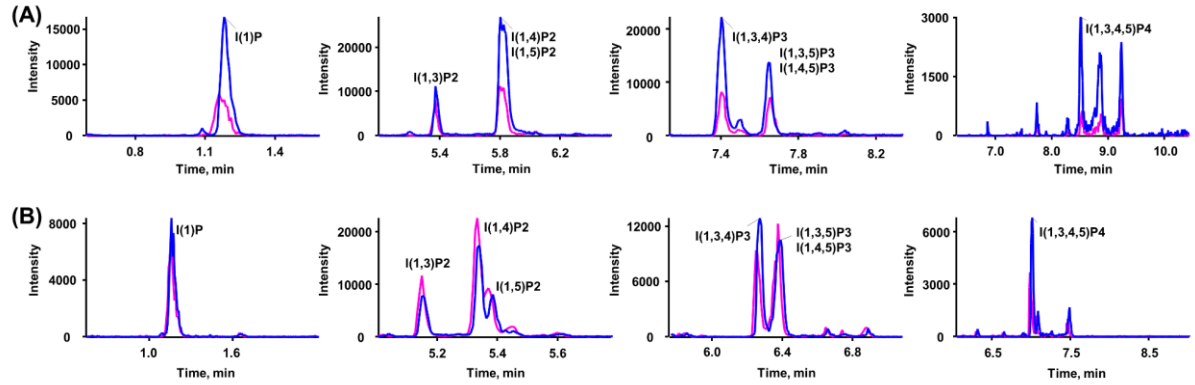

Figure S12. Column screen results on 2.6Cholester column. Mobile phases used: (A) 10 mM NH4FA in water and methanol; (B) 10 mM NH4FA in water and acetonitrile.

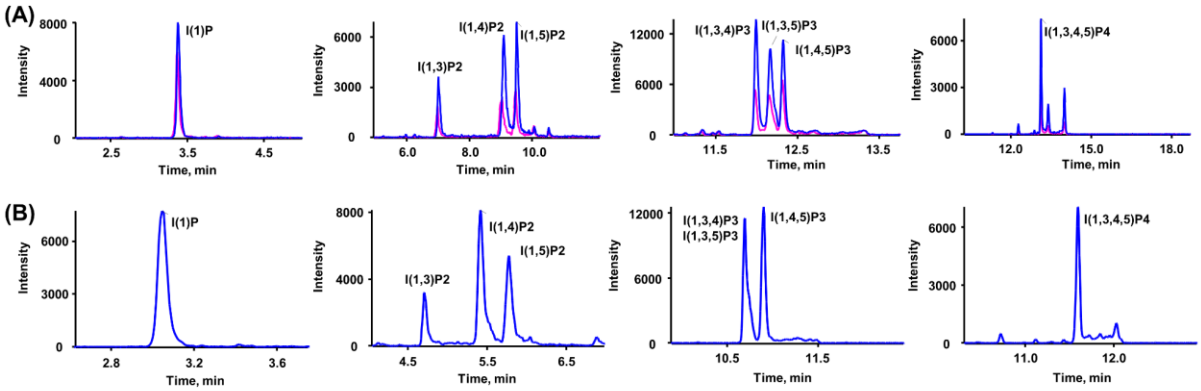

Figure S13. Results of reconstitution solvent optimization. Three levels of methanol content in reconstitution solvent were tested: 5% (blue), 10% (pink), and 20% (red).

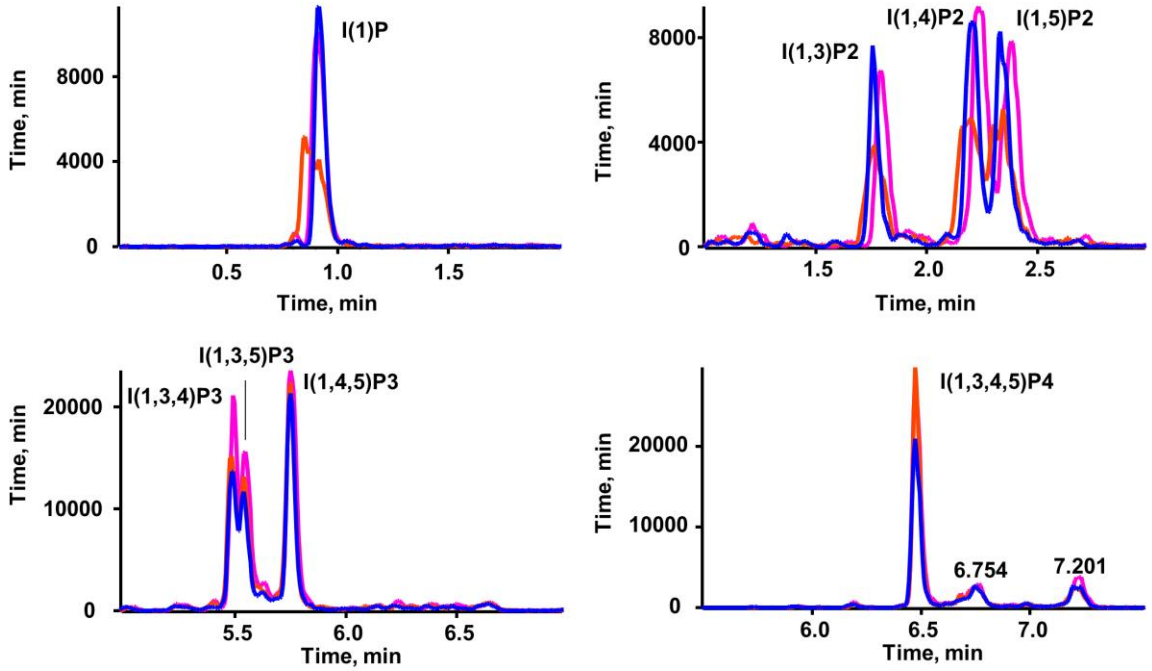

Figure S14. Sample preparation method with extraction kit.

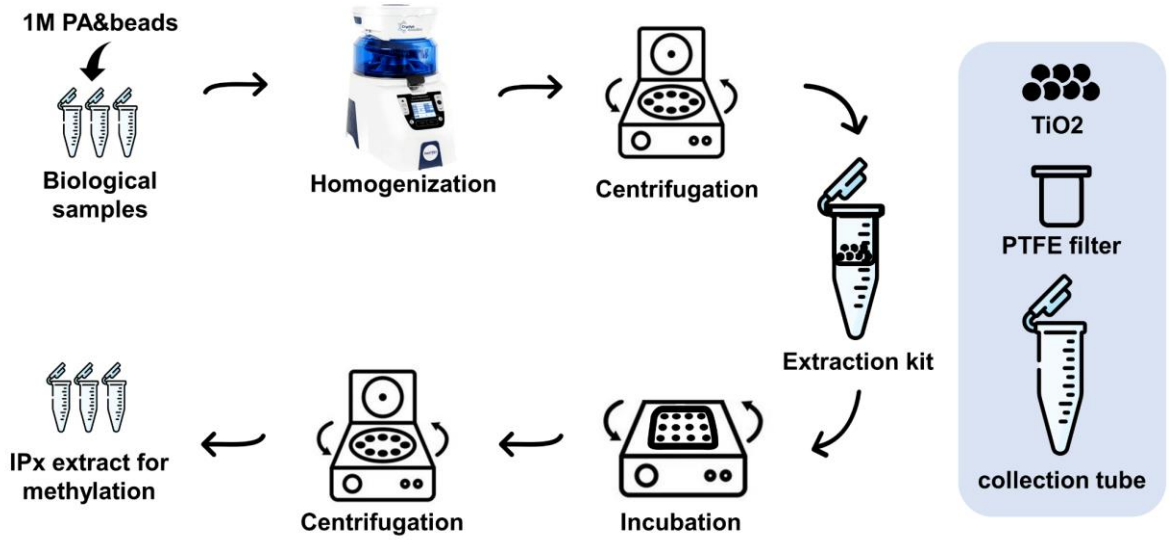

Figure S15. Calibration curves of IPx analytes.

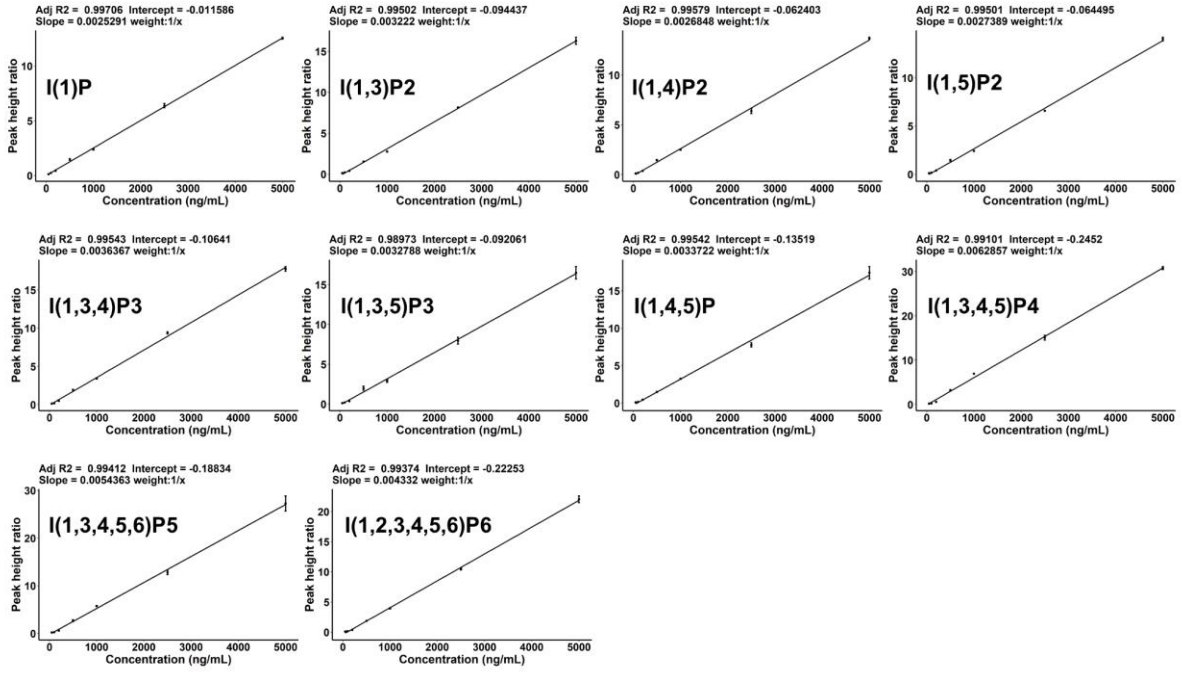

Figure S16. Representative EICs of IPx at LOQs. Estimate signal-to-noise ratio (S/N) obtained in PeakView.

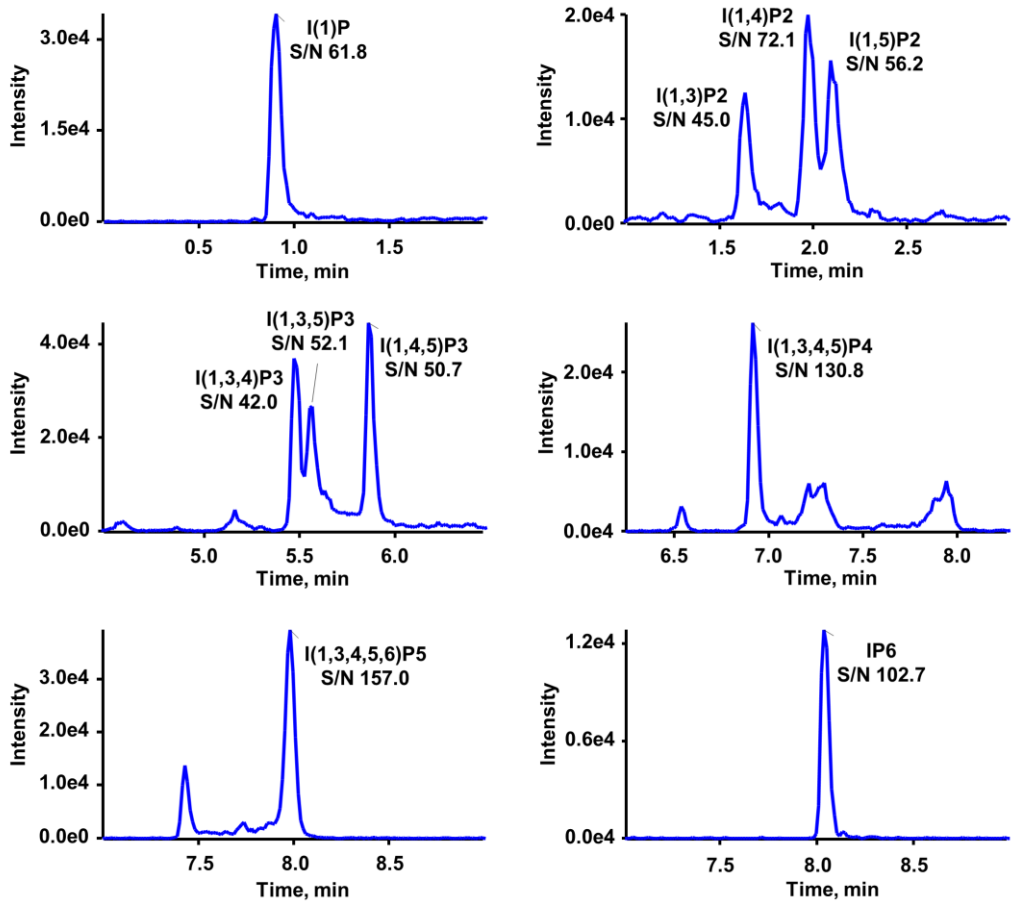

Figure S17. Autosampler stability results.

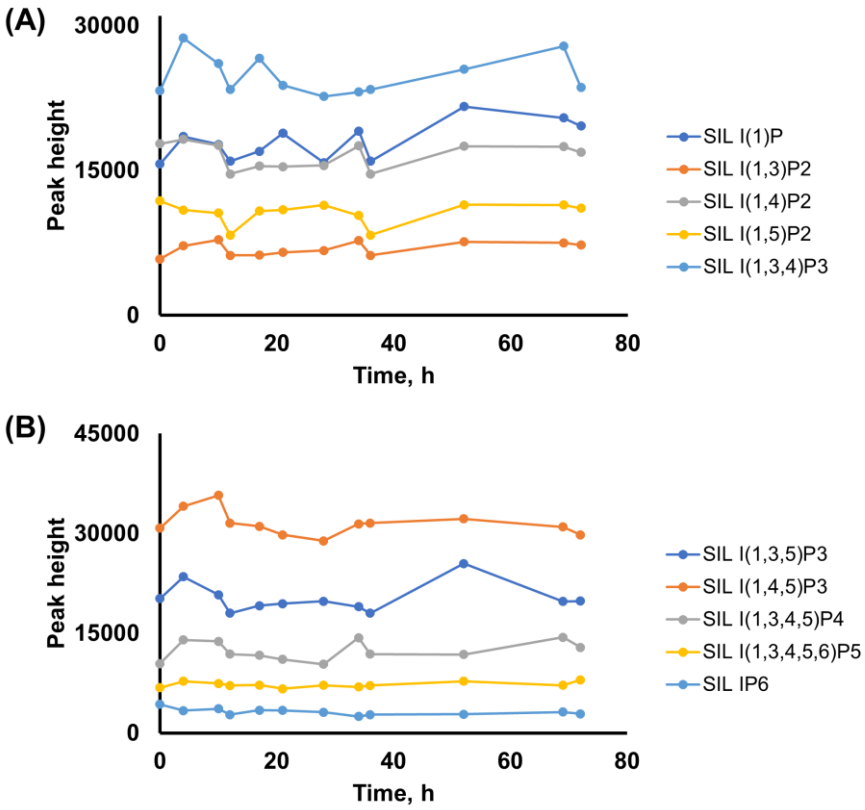

Figure S18. Cross-signal contribution of SIL IS in this study: XICs of analyte and corresponding SIL IS in sample solution of (A) SIL IP1, (B) SIL IP2, (C) SIL IP3, (D) SIL IP4, (E) SIL IP5, and (F) SIL IP6.

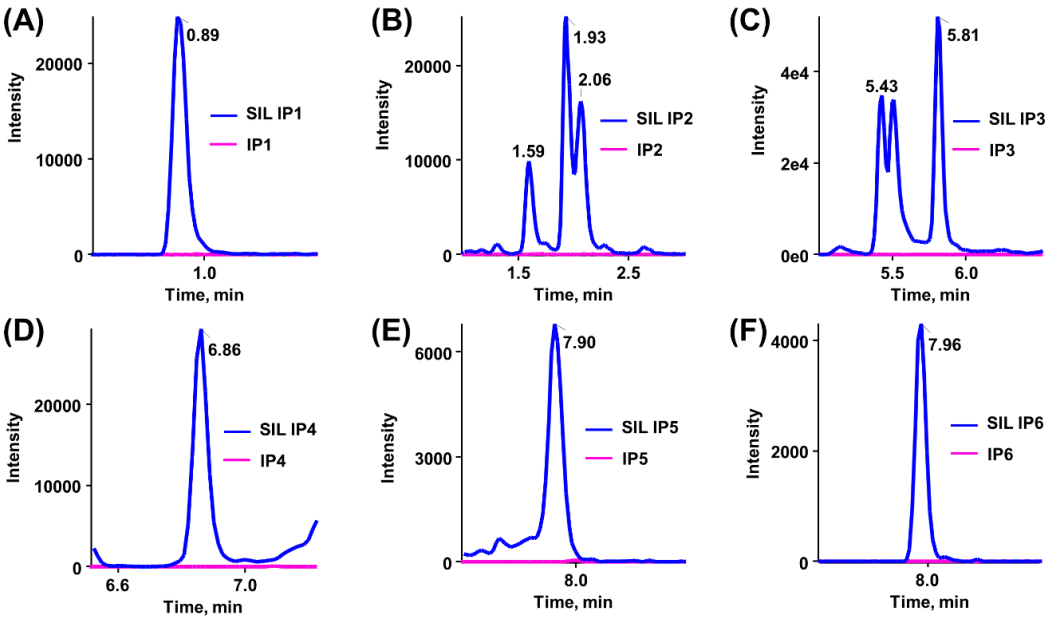

Figure S19. IPx profiles in different biological samples.

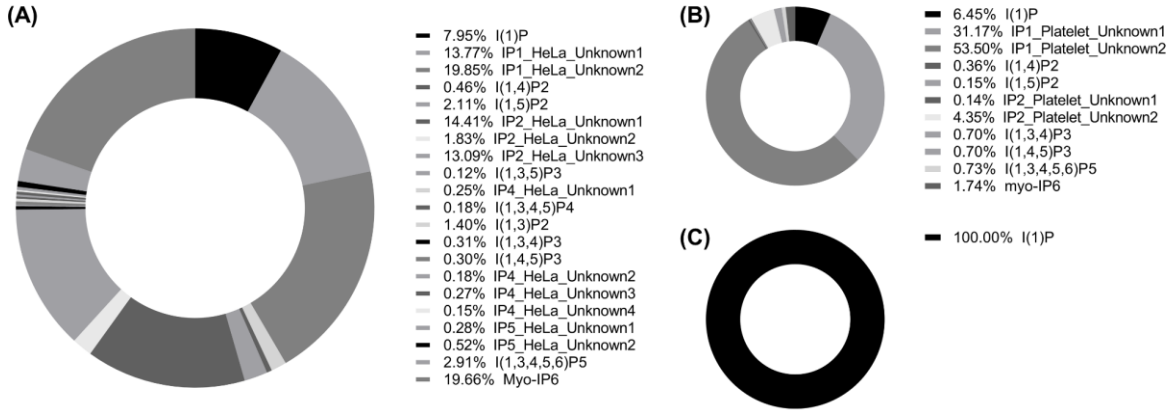

12. Publication IV

Targeted analysis of sugar phosphates from glycolysis pathway by phosphate methylation with liquid chromatography coupled to tandem mass spectrometry

Peng Li [a], Min Su [a], Madhumita Chatterjee [b], Michael Lämmerhofer [a*]

[a] Institute of Pharmaceutical Sciences, Pharmaceutical (Bio-)Analysis, University of Tübingen, Tübingen, Germany

[b] Department of Cardiology and Angiology, University Hospital Tübingen, 72076 Tübingen, Germany

Anal. Chim. Acta.

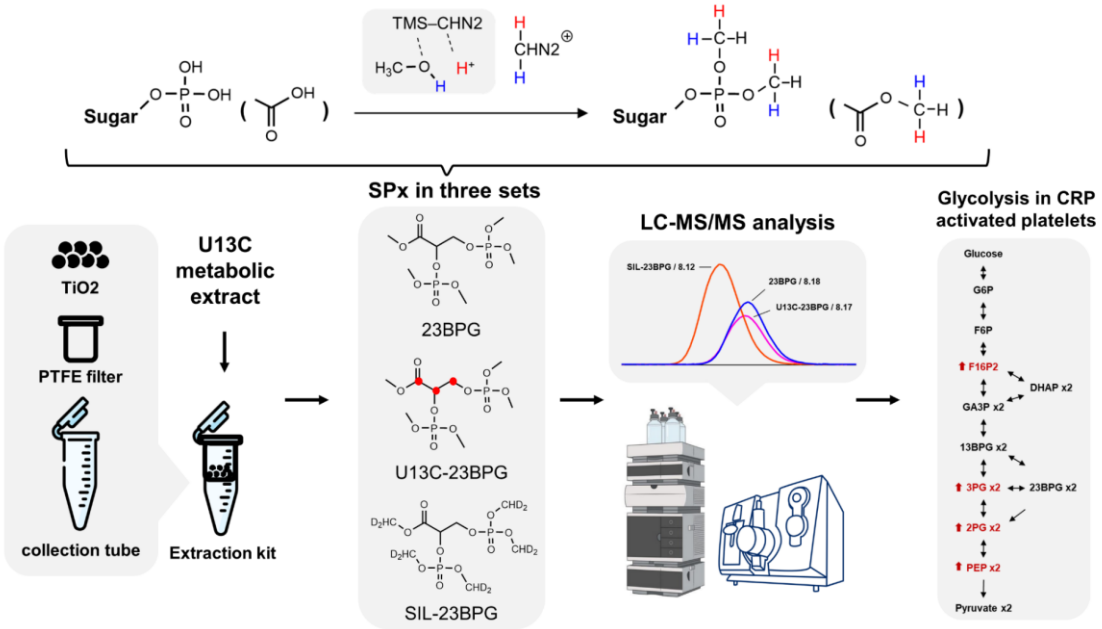

Targeted analysis of sugar phosphates from glycolysis pathway by phosphate methylation with liquid chromatography coupled to tandem mass spectrometry

Peng Li [a], Min Su [a], Madhumita Chatterjee [b], Michael Lämmerhofer [a] *

[a] Institute of Pharmaceutical Sciences, Pharmaceutical (Bio-)Analysis, University of Tübingen, Tübingen, Germany

[b] Department of Cardiology and Angiology, University Hospital Tübingen, 72076 Tübingen, Germany

*Author for correspondence:
Prof. Dr. Michael Lämmerhofer
Pharmaceutical (Bio-)Analysis
Institute of Pharmaceutical Sciences
University of Tübingen
Auf der Morgenstelle 8
72076 Tübingen, Germany
T +49 7071 29 78793, F +49 7071 29 4565
e-mail: michael.laemmerhofer@uni-tuebingen.de

Abstract

The glycolysis pathway breaks glucose into pyruvates and plays important roles in central carbon metabolism. It represents the basic anaerobic energy supply chain of cells. From analytical viewpoint, monitoring the glycolysis pathway remains a challenge as most metabolites involved are sugar phosphates. Structural similarity, instability, high polarity, and rich negative charges of sugar phosphates make LC-MS based analysis challenging. Here, we developed an improved workflow integrating uniformly 13C-labeled yeast metabolite extract, TiO2-based enrichment, differential stable isotope labeling phosphate methylation, porous graphic carbon column, and selected reaction monitoring acquisition. Uniformly 13C labeled yeast metabolite extract was used as internal standards while differential stable isotope labeled sugar phosphates worked as calibrants. The established method was validated for human plasma. The limits of quantification ranged between 0.25 and 0.54 pmol on column. The method was adapted and applied for more biological samples including cultured HeLa cells and human platelets. Compared to the group of resting platelets, most sugar phosphates from the glycolysis pathway were significantly upregulated in the group of platelets treated with collagen-related peptide (CRP) driving platelet activation. It indicates that platelets trigger glycolysis to meet energetic demands. The results document that this newly established method can be successfully used to monitor glycolysis in different biological samples. This method is able to deepen our understanding of the roles of the glycolysis pathway under different metabolic conditions.

Keywords

Sugar phosphate; porous graphitic carbon column; solid-phase extraction; derivatization; isotope labeling; targeted metabolomics

Abbreviations

SPx, sugar phosphates

PPP, pentose phosphate pathway

TCA, tricarboxylic acid cycle

CE, capillary electrophoresis

HILIC, hydrophilic interaction chromatography

IP, ion pairing

AEX, anion exchange chromatography

IC, ion chromatography

IEX, ion exchange chromatography

EDC, N-(3-dimethylaminopropyl)-N-ethylcarbodiimide hydrochloride

DCl, deuterium chloride

AA, acetic acid

PA, perchloric acid

TMSD, trimethylsilyl diazomethane

G1P, glucose 1-phosphate

G6P, glucose 6-phosphate

F6P, fructose 6-phosphate

M6P, mannose 6-phosphate

M1P, mannose 1-phosphate

Gal1P, galactose 1-phosphate

Gal6P, galactose 6-phosphate

S1P, sorbose-1-phosphate

F16P2, fructose 1,6-bisphosphate

GA3P, glyceraldehyde-3-phosphate

23BPG, 2,3-bisphospho-D-glycerate

3PG, 3-phosphoglyceric acid

2PG, 2-phosphoglyceric acid

PEP, phospho(enol)pyruvic acid

Pyr, pyruvate

Lac, lactate

DHAP, glycerone phosphate

A6P, allose 6-phosphate

PRP, platelet-rich plasma

SIL, stable isotope labeled

U13C, uniformly 13C labeled

SWATH, Sequential Windowed Acquisition of All Theoretical Fragment Ion Mass Spectra

PGC, porous graphitic carbon

ER, extraction recovery

ME, matrix effect

1 Introduction

Sugar phosphates (SPx) are phosphorylated monosaccharides, which play important roles in various metabolic pathways. As central educts of most biosynthetic processes, sugars are converted into various metabolic precursors in the central carbon metabolism, including glycolysis pathway, pentose phosphate pathway (PPP), and tricarboxylic acid cycle (TCA). In the glycolysis pathway (shown in Figure 1, inspired by KEGG [1]), which is a universal cellular pathway for anaerobic energy production, glucose is converted into pyruvate with several SPx generated as intermediates. The flux through the glycolysis pathway is enhanced under hypoxia such as in various disease states [2,3]. Most cancer cells have increased glycolysis rates to cope with the higher energy demand, which is known as The Warburg Effect [4]. Similarly, stimulated platelets were reported to switch their energy metabolism to anaerobic glycolysis to meet their enhanced energy demand during activation [5,6]. This in turn upregulates the PPP to support platelet activation [6]. Platelets exhibit commendable

metabolic plasticity in switching between glycolysis and mitochondrial oxidative phosphorylation [7]. However, glycolysis is triggered upon stimulation with thrombin utilizing internal glucose reserves of that from extracellular source [8]. Currently we have focused on collagen (collagen related peptide-CRP) induced changes in metabolic status, since platelets encounter collagen upon vascular disintegration. To monitor this metabolic pathway of central physiologic importance, a comprehensive and robust method is required to quantify SPx in various bio-samples.

As phosphorylated metabolites, the analysis of SPx remains challenging due to their chemical instability, low abundance in many biological samples, high polarity, and rich negative charge. Thus, many efforts have been made to achieve efficient, sensitive, and accurate analysis. Traditionally, SPx were separated by capillary electrophoresis (CE) [9,10], gas chromatography (GC) [11], and liquid chromatography (LC) [12] followed by mass spectrometry (MS) detection. Among these hyphenated techniques, LC with tandem-MS establishes itself as the preferred approach due to its ease-of-use, robustness, sensitivity, and resolution [13]. The most widely used reversed phase (RP) LC-MS is not appropriate for SPx, as these metabolites are too polar to be retained on RP columns [14]. Hence, different approaches of LC-MS have been reported for SPx, including hydrophilic interaction chromatography (HILIC [15]), ion pairing (IP [16]), anion exchange chromatography (AEX [17,18]), and mixed-mode chromatography [19,20]. HILIC is suitable for highly polar compounds like SPx as it retains analytes by their hydrophilicity [21,22]. To ensure the best performance of HILIC, analytes are usually prepared in high-organic solutions, which compromises the solubility of SPx. It should be noted that for multiple phosphorylated SPx, e.g. Fructose-1,6-bisphosphate (F16P2), HILIC still cannot provide satisfying peak shape. In IP-based methods, ion pairing reagents were added to form ion pairs with analytes for better retention and peak shape. Recently, a method that combines IP and HILIC was reported to analyse SPx [23]. Although, retention and peak shape could be improved, contamination and ion suppression raised from ion pairing reagents are inevitable. Ion chromatography (IC) or ion exchange chromatography (IEX) employs ionic interaction for retention, which is suitable

for charged and polar analytes [24]. AEX was adopted for SPx for better peak shape [25]. When coupled to MS, IEX instrumental configuration is more complex as it requires membrane device (e.g. online suppressor) to remove concentrated buffer required in the eluent for efficient elution of analytes. To assist desolvation during the ESI process, post column addition of organic solvent should be considered as well.

Without chemical modification of phosphate groups, SPx is prone to strong adhesion to glassware and stainless steel. This property poses great challenges both for sample preparation and instrumental analysis with low recovery and carry-over effect. To overcome these issues, chemical derivatization was introduced for SPx analysis to gain better chromatographic and MS performance. Precolumn derivation by formation of phosphoramid(at)es with aniline, 3-aminomethyl pyridine and 3-amino-9-ethylcarbazole (AEC) were evaluated to modify SPx [26–28]. Derivatization of phosphate groups to phosphoramides usually involves activation with *N*-(3-dimethylaminopropyl)-N-ethylcarbodiimide hydrochloride (EDC) and requires relatively long reaction time, especially with aromatic amines, or high temperature [29]. O-Alkylation of phosphates with diazo compounds were also introduced for phosphate derivatization [30–32]. Diazo based methods have many advantages including fast reaction speed, ease to remove by-product (e.g., nitrogen), among others. For example, it was reported that 8-(diazomethyl) quinoline can efficiently label trehalose-6-phosphate and related sugar phosphates in plant tissues and the resultant derivatives exhibited improved chromatographic performance [33]. Recently, 2-(diazo-methyl)-*N*-methyl-*N*-phenyl-benzamide (2-DMBA) was reported to derivatize sugar phosphates. Better resolution of isomers with improved sensitivity was achieved in this method but multiple phosphorylated analytes were not included [34]. These derivatization schemes, however, face the problem of incomplete labelling which they have in common due to space resistance arising from sterically demanding labelling reagent. On the contrary, smaller alkyl labelling reagents, diazomethane and trimethylsilyldiazomethane, showed complete derivatization in the literature. However, due to their poor solubility in aqueous solutions, application for polar metabolites has not been explored yet.

In this study, we propose a method based upon phosphate methylation and LC-MS/MS for SPx analysis. As primary focus, SPx from the glycolysis pathway were studied herein for method development. To realize robust and accurate quantification, uniformly 13C-labeled metabolite extract and deuterated stable isotope methylated SPx were taken as internal standards and calibrants, respectively. As a result, the established method was applied for glycolysis SPx in different biological samples, including NIST SRM1950 plasma, cultured HeLa cells, and human platelets.

2 Materials and methods

2.1 Materials

Acetonitrile, methanol (MeOH) of Ultra LC-MS grade and zirconia / glass beads were purchased from Carl Roth (Karlsruhe, Germany). Methanol-d4, ammonium hydroxide solution (NH4OH, ~30% NH3), ammonium formate (NH4FA), hydrochloric acid (HCl, ACS reagent, 37%), hydrogen chloride solution (HCl, 3 M in methanol), deuterium chloride solution (DCl, 35 % in D2O), acetic acid (AA), perchloric acid (PA), and NIST SRM1950 plasma were supplied by Sigma–Aldrich (Taufkirchen, Germany). Trimethylsilyl diazomethane (TMSD, 2M in hexane) was obtained from Alfa Aesar (supplied by Thermo Fisher Co., Ltd, Kandel, Germany). Water (H2O) was purified by a Purelab Ultra purification system (ELGA LabWater, Celle, Germany).

2.2 SPx standards

α-D-glucose 1-phosphate disodium salt hydrate (G1P), D-glucose 6-phosphate sodium salt (G6P), D-fructose 6-phosphate disodium salt hydrate (F6P), D-mannose 6-phosphate disodium salt hydrate (M6P), α-D(+)-mannose 1-phosphate sodium salt hydrate (M1P), α-D-galactose 1-phosphate dipotassium salt pentahydrate (Gal1P), D-Galactose 6-phosphate lithium salt (Gal6P), L-sorbose-1-phosphate lithium salt (S1P), D-fructose 1,6-bisphosphate trisodium salt hydrate (F16P2), L-glyceraldehyde-3-phosphate solution (GA3P, 8-12 mg/ml in H2O), 2,3-bisphospho-D-glycerate (23BPG), D-(−)-3-phosphoglyceric acid disodium salt (3PG), D(+)-2-phosphoglyceric acid sodium salt hydrate (2PG), phospho(enol)pyruvic acid

monopotassium salt (PEP), sodium pyruvate (Pyr), and sodium L-lactate (Lac) were supplied by Sigma-Aldrich (Taufkirchen, Germany). Glycerone phosphate dilithium salt (dihydroxyacetone phosphate, DHAP) and allose 6-phosphate (A6P) were obtained from BioZol (Eching, Germany). SPx standards were dissolved and diluted with acetonitrile-water (50:50; v/v) to the desired concentrations. Uniformly 13C-labeled metabolite extract of around 2 x 10^9 *Pichia pastoris* cells (~ 15 mg, strain CBS 7435) was obtained from ISOtopic Solutions (Vienna, Austria). A stock solution of internal standards was prepared by resuspending this metabolite extract with 2.0 mL H2O. All standards and internal standard solutions were kept at -20 °C till use.

2.3 Preparation of cultured HeLa cells

The human cervical HeLa cells adapted to serum free conditions (AC free, ECACC 08011102) were grown in a humidified incubator at 37 °C with 5% CO2. Cells were cultured with EX-CELL HeLa serum free media (Sigma Aldrich) with 2 mM L-glutamine (Sigma Aldrich), 12 U/mL penicillin and 12 µg/mL streptomycin until a cell density of around 2 × 10^6 cells/mL was reached. Cell counting was performed in triplicate with a hemocytometer. Aliquots of 10^6 HeLa cells were transferred into 2 mL homogenization tubes and centrifuged for 5 min (100 g at 4°C). After removing the supernatant, cell pellets were washed twice with ice-cold Dulbecco's Phosphate Buffered Saline (Sigma Aldrich) with repeated centrifugation. Cell samples were snap frozen in liquid nitrogen and kept at -80°C till use.

2.4 Isolation and treatment of human platelets

Human platelet samples were isolated from acid-citrate-dextrose (ACD) anticoagulated (12.5 g sodium citrate, 6.82 g of citric acid, 10 g glucose, 500 mL distilled water, adjusted to pH 4.69 with NaOH) (1:4) blood of healthy volunteers free of cardiovascular risk factors and medications. Washed platelets were isolated as previously described [34–36] and aliquoted for treatments. Briefly blood was centrifuged at 190 g for 20 min without break or acceleration. Platelet-rich plasma (PRP) was collected from the upper 2/3 layer. PRP was diluted with Tyrodes-HEPES buffer (2.5 mM HEPES,150 mM NaCl,1 mM KCl, 2.5 mM NaHCO3, 0.36 mM

NaH2PO4, 5.5 mM glucose, 1 mg/mL BSA, pH 6.5) and centrifuged at 800 g for 10 min without break or acceleration. The platelet pellet thus obtained was suspended in PBS (pH 7.4) supplemented with CaCl2. Platelet count was estimated with Sysmex. Isolated platelets were either kept under resting condition or treated with CRP (5µg/mL; CambCol laboratories, Cambridge, UK) for 5 minutes at room temperature to activate them. Thereafter samples were snap frozen in liquid nitrogen and kept at -80 °C till further analysis. Blood collection and platelet isolation were carried out at the Dept. of Cardiology and Angiology, University Hospital Tübingen, in accordance to ethical guidelines and approved by regional authorities (number 237/ 2018BO2).

2.5 SPx extraction

The SPx extraction was performed as we reported previously for inositol phosphates with slight modifications [38]. Briefly, around 5 mg TiO2 was transferred into centrifuge filter units after consecutive washing with 300 µL cold H2O and cold 1 M PA solution. Samples were prepared in homogenization tubes (e.g., 10^6 HeLa cells or 50 µL human plasma). After adding 50 µL internal standard stock solution, 300 µL pre-chilled 1 M PA solution and 0.15 g zirconia / glass beads, samples were homogenized at 4°C for 10 cycles (10 s per cycle, 6800 rpm, pause 30s) with Precellys Evolution using Cryolys Evolution cooling unit with dry ice cooling (Bertin Technologies, France). The samples were spun down for 5 min (16000 g at 4°C). The supernatant was transferred into the centrifuge filter units with washed TiO2. After shaking for 15 min (1400 rpm at 4°C) followed by a centrifugation step (3500 g at 4°C for 1 min), the filtrate was discarded. The homogenization and loading steps were repeated once. For the washing step of the loaded TiO2 beads, 300 µL of cold 100 mM aqueous HCl solution was added. After shaking (1400 rpm at 4°C for 1 min) and centrifugation (3500 g at 4°C for 1 min), the filtrate was discarded. The washing step was repeated once. Two-hundred-microliter 10% (v/v) NH4OH solution was added for elution. After shaking (1400 rpm at 4°C for 5 min) and centrifugation (3500 g at 4°C for 1 min), the filtrate containing SPx was transferred into fresh tubes. After repeating the elution step once, the filtrates were combined. Samples and SPx standards at different concentrations were lyophilized respectively for methylation.

2.6 Differential isotope labeling methylation

Lyophilized samples and SPx standards were reconstituted with 1 mM HCl in MeOH (light label) and 1 mM DCl in MeOH-d4 (heavy label), respectively. Hundred-microliter of 2 M TMSD solution were added. The samples were allowed to stand for 10 min at R.T. after brief vortexing and fume releasing. The derivatization was quenched by addition of 5 µL glacial acetic acid. Samples were dried under N2 in an evaporator (Genevac EZ-2, for around 2 hours). After reconstitution with 50 µL MeOH/H2O (1:9, v/v), facilitated by vortexing and sonication, samples were ready for LC-MS analysis. For calibrant samples, the SPx standards and sample matrix were combined during sample reconstitution step.

2.7 UHPLC-ESI-QqQ-MS/MS analysis with SRM acquisition

Chromatographic separation was performed on a 1290 Infinity UHPLC system (Agilent Technologies, Santa Clara, CA, USA) with a Hypercarb porous graphitic carbon column (2.6 µm, 1.0 × 100 mm, Thermo Fisher Scientific) equipped with a KrudKatcher Ultra HPLC in-line filter (0.5 µm) (Phenomenex, Torrance, CA, USA). Mobile phase A and B were 10 mM ammonium formate in water and methanol, respectively. The gradient elution (0.0 min, 0% B; 1.0 min, 0% B; 10 min, 100% B; 13 min, 100% B; 13.1 min, 95% B; 18 min, 95% B; 18.1 min, 5% B; 24 min, 5% B) was carried out at a flow rate of 0.1 mL/min and a constant column temperature of 60°C. Injection volume was 5 µL. MS detection was conducted with the above chromatographic system hyphenated to a QTRAP4500 mass spectrometer with a Turbo V source (Sciex, Framingham, MA, USA) operated with the ESI probe in positive mode. Ion source parameters were as follows: curtain gas (N2) 30 psi, nebulizer gas (zero grade air) 30 psi; heater gas (zero grade air) 30 psi, ion source voltage +4500 V, and source temperature 500 °C. SRM transitions and compound dependent parameters for analytes, surrogate calibrants, and internal standards are summarized in Table 1. The peak widths were 0.2 – 0.3 min. The total cycle time was 800 ms, which ensures around 15 data points for all analytes.

2.8 Data processing

Analyst 1.7 with Analyst Device Driver was utilized for data acquisition and system control. PeakView 2.2 was used for manual data evaluation. MultiQuant 3.0 was employed for peak integration, linear regression, and concentration calculation. Statistical analysis and visualization were performed with R language.

3 Results and discussion

3.1 Methylation strategy for SPx

Comprehensive coverage and accurate quantification are ultimate goals in metabolomics, yet both difficult to achieve. Structural diversity, high polarity, multiple charges and existence of many isomeric metabolites are just some factors making corresponding method development in complex biological matrices challenging in analytical perspectives. HILIC coupled to tandem MS emerged as the standard method for general polar metabolome analysis. Unfortunately, many metabolites carry multiple ionizable groups such as phosphate and carboxyl groups, which may cause poor peak shape, low recovery, and instrumental carryover. While recent column technology with polymer deactivated surface technology (MaxPeak High Performance Surfaces, HPS) partly mitigated some of those problems [39,40], it still persists for multiply phosphorylated metabolites [20]. Moreover, such technology may not be available for all hardware used throughout an entire analytical workflow, including sample preparation. Chemical derivatization is an alternative approach to alleviate several of the problems (peak shape, in-source fragmentation, recovery) of metabolites with multiple negative charges such as SPx. Previously, we established several methods for such critical metabolites based on phosphate methylation [38,41,42]. Analytical performance was improved after methylation. To further extend the coverage, we propose herein that this promising strategy can be used for more polar phosphorylated metabolites such as SPx as well.

Conventionally, underivatized SPx are detected with ESI-MS in negative mode. In preliminary experiments, we tested the fragmentation of various glycolytic metabolites without

derivatization, including G6P, 23BPG, lactate, and pyruvate, without derivatization. As shown in Figure S1, two characteristic fragments (m/z 79 and 97) are found for hexose phosphates. Metabolites with carboxylic groups (pyruvate and lactate) generated small fragments after the neutral loss of the carboxylic acid moiety (as CO2). Carrying two phosphates and one carboxylic group, one fragment (m/z 167) was observed for 23BPG with neutral loss of phosphoric acid. Afterwards, the glycolytic SPx metabolites were subjected to MS2 analysis after methylation. As indicated in Figure S2, after methylation, two characteristic fragments were observed for all SPx (m/z 109 and m/z 127). Therefore, a targeted method could be conveniently constructed with these SRM transitions. However, several SPx including G1P, GA3P, DHAP, pyruvate, and lactate could not be detected after methylation. It was proposed that some small methylated (C3) SPx (except G1P) become volatile after methylation and are lost during evaporation step. G1P was further checked further as G6P and F6P could be detected in the MS analysis. Afterwards, the MS parameters were optimized by direct infusion of derivatized standards. We tested different methylation times to get optimal derivatization conditions. Optimization results (Figure S3) showed that the methylation occurs fast (within 5 min) and signal intensity started to decrease afterwards. Therefore, methylation for 10 min was chosen for further study.

After optimization of derivatization and the successful selection of SRM transitions for MS2 analysis, a differential stable isotope labeling (SIL) strategy was developed for matrix-matched surrogate calibration. Surrogate calibration was required due to lack of analyte-free matrix and to enable favorable matrix-matched calibration. To this end, another standard set which does not exist in real samples was generated. As illustrated in Figure 3, in this SIL set, methylation was conducted with MeOH-d4, DCl, and D2O in replacement of MeOH, HCl, and H2O respectively. To confirm the fragmentation of methylated SPx, 23BPG in these three sets were analyzed for MS2 spectra. As shown in Figure 2, apart from the two common fragments (m/z 109 and m/z 127) arising from methylated phosphate, 23BPG generates another most abundant fragment 211 after methylation. This fragmentation resulted from neutral loss of methylated phosphate group, which follows the similar fragmentation pattern prior methylation.

By comparing MS2 spectra of 23BPG in the three sets, precursors were observed at m/z value of 337, 340, and 347, which indicates that U13C-23BPG and SIL-23BPG have reasonable mass shifts of 3 Da and 10 Da. SIL-23BPG showed that there are two deuterium introduced with each SIL methylation. Comparison of fragments lead to the conclusion that fragments of m/z 127 and 109 only shifted by the SIL methylation while fragment of m/z 211 keeps the backbone of glycerate. Therefore, additionally, another two sets of unique SRM transitions could be obtained also from U13C labeled yeast extract and SIL methylation, which makes the choice more flexible. Ideally, IS should be spiked before the sample preparation to compensate for sample loss and matrix effect. SIL-SPx could only be spiked before injection. Therefore, U13C metabolic extract was taken as IS while SIL-SPx was taken as surrogate calibrant.

3.2 LC analysis of methylated SPx

Underivatized phosphorylated metabolites such as SPx give usually bad peak shape in liquid chromatography due to strong adsorption of column hardware and surfaces of the flow path driven by the multiple negative charges of the compounds. Instrumental carryover is significant as well for this reason. Methylation of phosphate groups were reported to have favorable effects on peak shapes reducing tailing and increasing retention in RP-LC. Inspired by our previous method for inositol phosphates [38], preliminary experiments on LC method development started with a cholesterol-bonded column (Cosmocore 2.6Cholester, 2.6 µm core shell particle column). ACN and MeOH were tested as organic modifiers in this RP-type separation, during which MeOH exhibited better separation for the constitutional isomers 2PG and 3PG. According to the number of phosphate and carboxylate groups, retention times of SPx increased from sugar monophosphate, 2PG/3PG, F16P2, 23BPG, to PEP. This was expected as both phosphate and carboxylate groups of SPx can be methylated and lead to hydrophobicity increase. The methylated SPx showed improved peak shapes and enhanced sensitivity compared to conventional methods without derivatization (not shown). However, several issues emerged during this preliminary experiment of RPLC-MS analysis, which were addressed in the further method development.

There was little selectivity for hexose monophosphates such as F6P and G6P. As shown in Figure S4, G6P and F6P had both retention time close to dead time (t0), which indicates insufficient retention on the Cholester phase. Sugar monophosphates remain too polar to be sufficiently retained on RP column even after phosphate methylation. Additionally, G1P could not be detected by LC-MS after methylation. Then we organized several more SPx with phosphate group at 1' position. Results indicate that only SPx with phosphate at position 6 could be detected by this method. So, we supposed that when the 1' position is blocked by a phosphate group, the methylation reaction becomes more difficult, which leads to much lower sensitivity compared to SPx with 6' position. This difference makes our method more selective to SPx with 6' phosphate while it is below LODs for SPx with 1' phosphates. Furthermore, more chromatographic resolution between 23BPG and PEP is desirable due to interference arising from in-source fragmentation of 23BPG. By measurements of single standards of 23BPG and PEP (Figure S5), it was observed that the in-source fragment of 23BPG (m/z 337 → 211) overlaps with PEP (m/z 211 → 109). The last problematic issue of the Cholester-RP method was inter-conversion between 2PG and 3PG during methylation. When 2PG and 3PG were analyzed by LC-MS, they showed close but distinct retention times. However, the signal representing 3PG was also observed in the single standard of 2PG, which could have resulted from standard impurity or conversion during methylation.

Next, the derivatized standard mixture of SPx were analyzed with untargeted sequential windowed acquisition of all theoretical fragment ion mass spectra (SWATH) method (Suppl. Table S1) to get comprehensive data. In the SWATH data, we checked 2/3 PG with different numbers of methylation (phosphate, carboxylate, and hydroxyl groups). Results in Figure S6 showed that both full-methylation (methylated phosphate and carboxylate groups) and per-methylation (methylated phosphate, carboxylate, and hydroxyl group) were observed. It was a matter of course that per–methylated 2/3-PG has better retention than full–methylated 2/3-PG and thereby better separation in the RPLC-MS method. But interestingly, elution order of 2/3-PG switched for the per–methylated forms as compared to the full–methylated forms. The signal of the other 2/3-PG constitutional isomer was negligible in the chromatogram of the

respective other form after per–methylation, which indicates that the signal of 3PG in the 2PG standard comes from inter–conversion during methylation rather than an impurity in the standard. Once the hydroxyl of 2/3-PG is methylated, phosphate group transfer cannot occur anymore. Therefore, the derivatization was optimized for per-methylation of 2/3-PG and per–methylated 2/3 PG were chosen for the further study.

The LC method development was therefore continued with column screening experiments for achieving better retention of sugar monophosphates and better resolution between 23BPG and PEP. Different columns were tested for methylated SPx, including C30, chiral polysaccharide, and porous graphitic carbon (PGC) columns. The C30 RP column was tested for its perceived better retention of methylated sugar monophosphates owing to the increased hydrophobicity of this stationary phase. MeOH and ACN were tested as organic modifiers with the same gradient starting with low organic condition (5% B). As shown in Figure S7, there was little selectivity between G6P and F6P. Moreover, as reported for sugars SPx with free semiacetalic hydroxyl in position 1 show double peaks in C30 RP-LC due to the presence of anomers with distinct retention. In contrast, if this C1-hydroxyl is phosphorylated anomerization cannot occur anymore, and a single peak is observed. In our experiment, G6P showed double peaks, which is detrimental in this method. Chiral polysaccharide columns were tested due to their multiple interaction sites and favorable selectivity for isomeric species. Unfortunately, the tests with the chiral columns were not successful as summarized in Figure S8 – S9. Although some analytes had decent retention and showed symmetric peaks, most targeted SPx showed unsatisfactory peak shapes on the polysaccharide columns. Furthermore, retention of sugar monophosphates was not improved significantly. Meanwhile, 23BPG was not separated from PEP.

Finally, a PGC column was evaluated. It was reported to have better retention for polar compounds even under highly aqueous conditions [14]. In our screening experiments, PGC showed improved retention of methylated SPx and was chosen for further method development. To further check specificity of this method, more isobaric sugar monophosphates were organized and tested. Results are summarized in Figure S10. There

was no signal obtained in derivatization blanks at retention times of SPx. As mentioned previously, sugar 1' phosphates were not detected in our method (tested with concentrations at 2 x upper limit of quantifications, 2 µg/mL), which contributes to assay selectivity to some extent. Sugar 6' phosphates eluted close to each other. G6P, M6P, and F6P were separated in part by the employed screening gradient. Gal6P showed double peaks and eluted later than the above three SPx. A6P showed extremely bad peak shape and wide retention time range overlapping all SPx tested. Since allose is a rare monosaccharide in the leaves of the African shrub Protea rubropilosa, the risk of interference of A6P is low; it should not be present in the human samples of interest in our research. However, potential interference from diet should be considered when sugar monophosphates in real samples are analyzed with this method. The three critical sugar monophosphates (F6P, M6P, and G6P) as well as other SPx were taken for further optimization by column head focusing approach. One hundred % aqueous was held for 1 min, 2 min, and 3 min followed by identical gradient as before. Results of sugar monophosphates are shown in Figure S11. With increased holding time, the retention and selectivity between G6P and F6P were improved. However, M6P shifted to double peaks and gradually coeluted with G6P. Most importantly, there was little isomer selectivity when tested with a mixture. Additionally, better response and peak shape were observed from holding time of 1 min (shown in Figure S12). Eventually, the signal was taken to represent the sum of F6P, M6P, and G6P in this method which has therefore left some room for further improvements. The gradient started with 1 min holding at 100% aqueous to make analytes focused at the column head when the method starts. After optimization of LC conditions, the final method was established with PGC column. Representative chromatograms are shown in Figure 4. Symmetric peak shapes were achieved in typical RP-LC conditions. Adequate separation of critical peak pairs including 3PG / 2PG, and 23BPG / PEP was achieved. Interestingly, as shown in Figure 4F, similar to reports for SIL analogs in RP-LC, deuterated species elute earlier than 13C labeled– and original species. It is appropriate to have U13C - SPx as internal standards, as matrix effect in LC-MS analysis is retention time specific.

3.3 **Method evaluation and validation**

For a successful application to biological samples, another critical step of the entire workflow of SPx analysis is their efficient extraction, which is problematic as well. Due to their phosphate moiety and possible carboxyl groups, SPx are prone to bind to proteins in biological samples, which makes their extraction challenging. Strong acid-based liquid extraction methods, based on strong acids like HCl and PA, were reported to show decent extraction recovery (ER) for phosphorylated metabolites. As reported above, when extracted with HCl containing solvent mixture, there is a risk of hydrolysis and phosphate migration. Therefore, a weaker acid like acetic acid was proposed to improve extraction performance. Due to selective affinity of the phosphate group, metal oxide-based affinity chromatography (MOAC) has been successfully utilized to extract phosphopeptides, phosphoproteins and phosphorylated metabolites [43]. Recently, we developed an extraction kit consisting of centrifuge filter and TiO2 for analysis of inositol phosphates [38]. It combines PA based protein precipitation, MOAC extraction, and particle removal. After introducing washing steps with diluted HCl solution, this extraction kit was compatible with further phosphate methylation. Taking this knowledge, this extraction protocol was tested for SPx in plasma in this study. As shown in Table S2, ERs of SPx from 30% to 78% were achieved. The ER of SPx increases with the number of phosphate and carboxylate groups, which arises from increased affinity with more negatively charged groups. Internal standards are necessary in MS–based methods to compensate not only for sample loss during sample preparation, but also for the matrix effect (ME) during ionization. ME can result from coextracted and coeluted endogenous compounds. Commonly chosen internal standards include structurally similar analogs and stable isotope labeled (SIL) analogs. Ideally, SIL compounds should be used as they share closest chemical and physical properties to analytes, thereby undergoing the same extraction efficiency, chromatographic process and can compensate for MEs. When it comes to SIL internal analogs, 13C-labeled ones were reported to have closer retention time compared to deuterated ones, which was confirmed on PGC column as well. ME was evaluated for the target analytes using strategies reported before [44]. ME without internal standards were obtained by comparing

the response of internal standards in plasma matrix (post-extraction spiked) and that in solution. As shown in Table S3, ion suppression and ion enhancement were not significant even without internal standards. With compensation by 13C-labelled internal standards (from U13C-labelled cell extract), slightly improved ME was obtained (Table S4). In this study, internal standards had mainly the effect to correct variations from the sample preparation process. Method evaluation and validation, including accuracy, precision, linearity, and limit of quantification (LOQ), was carried out according to the FDA guideline with some modifications. As described before, SIL–SPx were taken as surrogate calibrants. Calibration series were constructed with pre-spiked U13C-labeled yeast extract in plasma followed by combination of different concentration levels of SIL–SPx before injection. As shown in Table 2 and Figure S13, good linearity was obtained over the tested concentration ranges. LOQ (on column) from 0.25 pmol to 0.54 pmol was achieved. Calibrants were analyzed in three batches for intra-batch and inter-batch accuracy and precision testing. As shown in Table S5 – S6, this method was proven to be accurate and reliable for SPx quantification in biological samples, with improved performance.

3.4 **Application to biological samples**

After method establishment and validation with human plasma, we applied this method to profile SPx in different biological samples, including NIST SRM1950 plasma, cultured HeLa cells, and human platelet samples. The quantification results in NIST plasma and cultured HeLa cells are summarized in Table S7. NIST plasma and HeLa exhibited distinct SPx profiles (representative chromatograms in Figure S14 for NIST plasma and Figure S15 for HeLa). These results indicate that this established method is suitable for quantitative analysis of SPx from the glycolysis pathway in biological samples. To further explore the performance of this method in a biological scenario, a pilot study on alteration of glycolytic pathway during platelet activation was conducted. Platelets from healthy donors were collected and aliquoted for treatment. CRP was used to activate the platelets and this experimental set was compared to resting platelets. Results are shown in Figure 5. Compared to the resting group (control), most SPx in glycolysis pathway got significantly upregulated in the CRP group, which indicates

increased glycolysis activity during platelet activation. It is in line with the reports before that platelets use the glycolysis pathway to generate adenosine 5'-triphosphate (ATP) to support its activation [6]. These results confirm that this method can be used in research exploring glycolysis and that it can provide reliable results on the SPx profile.

4 Conclusions

The accurate quantitative analysis of SPx with LC–MS remains challenging due to their high polarity and rich negative charge. In this study, the strategy of phosphate methylation was applied to improve the performance of the analysis of sugar phosphates from the glycolysis pathway. A LC–MS/MS method was established on a PGC column with better chromatographic performance than on other evaluated (C30, cholesteryl-bonded, chiral) columns. U13C-labeled yeast extract from *Pichia pastoris* and deutero-SIL methylated SPx were taken for internal standards and calibrants respectively. A TiO2–based extraction kit was used for the efficient extraction from biological samples. The established workflow was validated in human plasma. To further demonstrate the potential of this method, we used it to profile SPx in cultured HeLa cells, as model for platelets with limited availability for method development. In a pilot study, SPx of the glycolysis pathway were observed to be significantly upregulated in CRP-activated human platelets. These results demonstrate that this method can be used for monitoring glycolysis pathway. It holds the potential to facilitate our understanding of the role and alterations of the glycolytic pathway under different pathophysiological conditions.

Declaration of conflict of interests

The authors declare no conflict of interests.

Acknowledgements

P.L. gratefully acknowledges the support from the China Scholarship Council (grant number 201807060010). M.L. acknowledges the support by the German Research Foundation (DFG, Deutsche Forschungsgemeinschaft), project number 374031971-TRR 240.

References

[1] H. Ogata, S. Goto, K. Sato, W. Fujibuchi, H. Bono, M. Kanehisa, KEGG: Kyoto encyclopedia of genes and genomes, Nucleic Acids Res. 27 (1999) 29–34. https://doi.org/10.1093/nar/27.1.29.

[2] S. Ganapathy-Kanniappan, J.F.H. Geschwind, Tumor glycolysis as a target for cancer therapy: Progress and prospects, Mol. Cancer. 12 (2013) 1–11. https://doi.org/10.1186/1476-4598-12-152.

[3] H. Pelicano, D.S. Martin, R.H. Xu, P. Huang, Glycolysis inhibition for anticancer treatment, Oncogene. 25 (2006) 4633–4646. https://doi.org/10.1038/sj.onc.1209597.

[4] M. Lopez-Lazaro, The Warburg Effect: Why and How Do Cancer Cells Activate Glycolysis in the Presence of Oxygen?, Anticancer. Agents Med. Chem. 8 (2008) 305–312. https://doi.org/10.2174/187152008783961932.

[5] M. Aibibula, K.M. Naseem, R.G. Sturmey, Glucose metabolism and metabolic flexibility in blood platelets, J. Thromb. Haemost. 16 (2018) 2300–2314. https://doi.org/10.1111/jth.14274.

[6] P.P. Kulkarni, A. Tiwari, N. Singh, D. Gautam, V.K. Sonkar, V. Agarwal, D. Dash, Aerobic glycolysis fuels platelet activation: Small-molecule modulators of platelet metabolism as anti-thrombotic agents, Haematologica. 104 (2019) 806–818. https://doi.org/10.3324/haematol.2018.205724.

[7] M. Chatterjee, Platelet lipidome: Dismantling the “Trojan horse” in the bloodstream, J. Thromb. Haemost. 18 (2020) 543–557. https://doi.org/10.1111/jth.14721.

[8] M. Aibibula, K.M. Naseem, R.G. Sturmey, Glucose metabolism and metabolic flexibility in blood platelets, J. Thromb. Haemost. 16 (2018) 2300–2314. https://doi.org/10.1111/jth.14274.

[9] J.P.M. Hui, J. Yang, J.S. Thorson, E.C. Soo, Selective detection of sugar phosphates by capillary electrophoresis/mass spectrometry and its application to an engineered E. coli host, ChemBioChem. 8 (2007) 1180–1188. https://doi.org/10.1002/cbic.200700116.

[10] T. Soga, K. Igarashi, C. Ito, K. Mizobuchi, H.P. Zimmermann, M. Tomita, Metabolomic profiling of anionic metabolites by capillary electrophoresis mass spectrometry, Anal. Chem. 81 (2009) 6165–6174. https://doi.org/10.1021/ac900675k.

[11] D.B. Chu, C. Troyer, T. Mairinger, K. Ortmayr, S. Neubauer, G. Koellensperger, S. Hann, Isotopologue analysis of sugar phosphates in yeast cell extracts by gas chromatography chemical ionization time-of-flight mass spectrometry, Anal. Bioanal. Chem. 407 (2015) 2865–2875. https://doi.org/10.1007/s00216-015-8521-9.

[12] P. Vizán, G. Alcarraz-Vizán, S. Díaz-Moralli, J.C. Rodríguez-Prados, M. Zanuy, J.J. Centelles, O. Jáuregui, M. Cascante, Quantification of intracellular phosphorylated carbohydrates in HT29 human colon adenocarcinoma cell line using liquid chromatography-electrospray ionization tandem mass spectrometry, Anal. Chem. 79 (2007) 5000–5005. https://doi.org/10.1021/ac070170v.

[13] J.M. Buescher, S. Moco, U. Sauer, N. Zamboni, Ultrahigh performance liquid chromatography-tandem mass spectrometry method for fast and robust quantification of anionic and aromatic metabolites, Anal. Chem. 82 (2010) 4403–4412. https://doi.org/10.1021/ac100101d.

[14] C. Antonio, T. Larson, A. Gilday, I. Graham, E. Bergström, J. Thomas-Oates, Quantification of sugars and sugar phosphates in Arabidopsis thaliana tissues using porous graphitic carbon liquid chromatography-electrospray ionization mass spectrometry, J. Chromatogr. A. 1172 (2007) 170–178. https://doi.org/https://doi.org/10.1016/j.chroma.2007.10.011.

[15] E. Iturrospe, K.M. Da Silva, B. Talavera Andújar, M. Cuykx, J. Boeckmans, T. Vanhaecke, A. Covaci, A.L.N. van Nuijs, An exploratory approach for an oriented development of an untargeted hydrophilic interaction liquid chromatography-mass spectrometry platform for polar metabolites in biological matrices, J. Chromatogr. A. 1637 (2021) 461807. https://doi.org/10.1016/j.chroma.2020.461807.

[16] D. McCloskey, J.A. Gangoiti, B.O. Palsson, A.M. Feist, A pH and solvent optimized reverse-phase ion-paring-LC–MS/MS method that leverages multiple scan-types for

targeted absolute quantification of intracellular metabolites, Metabolomics. 11 (2015) 1338–1350. https://doi.org/10.1007/s11306-015-0790-y.

[17] M. Schwaiger, E. Rampler, G. Hermann, W. Miklos, W. Berger, G. Koellensperger, Anion-Exchange Chromatography Coupled to High-Resolution Mass Spectrometry: A Powerful Tool for Merging Targeted and Non-targeted Metabolomics, Anal. Chem. 89 (2017) 7667–7674. https://doi.org/10.1021/acs.analchem.7b01624.

[18] D.B. Chu, K. Klavins, G. Koellensperger, S. Hann, Speciation analysis of sugar phosphates via anion exchange chromatography combined with inductively coupled plasma dynamic reaction cell mass spectrometry-optimization for the analysis of yeast cell extracts, J. Anal. At. Spectrom. 29 (2014) 915–925. https://doi.org/10.1039/c4ja00043a.

[19] H. Hinterwirth, M. Lämmerhofer, B. Preinerstorfer, A. Gargano, R. Reischl, W. Bicker, O. Trapp, L. Brecker, W. Lindner, Selectivity issues in targeted metabolomics: Separation of phosphorylated carbohydrate isomers by mixed-mode hydrophilic interaction/weak anion exchange chromatography, J. Sep. Sci. 33 (2010) 3273–3282. https://doi.org/10.1002/jssc.201000412.

[20] K.M. Smith, I.D. Wilson, P.D. Rainville, Sensitive and Reproducible Mass Spectrometry-Compatible RP-UHPLC Analysis of Tricarboxylic Acid Cycle and Related Metabolites in Biological Fluids: Application to Human Urine, Anal. Chem. 93 (2021) 1009–1015. https://doi.org/10.1021/acs.analchem.0c03863.

[21] P. Hemström, K. Irgum, Hydrophilic interaction chromatography, J. Sep. Sci. 29 (2006) 1784–1821. https://doi.org/10.1002/jssc.200600199.

[22] P. Jandera, P. Janás, Recent advances in stationary phases and understanding of retention in hydrophilic interaction chromatography. A review, Anal. Chim. Acta. 967 (2017) 12–32. https://doi.org/10.1016/j.aca.2017.01.060.

[23] C. Mathon, G.A. Barding, C.K. Larive, G.A. Barding Jr., C.K. Larive, Separation of ten phosphorylated mono-and disaccharides using HILIC and ion-pairing interactions, Anal. Chim. Acta. 972 (2017) 102–110. https://doi.org/10.1016/j.aca.2017.03.029.

[24] J. Walsby-Tickle, J. Gannon, I. Hvinden, C. Bardella, M.I. Abboud, A. Nazeer, D. Hauton, E. Pires, T. Cadoux-Hudson, C.J. Schofield, J.S.O. McCullagh, Anion-exchange chromatography mass spectrometry provides extensive coverage of primary metabolic pathways revealing altered metabolism in IDH1 mutant cells, Commun. Biol. 3 (2020) 1–12. https://doi.org/10.1038/s42003-020-0957-6.

[25] J. Wang, T.T. Christison, K. Misuno, L. Lopez, A.F. Huhmer, Y. Huang, S. Hu, Metabolomic Profiling of Anionic Metabolites in Head and Neck Cancer Cells by Capillary Ion Chromatography with Orbitrap Mass Spectrometry, Anal. Chem. 86 (2014) 5116–5124. https://doi.org/10.1021/ac500951v.

[26] W.-C. Yang, M. Sedlak, F.E. Regnier, N. Mosier, N. Ho, J. Adamec, Simultaneous Quantification of Metabolites Involved in Central Carbon and Energy Metabolism Using Reversed-Phase Liquid Chromatography−Mass Spectrometry and in Vitro 13C Labeling, Anal. Chem. 80 (2008) 9508–9516. https://doi.org/10.1021/ac801693c.

[27] J. Han, V. Tschernutter, J. Yang, T. Eckle, C.H. Borchers, Analysis of Selected Sugars and Sugar Phosphates in Mouse Heart Tissue by Reductive Amination and Liquid Chromatography-Electrospray Ionization Mass Spectrometry, Anal. Chem. 85 (2013) 5965–5973. https://doi.org/10.1021/ac400769g.

[28] N. Sheng, H. Zhao, X. Chen, D. Wang, M. Li, Z. Wang, J. Zhang, J. Jiang, A novel derivatization strategy for profiling phosphate ester/anhydride metabolic network and application on glioma rats using HILIC-MS/MS, Talanta. 228 (2021) 122238. https://doi.org/10.1016/j.talanta.2021.122238.

[29] H. Zeng, C.B. Qi, T. Liu, H.M. Xiao, Q.Y. Cheng, H.P. Jiang, B.F. Yuan, Y.Q. Feng, Formation and Determination of Endogenous Methylated Nucleotides in Mammals by Chemical Labeling Coupled with Mass Spectrometry Analysis, Anal. Chem. 89 (2017) 4153–4160. https://doi.org/10.1021/acs.analchem.7b00052.

[30] J. Clark, K.E. Anderson, V. Juvin, T.S. Smith, F. Karpe, M.J.O. Wakelam, L.R. Stephens, P.T. Hawkins, Quantification of PtdInsP3 molecular species in cells and tissues by mass spectrometry, Nat. Methods. 8 (2011) 267–272.

https://doi.org/10.1038/nmeth.1564.

[31] F. Wei, X. Wang, H. fang Ma, X. Lv, X. yan Dong, H. Chen, Rapid profiling and quantification of phospholipid molecular species in human plasma based on chemical derivatization coupled with electrospray ionization tandem mass spectrometry, Anal. Chim. Acta. 1024 (2018) 101–111. https://doi.org/10.1016/j.aca.2018.04.012.

[32] J.C. Lee, S.K. Byeon, M.H. Moon, Relative Quantification of Phospholipids Based on Isotope-Labeled Methylation by Nanoflow Ultrahigh Performance Liquid Chromatography-Tandem Mass Spectrometry: Enhancement in Cardiolipin Profiling, Anal. Chem. 89 (2017) 4969–4977. https://doi.org/10.1021/acs.analchem.7b00297.

[33] X.T. Luo, B.D. Cai, H.P. Jiang, H.M. Xiao, B.F. Yuan, Y.Q. Feng, Sensitive analysis of trehalose-6-phosphate and related sugar phosphates in plant tissues by chemical derivatization combined with hydrophilic interaction liquid chromatography–tandem mass spectrometry, J. Chromatogr. A. 1592 (2019) 82–90. https://doi.org/10.1016/j.chroma.2019.01.040.

[34] S. Li, F. Liu, Z. Zhang, X. Yin, T. Ye, F. Yuan, Y. Feng, I. Biology, B.-F. Yuan, Y. Feng, Ultrasensitive Determination of Sugar Phosphates in Trace Samples by Stable Isotope Chemical Labeling Combined with RPLC–MS, Anal. Chem. (2022) 1–21. https://doi.org/10.1021/acs.analchem.2c00346.

[35] M. Chatterjee, D. Rath, J. Schlotterbeck, J. Rheinlaender, B. Walker-Allgaier, N. Alnaggar, M. Zdanyte, I. Muller, O. Borst, T. Geisler, T.E. Schaffer, M. Lammerhofer, M. Gawaz, Regulation of oxidized platelet lipidome: implications for coronary artery disease, Eur Hear. J. 38 (2017) 1993–2005. https://doi.org/10.1093/eurheartj/ehx146.

[36] T. Harm, A. Bild, K. Dittrich, A. Goldschmied, J. Nestele, M. Chatterjee, X. Fu, K. Kolb, T. Castor, O. Borst, T. Geisler, D. Rath, M. LäMmerhofer, M. Gawaz, Acute coronary syndrome is associated with a substantial change in the platelet lipidome, Cardiovasc. Res. (2021). https://doi.org/10.1093/cvr/cvab238.

[37] M. Cebo, C. Calderón Castro, J. Schlotterbeck, M. Gawaz, M. Chatterjee, M. Lämmerhofer, Untargeted UHPLC-ESI-QTOF-MS/MS analysis with targeted feature

649 extraction at precursor and fragment level for profiling of the platelet lipidome with ex
650 vivo thrombin-activation, J. Pharm. Biomed. Anal. 205 (2021) 114301.
651 https://doi.org/10.1016/j.jpba.2021.114301.
652 [38] P. Li, M. Gawaz, M. Chatterjee, M. Lämmerhofer, Isomer-selective analysis of inositol
653 phosphates with differential isotope labelling by phosphate methylation using liquid
654 chromatography with tandem mass spectrometry, Anal. Chim. Acta. 1191 (2022)
655 339286. https://doi.org/10.1016/j.aca.2021.339286.
656 [39] M. Lauber, T.H. Walter, M. Gilar, M. Delano, C. Boissel, K. Smith, R. Birdsall, P.
657 Rainville, J. Belanger, K. Wyndham, H. Separations, O.F.M. Analytes, [WHITE PAPER
658] Low Adsorption HPLC Columns Based on MaxPeak High Performance Surfaces [
659 WHITE PAPER], (n.d.) 1–7.
660 [40] D.G. Thelen, J.A. Martin, J.D. Roth, Patent Application Publication: US 2019 / 0125831
661 A1, 2019.
662 [41] P. Li, M. Gawaz, M. Chatterjee, M. Lämmerhofer, Targeted Profiling of Short-, Medium-
663 , and Long-Chain Fatty Acyl-Coenzyme As in Biological Samples by Phosphate
664 Methylation Coupled to Liquid Chromatography-Tandem Mass Spectrometry, Anal.
665 Chem. 93 (2021) 4342–4350. https://doi.org/10.1021/acs.analchem.1c00664.
666 [42] P. Li, M. Lämmerhofer, Isomer Selective Comprehensive Lipidomics Analysis of
667 Phosphoinositides in Biological Samples by Liquid Chromatography with Data
668 Independent Acquisition Tandem Mass Spectrometry, Anal. Chem. 93 (2021) 9583–
669 9592. https://doi.org/10.1021/acs.analchem.1c01751.
670 [43] L. Si-Hung, C. Troyer, T. Causon, S. Hann, Sensitive quantitative analysis of
671 phosphorylated primary metabolites using selective metal oxide enrichment and GC-
672 and IC- MS/MS, Talanta. 205 (2019) 120147.
673 https://doi.org/10.1016/j.talanta.2019.120147.
674 [44] B.K. Matuszewski, M.L. Constanzer, C.M. Chavez-Eng, Strategies for the assessment
675 of matrix effect in quantitative bioanalytical methods based on HPLC-MS/MS, Anal.
676 Chem. 75 (2003) 3019–3030. https://doi.org/10.1021/ac020361s.

677 **Tables with captions**

678 **Table 1:** SRM transitions with MS parameters (dt, dwell time; DP, declustering potential; EP,
679 entrance potential; CE, collision energy; CXP, collision cell exit potential).

SPx	Q1	Q3	dt	DP, V	EP, V	CE, V	CXP, V
F6P/M6P/G6P-1	289.1	127	30	80	10	20	10
F6P/M6P/G6P-2	289.1	109	30	80	10	25	10
F16P2-1	397.1	109	30	70	10	30	15
F16P2-2	397.1	127	30	70	10	20	15
23BPG-1	337.0	211	30	70	10	18	10
23BPG-2	337.0	127	30	70	10	40	10
3PG/2PG-1	243.1	109	30	60	10	38	10
3PG/2PG-2	243.1	127	30	60	10	15	10
PEP-1	211.0	109	30	60	10	30	10
PEP-2	211.0	127	30	60	10	25	10
U13C-F6P/M6P/G6P-1	295.1	127	30	80	10	20	10
U13C-F6P/M6P/G6P-2	295.1	109	30	80	10	25	10
U13C-F16P2	403.1	127	30	70	10	20	15
U13C-23BPG	340.0	214	30	70	10	18	10
U13C-3PG/2PG	246.1	127	30	60	10	15	10
U13C-PEP	214.0	109	30	60	10	30	10
SIL-F6P/M6P/G6P-1	293.1	131	30	80	10	25	10
SIL-F6P/M6P/G6P-2	293.1	113	30	80	10	20	10
SIL-F16P2	405.1	131	30	70	10	20	15
SIL-23BPG	347.1	217	30	70	10	18	10
SIL-3PG/2PG	251.1	131	30	60	10	15	10
SIL-PEP	217.1	113	30	60	10	30	10

680

681 **Table 2:** Calibration curves of SPx in this method (plasma as matrix).

SPx	range, ng/mL	linear equation	r	LOQ on column, pmol
F6P/M6P/G6P	20 - 1000	y = 0.00088673x + 0.011223	0.9987	0.33
F16P2	20 - 1000	y = 0.0016019x - 0.007057	0.9958	0.25
3PG	10 - 500	y = 0.0022836x + 0.019088	0.9889	0.43
2PG	10 - 500	y = 0.0050257x + 0.057711	0.9956	0.54
23BPG	10 - 500	y = 0.0144496x + 0.095651	0.9978	0.27
PEP	10 - 500	y = 0.0015483x + 0.011082	0.9972	0.49

682

Figures with captions

Figure 1: Sugar phosphates and related metabolites in glycolysis pathway (inspired by KEGG [1]). As part of central carbon metabolism, glycolysis pathway provides precursors for most biosynthesis processes.

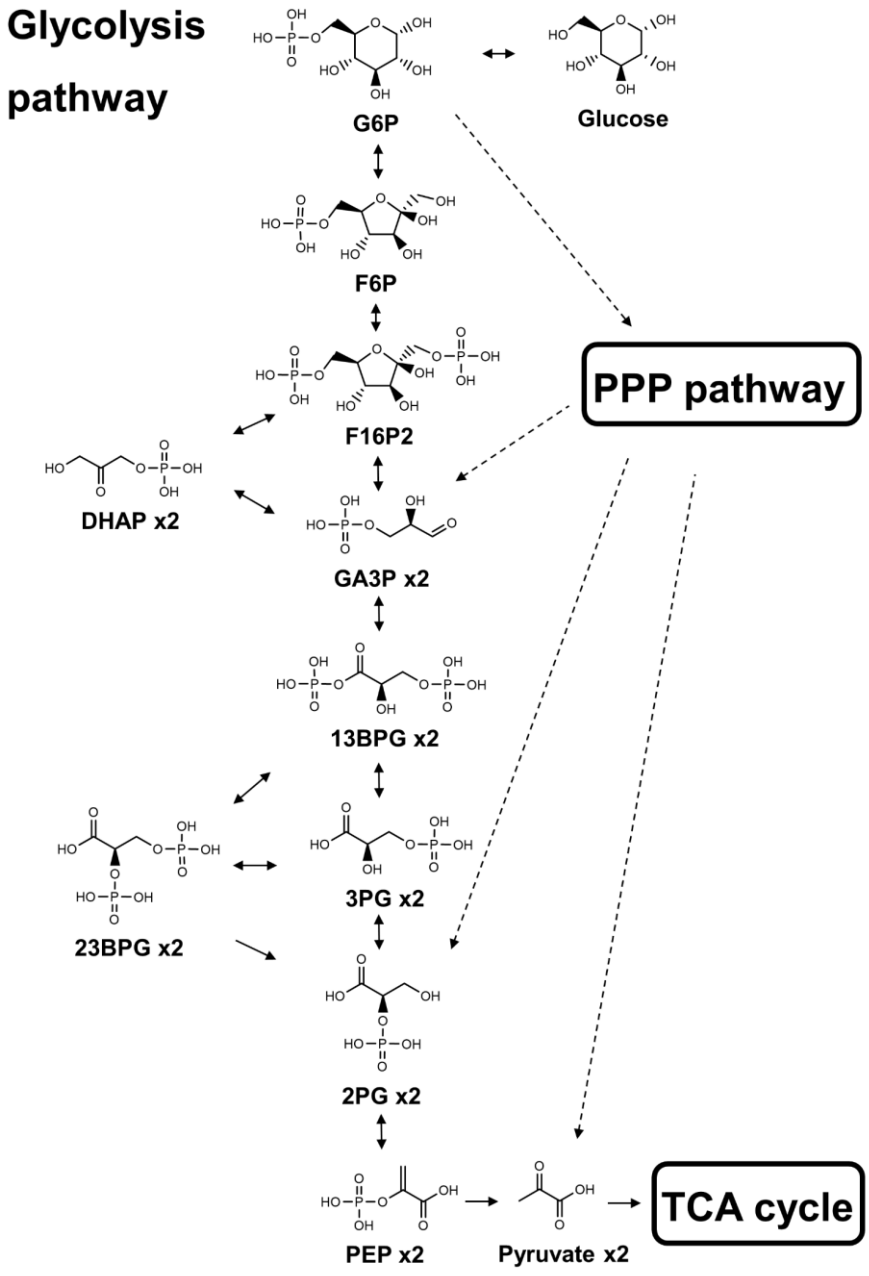

Figure 2: Product ion spectra of 23BPG in three sets: (A) methylated 23BPG; (B) methylated uniformly 13C-labeled 23BPG; (C) Stable isotope labeled deutero-methylated 23BPG. MS2 spectra of analytes in three sets improved confidence of fragmentation elucidation, SRM transition construction and identification in real samples.

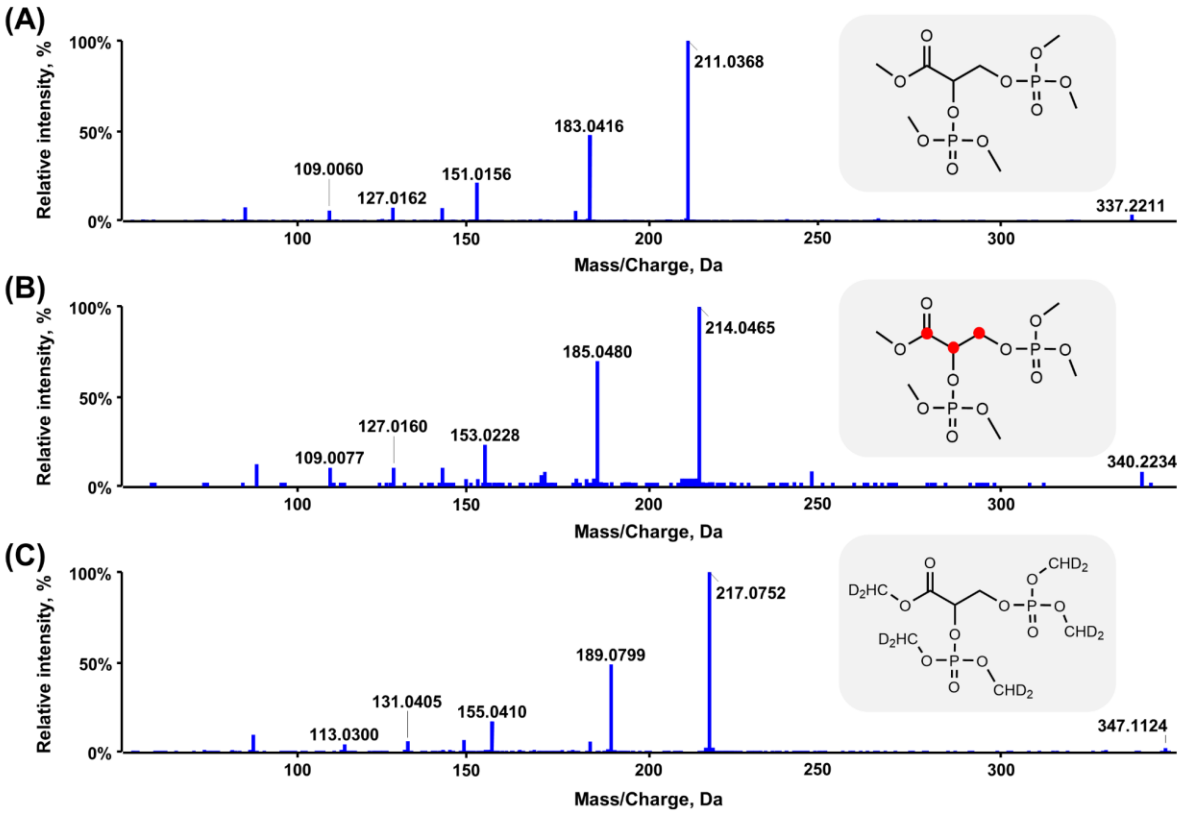

Figure 3: Summary of standard design including analytes, internal standards, and surrogate calibrants. (A) The phosphate methylation of sugar phosphates by trimethylsilyl diazomethane under acidic condition. Hydrogen was colored to show different contributors, which is the base for differential stable isotope labeling methylation in (B). Pre-spiked internal standards (uniformly 13C labeled sugar phosphates) and analytes were lightly methylated (colored in gray) while standards were heavily methylated (colored in red) as surrogate calibrants.

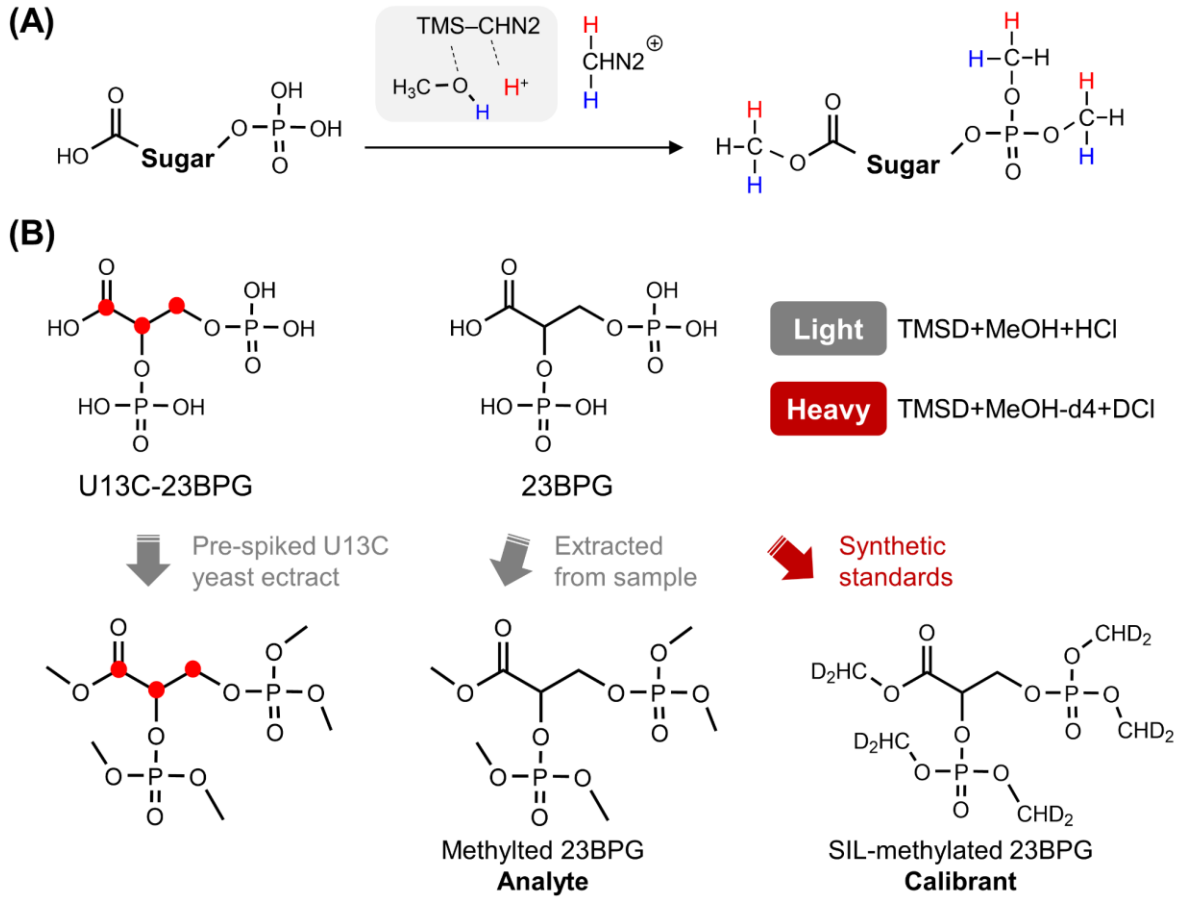

Figure 4: Representative chromatograms obtained with porous graphic carbon column of SPx standard mixture after methylation: (A) F6P/M6P/G6P; (B) F16P2; (C) 23BPG; (D) 3PG and 2PG; (F) 23BPG, SIL-23BPG, and U13C-23BPG. The chromatograms were obtained with: porous graphitic carbon column (2.6 µm, 1.0 × 100 mm), mobile phase: 10 mM NH4FA in water and methanol (details described in materials and methods section).

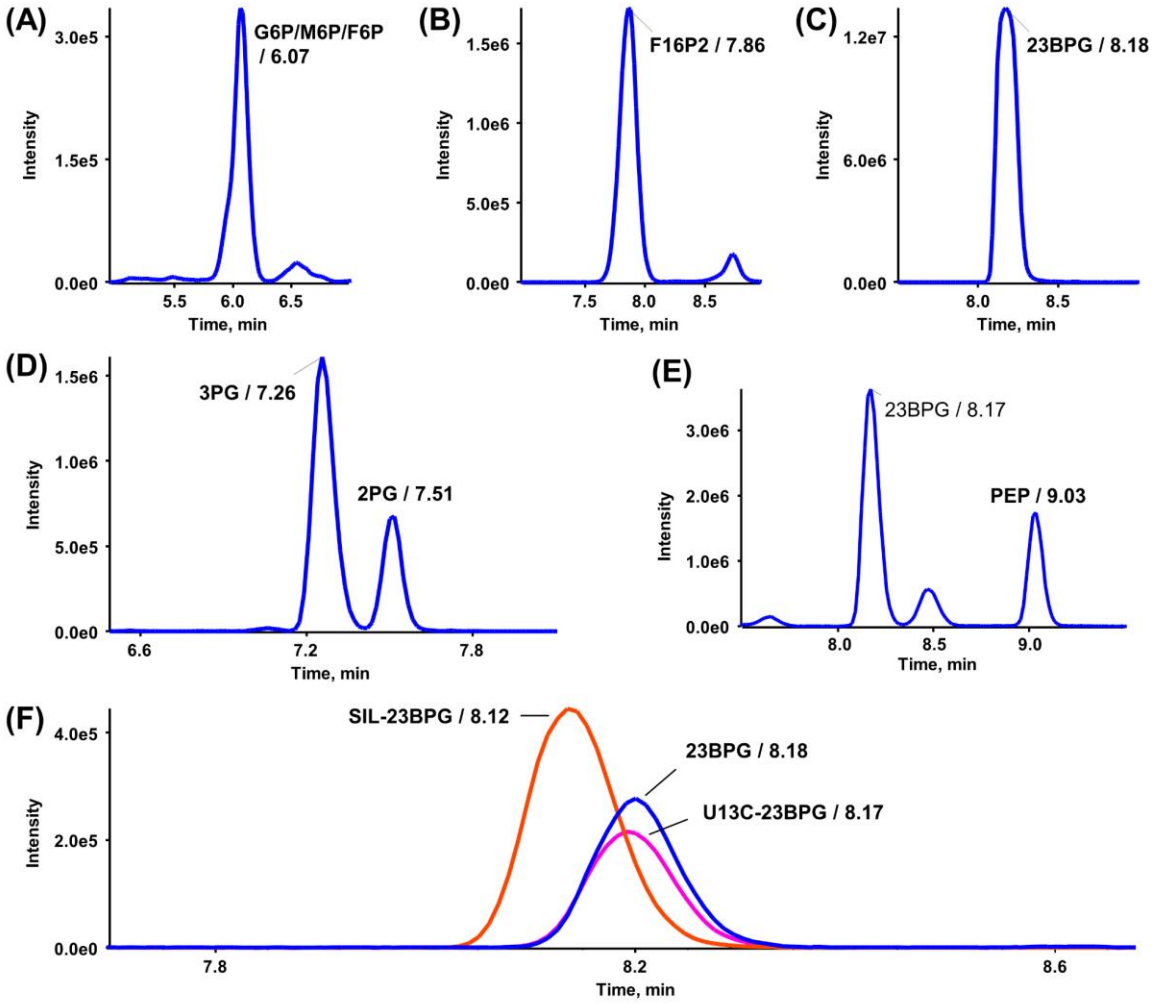

Figure 5: Alterations of SPx generated during glycolysis in experimental human platelet samples. Human platelets from healthy donors (n = 10) were aliquoted and either kept under resting condition or treated with collagen-related peptide (CRP) to activate them. (A) Relative quantification of SPx achieved after normalization by internal standards. P-values were obtained from paired sample Wilcoxon test. Significance levels are *p < 0.05, **p < 0.01, and ***p < 0.001. (B) gives the summary of upregulation of SPx in glycolysis pathway.

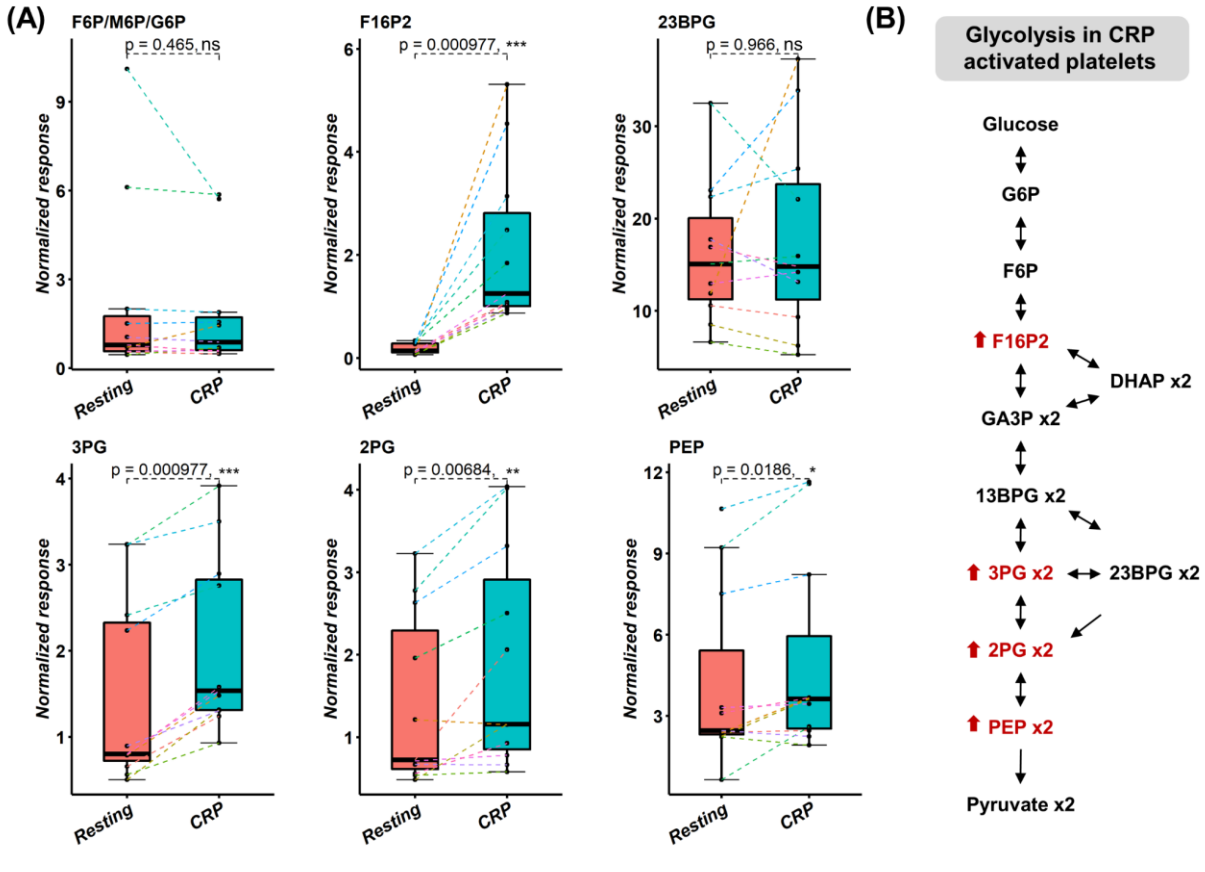

Supporting information

Targeted analysis of sugar phosphates from glycolysis pathway by phosphate methylation with liquid chromatography coupled to tandem mass spectrometry

Peng Li [a], Min Su [a], Madhumita Chatterjee [b], Michael Lämmerhofer [a *]

[a] Institute of Pharmaceutical Sciences, Pharmaceutical (Bio-)Analysis, University of Tübingen, Tübingen, Germany

[b] Department of Cardiology and Angiology, University Hospital Tübingen, 72076 Tübingen, Germany

***Authors for correspondence:**

Prof. Michael Lämmerhofer
Pharmaceutical (Bio-)Analysis
Institute of Pharmaceutical Sciences
University of Tuebingen
Auf der Morgenstelle 8
72076 Tuebingen, Germany
T +49 7071 29 78793, F +49 7071 29 4565
e-mail: michael.laemmerhofer@uni-tuebingen.de
http://www.bioanalysis.uni-tuebingen.de/

Content

Text S1 | High resolution mass spectrometry (HR - MS) method information.

The HR-MS detection was performed on a TripleTOF 5600+ mass spectrometer with a DuoSpray source (Sciex, Framingham, MA, USA) operated with the ESI probe. Ion source parameters were: curtain gas (N2) 30 psi, nebulizer gas (zero grade air) 30 psi; heater gas (zero grade air) 30 psi, ion source voltage +4500 V (positive mode) and source temperature 500 °C. Sequential window acquisition of all theoretical fragment ion mass spectra (SWATH) experiments were performed to obtain comprehensive MS/MS data. The detailed SWATH information is listed in Table S1. Briefly, in the TOF scan, MS parameters were: DP 100 V, CE 10 V, mass range m/z 50 – 2000, accumulation time 200 ms. SWATH experiments were conducted from 50 – 1250 Da. The SWATH window width was 50 Da with accumulation time 20 ms. Other MS parameters were DP 100 V, CE 50 V, and CES 15 V. The total cycle time was 729 ms. The instrument was automatically calibrated every 5 samples via calibration delivery system (CDS) using commercial calibration solution. The EIC of precursor ion was extracted in MasterView software according to chemical formula. Corresponding product ion spectra were obtained after deconvolution according to Rt in chromatography.

Table S1 | SWATH window parameters in this study.

Exp Index	Experiment type	Start mass (Da)	Stop mass (Da)	CE (V)	CES (V)	Accumulation time (ms)
1	TOFMS	50	2000	10	0	200
2	SWATH	50	100	50	15	20
3	SWATH	99	150	50	15	20
4	SWATH	149	200	50	15	20
5	SWATH	199	250	50	15	20
6	SWATH	249	300	50	15	20
7	SWATH	299	350	50	15	20
8	SWATH	349	400	50	15	20
9	SWATH	399	450	50	15	20
10	SWATH	449	500	50	15	20
11	SWATH	499	550	50	15	20
12	SWATH	549	600	50	15	20
13	SWATH	599	650	50	15	20
14	SWATH	649	700	50	15	20
15	SWATH	699	750	50	15	20
16	SWATH	749	800	50	15	20
17	SWATH	799	850	50	15	20
18	SWATH	849	900	50	15	20
19	SWATH	899	950	50	15	20
20	SWATH	949	1000	50	15	20
21	SWATH	999	1050	50	15	20
22	SWATH	1049	1100	50	15	20
23	SWATH	1099	1150	50	15	20
24	SWATH	1149	1200	50	15	20
25	SWATH	1199	1250	50	15	20

The extracted peaks of SPx have peak widths of around 0.25 min. The cycle time is 729 ms.

Table S2 | Extraction recovery (ER) of SPx in this method (plasma as matrix, n = 3).

ER, %	F6P	G6P	F16P2	23BPG	3PG	2PG	PEP
QC1 (low)	39.3 ± 3.7	42.2 ± 2.0	61.5 ± 8.5	77.8 ± 12.4	55.0 ± 5.7	48.7 ± 2.6	75.9 ± 4.8
QC2 (medium)	41.2 ± 5.3	42.6 ± 3.2	70.1 ± 2.6	70.6 ± 5.7	47.8 ± 9.8	51.2 ± 6.5	63.8 ± 6.5
QC3 (high)	30.2 ± 2.8	30.2 ± 2.8	74.2 ± 5.3	71.2 ± 4.1	67.5 ± 6.9	35.4 ± 7.6	52.1 ± 4.4

For F6P, G6P, and F16P2, the concentrations of QC1, QC2, and QC3 were 100 ng/mL (~ 5 x LOQ), 500 ng/mL, and 1000 ng/mL respectively. For 23BPG, 3PG, 2PG, and PEP, the concentrations of QC1, QC2, and QC3 were 50 ng/mL (~ 5 x LOQ), 250 ng/mL, and 500 ng/mL respectively.

Table S3 | Matrix effect (ME) of SPx without internal standards (plasma as matrix, n = 3).

ME wo IS, %	F6P	G6P	F16P2	23BPG	3PG	2PG	PEP
QC1 (low)	96.4 ± 1.8	88.7 ± 6.2	79.3 ± 8.1	92.1 ± 3.8	123.4 ± 9.6	138.9 ± 1.1	70.9 ± 4.2
QC2 (medium)	99.2 ± 11.8	84.3 ± 2.6	95.6 ± 3.8	86.9 ± 3.0	118.1 ± 4.6	121.6 ± 11.0	89.3 ± 8.9
QC3 (high)	90.5 ± 3.9	83.4 ± 2.9	101.2 ± 0.8	81.8 ± 3.9	117.7 ± 6	125.0 ± 6.7	79.0 ± 6.5

The concentrations were the same as in Table S1 above.

Table S4 | Matrix effect (ME) of SPx with internal standards (plasma as matrix, n = 3).

ME w/ IS %	F6P	G6P	F16P2	2,3BPG	3PG	2PG	PEP
QC1 (low)	106.1 ± 2.6	105.4 ± 1.6	97.2 ± 8.4	106.7 ± 3.9	103.5 ± 6.5	106.7 ± 3.6	102.0 ± 9.8
QC2 (medium)	107.2 ± 1.5	107.3 ± 1.4	100.1 ± 4.3	91.4 ± 7.2	100.5 ± 11.1	91.3 ± 8.2	107.7 ± 3.5
QC3 (high)	106.7 ± 4.9	106.6 ± 5.5	103.7 ± 6.6	97.9 ± 9.6	101.7 ± 3	104.4 ± 9.6	102.8 ± 11.6

The concentrations were the same as in Table S1 above.

Table S5 | Intra – batch accuracy (as determined by % recovery) and precision (as % RSD) (plasma as matrix, n = 3).

Accuracy and precision (intra-batch)	F6P	G6P	F16P2	23BPG	3PG	2PG	PEP
QC1 (low)	69.6 ± 11.6	75.1 ± 5.2	80.1 ± 13.2	105.2 ± 2.6	105.6 ± 2.4	105.3 ± 8.1	88.9 ± 5.2
QC2 (medium)	87.8 ± 2.9	93.3 ± 10.4	86.1 ± 3.4	90.7 ± 4.7	104.1 ± 1.2	95.2 ± 16.1	99.4 ± 3.9
QC3 (high)	103.2 ± 1.6	108.7 ± 7.5	108.9 ± 6.2	101.8 ± 2.7	90.6 ± 3.1	99.3 ± 4.3	96.1 ± 2.0

The concentrations were the same as in Table S1 above.

Table S6 | Inter – batch accuracy (as determined by % recovery) and precision (as % RSD) (plasma as matrix, n = 3).

Accuracy and precision (inter-batch)	F6P	G6P	F16P2	23BPG	3PG	2PG	PEP
QC1 (low)	74.2 ± 1.3	75.8 ± 0.5	81.9 ± 4.6	108.3 ± 3.2	108.0 ± 0.9	109.2 ± 3.1	85.4 ± 2.9
QC2 (medium)	88.6 ± 8.4	89.4 ± 7.9	85.1 ± 2.0	94.1 ± 3.0	104.6 ± 4.0	91.6 ± 5.3	100.8 ± 2.2
QC3 (high)	101.5 ± 6.0	108.7 ± 7.2	108.1 ± 3.5	99.9 ± 2.7	88.9 ± 1.1	98.4 ± 5.1	96.2 ± 2.7

The concentrations were the same as in Table S1 above.

Table S7 | SPx in glycolysis quantified in biological samples.

SPx	F6P/M6P/G6P	F16P2	23BPG	3PG	2PG	PEP
NIST SRM1950 plasma (50 µL)	2.7 ± 0.3	0.8 ± 0.3	0.8 ± 0.05	0.1 ± 0.05	22.3 ± 3.9	ND
HeLa cells (10^6 cells)	261.5 ± 32.9	389.5 ± 21.7	31.2 ± 2.5	20.8 ± 4.1	33.6 ± 3.6	ND

ND, lower than LOQ in this method.

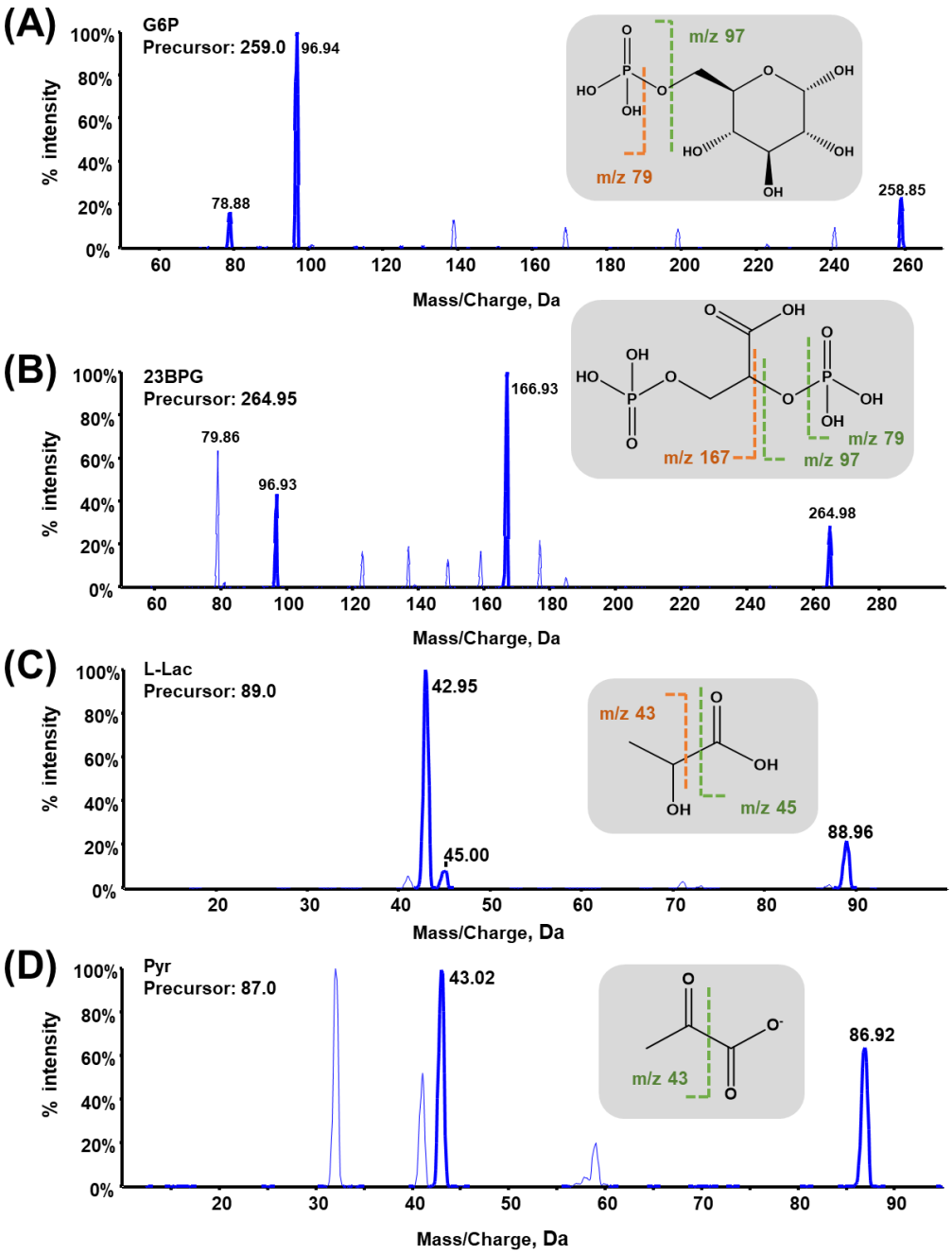

Figure S1 | Product ion spectra of metabolites in the glycolysis pathway before methylation, including (A) G6P, (B) 23BPG, (C) Lac, and (D) Pyr.

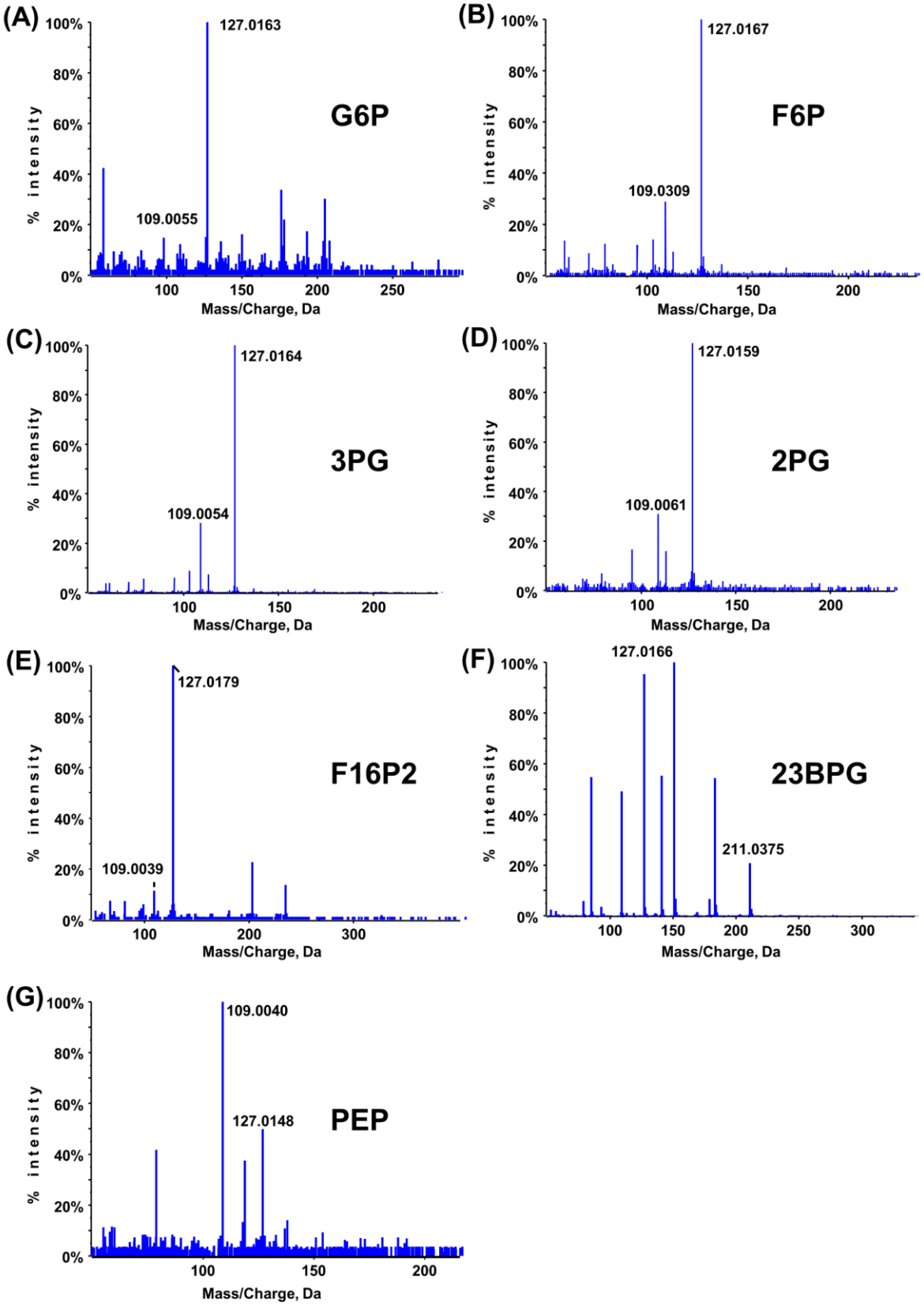

Figure S2 | Product ion spectra of metabolites in the glycolysis pathway after methylation, including (A) G6P, (B) F6P, (C) 3PG, (D) 2PG, (E) F16P2, (F) 23BPG, and (G) PEP.

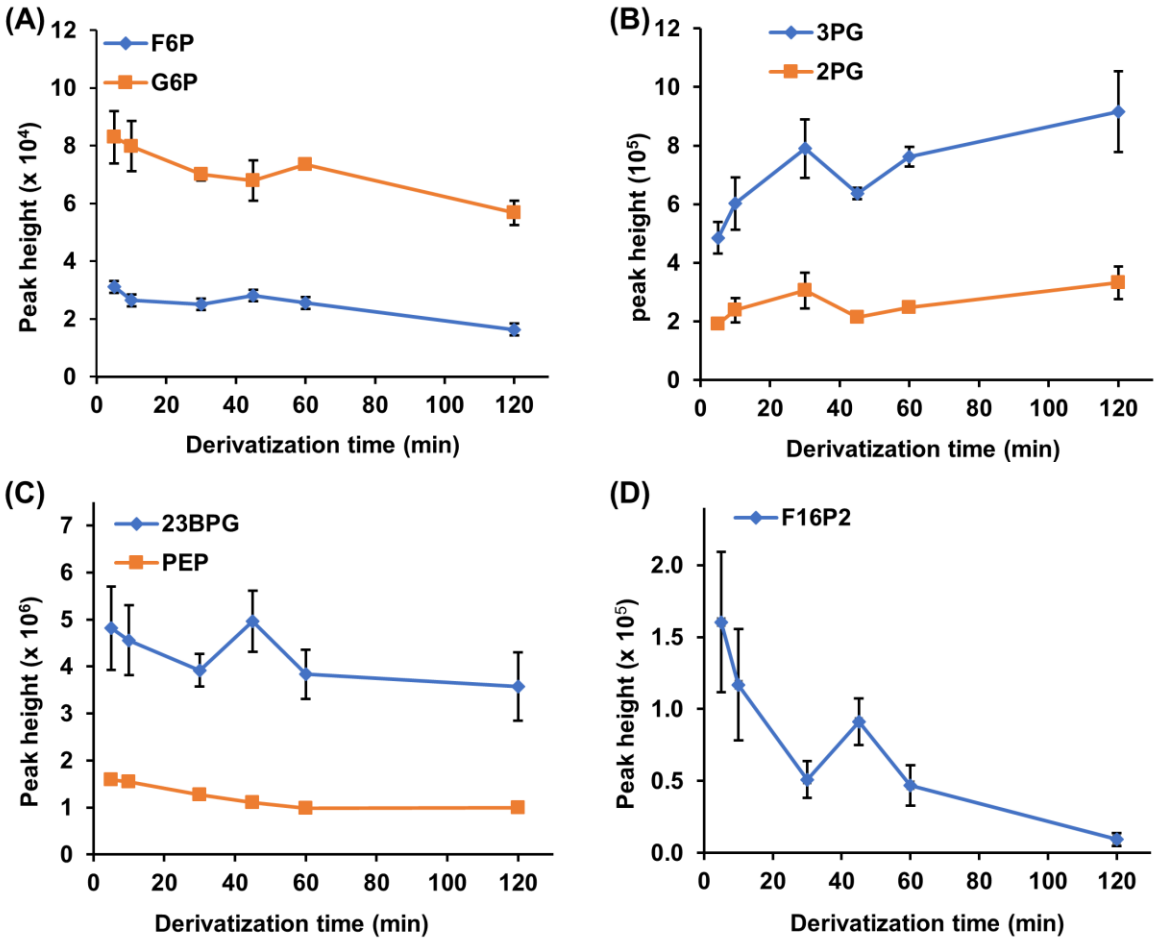

Figure S3 | Optimization of methylation time.

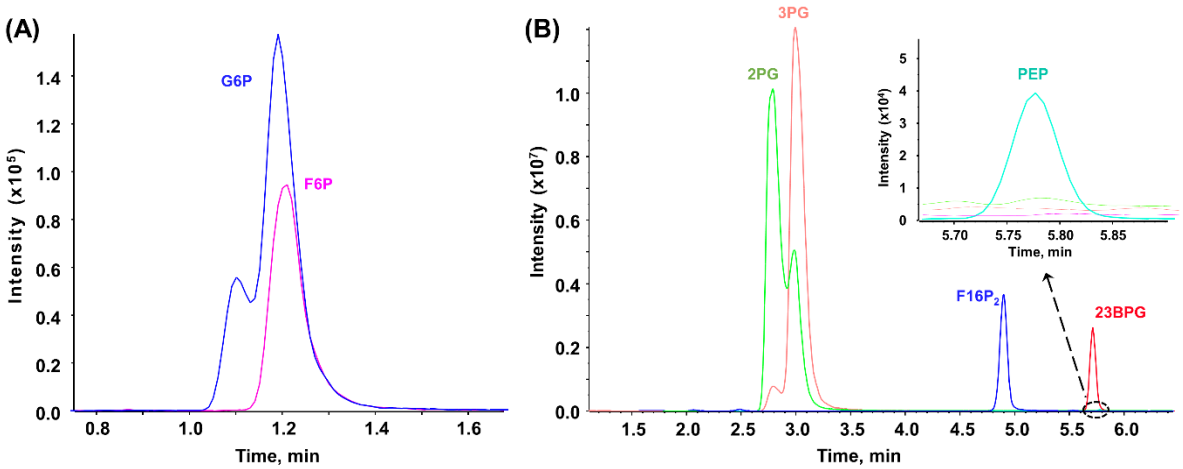

Figure S4 | Chromatograms of SPx on cholesterol-bonded column. The chromatograms were obtained with: COSMOCORE 2.6Cholester packed column (2.6 µm, 2.1 x 150 mm). Mobile phases: A 10 mM NH4FA in water and B methanol. Gradient: 0 min, 5% B; 3 min 5% B; 9 min, 100% B; 10 min, 100% B; 10.1 min, 5% B; 15 min, 5% B. Flow: 0.4 mL/min. Column temperature: 60 °C.

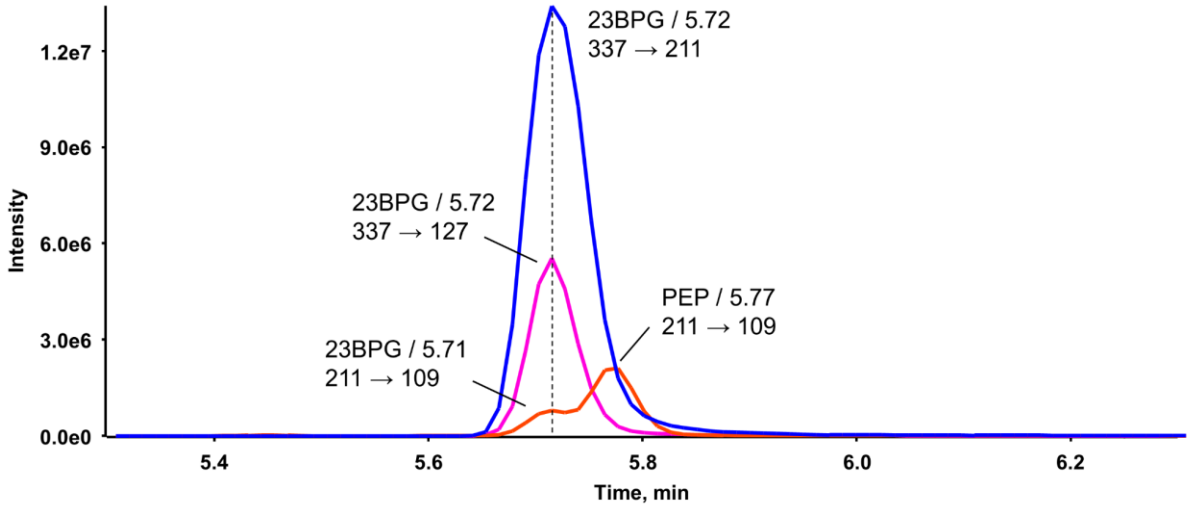

Figure S5 | In-source fragmentation of methylated 23BPG and its potential interference for PEP. Blue and pink traces are characteristic transitions of 23BPG. The red trace is the overlapped transition of 23BPG and PEP. Conditions as in Figure S4.

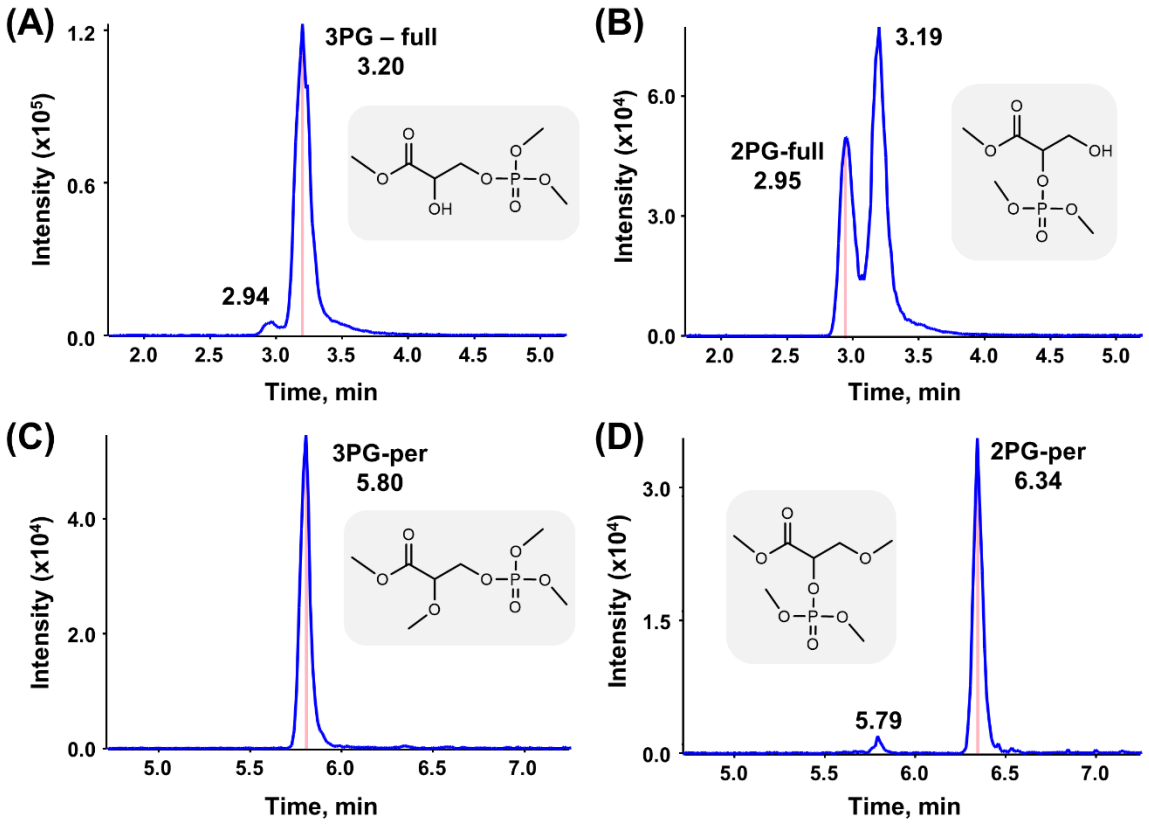

Figure S6 | Chromatograms with chemical structures of 2/3-PG in full-methylation and per-methylation states. (A) full methylated 3PG. (B) full methylated 2PG. (C) per-methylated 3PG. (D) per-methylated 2PG. Conditions as in Figure S4.

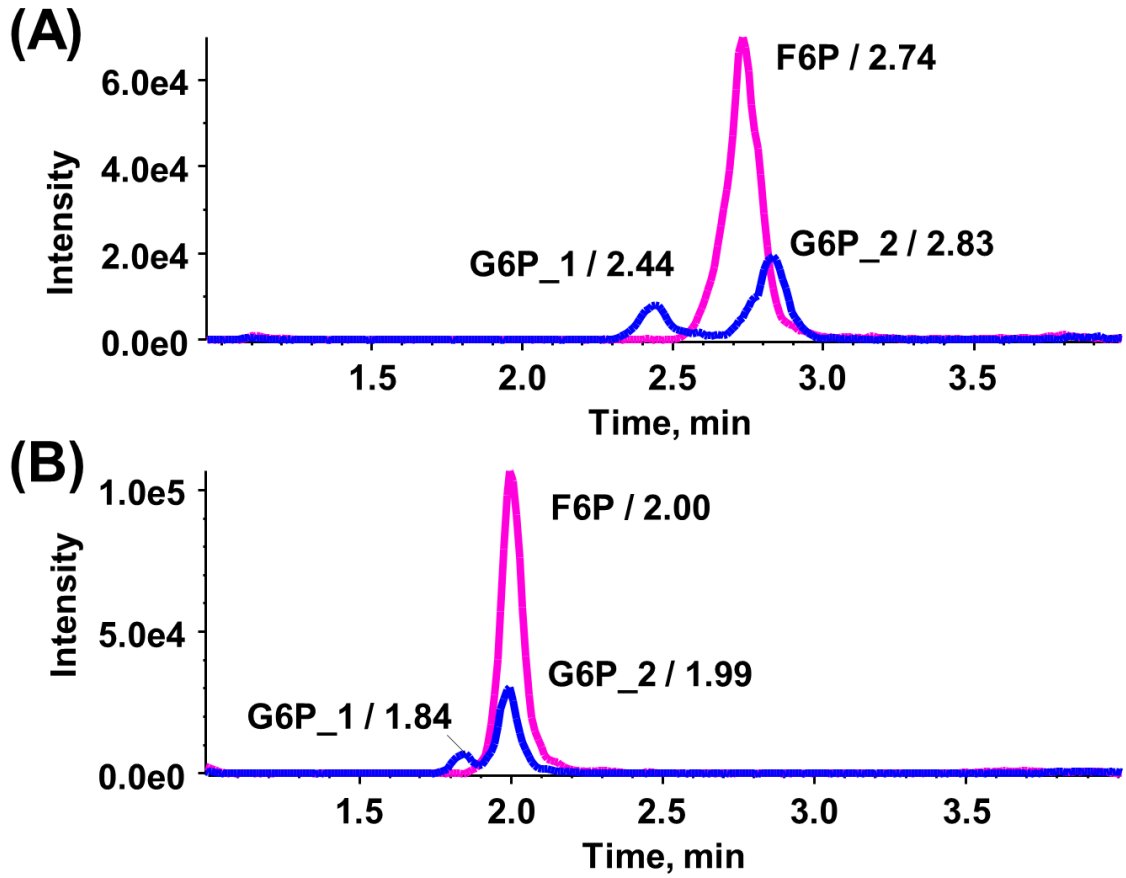

Figure S7 | Chromatograms of G6P and F6P on C30 column. The chromatograms were obtained with: ProntoSIL C30 column (5 µm, 2 x 200 mm). Mobile phases: A 10 mM NH4FA in water. MeOH (A) and AcN (B) was used as organic modifier respectively. Gradient: 0 min, 5% B; 6 min 5% B; 20 min, 100% B; 24 min, 100% B; 24.5 min, 5% B; 30 min, 5% B. Flow: 0.4 mL/min. Column temperature: 40 °C.

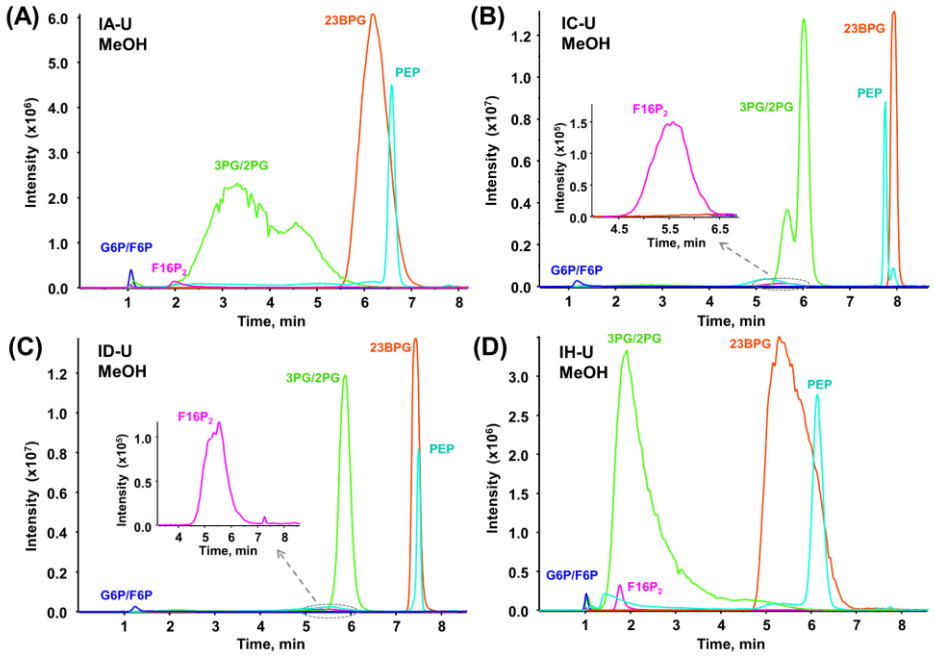

Figure S8 | Chromatograms of SPx on chiral columns. The chromatograms were obtained with: column: Daicel Chiralpak UPLC columns are with the same dimension (1.6 µm, 3.0 x 100 mm). Mobile phases: A 10 mM NH4FA in water. MeOH was tested as organic modifier B. Gradient: 0 min, 5% B; 6 min 5%; 20 min, 100% B; 24 min, 100% B; 24.5 min, 5% B; 30 min, 5% B. Flow: 0.5 mL/min. Column temperature: 40 °C.

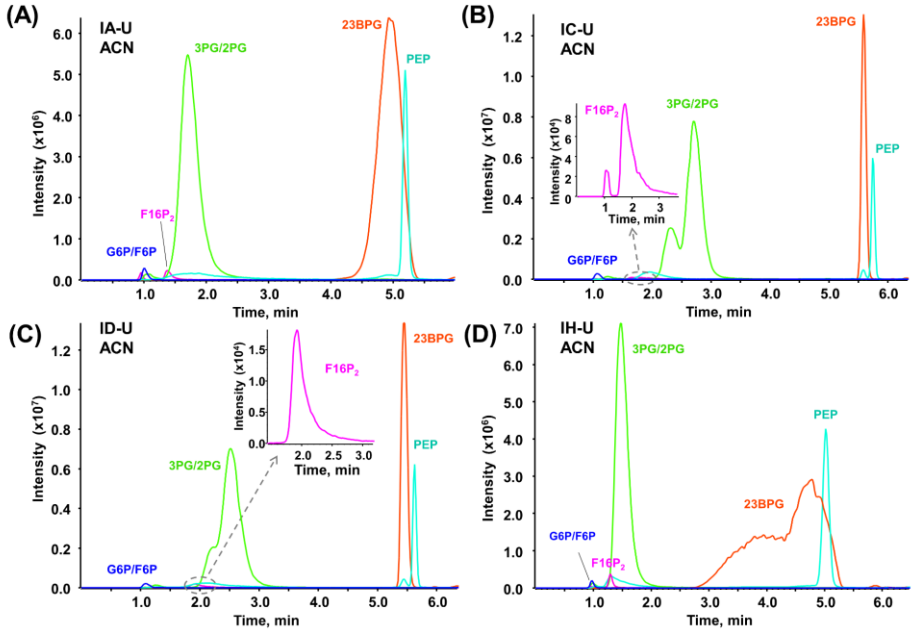

Figure S9 | Chromatograms of SPx on chiral columns. AcN was tested as organic modifier B. Other conditions were as that in Figure S8.

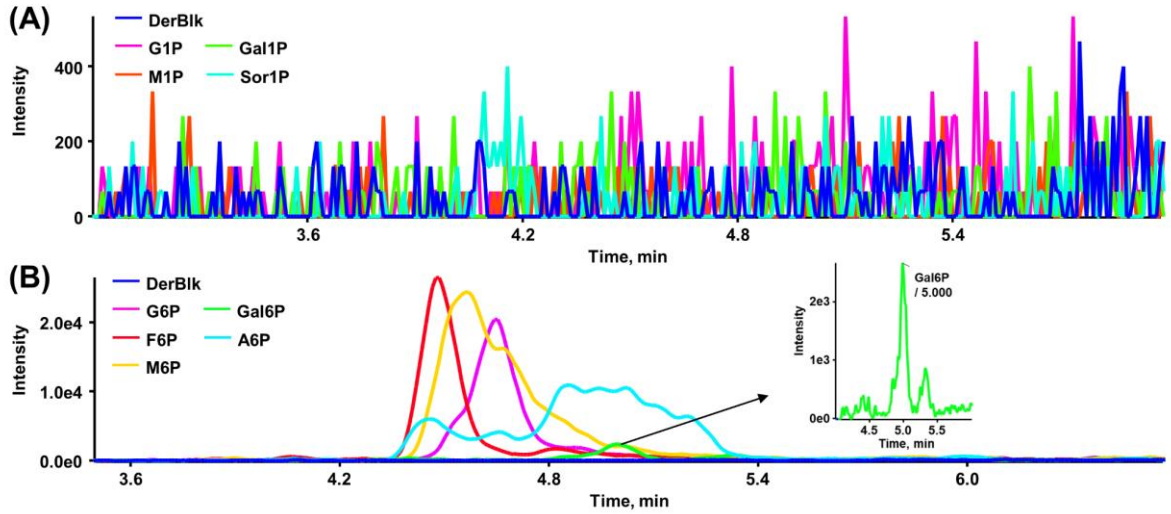

Figure S10 | Results of specificity test. Two groups of isobaric sugar monophosphates were tested. (A) sugar 1' phosphate: G1P, Gal1P, M1P, and Sor1P. (B) sugar 6' phosphate: G6P, Gal6P, F6P, A6P, and M6P. The chromatograms were obtained with: column: porous graphitic carbon column (2.6 µm, 1.0 x 100 mm). Mobile phases: A 10 mM NH4FA in water and B MeOH. Gradient: 0 min, 5% B; 9 min 100% B; 12 min, 100% B; 12.1 min, 95% B; 17 min, 95% B; 17.1 min, 5% B; 23 min, 5% B. Flow: 0.1 mL/min. Column temperature: 60 °C.

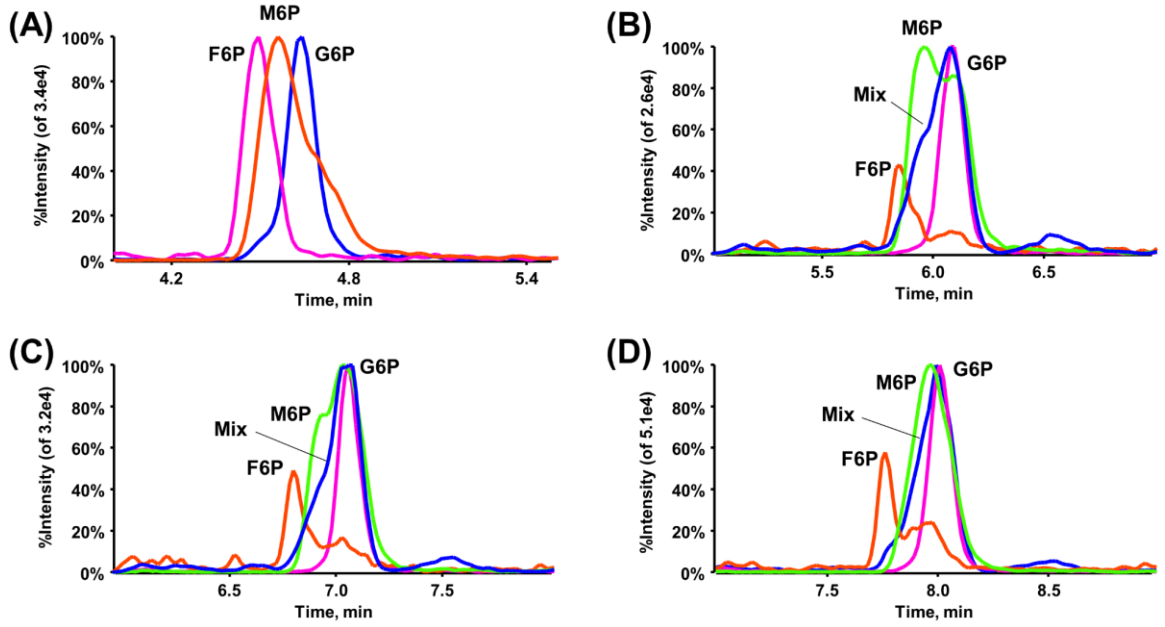

Figure S11 | Results of LC optimization for sugar monophosphates. The chromatograms were obtained with: column: porous graphitic carbon column (2.6 µm, 1.0 x 100 mm). Mobile phases: A 10 mM NH4FA in water and B MeOH. Flow: 0.1 mL/min. Column temperature: 60 °C. Different gradients were tested: (A) gradient was the same as Figure S10; (B) gradient: 0 min, 0% B; 1 min, 0% B; 10 min 100% B; 13 min, 100% B; 13.1 min, 95% B; 18 min, 95% B; 18.1 min, 0% B; 24 min, 0% B. (C) gradient: 0 min, 0% B; 2 min, 0% B; 11 min 100% B; 14 min, 100% B; 14.1 min, 95% B; 19 min, 95% B; 19.1 min, 0% B; 25 min, 0% B. (D) gradient: 0 min, 0% B; 3 min, 0% B; 12 min 100% B; 15 min, 100% B; 15.1 min, 95% B; 20 min, 95% B; 20.1 min, 0% B; 26 min, 0% B.

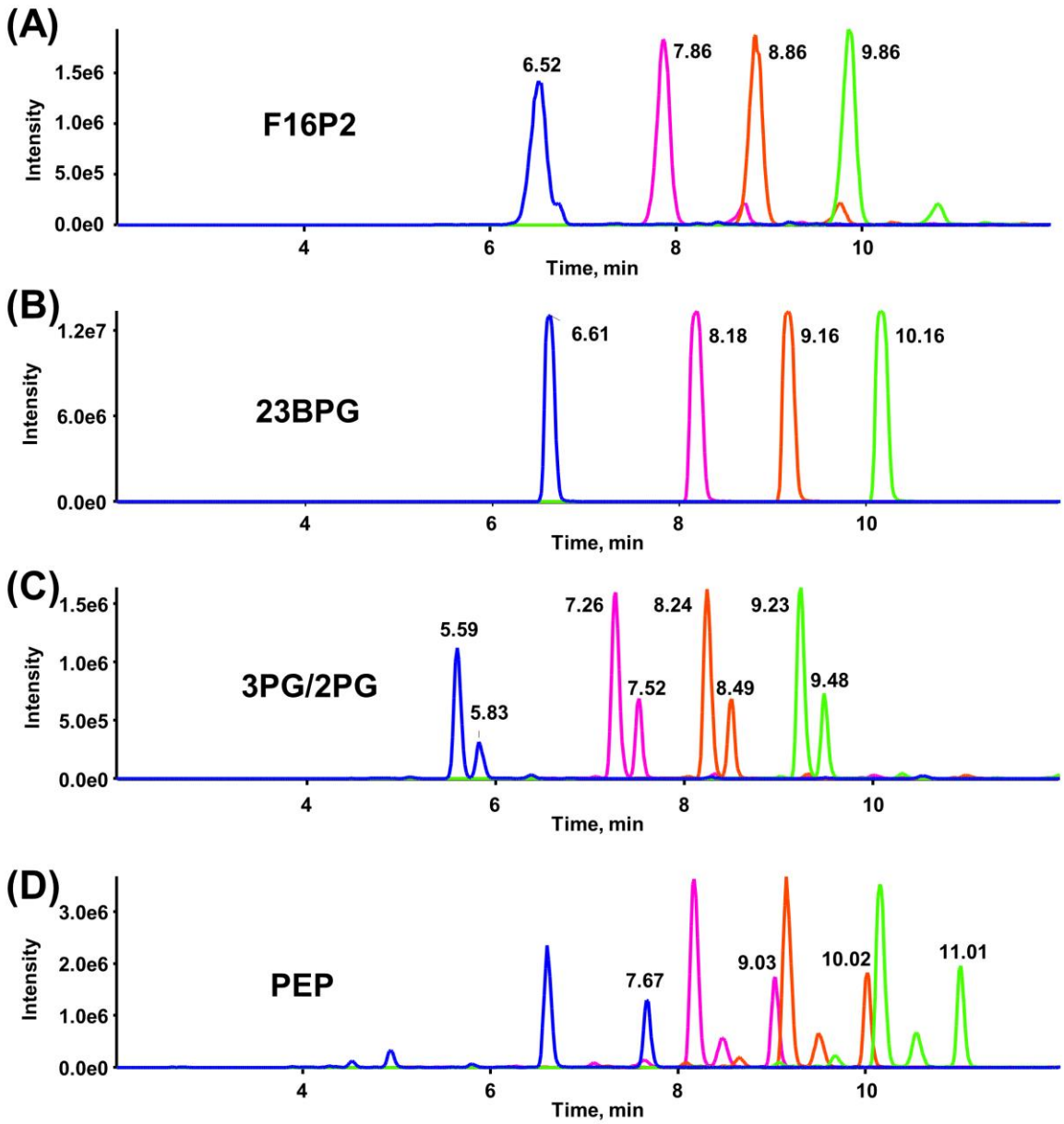

Figure S12 | Results of LC optimization for other sugar phosphates in this study. The chromatograms were obtained with: column: porous graphitic carbon column (2.6 µm, 1.0 x 100 mm). Mobile phases: A 10 mM NH4FA in water and B MeOH. Flow: 0.1 mL/min. Column temperature: 60 °C. For SPx analytes: (A) F16P2, (B) 23BPG, (C) 3PG and 2PG, and (D) PEP, different gradients were tested as follows. The blue trace stands for gradient in Figure S10; The pink trace stands for gradient: 0 min, 0% B; 1 min, 0% B; 10 min 100% B; 13 min, 100% B; 13.1 min, 95% B; 18 min, 95% B; 18.1 min, 0% B; 24 min, 0% B. The red trace stands for gradient: 0 min, 0% B; 2 min, 0% B; 11 min 100% B; 14 min, 100% B; 14.1 min, 95% B; 19 min, 95% B; 19.1 min, 0% B; 25 min, 0% B. the green trace stands for gradient: 0 min, 0% B; 3 min, 0% B; 12 min 100% B; 15 min, 100% B; 15.1 min, 95% B; 20 min, 95% B; 20.1 min, 0% B; 26 min, 0% B.

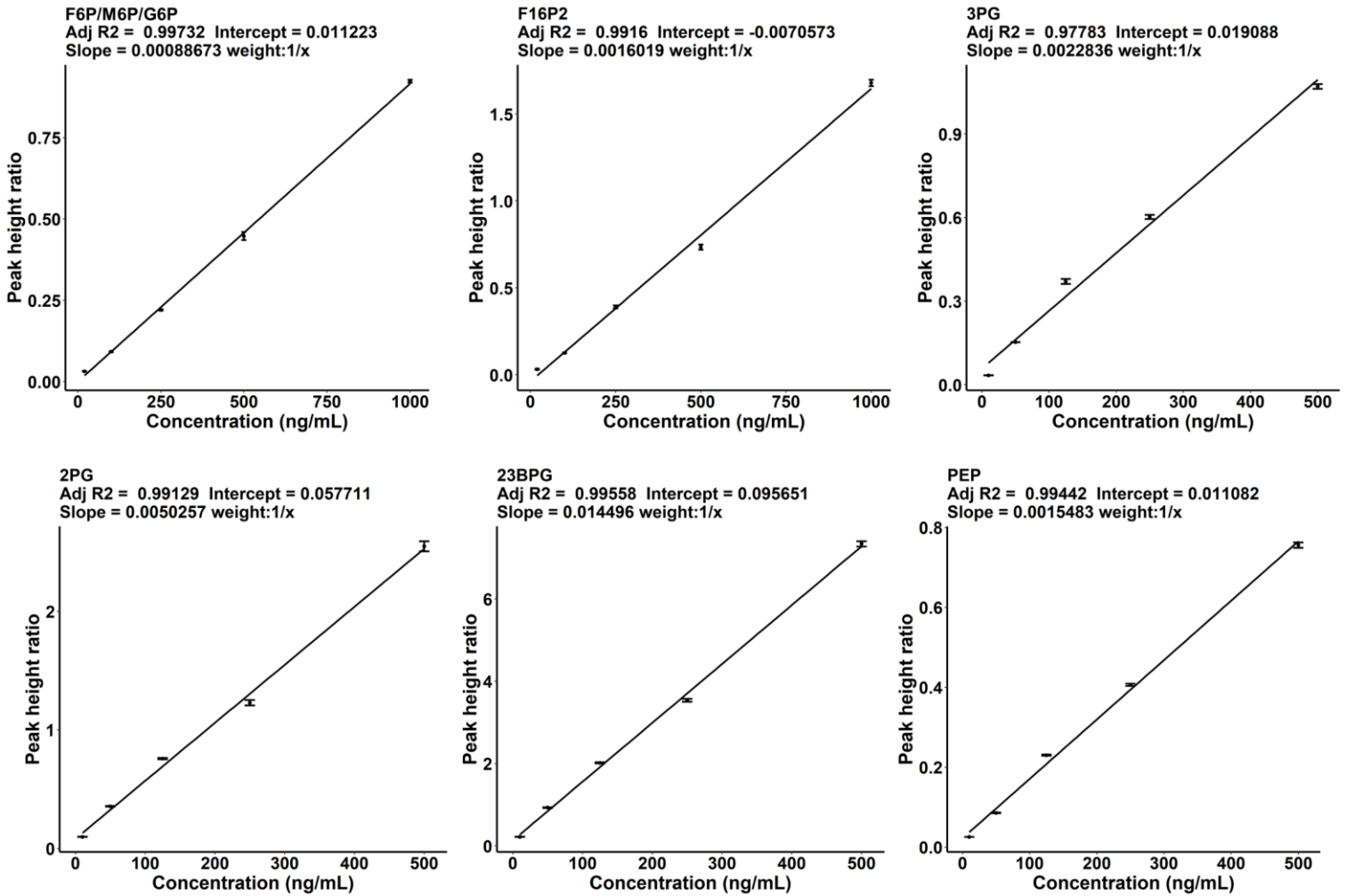

Figure S13 | Results of calibration curves (weighing regression of 1/x was used) in plasma.

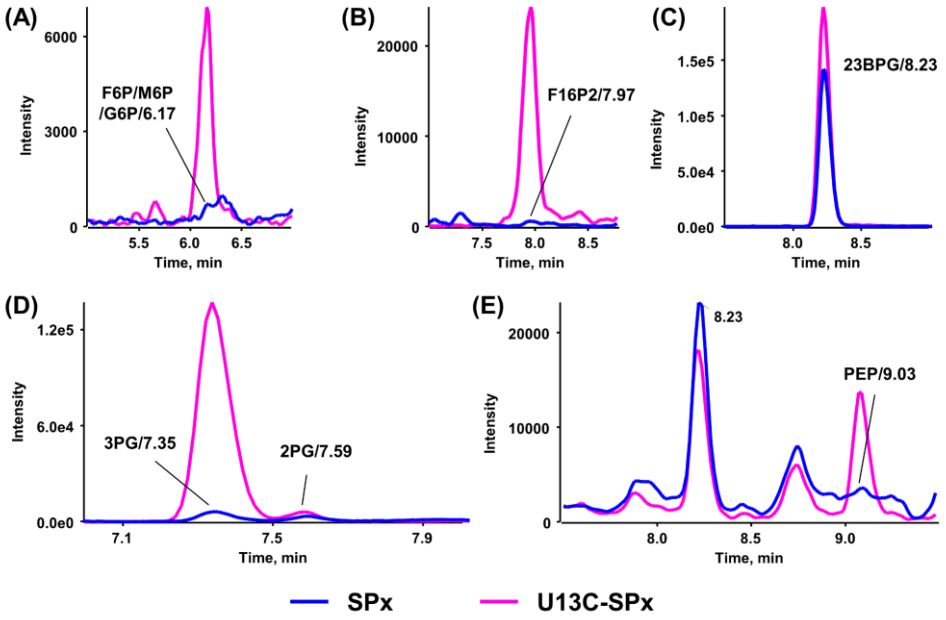

Figure S14 | Representative chromatograms (SPx analyte in blue while U13C-SPx in pink) in NIST SRM1950 plasma sample. The analytes with concentrations in solution were as follows: (A) F6P/M6P/G6P, 17.2 ng/mL; (B) F16P2, 25.2 ng/mL; (C) 23BPG, 73.6 ng/mL; (D) 3PG, 11.1 ng/mL and 2PG, 74.2 ng/mL; (E) PEP, 5.3 ng/mL.

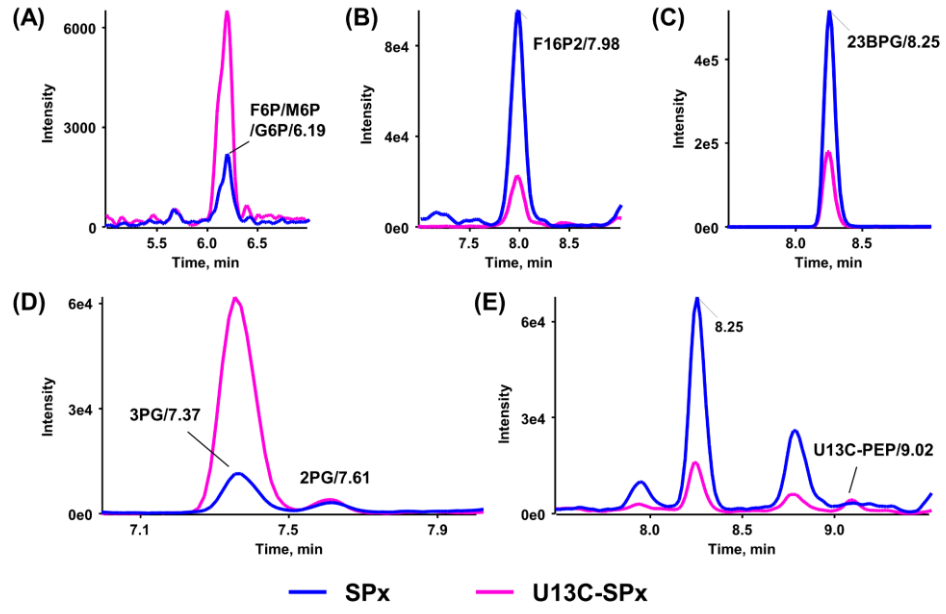

Figure S15 | Representative chromatograms (SPx analyte in blue while U13C-SPx in pink) in cultured HeLa cell sample. The analytes with concentrations in solution were as follows: (A) F6P/M6P/G6P, 464.1 ng/mL; (B) F16P2, 2973.1 ng/mL; (C) 23BPG, 217.7 ng/mL; (D) 3PG, 88.6 ng/mL and 2PG, 125.9 ng/mL; (E) PEP, ND (lower than LOQ).

XII. Acknowledgement

At the end of my doctoral study, I would like to express my sincere thank you to all the people who inspired and helped me during this period.

First, I would like to thank Prof. Dr. Michael Laemmerhofer for having me working in his laboratory and his supervision. After first interview just before the Christmas in 2017, we made it together applying for the CSC scholarship with interesting research proposal. I really enjoy working with him, as well as the research topics. He is encouraging, inspiring, and supportive. I could not finish the study without his endless support throughout my study. I am also grateful to Prof. Dr. Stefan Laufer to be my second supervisor. Many thanks for reviewing my thesis and organizing the defence.

Many thanks to Bernhard Drotleff, Jorg Schlotterbeck, and Carlos Calderón Castro. Thank them for the introduction when I started my PhD study. I learnt so much from them, not only the knowledge of instruments but also the way to handle multiple projects efficiently.

Many thanks to Jeannie Horak, who taught me general knowledge of research and particularly the cell culture. I learnt the careful working style of designing experiments from her, which benefits me so much.

Many thanks to Min Su, who worked with me for her master thesis. It was my first time to be responsible for a complete master thesis. Thank her for her work and cooperation. Wish you all the best for your PhD study in the future.

Special thanks to Feiyang Li and Simon Jaag. We spend the most time together in the lab. Every discussion during the lunch break is encouraging and inspiring.

Many thanks to all my colleagues and former lab members: Adrian Sievers-

Engler, Mike Kaupert, Siyao Liu, Stefanie Bäurer, Ryan Karongo, Kristina Schmitt, Ece Aydin, Malgorzata Cebo, Stefan Neubauer, Christian Geibel, Marc Wolter, Min Ge, Luke Tu, Adrian Brun, Xiaoqing Fu, Franz Fießinger, Cornelius Knappe, Mirna Maalouf, Matthias Olfert, Kristian Serafimov, Zhanjian Xu, Chunmei Wen, Zaiwei Zhang, Shenkai Chen, Li Zhang, Shereen Ahmed, Tayser Alfadel, Jose' Juan Borra's Cruzado, and Bushra Alissa. Due to your work and contribution, the working group is running so efficiently. It is a lovely group in which we support and inspire each other.

I would like thank my girlfriend, Yali Liu. We are fortunate to start our PhD study together. Her loving care and unconditional supports motivate me to move forward all the time. I think I am the lucky guy who gets her in my life.

Last but not the least, I would like to thank my parents, Luping Li and Guofang Xue for their endless support and understanding.